



**HAL**  
open science

# Development of novel mass spectrometry-based approaches for searching for low-mass tyrosinase inhibitors in complex mixtures

Aleksander Salwiński

► **To cite this version:**

Aleksander Salwiński. Development of novel mass spectrometry-based approaches for searching for low-mass tyrosinase inhibitors in complex mixtures. Other. Université d'Orléans, 2014. English. NNT : 2014ORLE2013 . tel-01223001

**HAL Id: tel-01223001**

**<https://theses.hal.science/tel-01223001v1>**

Submitted on 1 Nov 2015

**HAL** is a multi-disciplinary open access archive for the deposit and dissemination of scientific research documents, whether they are published or not. The documents may come from teaching and research institutions in France or abroad, or from public or private research centers.

L'archive ouverte pluridisciplinaire **HAL**, est destinée au dépôt et à la diffusion de documents scientifiques de niveau recherche, publiés ou non, émanant des établissements d'enseignement et de recherche français ou étrangers, des laboratoires publics ou privés.

**ÉCOLE DOCTORALE**  
**SANTE, SCIENCES BIOLOGIQUES ET CHIMIE DU VIVANT**

Institut de Chimie Organique et Analytique

**THÈSE** présentée par :  
**Aleksander SALWIŃSKI**

soutenue le : **24 avril 2014**

pour obtenir le grade de : **Docteur de l'université d'Orléans**  
Discipline/ Spécialité : Chimie

**Development of novel mass  
spectrometry-based approaches for  
searching for low-mass tyrosinase inhibitors  
in complex mixtures**

**THÈSE dirigée par :**

**Benoît MAUNIT**

**Raphaël DÉLÉPEE**

Professeur – Université d'Orléans

Professeur – Université de Caen Basse Normandie

**RAPPORTEURS :**

**Francesc Xavier AVILÉS**

**Benjamin CARBONNIER**

Professeur – Université Autonome de Barcelone

Professeur – Université Paris-Est Créteil Val de Marne

**JURY :**

**Francesc Xavier AVILÉS**

**Benjamin CARBONNIER**

**Patrice ANDRÉ**

**Claire DEMESMAY-GUILHIN**

**Paul HANNEWALD**

**Raphaël DÉLÉPEE**

**Benoît MAUNIT**

Professeur – Université Autonome de Barcelone

Professeur – Université Paris-Est Créteil Val de Marne

Président de BOTANICOSM'ETHIC

Professeur – Université Claude Bernard Lyon 1

Docteur – Directeur Général Adjoint de 'Plant Advanced Technologies'

Professeur – Université de Caen Basse Normandie

Professeur – Université d'Orléans

**CONFIDENTIAL**



## **Acknowledgements**

This thesis was conducted in the Institute of Organic and Analytical Chemistry (ICOA) in Orleans, France. I would like to thank **Professor Olivier Martin**, director of ICOA, and **Professor Claire Elfakir**, head of the laboratory of analytical chemistry, for Their kind welcome in the Institute.

I would like to thank my scientific supervisors: **Professor Benoît Manunit** and **Professor Raphaël Delépée** for giving me the opportunity to conduct the PhD research project in Their scientific team. I would like to thank each of You for Your support, assistance and suggestions.

I would also like to thank **Doctor David Da Silva** for His help in conducting various FA and ENALDI-MS experiments in the final stage of my work and numerous precious advices and remarks concerning the final form of the present manuscript.

I would like to thank **Professor Francesc Xavier Avilés** (Autonomous University of Barcelona) and **Professor Benjamin Carbonnier** (University Paris-Est Créteil) for giving me a honour to review this work and to become Reporters of my Thesis manuscript.

I thank **Professor Claire Demesmay-Guilhin**, **Doctor Paul Hannewald** and **Mr Patrice André** for giving me a honour to join the Jury in the role of Examiners.

I thank **Doctor Cyril Colas**, **Doctor Emilie Destandau**, **Sandrine Zubrzycki** and **Laëtitia Fougere** for Their inestimable help and assistande during my work in the laboratory.

A number of other people deserve many thanks for Their presence in my everyday laboratory work. I would like thank them for their enthusiasm and kindness: **Syame**, **Hanane**, **Ludivine**, **Manabu-san**, **Aleksandra**, **Nathaly**, **Hala**, **Reine**, **Ozkan** and **Kinga**.

I am thankful to the **Conseil régional du Centre** for financial support.

I would like to thank **Mr. Patrice André**, director of the Ethnobotany Innovation Department of LVMH Recherche, for providing us with the samples of plant extract and glabridin.



## TABLE OF CONTENTS

### List of abbreviations

### GENERAL INTRODUCTION

#### Chapter I – Introduction

<b>I. Preface.....</b>	<b>1</b>
<b>I.1. Skin hyperpigmentation: a general outlook.....</b>	<b>2</b>
<b>I.2. Tyrosinase - the main enzyme responsible for skin pigmentation.....</b>	<b>3</b>
I.2.1. The pathway of melanin biosynthesis – enzymatic conversion of L-Tyr and L-DOPA.....	6
I.2.2. General introduction to enzyme kinetics and types of enzyme inhibition.....	7
I.2.2.1. An outlook of tyrosinase inhibitors.....	8
<b>II. High-throughput screening as a tool for finding biologically active substances.....</b>	<b>14</b>
<b>II.1. Affinity-based screening.....</b>	<b>15</b>
II.1.1. Affinity chromatography.....	16
II.1.2. Surface plasmon resonance coupled with HPLC/MS.....	17
II.1.3. Ultrafiltration and related techniques.....	19
II.1.4. Direct detection of protein-ligand complexes.....	20
II.1.5. Intensity ion fading MS.....	22
<b>II.2. On-line enzymatic activity-based screening.....</b>	<b>23</b>
<b>II.3. A short overview of high-throughput screening methods developed in present work.....</b>	<b>25</b>
<b>III. Mass spectrometry.....</b>	<b>25</b>
<b>III.1. Introduction.....</b>	<b>25</b>
<b>III.2. Mass spectrometer with electrospray ion source.....</b>	<b>26</b>
III.2.1. Electrospray ion source.....	26
III.2.2. Collision-induced dissociation and its application in metabolite identification.....	28
III.2.3. An outlook of Bruker maXis™ UHR-Qq-TOF spectrometer.....	30
<b>III.3. Matrix-assisted laser desorption/ionisation and related techniques.....</b>	<b>34</b>
<b>IV. The strategies for protein immobilisation.....</b>	<b>39</b>
<b>IV.1. Non-covalent protein immobilisation.....</b>	<b>39</b>
IV.1.1. Immobilisation based on specific protein-ligand interactions.....	39
IV.1.2. Immobilised artificial membranes.....	41
IV.1.3. Enzyme immobilisation by entrapment within a polymer network.....	41
<b>IV.2. Covalent protein immobilisation.....</b>	<b>41</b>
IV.2.1. General outlook.....	41
IV.2.2. Impact of protein immobilisation on its kinetic parameters: $K_M$ and $V_{max}$ .....	44

#### Chapter II – Frontal affinity chromatography

<b>I. Frontal affinity chromatography: from theory to practice.....</b>	<b>45</b>
<b>I.1. An introduction to frontal affinity chromatography.....</b>	<b>45</b>
I.1.1. The historical background of frontal affinity chromatography.....	45
I.1.2. The principle and mathematical description of frontal analysis.....	45

1.1.2.1. A 'single infusion' approach.....	46
1.1.2.2. Staircase frontal analysis.....	48
<b>1.2. Selection of appropriate detection method.....</b>	<b>51</b>
<b>1.3. Non-specific interactions of analyte with the stationary phases. Selection of appropriate immobilisation support.....</b>	<b>52</b>
<b>1.4. The pathways of protein immobilisation commonly applied for frontal affinity chromatography.....</b>	<b>53</b>
<b>II. Stationary phases for FAC: development and application of FAC for searching for the inhibitors of tyrosinase and trypsin.....</b>	<b>57</b>
<b>II.1. Aims and objectives.....</b>	<b>57</b>
<b>II.2. Stationary phases for FAC.....</b>	<b>57</b>
<b>II.2.1. Capillary-format monoliths.....</b>	<b>57</b>
II.2.1.1. Organic monoliths based on esters of acrylic and methacrylic acid.....	58
II.2.1.1.1 Preparation of amine-covered hydrophilic organic poly(SBMA-co-AEMA-co-EGDMA) monolith with the surface hydrophilized by zwitterionic moieties.....	59
II.2.1.1.2 Preparation of hydrophilic monolith based on N-acryloxysuccinimide.....	61
II.2.1.2. Silica monoliths.....	61
II.2.1.2.1 Preparation of organic-inorganic silica monolith based on APTES/TEOS using surfactant as a porogen.....	62
II.2.1.2.2 Preparation of organic-inorganic silica monolith based on APTES/TEOS using room-temperature ionic liquid as co-porogen.....	62
<b>II.2.2. Silica beads as an immobilisation support.....</b>	<b>63</b>
II.2.2.1. Chromatographic support for silica beads.....	64
<b>II.3. Protein immobilisation on the surface of monoliths and silica particles.....</b>	<b>64</b>
<b>II.3.1. Capillary-format monoliths.....</b>	<b>65</b>
II.3.1.1. Derivatisation and preparation of the capillaries for enzyme immobilisation.....	66
II.3.1.1.1. Amine-bearing monoliths.....	66
II.3.1.1.2. Poly(NAS-co-EGDMA) monolith.....	66
II.3.1.2. Enzyme immobilisation: capillary-format monoliths.....	67
<b>II.3.2. Silica beads.....</b>	<b>67</b>
<b>II.3.2.1. Derivatisation of silica beads.....</b>	<b>67</b>
II.3.2.1.1 Activation of silica-APTES beads.....	67
II.3.2.1.2 Activation of silica-GPTMS beads.....	68
<b>II.3.2.2. Enzyme immobilisation: silica beads.....</b>	<b>68</b>
II.3.2.2.1. Immobilisation of tyrosinase on silica-APTES-GLA beads.....	68
II.3.2.2.2. Immobilisation of trypsin on silica-oxGPTMS beads.....	68
<b>III. Evaluation of the stationary phases for FAC.....</b>	<b>69</b>
<b>III.1. Trypsin as a biological target for method validation.....</b>	<b>69</b>
<b>III.2. Configuration of the experimental system.....</b>	<b>70</b>
III.2.1. Silica-packed cartridges.....	70
III.2.2. Capillary-format FAC.....	70
<b>III.3. Assessment of the nature of non-specific interactions for developed stationary phases.....</b>	<b>71</b>
<b>III.3.1. Capillary-format stationary phase.....</b>	<b>72</b>
III.3.1.1. Organic monoliths.....	72
III.3.1.2. Silica monoliths.....	75
<b>III.3.2. Silica particle-based stationary phases.....</b>	<b>76</b>
<b>III.3.3. Selection of the stationary phase for FAC: conclusions.....</b>	<b>78</b>

<b>IV.1. FAC experiment using tyrosinase and trypsin as biological targets.....</b>	<b>78</b>
IV.1.1. Capillary-format organic monoliths.....	78
IV.1.2. Silica particles.....	81
<b>IV.2. FAC – conclusions.....</b>	<b>84</b>
<b>V. Continuous-flow step gradient mass spectrometry based method for the determination of kinetic parameters of immobilised mushroom tyrosinase in equilibrating conditions: comparison with free enzyme.....</b>	<b>84</b>
<b>Appendix I: Supplementary Information.....</b>	<b>91</b>
<b><u>Chapter III</u> – Enzyme-coupled nanoparticles-assisted laser desorption ionisation MS for searching for low-mass inhibitors of enzymes in complex mixtures</b>	
<b>I. Ion Fading/ Ion Hunting Enzyme-coupled nanoparticles-assisted laser desorption ionisation MS..</b>	<b>95</b>
<b>I.1. Introduction.....</b>	<b>95</b>
<b>I.2. Experimental.....</b>	<b>97</b>
<b>I.2.1. Extraction of plant material.....</b>	<b>97</b>
<b>I.2.2. Synthesis of functional magnetic nanoparticles.....</b>	<b>97</b>
I.2.2.1. Synthesis of raw magnetic nanoparticles.....	97
I.2.2.2. Derivatisation of raw MPs.....	98
I.2.2.2.1. Aldehyde-covered MPs-APTES-GLA.....	98
I.2.2.2.2. Aldehyde-covered MPs-oxyGPTMS.....	98
<b>I.2.3. Immobilisation of enzymes: trypsin and tyrosinase.....</b>	<b>99</b>
<b>I.2.4. Kinetic assay of free and immobilised tyrosinase.....</b>	<b>99</b>
I.2.4.1. Determination of kinetic parameters of free and immobilised tyrosinase.....	99
I.2.4.2. Stability of immobilised tyrosinase.....	100
I.2.5. Mass spectrometry.....	100
<b>I.3. IF/IH-ENALDI MS: results and discussion.....</b>	<b>101</b>
<b>I.3.1. Characterisation of MPs as a non-organic matrix and host for enzyme immobilisation.....</b>	<b>101</b>
I.3.1.1. Structural characterization of MPs.....	101
I.3.1.2. Magnetic nanoparticles as an immobilisation support.....	102
I.3.1.3. Application of EMPs as non-organic matrix.....	104
<b>I.3.4. 'Ion Fading' IF-ENALDI MS and 'Ion Hunting' IH-ENALDI MS - illustration of the experimental approach using standard inhibitors.....</b>	<b>104</b>
I.3.4.1. Experimental design and evaluation of IF-ENALDI MS.....	104
I.3.4.2. Experimental design and evaluation of IH-ENALDI MS.....	107
<b>I.3.5. An application of IF-ENALDI MS to the samples of plant extracts.....</b>	<b>109</b>
<b>I.3.6. The complement of IF-ENALDI MS: identification of inhibitor and substrate candidates by ESI-Qq-TOF MS.....</b>	<b>112</b>
I.3.6.1. Aqueous extract of liquorice roots.....	115
I.3.6.2. Methanol extract of Sparrmannia discolor leaves and stems.....	120
<b>I.4. IF/IH-ENALDI MS – conclusions.....</b>	<b>126</b>
<b>II. The use of enzyme-coupled magnetic particles to study the spectrum of unusual substrates of tyrosinase by direct surface-assisted laser desorption/ionisation and ESI-Qq TOF MS.....</b>	<b>128</b>
<b>II.1. Introduction.....</b>	<b>128</b>
<b>II.2. The rationale for this study.....</b>	<b>131</b>
<b>II.3. ESI-Qq-TOF MS evaluation of tyrosinase-driven oxidation of 2,4-resorcinol-containing tyrosinase inhibitors.....</b>	<b>131</b>



<b>II.4. The experiment design and results</b> .....	132
<b>II.5. Conclusions</b> .....	135
<b>Appendix II: Supplementary Information</b> .....	137
<b>Chapter IV</b> – <i>An application of magnetic nanoparticles for evaluating the substrate specificity of human and viral thymidylate kinase using ESI-Qq TOF MS. Magnetic nanoparticles as non-organic matrix for SALDI-TOF coupled with thin layer chromatography</i>	
<b>I. An application of magnetic nanoparticles for evaluating the substrate specificity of human and viral thymidylate kinase using ESI-Qq TOF MS</b> .....	140
<b>I.1. Introduction</b> .....	140
I.1.1. Multidimensional potential of MPs as the carrier of enzymes.....	141
I.1.2. Nucleotide analogs as antiviral drugs.....	141
I.1.3. The importance of the selectivity of antiviral therapy.....	141
I.1.4. The design of selective antiviral therapy against poxviruses on the basis of the comparative study on substrate spectrum of viral and human TMP kinase (TMPK).....	142
<b>I.2. Materials and methods</b> .....	143
I.2.1 The chemistry of TMPK kinase immobilisation.....	143
I.2.2. The experiment design.....	144
<b>I.3. Experimental part</b> .....	146
I.3.1. Immobilisation of TMPK kinases.....	146
I.3.2. Typical assay of enzymatic activity by ESI-Qq-TOF MS.....	146
<b>I.4. Preliminary results</b> .....	146
I.4.1. Enzymatic activity of TMPK kinase in the context of mass spectrometry.....	146
I.4.2. Comparison of the two pathways of kinase immobilisation using vvTMPK as a model enzyme.....	146
I.4.3. Immobilisation of viral and human TMPK kinase to MPs-APTES-GLA nanoparticles.....	147
<b>I.5. The stability assay of viral/human thymidylate kinases</b> .....	148
<b>I. 6. Prospective applications of kinase-MPs in future experiments</b> .....	149
<b>I.7. General conclusions</b> .....	149
<b>II. Magnetic nanoparticles as non-organic matrix for SALDI-TOF coupled with thin layer chromatography</b> .....	150
II.1. Introduction.....	150
II.2. Experimental part.....	151
II.3. Results.....	151
II.3.1. Direct ionisation of plant metabolites. Comparison to an organic matrix, 9-aminoacridine.....	151
II.3.2. An impact of MPs deposition on separation and visualization of plant metabolites.....	154
<b>II.4. Conclusions</b> .....	157
<b>GENERAL CONCLUSIONS</b> .....	158
<b>The list of chemical products and solvents</b> .....	166
<b>List of Author's scientific papers</b> .....	168
<b>Bibliography</b> .....	172

## List of abbreviations

<b>AA</b> .....	acrylic acid
<b>AEMA</b> .....	2-aminoethyl methacrylate
<b>AIBN</b> .....	2,2'-Azobis(2-methylpropionitrile)
<b>APTES</b> .....	(3-aminopropyl)triethoxysilane
<b>ASM</b> .....	amine-bearing silica monolith
<b>ATP</b> .....	adenosine triphosphate
<b>BSA</b> .....	bovine serum albumin
<b>CID</b> .....	collision-induced dissociation
<b>COSY</b> .....	correlation spectroscopy
<b>DEPT</b> .....	Distortionless Enhancement by Polarization Transfer
<b>DHPA</b> .....	3-(2,4-Dihydroxyphenyl)propionic acid
<b>dTMP</b> .....	Thymidine monophosphate
<b>EGDMA</b> .....	Ethylene glycol dimethacrylate
<b>EIC</b> .....	extracted ion chromatogram
<b>EMPs</b> .....	enzyme-coupled magnetic nanoparticles
<b>ENALDI</b> .....	enzyme-coupled nanoparticles-assisted laser desorption/ionisation
<b>ESI</b> .....	electrospray ionisation
<b>FAC/FA</b> .....	frontal affinity chromatography/frontal analysis
<b>GLA</b> .....	glutaraldehyde; 1,5-pentanedial
<b>GPTMS</b> .....	(3-glycidyloxypropyl)trimethoxysilane
<b>HTS</b> .....	high-throughput screening
<b>L-Arg</b> .....	L-arginine
<b>L-DOPA</b> .....	L-3,4-dihydroxyphenylalanine
<b>L-Glu</b> .....	L-Glutamine
<b>L-Tyr</b> .....	L-tyrosinase
<b>m/z</b> .....	mass to charge ratio
<b>MAA</b> .....	methacrylic acid
<b>MALDI</b> .....	matrix-assisted laser desorption/ionisation
<b>MM</b> .....	monoisotopic mass
<b>MPs</b> .....	magnetic nanoparticles
<b>MPs-APTES-GLA</b> ...	MPs derivatised with APTES and GLA
<b>MPs-oxyGPTMS</b> ...	MPs derivatised with GPTMS subsequently oxidised to aldehyde
<b>MS</b> .....	mass spectrometry
<b>NAS</b> .....	N-acryloxysuccinimide
<b>NMR</b> .....	nuclear magnetic resonance
<b>PEG</b> .....	polyethylene glycol
<b>SALDI</b> .....	surface-assisted laser desorption/ionisation
<b>SBMA</b> .....	[3-(Methacryloylamino)propyl]dimethyl(3-sulfopropyl)ammonium
<b>TEM</b> .....	Transmission electron microscopy
<b>TEOS</b> .....	Tetraethyl orthosilicate
<b>TIC</b> .....	total ion chromatogram (total ion current)
<b>TMPK</b> .....	thymidylate kinase
<b>TMSPA</b> .....	3-(trimethoxysilyl)propyl acrylate
<b>TOF</b> .....	time of flight
<b>TRIS</b> .....	2-Amino-2-hydroxymethyl-propane-1,3-diol
<b>VS</b> .....	virtual screening



## INTRODUCTION GÉNÉRALE

Les végétaux supérieurs tout comme d'autres ressources naturelles constituent une réserve encore fortement inexploitée riche en substances biologiquement actives qui ont trouvées pour certaines des applications dans l'industrie cosmétique et thérapeutique. Aussi, dans le passé, les propriétés thérapeutiques des plantes ont été découvertes par la méthode dite «par tâtonnements ». Ces découvertes recueillies au cours de nombreuses générations ont donné le fondement même des systèmes médicaux traditionnels, en Chine, Inde et Europe par exemple.

Les connaissances en ethnobotanique permettent en premier lieu de cibler des plantes ou parties de plantes qui sont potentiellement intéressantes pour répondre à une approche cosmétique permettant, par exemple, d'estomper les taches brunes de la peau. Il est alors nécessaire de mettre en place et d'optimiser les protocoles d'extraction, de séparations des molécules constitutives des extraits afin d'identifier la ou les molécules actives lors de tests biologiques. Tout cela demande du temps. Aussi, l'industrie exprime le besoin de pouvoir s'appuyer sur des techniques simples, rapides, efficaces et fiables pour tester l'activité des composés issus d'extraits de plantes. Ces tests sont utilisés en « screening », c'est-à-dire qu'ils servent à identifier les molécules en recherchant des activités spécifiques, dans notre cas, une activité vis-à-vis de l'enzyme tyrosinase qui intervient dans le processus de la mélanogénèse.

Ce travail s'inscrit dans la continuité des efforts entrepris depuis de nombreuses années, sur le développement de méthodologies innovantes permettant le criblage primaire de nouvelles molécules bioactives naturelles en milieu complexe (*Chapitre I, p. II*).

Ainsi, ce projet de recherche a été consacré au développement des nouvelles méthodologies en spectrométrie de masse basées sur l'interaction enzyme/inhibiteur afin d'identifier des inhibiteurs d'origine naturelle de l'enzyme tyrosinase. La tyrosinase catalyse notamment la réaction de transformation de la tyrosine en Dopa (dihydroxyphénylalanine) grâce à son activité hydroxylase et la réaction de transformation de la Dopa en dopaquinone grâce à son activité oxydase avec comme finalité métabolique la synthèse des phéomélanines et/ou des eumélanines. Dans des conditions normales, la pigmentation de la peau est uniforme. Toutefois, au cours du temps, une pigmentation excessive peut se manifester localement par des taches de vieillissement (lentigo sénile) due à une sécrétion accrue localisée de mélanine. Les substances dépigmentantes peuvent agir directement sur la vitalité des mélanocytes épidermiques où se déroule la mélanogénèse et/ou interférer avec une des étapes de la biosynthèse de la mélanine. Ces substances dites actives opèrent soit en inhibant une des enzymes (par exemple la tyrosinase) impliquées dans la mélanogénèse, soit en s'intercalant comme analogue structural d'un des composés chimiques de la chaîne de synthèse de la

mélanine, chaîne qui peut alors être bloquée et ainsi assurer la dépigmentation. Ainsi, une molécule est reconnue comme dépigmentante si elle agit directement sur les mélanocytes épidermiques en inhibant l'activité de ces cellules et/ou si elle bloque l'une des étapes de la biosynthèse des mélanines. C'est pourquoi, la recherche d'inhibiteurs de cette enzyme présente un grand intérêt pour l'industrie cosmétique intéressée par l'identification d'agents dépigmentants agissant sur le processus de la mélanogénèse, destiné à lutter contre l'hyperpigmentation cutanée à savoir lorsque la peau présente une hétérogénéité de pigmentation.

Le mémoire présenté s'articulera autour des quatre chapitres suivants :

Dans le premier chapitre, nous présenterons un rapport bibliographique faisant l'état de l'art des différents étapes et approches en liaison avec les techniques de criblage d'inhibiteurs de la tyrosinase qui est dans le cadre de ses travaux la cible biologique choisie. La première partie du chapitre I sera consacrée à la description de sa structure, suivi du mécanisme de son activité et des caractéristiques structurelles de ses inhibiteurs. Puis nous présenterons, dans la deuxième partie de ce chapitre, un descriptif général des méthodes basées sur la spectrométrie de masse dans le cadre d'un criblage de haut débit d'inhibiteur avec un accent particulier apporté aux techniques en spectrométrie de masse spécifiquement utilisées lors de nos études expérimentales. Enfin, la fin du chapitre I traitera des différentes méthodes existantes d'immobilisation des protéines sur support solide, ce qui constitue une part essentielle dans les protocoles analytiques développés au cours de ce projet de recherche.

Le second chapitre sera consacré à la mise en place et l'optimisation de la chromatographie d'affinité frontale (**Frontal Affinity Chromatography, FAC**), utilisée dans le cadre de ses recherches afin d'obtenir le classement des ligands/inhibiteurs présent dans un mélange complexe en fonction de leurs affinités avec la cible biologique tyrosinase. Après une partie théorique sur l'approche analytique par chromatographie d'affinité frontale, le chapitre sera consacré à la conception et l'utilisation de phases monolithiques au sein de capillaires avec pour objectifs de réduire au maximum les interactions non spécifiques indésirables entre les analytes et les dites phases monolithiques.

Le troisième chapitre sera consacré au développement d'une nouvelle méthodologie nommée ENALDI-MS (**Enzyme-coupled Nanoparticles-Assisted Laser Desorption/Ionisation Mass Spectrometry**) basée sur la spectrométrie de masse couplée à la désorption/ionisation laser assistée par matrice constituée d'un support solide enzymes-nanoparticules magnétiques de silice. La pertinence et l'efficacité de cette nouvelle méthodologie, appliquée notamment à deux extraits préparés à partir de racines de Réglisse (*Glycyrrhiza glabra*) et de tiges et feuilles de *Sparrmannia*

discolor, seront discutées dans le cadre du criblage de molécules bioactives effectué selon deux approches à savoir par 'extinction d'ions' (Ion Fading, IF-ENALDI), et par une approche de pré-concentration sélective des inhibiteurs présents dans l'échantillon nommée Ion Hunting, (IH-ENALDI).

Le quatrième chapitre présentera la possibilité d'étendre les applications de notre méthodologie basée sur l'immobilisation d'enzymes sur billes magnétiques de silice. En premier lieu, il sera montré dans ce chapitre la possibilité d'utiliser un tel support, d'une part afin d'évaluer avec une grande précision en masse les produits émanant d'une catalyse enzymatique particulière et d'autre part comme matrice non organique exceptionnelle. La première partie du chapitre IV illustrera le potentiel dans le domaine de criblage basée sur une détection par spectrométrie de masse de l'utilisation des billes magnétiques de silice sur lesquelles a été fixée l'enzyme Thymidylate Kinase (TMPK) de souche humaine ou virale afin de suivre en simultané d'une part la phosphorylation de la thymidine monophosphate en thymidine phosphate et d'autre part la transformation de l'ATP en ADP. La seconde partie du chapitre IV traitera des potentialités de l'utilisation des particules magnétiques de silice vierges en tant que matrice inorganique dans le cadre d'études d'extraits de plantes par Chromatographie en Couche Mince couplée à la spectrométrie de masse.



## GENERAL INTRODUCTION

The plants and other natural products constitute a rich and still unexploited source of bioactive substances that have found numerous applications in both cosmetic and therapeutic industry. In the past times, the therapeutic properties of plants were being discovered by 'trial and error'. These findings collected over many generations gave the foundation of the traditional medicine systems, *e.g.* in China or India.

An information about the presence of a positive, desirable biological effect of given plant (*e.g.* whitening of the skin spots caused by one of hyperpigmentation disorders), although fundamental, is just one small step towards finding a *unique molecule* responsible for this effect. The way from the intact plant to a single biologically active molecule is work- and time-consuming and includes an extraction, multistep separations and numerous biological assays of individual fractions of studied plant extract (the approach called bioassay-guided fractionation). For this reason, the cosmetic and pharmaceutical industries expect faster and more efficient methods of finding the individual biologically active compounds in the masses of plants that are still unexplored and thus far from the commercial application.

This work is devoted to development of the novel mass spectrometry-based methodologies to identify the interactions between tyrosinase enzyme and its prospective inhibitors of natural origin. Tyrosinase is the key enzyme involved in a process of the synthesis of melanin, the natural pigment responsible for the skin coloration. Tyrosinase inhibitors raise a high interest for the cosmetic industry for the reason of their potential application in reducing the visible outcome of hyperpigmentation, manifested in the appearance of undesirable skin spots.

The first chapter constitutes a multidimensional review of the subjects and approaches related with the thematic of the present work. The first part of *Chapter I* is sacrificed to tyrosinase – a biological target of key importance in this research project: *i*) the structure, *ii*) mechanism of its activity and *iii*) the structural characteristics of its inhibitors. The second part of *Chapter I* is devoted to current mass spectrometry-based methods of high-throughput inhibitor screening and the characteristics of MS approaches applied in the experimental part. The last part of *Chapter I* is a review of current methods for protein immobilisation to a solid support which is crucial element of all methodologies developed during this research project.

The second chapter is fully devoted to the work on frontal affinity chromatography (FAC), an approach enabling simultaneous ranking the ligands/inhibitors within the complex mixture according to their affinities to the biological target (enzyme/receptor respectively). If ligands/inhibitors are used separately, FAC allows to determine their binding affinities and the amount of biological target immobilised onto the solid support. In the first part Reader will find a comprehensive review of the theory and types of FAC, the technical solutions crucial for this approach and the range of FAC application in the



context of the optimal stationary phases and the types of biological targets. The second part of the *Chapter II* is devoted to the description of development and evaluation of two hydrophilic capillary-scale polymer-based bioaffinity stationary phases for FAC with minimized undesirable nonspecific interactions between the analyte and the solid immobilisation support. The performance, range of their application and limitations will be compared with the classic solutions in this domain.

The third chapter is fully sacrificed to a novel approach developed in our laboratory – enzyme-coupled nanoparticles-assisted laser desorption ionisation MS (ENALDI MS), compatible with a standard MALDI mass spectrometer. Two variations of ENALDI MS are evaluated as an extension of existing 'Ion Fading MS' (IF-MS), based on on-the-spot binding of inhibitors by enzyme molecules and 'Ion Hunting MS' (IH-MS), based on selective pre-concentration of inhibitors present in the sample. The potential of IF-ENALDI MS (modified IF-MS) will be illustrated using two plant extracts: liquorice roots and *Sparrmannia discolor* stems and leaves. Enzyme-coupled magnetic nanoparticles (EMPs) will be shown to constitute an effective non-organic matrix enabling ionisation of low-mass molecules compatible with classic MALDI-TOF apparatus without any interferences in the low-mass range.

The second part of the *Chapter III* concerns the discovery of a novel group of tyrosinase substrates using tyrosinase-coupled magnetic nanoparticles. These compounds, such as glabridin or 3-(2,4-dihydroxyphenyl)propanoic acid, contain 1,3-resorcinol moiety and are considered as strong inhibitors of tyrosinase. They are shown to be oxidised to corresponding *o*-quinones in the presence of the classic tyrosinase substrates.

The fourth chapter shows the range of magnetic nanoparticles (MPs) applications other than those described in *Chapter III: i)* as a useful enzyme host dedicated for well-controlled experiments 'in solution' requiring high mass precision and *ii)* as an outstanding non-organic matrix. The first part of the *Chapter IV* concerns an evaluation of the substrate spectrum of thymidylate kinases (TMPK) of vaccinia virus and human origin, the biological targets of a high therapeutic interest. TMPK catalyses a phosphorylation of thymidine monophosphate to thymidine diphosphate with simultaneous dephosphorylation of ATP to ADP. The two types of EMPs hosting viral and human TMPK applied in parallel constitute a promising tool for evaluation of a selectivity of the antiviral drug candidates towards viral components of DNA replication system.

The final part of the *Chapter IV* reports the study on the coupling of blank MPs (without derivatisation of the silica surface) with a standard silica TLC plate as a ready-to-use base for direct ionisation of plant extract constituents after their separation.

In the final part of present manuscript the conclusions of this work and prospects for the future will be discussed.

# **CHAPTER I**

## **Introduction**



***Preface***

Tyrosinase was selected as the major biological target for the reason of an important role of its inhibitors in the cosmetic industry due to their skin-whitening properties. These compounds were successfully applied for the treatment of skin hyperpigmentation having a negative esthetical impact (**p. 1.1**). The screening approaches described in present work were partially applied to the real samples of plant extracts provided by Ethnobotany Innovation Department of LVMH Recherche – a division of LVMH Group – responsible for development of perfumes and cosmetics based on plant extracts. The Laboratory of Analytical Sciences of the Institute of Organic and Analytical Chemistry at the University of Orleans, in which the present work was conducted, maintains cooperative relations with the cosmetic industry, in particular, the companies united within the confines of the Cosmetic Valley – the world's leading cosmetics network.

### 1.1. Skin hyperpigmentation: a general outlook

Skin hyperpigmentation disorders are manifested in darkening of the skin pigmentation yielding a negative esthetical impact. Hyperpigmentation belongs to one of the most frequent diagnoses among dermatology patients in the USA [1]. The most common pigmentation disorders include melasma and solar lentigines and may be exacerbated by skin exposure to UV radiation [1].

Melanin is responsible for the coloration of widespread group of living organisms, including human's skin and hair. Melanin is produced in melanosomes, the organelles within melanocytes, the cells located in the epidermal layer of the skin (**fig. 1**) [1].

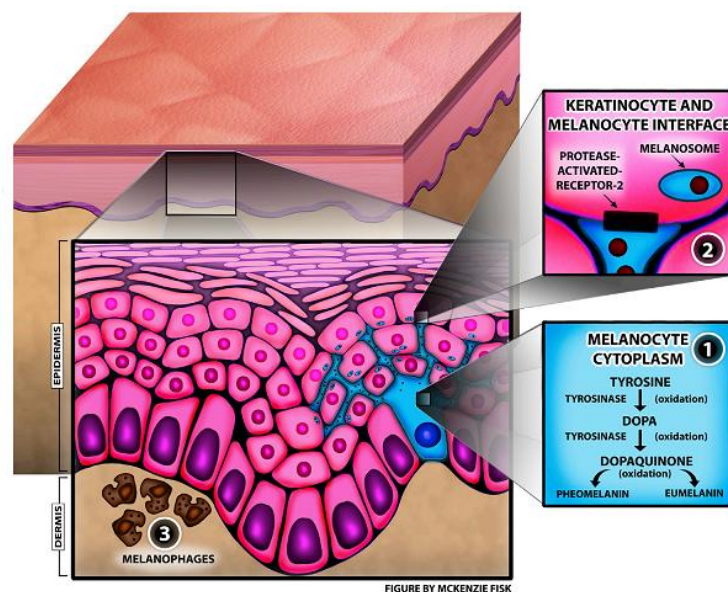


**Figure 1.** Simplified schema of melanin diffusion within skin dermis and epidermis. Illustration reprinted from the reference [1].

Melanin-filled melanosomes are then transferred to keratinocytes and are responsible for epidermal pigmentation [1, 2]. Melanins may also be found within dermis – the skin layer located below epidermis, as well as inside of macrophages (melanophages) that have the capability of melanin phagocytosis (**fig. 1**). The pathogenic mechanism of hyperpigmentation is usually related with *i*) an increased synthesis of melanin precursors by tyrosinase enzyme [1, 3]; *ii*) an increased transfer of melanin-containing melanosomes from melanocytes to keratinocytes [1, 4]; *iii*) according to Fisk *et al.* the presence of melanophages in dermis resulting in a hyperpigmentation resulting in a blue hyperpigmentation [1].

Tyrosinase is the main enzyme in the melanin biosynthetic pathway and is responsible for the oxygen-dependent conversion of L-tyrosine to L-dopaquinone (L-DOPA), the precursor of all types of melanins\* [5-7]. Tyrosinase-related abnormalities contribute to certain types of hyperpigmentation

\* Reader will find more details in **p. 1.2.1** of the present chapter, page 6.

disorders, *e.g.* Yamada *et al.* reported significantly increased tyrosinase expression (by 70%) in epidermal melanocytes within the area of solar lentigines, the common hyperpigmentation disorder [8]. Tyrosinase is the main target of anti-hyperpigmentation therapies involving topical application of certain tyrosinase inhibitors [9, 10]. This way of hyperpigmentation treatment is focused on the *causes* of increased melanin concentration and is less invasive for the patients than the treatment of the symptoms of the *presence* of melanin, *e.g.* thermal damage of melanin by laser or chemical peels leading to removal of this pigment from the skin.

### ***1.2. Tyrosinase - the main enzyme responsible for skin pigmentation***

Tyrosinase (EC 1.14.18.1) is a member of the type 3 copper protein family and catalyses an oxygen-based oxidation of monophenols and *o*-diphenols to corresponding *o*-quinones [11-14]. An active site of tyrosinase is composed of two copper atoms, each of which is chelated with three histidine residues [11-15]. This architecture of the active site is a characteristic feature for all copper proteins belonging to type 3 family, *e.g.* catechol oxidases of plant origin (EC 1.10.3.1) capable of oxidizing diphenols to corresponding *o*-quinones but not monophenols. In mammals, tyrosinase is a membrane glycoprotein accompanied with two additional tyrosinase-related proteins showing significant homology to tyrosinase [12].

Mushroom tyrosinase is routinely used for assessment of the inhibitory properties of tyrosinase inhibitors [16-24]. Crystallographic studies of mushroom tyrosinase published in 2011 (PDB accession code: 2y9w) revealed that the enzyme forms **H<sub>2</sub>L<sub>2</sub>** tetramers (**HL** structure was depicted in **fig. 2**) [15]. A copper-containing active site, responsible for catalytic activity of enzyme, is located in H subunit while L subunit shows high structural homology to lectin-like proteins [15]. The function of L subunit is unknown and it does not influence significantly the catalytic activity of H subunit. Each of two copper atoms located in the enzyme's active site is coordinated by three histidine residues.

Tyrosinase enzymes have very low substrate specificity and can accept numerous mono- and *o*-diphenols as substrates [25-28].

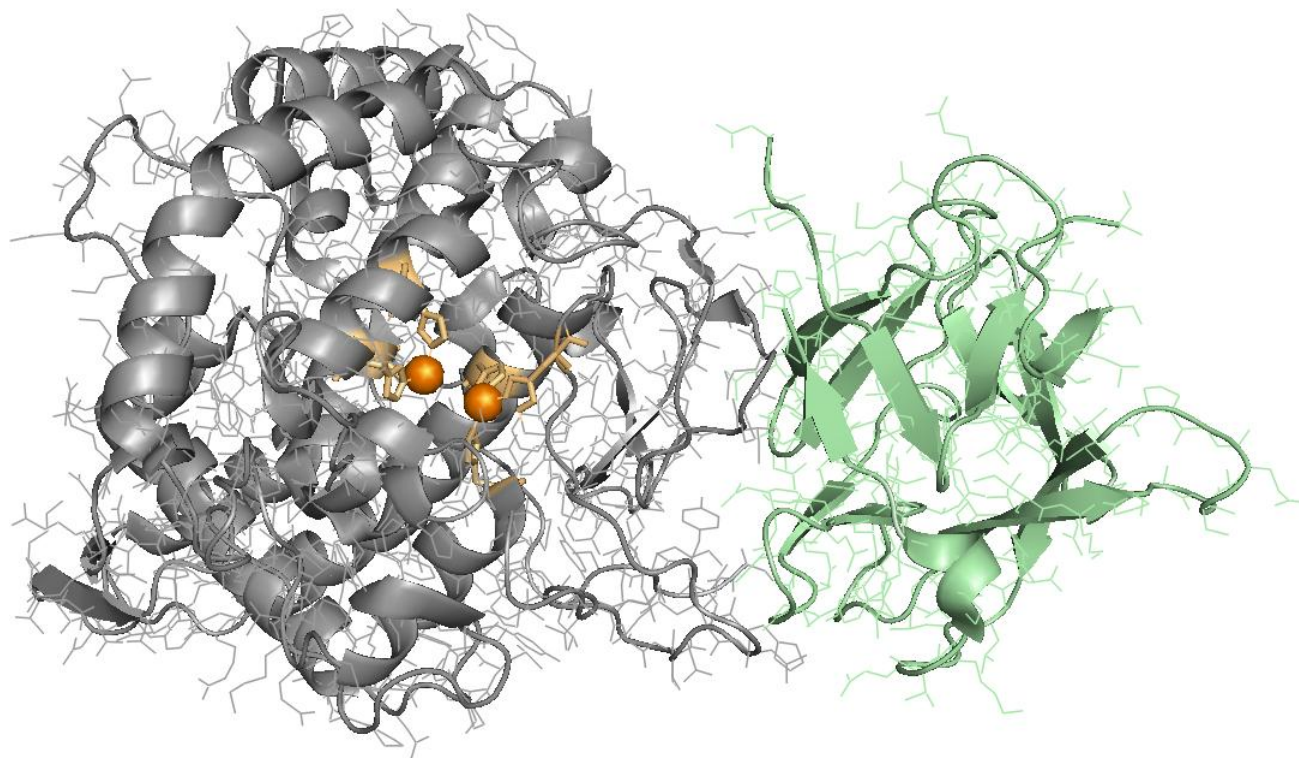
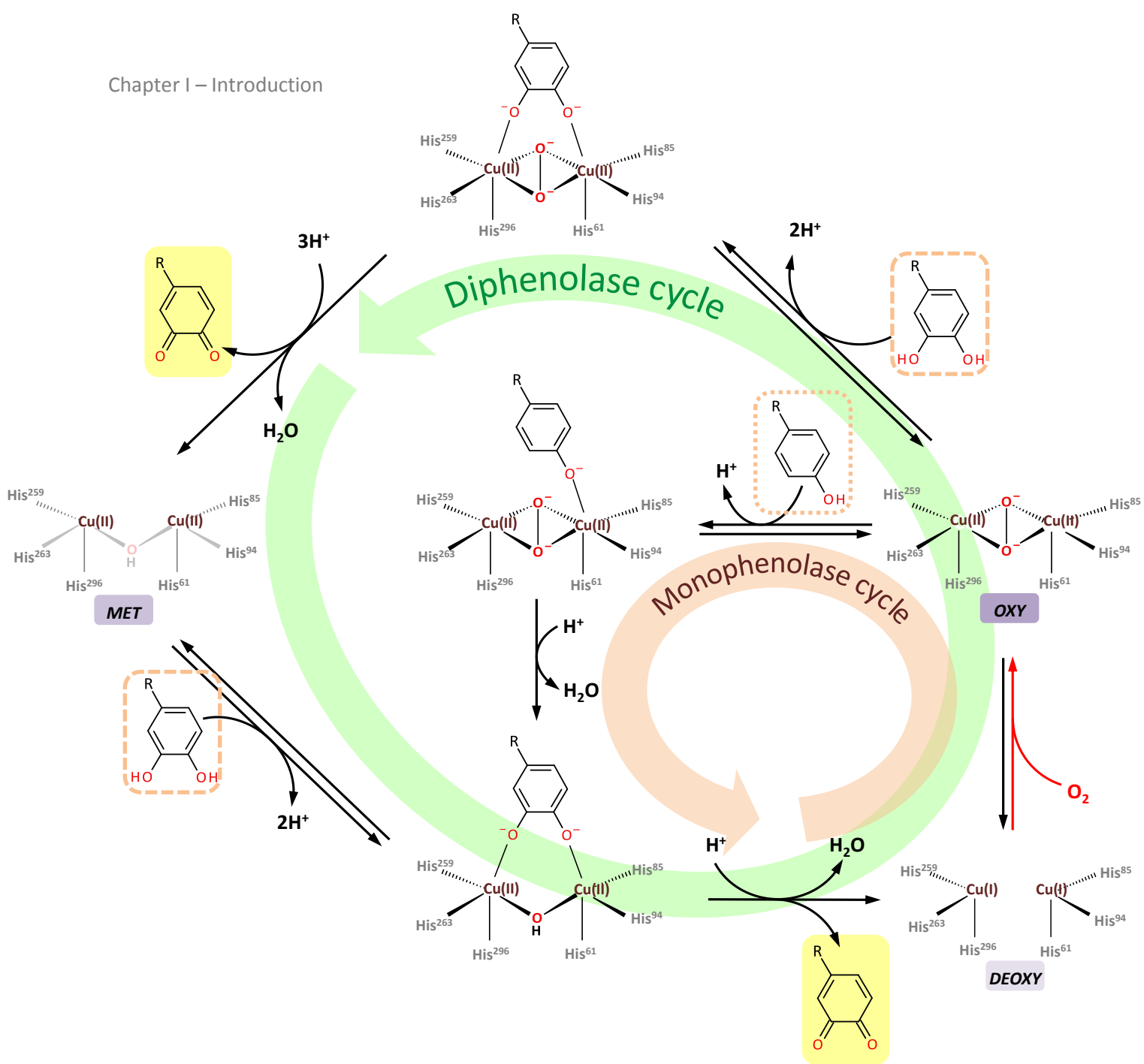
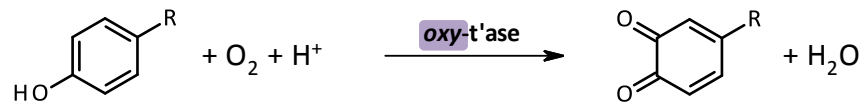


**Figure 2.** The structure of mushroom tyrosinase (PDB accession code: 2y9w [15]). Catalytic subunit was marked in gray, while lectin-like non-catalytic subunit in pale green. Copper atoms in the active site of tyrosinase were visualised as orange spheres and histidine residues chelating these copper atoms were marked in pale orange. This figure was generated using PyMOL (<http://www.pymol.org/>).

During the catalytic cycle, the active site of tyrosinase may be present in three alternative forms: *met-*, *deoxy-* and *oxy-* (*met-*, *deoxy-* and *oxy-t'*ase respectively). Only reduced *deoxy-t'*ase is capable of binding a molecule of dioxygen, indispensable in a process of tyrosinase-catalyzed phenol oxidation (**fig. 3**). Oxygen is embedded into *oxy-t'*ase copper-containing site that can accept both *p*-monophenols and *o*-diphenols as substrates [14]. The full process of hydroxylation of monophenols and their subsequent oxidation to *o*-quinones (**fig. 3**, *monophenolase cycle*) results in the reduction of enzyme's active site to *deoxy-* form and the consumption of one dioxygen molecule. The oxidation of *o*-diphenol-type substrates to corresponding *o*-quinones may be conducted by both oxygenated *oxy-t'*ase or oxidised *met-t'*ase (**fig. 3**, *diphenolase cycle*) [14, 26, 29]. The completion of a single cycle of the 'regeneration' of enzyme's active site to oxygenated *oxy-* form results in the oxidation of two molecules of *o*-diphenol.



**Monophenolase activity**



**Diphenolase activity**

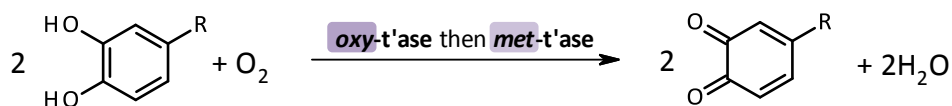


**Figure 3.** An outlook of the pathways of mono- and diphenol conversion to corresponding o-quinones catalyzed by tyrosinase. A single dioxygen molecule is sufficient for oxidation of one monophenol or two diphenol molecules to corresponding quinones [7, 29].



## 1.2.1. The pathway of melanin biosynthesis – enzymatic conversion of L-Tyr and L-DOPA

If L-tyrosine or its *o*-hydroxylated form – L-DOPA – are used as the substrates, resulting L-dopaquinone undergoes non-enzymatic intermolecular cyclisation to L-dopachrome, which in turn polymerizes to black eumelanin pigments (**fig. 4**) [6, 7]. If L-Tyr is the only substrate, L-DOPA is formed in a process of spontaneous, non-enzymatic reaction of L-dopaquinone and leukodopachrome and undergoes further oxidation. In case of elevated level of cysteine (>1  $\mu\text{M}$ ), the melanin biosynthesis pathway is partially diverted towards red pheomelanins (**fig. 4**) [5].

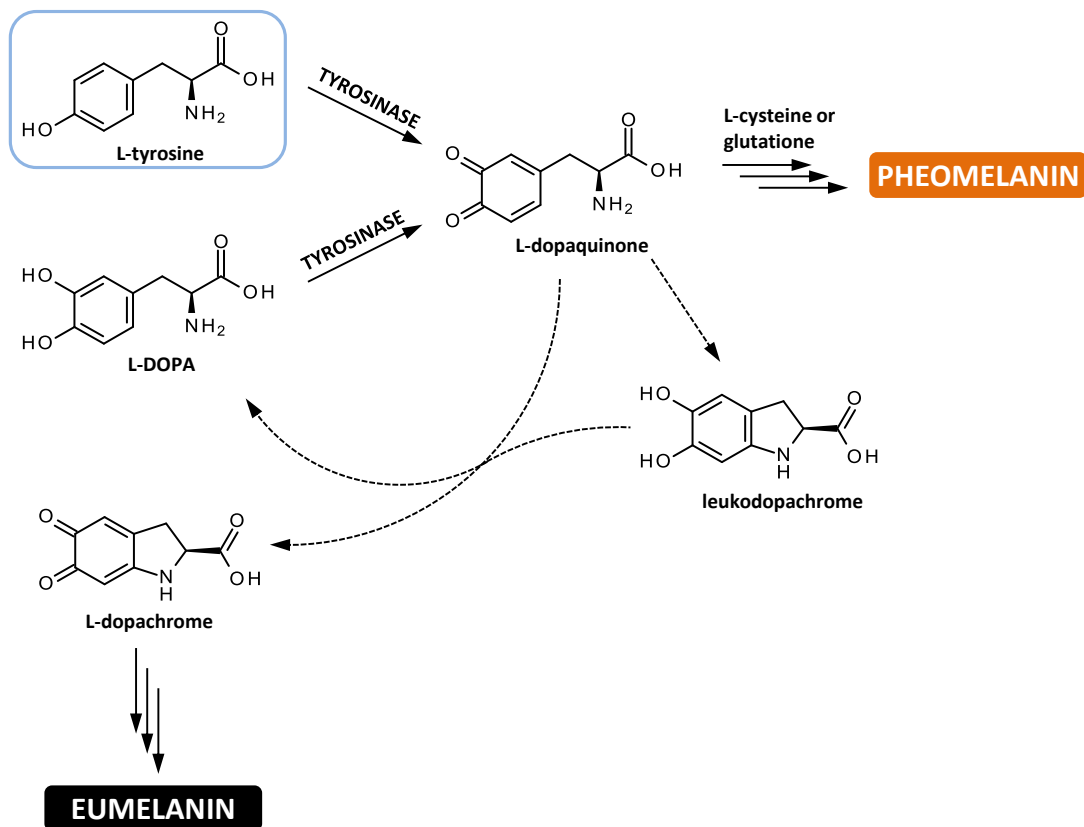


**Figure 4.** The pathway of melanin biosynthesis starting from L-tyrosine [5-7]. Dotted lines represent spontaneous, non-enzymatic processes.

## 1.2.2. General introduction to enzyme kinetics and types of enzymatic inhibition

The kinetics of enzymatic conversion of given substrate is classically described using two basic parameters, directly available from an experiment: maximum conversion rate,  $V_{max}$ , and Michaelis–Menten constant,  $K_M$  [29].  $V_{max}$  is the parameter describing the maximal rate of diminution of substrate's concentration or growth of the product concentration in a specified time unit and can be expressed in *e.g.* ( $\mu\text{M/s}$ ). In certain cases it is more convenient to use maximum *specific* activity ( $SA_{max}$ ) that is maximum conversion rate of given substrate per mass unit of enzyme, *e.g.* ( $\mu\text{mol/min/s}$ ) [30]. This expression of enzymatic activity is particularly convenient for the comparison of an impact of enzyme immobilisation (*Chapter III*). The classic model of enzymatic kinetics was proposed by L. Michaelis and M. Menten in 1913 and is based on the assumption that the process of enzyme (E)–substrate (S) association is reversible and conversion of substrate to product (P) irreversible [31, 32]:



and may be expressed using the **equation 1**:

$$SA = \frac{SA_{max}[S]}{[S] + K_M} \quad \text{or} \quad V = \frac{V_{max}[S]}{[S] + K_M} \quad (1)$$

where:  $[S]$  - substrate concentration,  $V/SA$  - an initial conversion rate/specific activity rate for the given substrate concentration  $[S]$  respectively.

$SA_{max}$  ( $V_{max}$ ) and  $K_M$  values may be obtained by fitting several experimental points for various substrate concentrations, ( $[S_i]$ ,  $V_i$ ), with Michaelis–Menten model described by the **equation 1** using non-linear regression.

As one may conclude from the **equation 1**,  $K_M$  constant represents the substrate's concentration for which the initial enzymatic conversion rate is equal to  $\frac{1}{2}V_{max}$ . If product formation is the rate-limiting step during the overall enzymatic reaction,  $K_M$  is the same as the dissociation constant ( $K_d$ ) of enzyme–substrate complex (ES) [33]. In other words, the higher  $K_M$ , the lower affinity constant of given substrate to enzyme's active site.

Enzymatic inhibitors are classified into two main groups: reversible (competitive, non-competitive, uncompetitive and mixed-type) and irreversible leading to enzyme inactivation [34]. The competitive inhibitors bind to unoccupied enzymes' active sites and thus alter the formation of ES complexes, but cannot bind to the ES. The competition of the substrate and inhibitor for an access to the active site decreases an apparent affinity of this substrate to the enzyme molecule. It leads to an increase of the  $K_M$  for the substrate in the presence of the competitive inhibitor. Simultaneously,  $V_{max}$  remains unchanged since the phenomenon of competition between substrate and inhibitor may be surpassed when the substrate's concentrations dramatically exceeds the concentration of the inhibitor (**fig. 5**).

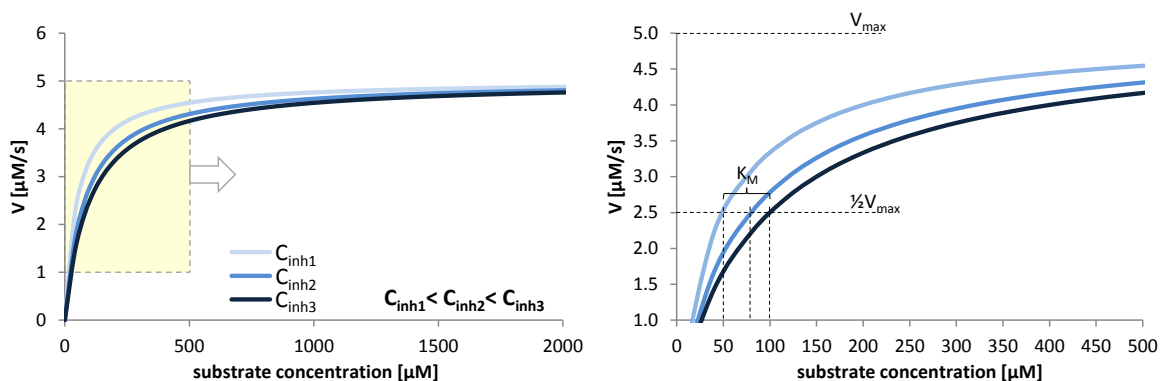


**Figure 5.** An impact of the **competitive** inhibitor on the kinetic curves of enzymatic activity. In all three cases the  $V_{max}$  value remains unchanged.

The non-competitive inhibitors have the same affinity to free enzyme (E) and to enzyme-substrate complex (ES). In other words, non-competitive inhibitors bind to the enzyme without blocking substrate's access to enzyme's active site. For this reason, this type of inhibitor does not affect the  $K_M$  constant, but alters catalytic properties of enzyme leading to decrease of its apparent  $V_{max}$  (fig. 6).

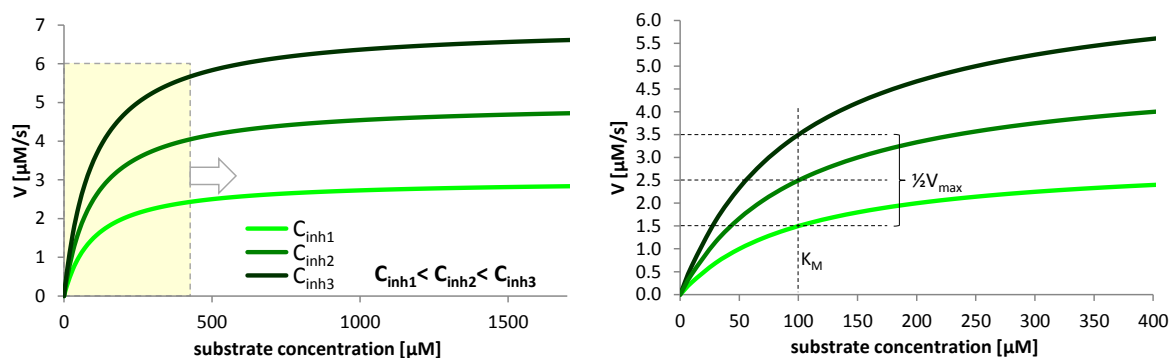


**Figure 6.** An impact of the **non-competitive** inhibitor on the kinetic curves of enzymatic activity. In all three cases the  $K_M$  value remains unchanged.

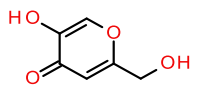
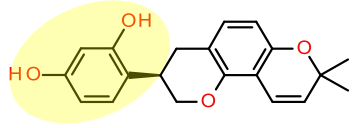
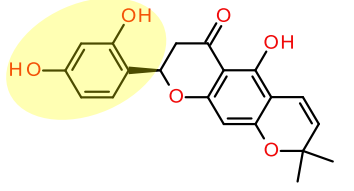
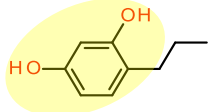
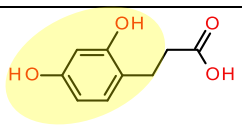
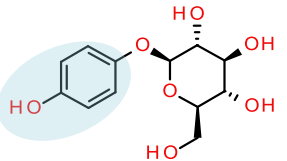
Mixed-type inhibitor binds to both E and ES partially blocking an access of substrate to enzyme's active site. It leads to increase of  $K_M$  value and decrease of  $V_{max}$  value. Uncompetitive inhibitors can bind only to ES complexes [34].

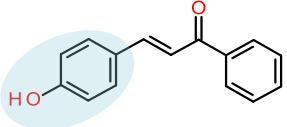
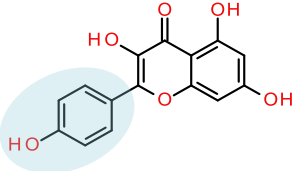
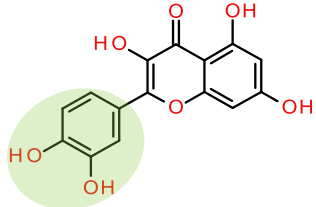
#### 1.2.2.1. An outlook of tyrosinase inhibitors

Numerous analogues of mono- or diphenols were identified as tyrosinase inhibitors, *e.g.* arbutin or quercetin respectively (table 1, entries 6 and 9 respectively). These compounds constitute the competitive inhibitors and bind to tyrosinase active site by mimicking enzyme's natural substrates (L-tyrosine, monophenol and L-DOPA, diphenol, fig. 4). Compounds possessing 2,4-substituted resorcinol moiety constitute the group of the strongest tyrosinase inhibitors, *e.g.* glabridin, described by Yokota *et*

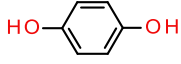
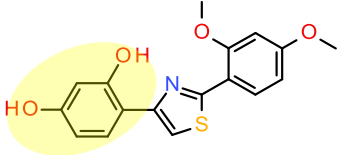
*al.* in 1998 as one of the strongest tyrosinase inhibitor. For this reason, resorcinol moiety is usually incorporated into newly designed synthetic tyrosinase inhibitors (**table 1**, entries **11-14**).

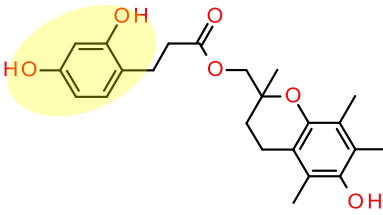
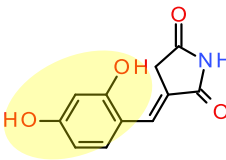
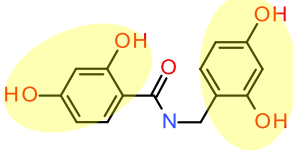
**Table 1.** The list of selected tyrosinase inhibitors of plant and synthetic origin. Enzymatic activity measured using monophenol (MA) or diphenol (DA) substrate. 2,4-substituted resorcinol moieties were marked in yellow, monophenol in blue and diphenol in green.

Naturally occurring tyrosinase inhibitors					
	Name	Inhibition type	Chemical structure	Organism of origin	Ref.
1	Kojic acid	competitive (MA); mixed-type (DA)  copper chelator		Fungi <i>Aspergillus oryzae</i> [35]	[7, 36]
2	Glabridin	noncompetitive (DA)		<i>Glycyrrhiza glabra</i> L.	[37, 38]
3	Dalenin	mixed-type (DA)		<i>Dalea elegans</i>	[16]
4	4-Propylresorcinol	competitive		<i>Artocarpus incisus</i>	[24, 39]
5	3-(2,4-Dihydroxyphenyl)propanoic acid, DHPA	competitive		The fig leaves and fruits	[23]
6	Arbutin	competitive		<i>Myrothamnus flabellifolia</i> [40]	[36]

	<b>Name</b>	<b>Inhibition type</b>	<b>Chemical structure</b>	<b>Organism of origin</b>	<b>Ref.</b>
7	4-Hydroxychalcone				[41]
8	Kaempferol	competitive (DA)		Lotus leaves, persian walnut, quinoa, green tea, <i>Maytenus aquifolium</i> and <i>Maytenus ilicifolia</i> leaves, oregano	[7, 42]
9	Quercetin	competitive (DA)		Green tea, <i>Maytenus aquifolium</i> and <i>Maytenus ilicifolia</i> leaves, lotus leaves, propolis, green tea, oregano, quinoa, apricot fruit, burdock leaves, cocoa, apple	[7]

#### Synthetic tyrosinase inhibitors

	<b>Name</b>	<b>Inhibition type</b>	<b>Chemical structure</b>	<b>Ref.</b>
10	Hydroquinone	The mechanism is not clear		[43, 44]
11	Bis-resorcinol-substituted thiazole	NA		[45]

	Name	Inhibition type	Chemical structure	Ref.
12	6''-hydroxy-2'',5'',7'',8''-tetramethylchroman-2''-yl)methyl 3-(2',4'-dihydroxy-phenyl)propionate	competitive (DA)		[46]
13	(E)-3-(2,4-dihydroxybenzylidene)pyrrolidine-2,5-dione	noncompetitive (MA)		[47]
14	N-Benzylbenzamide family	competitive (DA)		[21]

Resorcinol-containing compounds do not have well defined mechanism of tyrosinase inhibition. Some of them compete with the substrate for entering to the active site, *e.g.* 4-propylresorcinol or 3-(2,4-dihydroxyphenyl)propanoic acid (**table 1**, entries **4** and **5**), other molecules were shown to inhibit tyrosinase in the non-competitive way (*e.g.* glabridin, entry **2**) or showed mixed-type inhibition (*e.g.* dalenin, entry **2**). Further details and a discussion about the nature of resorcinol-containing inhibitors Reader may find in the *Chapter III, p. II.1* (page 128).



## **II. High-throughput screening as a tool for finding biologically active substances**

All cellular processes are based on specific interactions between biomolecules (*e.g.* DNA, RNA, proteins: enzymes, receptors) or biomolecules and small-molecule ligands (*e.g.* neurotransmitters and receptors, enzymes and substrates, *etc.*). Numerous biomolecules are targeted by small-molecule drugs. Their therapeutic effect is strictly related with the nature and role of biological target, *e.g.* inhibitor molecules are used for blocking disease-related enzymes (*e.g.* imatinib as the inhibitor of hybrid tyrosine kinase BCR-ABL for the treatment of chronic myeloid leukemia [48]); antagonist or reverse agonist molecules block disease-related signal transduction by interacting with appropriate receptors (*e.g.* fexofenadine as H<sub>1</sub>-receptor antagonist for the treatment of seasonal allergic rhinitis [49]). As of December 2006, the total number of 248 biological targets of small-molecule drugs were defined for FDA-approved drugs, including 207 targets of human origin (encoded by human genome). Over the past twenty years, an average number of newly introduced biological targets oscillates around 5.3 per year [50]. Simultaneously, new improved drugs towards already known targets are being introduced to the market every year.

The process of defining novel bioactive molecules interacting with disease-related biological target is based on experimental screening of the libraries of existing molecules (so called 'chemical space') that may be assisted by virtual screening (VS), an *in silico* complement of the classic high-throughput screening. VS helps to reduce the chemical space requiring biological evaluation. It may be realized either by high-throughput docking of candidate molecules to the biological target (if the structure of target's active site is known) or by computing the properties of pharmacophore – the set of steric and electronic features of a molecule required to ensure an appropriate interaction with the biological target of interest [50-52]. Desired biological activity of the set of compounds that were designed or pointed-out in a process of VS or selected manually in a form of appropriate library have to be evaluated experimentally. A systematic approach usually starts at *in vitro* verification if the candidate molecules interact with biological target. This step, involving purified biological targets, requires an efficient analytical method [53, 54]. The 'hits' of initial *in vitro* screening are subjected to cell-based assay of desired biological activity and toxicity [53].

Numerous modern screening approaches are based on mass spectrometry, for the reason of a multidimensional character of this method. While studying complex mixtures, the most pronounced advantage of mass spectrometry is the possibility of observation of many compounds simultaneously, thus avoiding (in many cases) the need of incorporation of the time-consuming separation steps into the experimental workflow. MS-based screening may be divided into two basic groups (**fig. 7**): *i*) approaches based on detecting the presence of specific affinity of the inhibitor to the active or allosteric sites of target enzyme or *ii*) methods based on monitoring the impact of individual inhibitor candidates or mixtures of interest on the enzymatic activity [55].

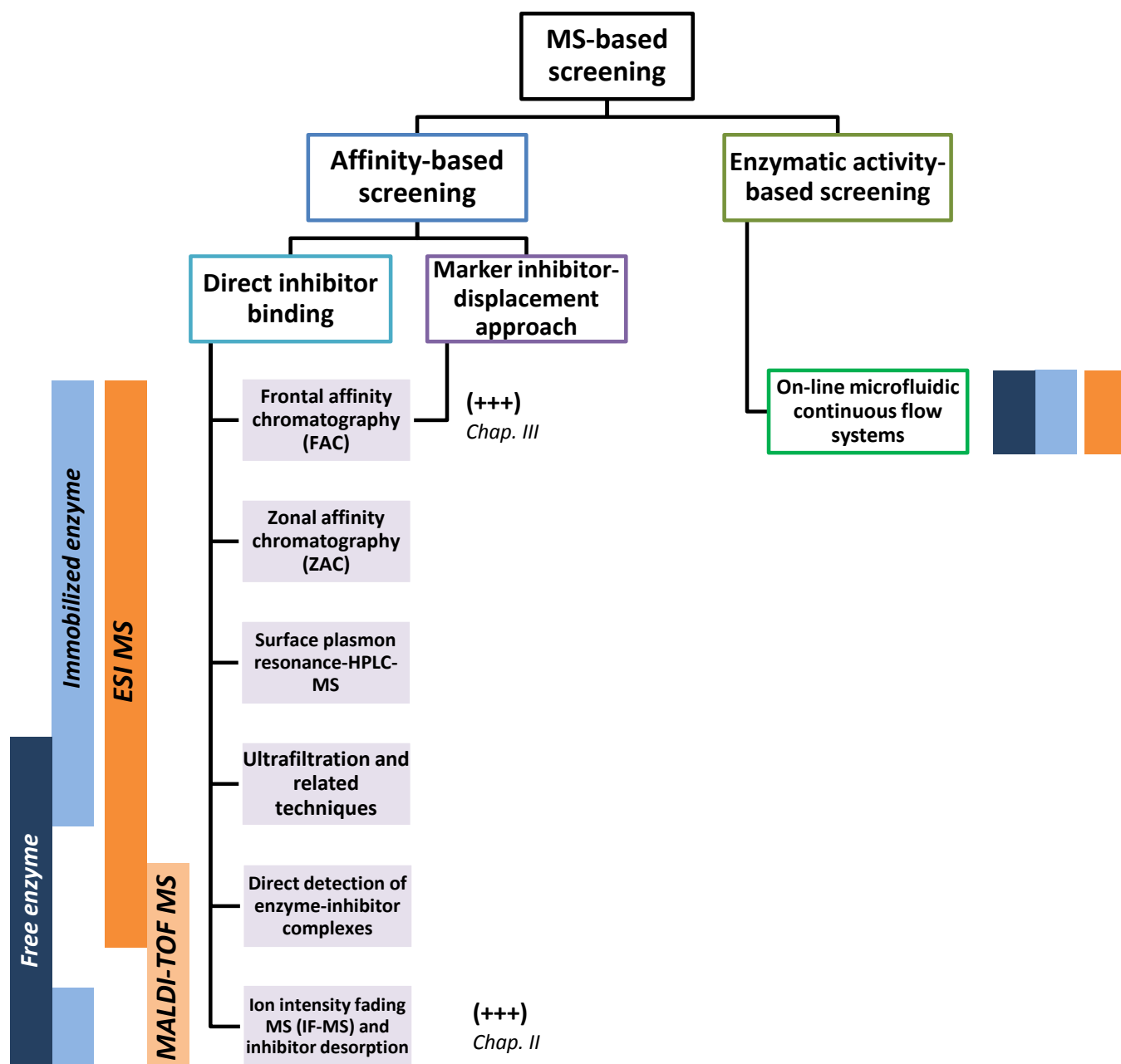


**Figure 7.** The leading MS-based methods for screening of enzyme-inhibitor complexes. Methods marked with (+) sign were of key interest during the research program described in this manuscript.

## II.1. Affinity-based screening

Affinity-based methods help to select inhibitor candidates from complex mixtures (such as plant extracts of drug libraries) on the basis of the assumption that if given compound strongly interacts with the target enzyme, there is a high probability that it will induce a biological effect by affecting its activity. Inhibitory properties of the 'hits' indicated by means of the methods from this group always have to be confirmed using the classic enzymatic assays. The biggest advantage of affinity-based approaches is that they do not

require any marker of the enzymatic activity and thus, once developed, may be usually extended to other types of proteic targets, *e.g.* antibodies, receptors or structural proteins. Affinity-based methods may be realized using both immobilised or free protein.

### ***Affinity-based methods utilizing immobilised proteins***

#### *11.1.1. Affinity chromatography*

Affinity chromatography (AC) in various varieties (*e.g.* frontal or zonal AC) is based on an application of a stationary phase covered with immobilised biological target that selectively retains interacting compound inside the chromatographic column. The simplest form of AC is the zonal affinity chromatography (ZAC) [53, 56-59] which involves injecting a small amount of studied mixture (*e.g.* library of drug candidates) followed by monitoring of the retention factors ( $k$ ) of all components present in the mixture (**fig. 8**). The stronger ligand-target interaction, the higher  $k$  value of this ligand is (**fig. 8-B**) [59]. Non-interacting compounds are eluted from the column in the first order. This approach was successfully applied for studying interactions between prednisolone and corticosteroid-binding globulin [60].

In a presence of a known marker ligand having an affinity to the same binding site as the studied compounds, retention factors of interacting analyte molecules will be reduced proportionally to the concentration of the marker [61]. This effect may be used to shorten long retention times of strongly interacting compounds if isocratic elution mode is applied. If no competitor is introduced in the experiment, an additional elution step is required to dissociate bound analyte (*e.g.* by changing pH or increasing an organic content of the mobile phase) [57]. Affinity chromatography may also be used to determine which enantiomer of given bioactive compound preferentially binds to the biological target [56].

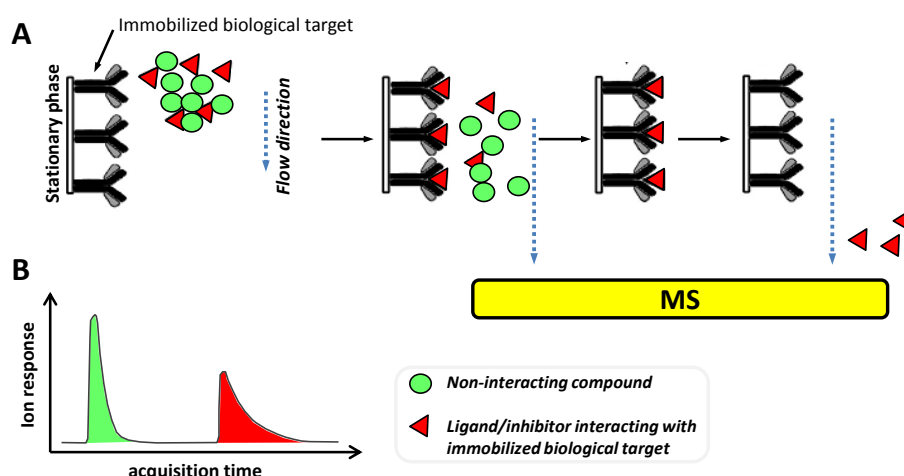


**Figure 8.** The schema of zonal affinity chromatography involving a single injection of the studied mixture (A) and exemplary chromatogram obtained for the mixture containing a non-interacting compound (green) and a specific ligand of immobilised biological target, assuming that there are no non-specific interactions between these both types of compounds and the solid support of the biological target.

Affinity chromatography applied as a screening tool was phased out by frontal affinity chromatography (FAC) which provides more data per analysis, *e.g.* step-gradient FAC provides dissociation constant ( $K_d$ ) and the amount of immobilised proteic target ( $B_t$ ) on the column within a single run [62]. The main difference in terms of the experimental design between FAC and ZAC is the way of sample supply to the column with immobilised biological target: in FAC it is continuously infused through the column. The most pronounced advantage of FAC over ZAC is the presence of the uniform analyte concentration in the entire column and thus full dynamic equilibrium between bound and solubilised fraction of interacting analyte. It allows to precisely determine  $K_d$  and  $B_t$  values by applying a simple equilibrium law. FAC was one of the main tools applied during the course of the research project described in present manuscript and was described in details in the *Chapter II*.

### II.1.2. Surface plasmon resonance coupled with HPLC/MS

Surface plasmon resonance (SPR), if used for screening small-molecule ligands, is based on an optical biosensor with superficially immobilised biological target. The optical sensor is deposited within a flow cell coupled with analyte-sensitive detector. If a plug of studied solution passing over the surface of the optical sensor contains ligand or inhibitor which binds the biological target, refractive index of the optical sensor changes in a way approximately proportional to a mass of bound compound [63]. SPR curve (**fig. 9-A**) shows the kinetics of ligand association to (**a**) and its dissociation from (**b**) immobilised target. For a series of experiments using several concentrations of pure ligand or inhibitor of interest it is possible to determine related association and dissociation constants ( $K_a$  and  $K_d$  respectively) [63, 64].

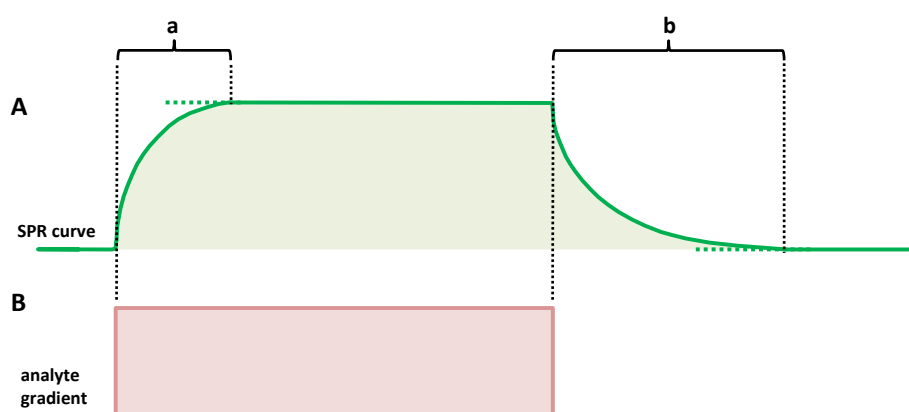


**Figure 9.** Typical SPR curve (**A**) and the profile of analyte gradient (**B**). The size of association (**a**) and dissociation (**b**) zones on SPR curve are determined by ligand-target binding kinetics.

SPR belongs to the group of non-selective screening methods and alone can only give a simple 'yes/no' answer concerning the presence of target's binding partner(s) in studied mixture. To address this issue, Zhang *et al.* developed an automated interface coupling SPR with HPLC (**fig. 4-A**) for identification of *Astragalus membranaceus* metabolites interacting with human serum albumin [65].

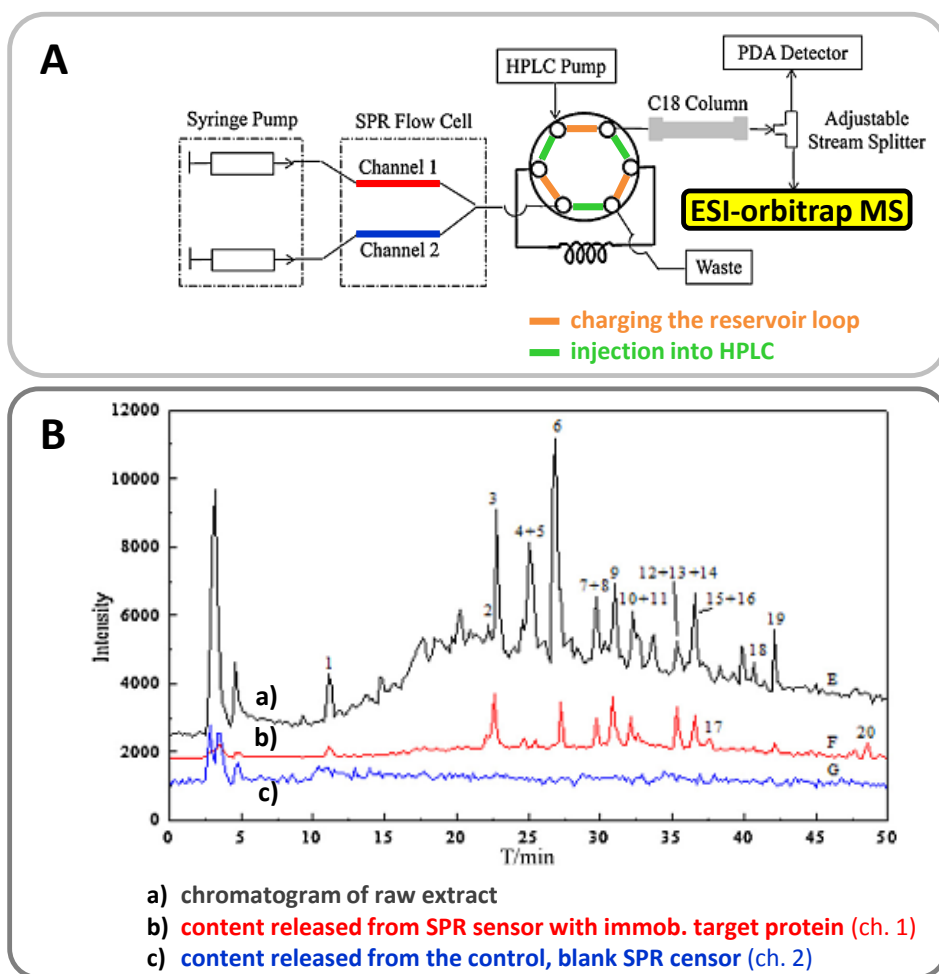


**Figure 10.** The layout of the interface coupling SPR and HPLC-MS/MS using six-port valve (A) and an exemplary outcome of the analysis of *Astragalus membranaceus* roots extract and using human serum albumin as biological target (B). Peaks on the chromatogram (b) represent compounds having an affinity to target protein (adapted from [65]).

The experimental system is composed of two SPR channels: one containing native target protein and the second, control channel without immobilised protein. This dual flow cell gives 'yes/no' answer if given extract fraction contains any binding partner for the studied proteic target. In case of a positive SPR response, associated ligands (fig. 9-A, zone b) are eluted from the SPR sensor directly to a sample loop (fig. 10-A). Thanks to the six-port valve, the loop content is then injected to HPLC-MS/MS system. On the basis of the comparison of the chromatograms of the mixtures released from *i*) protein-bound and *ii*) blank SPR cells, one can conclude which compounds within the extract were bound to the proteic target (fig. 10-B, chromatograms b and c). The procedure includes a negative control in a form of blank SPR sensor cell to eliminate the risk of 'false-positive' hits caused by possible non-specific interactions of extract components with blank, unoccupied sensor.

**Affinity-based methods utilizing free proteins***II.1.3. Ultrafiltration and related techniques*

Ultrafiltration technique is based on an application of free biological target trapped within the confines of a flow cell or reaction compartment with molecular weight cutoff membrane [53, 55, 61, 66, 67]. The classic experiment involves the following steps: *i)* infusion of studied mixture into the cell with entrapped free target protein; *ii)* incubation; *iv)* removal of unbound compound through weight cutoff membrane; *v)* dissociation of ligand-target protein complexes using disruption buffer; *vi)* detection and identification of the compounds released from the target protein.

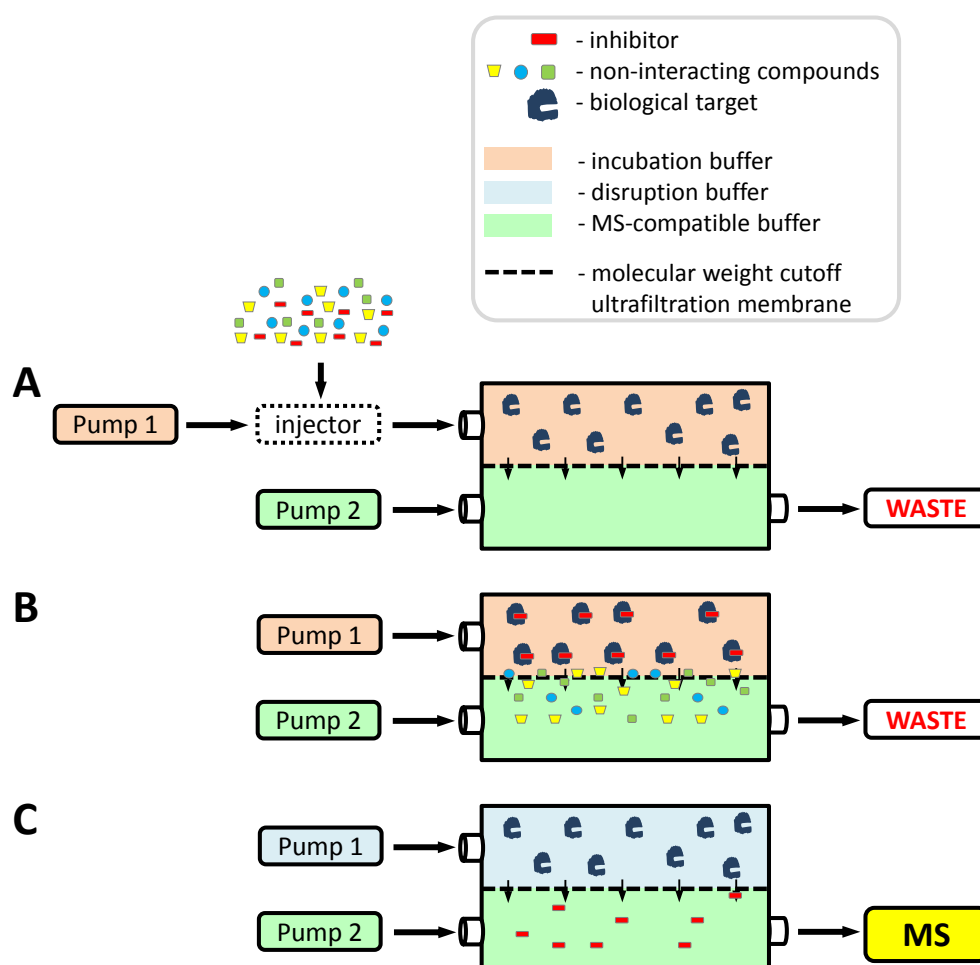


**Figure 11.** The layout of a classic automated pulsed ultrafiltration experiment: binding (A); wash-out unbound analyte (B); disruption of ligand-protein interaction and liberation of initially bound ligands and their subsequent analysis (C). This illustration was based on [61].

Richard B. van Breemen *et al.* published in 1997 an automated *pulsed* ultracentrifugation approach [66]. It is based on injection of a plug (described by Authors as a pulse) of studied mixture into the chamber containing free biological target (**fig. 11-A**). Mixture has to be prepared in a buffer compatible with biological target but not necessarily with mass spectrometry, since in a first stage used buffer is diverted

into the waste. This point shows a significant advantage over frontal affinity chromatography, in case of which the choice of sample buffer is limited to those compatible with MS. After flushing the chamber with binding buffer to wash-out unbound compounds (**fig. 11-B**), disruption mobile phase is infused into the chamber to dissociate protein-ligand complexes (**fig. 11-C**). In the original work water/MeOH (50/50) was applied making it fully compatible with ESI-MS. Pulsed ultrafiltration was successfully applied for various biological targets, including enzymes, *e.g.* calf intestine adenosine deaminase, human serum albumin [66] or cyclooxygenase (COX-2) [67].

Similar approach of screening may be accomplished using biological target immobilised to carrier easily separable from the solution (*e.g.* magnetic particles) [68, 69]. Due to simplicity of the separation of enzyme carrier from studied mixture, binding step may be conducted in a simple eppendorf tube without the need of using weight cut off membrane.

Marszałł *et al.* applied magnetic nanoparticles as a carrier for the family of heat shock proteins 90 $\alpha$  (HSP 90 $\alpha$ ) and successfully used this conjugate to separate standard, known ligands from the complex mixture [69]. Earlier, the same group of Professor Moaddel used magnetic nanoparticles to isolate ligands binding to human serum albumin [68].

#### *II.1.4. Direct detection of protein-ligand complexes*

Detection of non-covalent complexes provides a direct proof of the presence of protein-ligand specific interactions. This approach was successfully applied for determining dissociation (of binding) constants for various low-mass ligand candidates of known molecular mass [70-72] rather than for identification of the new ligands of unknown mass within the complex mixtures (**table 2**). An accuracy of ligand mass determination is in many cases limited due to large difference in masses of ligand and the biological target. For example, if we take into account that the charge of both free protein and the complex after ionisation using an electrospray is equal to 10, the error of ligand mass determination is multiplied by the factor 10 in relation to the accuracy of  $m/z$  value for both free protein and the complex peaks. Nevertheless, monitoring of the formation of protein-ligand complexes is very useful for high-throughput screening of the large set of **individual** inhibitor candidates, *e.g.* synthetic compounds that are available in a pure form [71].

**Table 2.** The examples of application of mass spectrometry for studying protein-ligand complexes

	Target protein		Ligand		Type of MS instrument	P and P/L ionisation charge	Remarks	Ref.
	name	MW [kDa]	type	mass range [Da]				
1	Carbohydrate-binding antibody, Se155-4 scFv	26.5	synthetic carbohydrate ligands	< 600	ESI FT-ICR	+7, +8	Indirect quantification of protein-ligand interactions by monitoring the ratio of P/PL <sub>M</sub> ; L and L <sub>M</sub> present together in the same sample	[72]
2	Fructose 1,6-bisphosphatase (tetrameric protein)	36.7 (monomer)	Low-mass inhibitors	< 500	ESI-TOF	+22, +23, +24	Determination of K <sub>d</sub> of individual ligands using P/PL ion responses.	[70]
3	Ribonuclease A (RNaseA)	13.7	cytosine	< 150	Electrospray ionisation triple quadrupole	+6, +7, +8	Determination which particular protein in a protein mixture interacts with a specified ligand using mass spectrometer operated in the precursor ion mode.	[73]
4	a) Lysozyme; b) Bcl-x <sub>L</sub>	a) 14.3; b) 21.3	Low-mass molecular inhibitors of studied proteins	< 650	nanoESI-TOF	a) +6, +7, +8; b) +7, +8, +9	One-point determination of K <sub>d</sub> of individual ligand candidates for Bcl-x <sub>L</sub> by comparing their P/PL ratios to P/PL <sub>M</sub> of the external control samples; lysozyme was used for method validation.	[71]
5	a) RNaseA; b) Lysozyme	13.7; 14.3	a) cytidine nucleotides; b) oligo-saccharides	a) < 500; b) < 1300	Desorption electrospray ionisation (DESI) ion mobility TOF MS	+7, +8, +9	DESI ion source consists of two sprayers: one of them produces droplets of a protein solution in a process of gas-driven nebulisation, the second one forms charged droplets of an analyte solution in a process of classic electronebulization. Protein and analyte-containing droplets emerge, evaporate and are delivered to mass spectrometer. Application of ion mobility TOF MS enabled complete separation of the complexes of RNaseA with various nucleotides (2'-CMP, CDP; CTP).	[74]
7	Bovine carboxypeptidase A (CPA)	34.2	Potato carboxypeptidase inhibitor (PCI)	4295	MALDI-TOF MS	+1	CPA-PCI complexes could only be observed when 'dried droplet' method was used for sample preparation, in contrast to 'thin layer'	[75]
8	Insulin-like growth factor-binding protein 3 (IGFBP-3)	29	Insulin-like growth factor 1 (IGF-1)	7600	MALDI-TOF MS	+4	An effect of 2-deoxy-D-glucose and glucose on IGFBP-3/IGF-1 complex formation. Epidermal growth factor (6.4 kDa) was used as an internal standard.	[76]


P - target protein;

L - ligand;

L<sub>M</sub> - marker ligand with known affinity to P;

PL - protein-ligand complex

 - liquid phase;

 - solid phase

FT-ICR - Fourier transform ion cyclotron resonance;

TOF - time of flight



## II.1.5. Intensity ion fading MS

Intensity ion fading matrix-assisted laser desorption ionisation time-of-flight mass spectrometry (IF-MS) was used for the first time by the scientific group of Professor Francesc X. Avilés for searching for the specific interactions between various proteases and their high mass peptidic inhibitors [77]. Despite being published 10 years ago, only a few studies have used IF-MS [75, 77-83], most of them in the laboratory headed by Prof. Avilés. IF-MS is based on the formation of specific complexes between target proteins and their binding partners leading to removal of bound molecules from the solution of studied extract or mixture. It leads to disappearance of corresponding ions from the mass spectrum of the extract, since they are not accessible for direct desorption and ionisation. The principal technique employed for IF-MS is MALDI-TOF MS [75-89]. IF-MS approach may be conducted using direct and/or indirect pathway (**fig. 12**). Direct protocol is based on a simple incubation of studied mixture with the target enzyme (protease) dissolved in a buffer compatible with the biological system (*i*), followed by addition of a solution of organic matrix (*ii*) and deposition of the mixture onto the MALDI spot for analysis (*iii*). Indirect protocol requires the use of the biological target immobilised onto the solid support and, besides the results provided by the direct protocol, enables observation of the ligands desorbed from biological target separately. It brings an additional dimension to the IF-MS by providing complementary results that might be used as a confirmation of the initial 'ion fading' results.

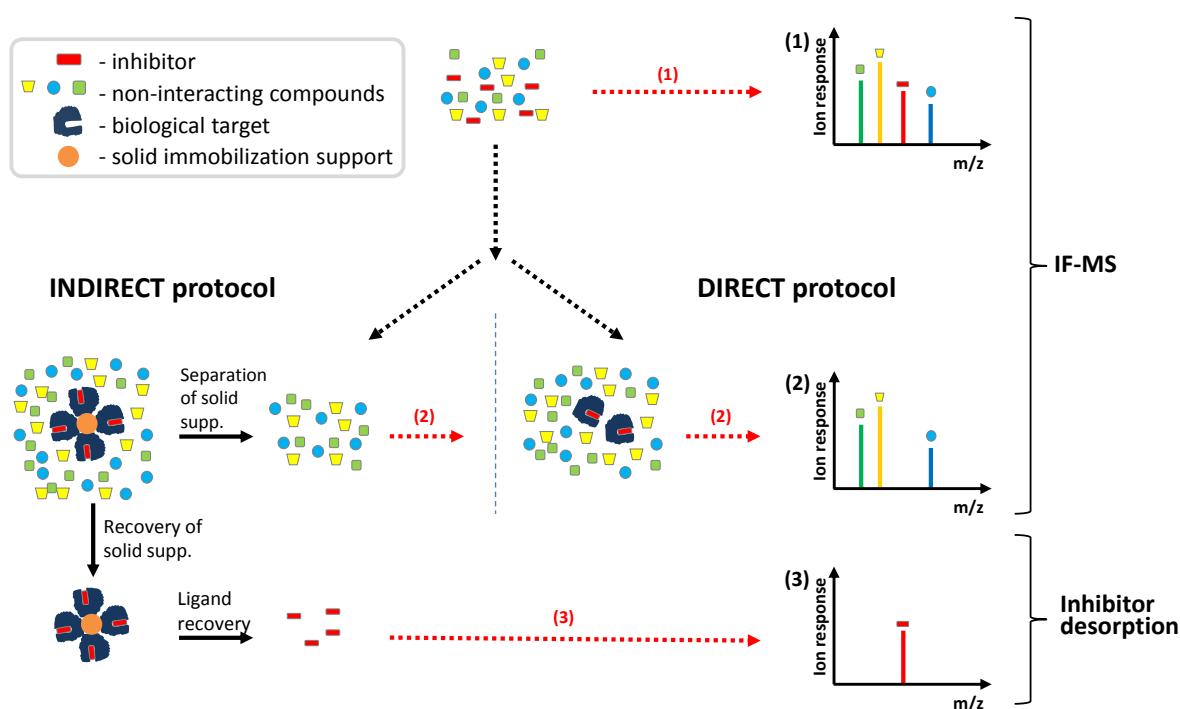


**Figure 12.** Simplified diagram of the strategies of ligand screening using IF-MS approach. (1) - mass spectrum of the complete sample; (2) - intensity ion fading phenomenon caused by retention of the inhibitor molecule within a binding site of the proteic target; (3) - ligand desorption and its subsequent analysis. The illustration was adapted from the reference [82].

## II.2. On-line enzymatic activity-based screening

Affinity-based screening methods do not require any marker of enzymatic activity since they are based purely on measuring protein-ligand affinity. An alternative approach, based on the monitoring of enzymatic activity, is based on the use of the natural or synthetic substrate of the target enzyme. Danny van Elswijk *et al.* developed a fluidic system for on-line identification of angiotensin-converting enzyme (ACE) inhibitors in hydrolysed milk [90]. On-line system was depicted in **fig. 13-A** and consists of injector, an analytical column (C18) and a split diverting separated sample directly to MS and to biochemical assay section coupled to fluorescence detector.

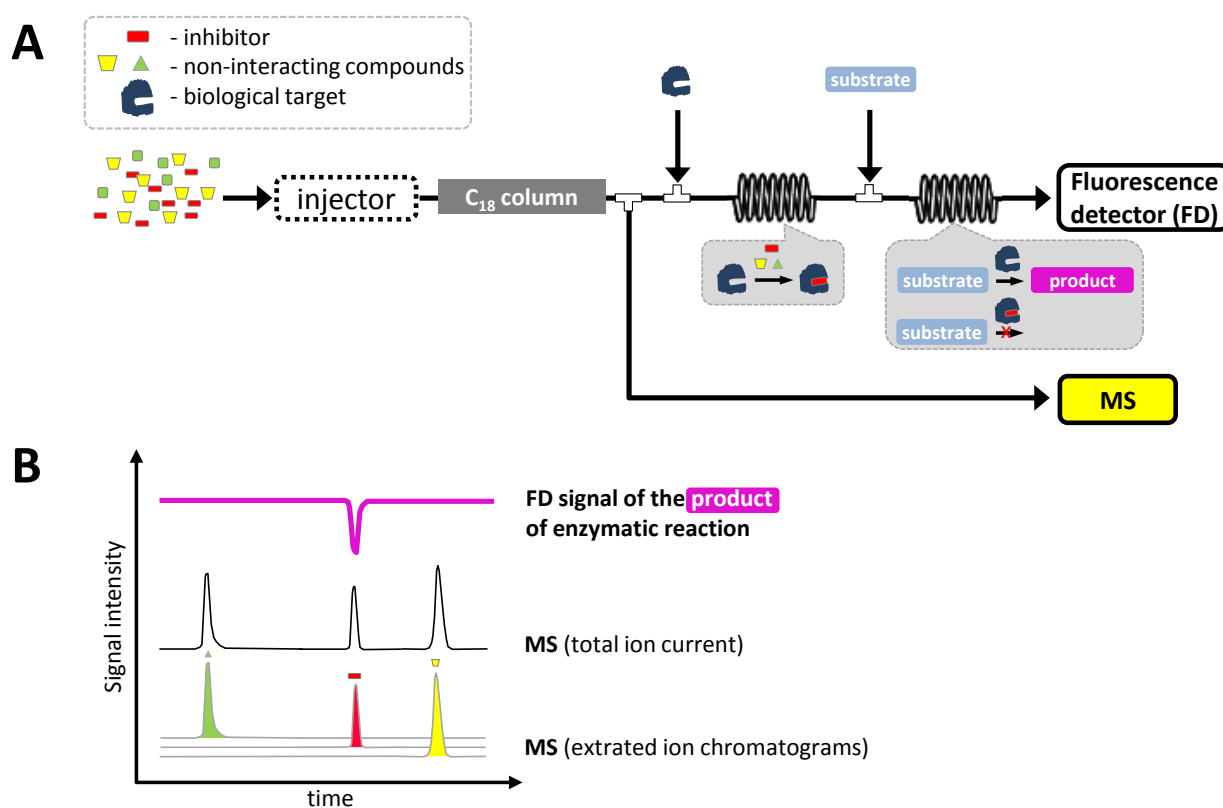


**Figure 13.** The layout of automated on-line enzymatic activity-based screening (**A**); an exemplary result of the analysis of a mixture of three compounds, including one inhibitor (**B**). This illustration was based on [90].

During the first stage of 'biochemical assay' section, a mobile phase containing separated analyte molecules is mixed with the solution of free ACE dispersed in a buffer optimal for the enzymatic reaction. In the following section, the ACE substrate (*ortho*-aminobenzoic acid–phenylalanine–arginine–lysine–dinitrophenol–proline, abz-FRK(dnp)P-OH) is introduced into the fluidic system. Abz-FRK(dnp)P-OH is internally quenched fluorogenic substrate of ACE – the fluorescence of this compound is released after its cleavage by ACE. It thus can be used to track ACE activity in a selective way. If the inhibitor is present in a

sample, it binds to ACE and blocks its activity. Consequently, no fluorogenic product of abz-FRK(dnp)P-OH conversion will be found within the segment of the mobile phase containing the inhibitor and, consequently, a negative peak on the signal of the fluorescence detector will be observed. The comparison of this signal with the total ion chromatogram of separated sample (**fig. 13-B**) identifies the inhibitor(s) peaks. The main and the most obvious disadvantage of this approach is the need of finding the selective marker of the enzymatic activity.

F.Heus *et al.* applied a modified system comprising just one infusion channel in the biochemical assay section, providing the mixture of the target enzyme – acetylcholine binding protein (AChBP) – in a complex with a marker (E)-3-(3-(4-diethylamino-2-hydroxybenzylidene)-3,4,5,6-tetrahydropyridin-2-yl)pyridine, DAHBA, for detection of neurotoxic (AChBP-binding) peptides in snake venoms [91]. In case of the presence of AChBP-binding peptides within the plug eluted from the analytical column, DAHBA, posing enhanced fluorescence properties only in a complex with AChBP, will be displaced from protein and, consequently, a negative peak on the signal of the fluorescence detector will be observed.

### II.3. A short overview of the ligand screening methods developed in present work

In our laboratory we decided to develop and optimize the screening approaches that can be easily transferred to other scientific groups and R&D laboratories working on discovering of novel bioactive substances of plant origin applicable in the cosmetic industry. On the other hand, we focused our main attention on approaches applicable to various types of biological targets other than enzymes (e.g. antibodies). Owing to our experience in a design and synthesis of capillary-format polymeric stationary phases, we decided to miniaturize and improve existing solutions in the domain of frontal affinity chromatography, FAC (*Chapter II*). The second reason justifying the selection of FAC is that our laboratory is equipped with a high-resolution ESI Qq-TOF mass spectrometer compatible with various ion sources (ESI, APPI, APCI) providing a powerful tool for detection and identification of a wide range of plant metabolites.

In addition, we extended an applicability of MALDI-TOF MS-based 'intensity ion fading' approach to low-mass molecules due to a simplicity in the experimental pathway and a large potential of its commercialization (*Chapter III*).

## III. Mass spectrometry

### III.1. Introduction

Mass spectrometry (MS) is an analytical technique that enables measuring a mass-to-charge ratio of intact molecules or their fragments. Well optimized instrument parameters, proper selection of an ion source and ionisation mode make possible to monitor many constituents of analyzed mixture simultaneously. It thus makes mass spectrometer a detector of choice for frontal affinity chromatography or other high-throughput screening methods (Reader may find more details on this subject in the *Chapter II*).

Mass spectrometer is a modular instrument and in its basic variant it consists of an ion source - the unit where ions are produced, a mass analyser and a detector - units responsible for determining  $m/z$  of chemical species and their abundance respectively (**fig. 14**).

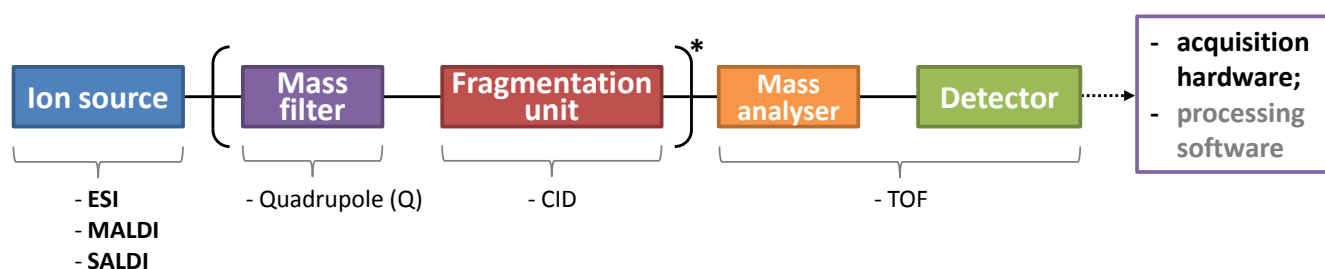


**Figure 14.** The classic segmented layout of a common mass spectrometer and selected hardware examples used in our laboratory. ESI - electrospray ionisation, MALDI/SALDI - matrix/surface assisted laser desorption ionisation, CID - collision-induced dissociation. \* - optional segments.

An appropriate ion optics provides an ion transfer between these segments. Apart from the ion source, all segments of the mass spectrometer operate at high vacuum to increase a mean free path of ions for the reason of reducing the risk of accidental ion collisions and their fragmentation.

The ion source is an interface between the zone of atmospheric pressure, where ionisation takes a place, and the low-pressure environment of the mass spectrometer. The most common ion source used for liquid samples is an electrospray ionisation (ESI) (**p. II.2** in the present chapter). Solid samples may be ionized e.g. by matrix or surface-assisted laser desorption/ionisation (MALDI/SALDI respectively) (**p. II.3** in the present chapter).

### **III.2. Mass spectrometer with electrospray ion source**

#### **III.2.1 Electrospray ion source**

Electrospray ion source (ESI) described for the first time in 1984 by Masamichi Yamashita and John Fenn [92] is the ion source most widely used for liquid samples. It supports ionisation of high to medium hydrophilic analyte and large biomolecules. ESI was used for all experiments with frontal affinity chromatography (*Chapter II*). The most important part of ESI is a sample nebuliser. It consists of the capillary attached to the source of a sample mixture which is placed coaxially into the tube attached to the source of compressed gas (nitrogen) supporting an electrospray process (**fig. 15**).

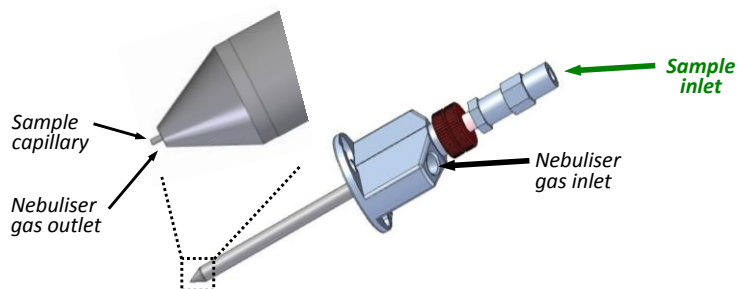


**Figure 15.** Bruker nebuliser for electrospray ion source. This illustration was adapted with modifications from Bruker Daltonique ESI-MS tutorial.

The capillary of the nebuliser is held at an electric potential having the polarity opposite to the potential of MS entrance (**fig. 16**). The difference of potential (usually around 2- 4 kV) between the capillary and the MS entrance draws the sample solution into the Taylor cone and leads to fine dispersion of the liquid. This effect is additionally supported by a coaxial flow of the nebulising gas. Resulted droplets have the same polarity as the capillary and opposite to the polarity of the MS entrance. Due to elevated temperature in the ion source, sample solvent evaporates and droplets shrink. When the force of Coulombic repulsion of the superficial charges (carried by ions) of the same sign is higher than the droplet's surface tension (in other words, if droplet-specific Rayleigh limit is exceeded), the droplet explodes producing even smaller droplets [93]. This process is repeated upon further solvent evaporation.

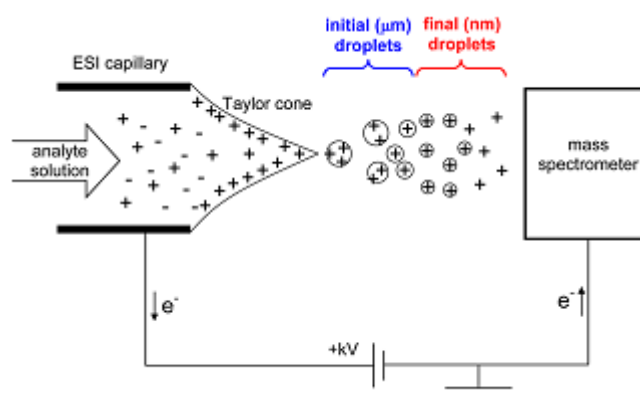


**Figure 16.** General outlook of the ESI ion source operated in a positive mode of ionisation [93]. For simplification of the illustration, the pathway of nebulising gas was omitted.

In accordance with the ion evaporation model (IEM), solvated ions of low-molecular analyte are believed to be ejected from the surface of nanodroplets [93]. The lower droplet's surface tension, the higher ejection rate constant. Large, globular biomolecules are believed to be ionized according to charge residue model (CRM). This model provides that the globular biomolecule is surrounded with the 'shell' of solvent that gradually shrinks upon evaporation to disappear completely at the end of this process [93].

#### Modes of ionisation

##### a) positive mode of ionisation

Positive ion mode for an observation of positively charged species. In this mode of ionisation, the nebuliser's capillary as well as droplets of the analyte are polarised positively and the sprayshield polarised negatively. The carriers of a positive charge within the droplets are usually protons, cations of metals (*e.g.* lithium, sodium or potassium) or salts (ammonium cation). Protons may come from acidified analyte solution or be generated in a process of water electrolysis on the surface of the nebuliser capillary [93]. These charge carriers form adducts with the analyte molecules and thus make them ionized. When diluted ammonium formate buffer is applied, proton adducts ( $[M+zH]^{z+}$ ) are the most common ions observed in the mass spectrum. They can be formed either by direct association of protons with the analyte molecules or by association of ammonium cations followed by liberation of ammonia. Sodium and potassium adducts are observed in a lesser extent unless salts containing these cations are intentionally added to the buffer solution. Organic salts can be visualised directly in their cationic forms, *e.g.* cetyltrimethylammonium bromide is observed as  $[M-Br]^+$ .

As it was stated above, positive ions are usually visualised in a form of the proton adducts. If in studied mixtures there is a vast number of compounds (*e.g.* in case of direct analysis of raw plant extract or complex library of drugs), we may encounter ion suppression phenomenon. It is caused by the fact that the pool of protons present in the buffer may be depleted by compounds having high proton affinity (*e.g.* amines). It will cause lower ionisation extent of the compounds having low proton-affinity (*e.g.* carboxylic

acids). If pH of the MS-compatible buffer is to be fixed at a certain level for the reason of adjusting it to the experimental conditions to the requirements of the biological target, it is usually necessary to add acidic make-up solvent (*e.g.* pure MeOH or a mixture of MeOH and diluted aqueous solution of formic acid) just before MS sample inlet [62, 94-96].

*b) negative mode of ionisation*

Negative ion mode is used to visualise negatively charged species. The polarity of the nebulizer and sprayshield are reversed in relation to the positive ion mode. Most of analyte molecules are ionized by detachment of a proton yielding  $[M-H]^-$  ion. Moreover, analyzed molecules may form adducts with anions present in the buffer, *e.g.* chloride, bromide, formate or acetate.

*III.2.2. Collision-induced dissociation and its application in metabolite identification*

More advanced instruments are equipped with additional units enabling selection of the ion of interest by means of an ion filter (*e.g.* quadrupole), its subsequent fragmentation and analysis of resulting fragments. This feature is of key importance for identification of unknown metabolites on the basis of their fragmentation pattern (Reader will find more details in the *Chapter III*). The most common fragmentation method for the small molecules is a collision-induced dissociation (CID) which is based on controlled collisions of the precursor ions with a static collision gas (usually nitrogen, argon or xenon). In a process of inelastic collisions, kinetic energy of the analyte ion is partially converted into its internal energy. It leads to decomposition of the ion into fragments (**fig. 17**) [97]. The collision energy may be regulated by changing the acceleration of the precursor ion within the collision cell.

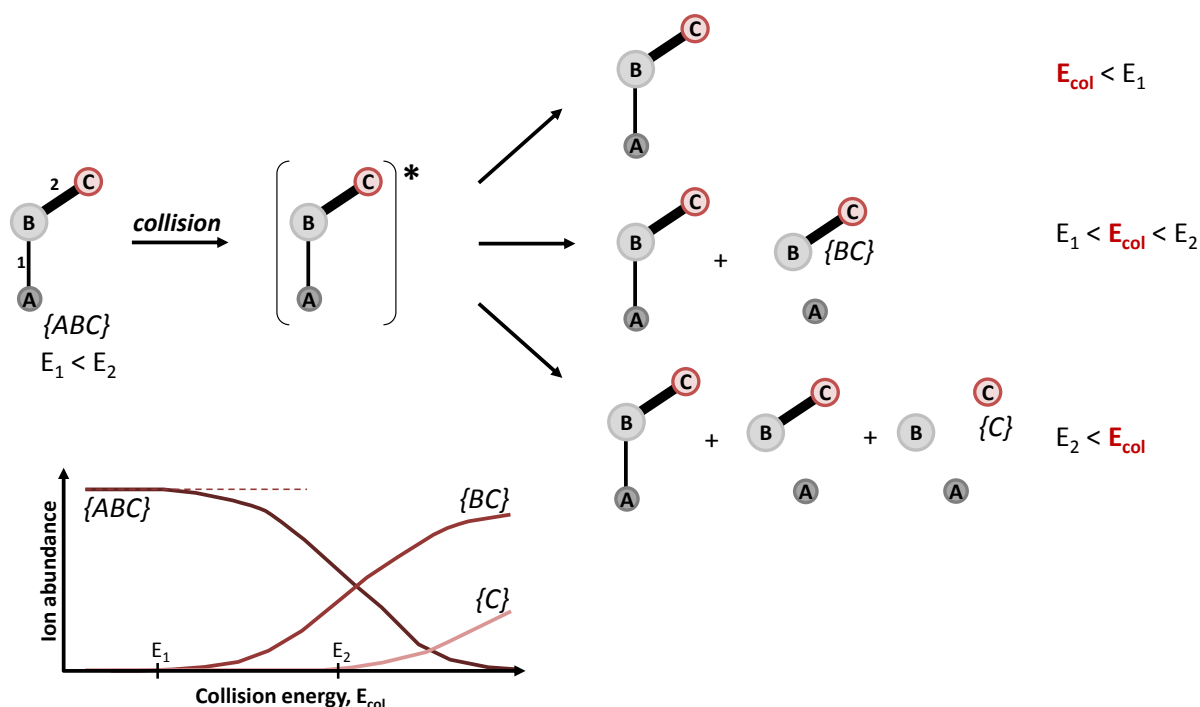


**Figure 17.** The visualization of CID-induced fragmentation.  $E_{col}$  - collision energy;  $E_i$  - dissociation energy of the bond  $i$ . A, B and C represent very stable molecular moieties with bond energies  $\gg E_{col}$  that remain intact during the fragmentation process. Let us assume that the C moiety is ionisable in studied conditions. Similar diagram of fragment abundances may be found in the ref. [98].

The nomenclature of common fragmentation patterns of flavonoids will be discussed taking eriocitrin as a model molecule (**fig. 18**). The flavonoids and their glycosylated derivatives constitute a large group of bioactive secondary metabolites of higher plants [99-104]. They have numerous beneficial features, *e.g.* may be applied as antibacterial agents and are effective scavengers of reactive oxygen species [103, 104]. Numerous flavonols are inhibitors of tyrosinase due to structural similarities to tyrosinase and DOPA, natural substrates of this enzyme (for example, *p. 1.2.2.1, table 1, entry 8 and 9*) and thus will be thoroughly discussed in further part of present manuscript. Flavonoids are composed of three rings marked as A, B and C and may be present as an aglycone or in a form of C- or O-glycosides (an example of the latter type: **fig. 18**). The aglycone core may be subjected to further modifications, *e.g.* methylation of some of its hydroxyl groups (*e.g.* hesperidin). Fragmentation nomenclature of aglycone is directly related with the annotation of their rings and marked as  $^{j,k}A_0$  and  $^{j,k}B_0$  for the fragments containing A or B ring respectively (**fig. 18**). The upper indexes  $j$  and  $k$  represent the numbers of the bonds within the ring C cleaved during the fragmentation process [102, 105]. The nomenclature for fragmentation or for carbohydrate part of the flavonoid structure presented herein is consistent with the general nomenclature for carbohydrate fragmentation, proposed by Domon and Costello in 1988 [106]. Charged fragments formed during the fragmentation process (and thus visualised on MS spectrum) may be divided into two groups: *i*) located within the confines of the considered sugar unit (denoted as  $^{p,q}A_m$ ,  $B_m$  and  $C_m$ ) or *ii*) within detached aglycone portion or reducing sugar unit (denoted as  $^{p,q}X_n$ ,  $Y_n$  and  $Z_n$ ), **fig. 18**. The



indexes  $m$  ( $m \geq 1$ ) represent the number of sugar unit counted from the non-reducing end while the indexes  $n$  represents the number of sugar unit counted from reducing end or from aglycone ( $n \geq 0$ ). As it was shown in **fig. 18**, fragments  ${}^{p,q}A_m$  and  ${}^{p,q}X_n$  are the result of the disruption of a sugar ring. The numbers of the cleaved bonds are provided in a form of front, upper indexes:  $p$  and  $q$ . Numeration of the bonds within the sugar ring starts from a hemiacetal bond which is assigned as 0 (**fig. 18**).

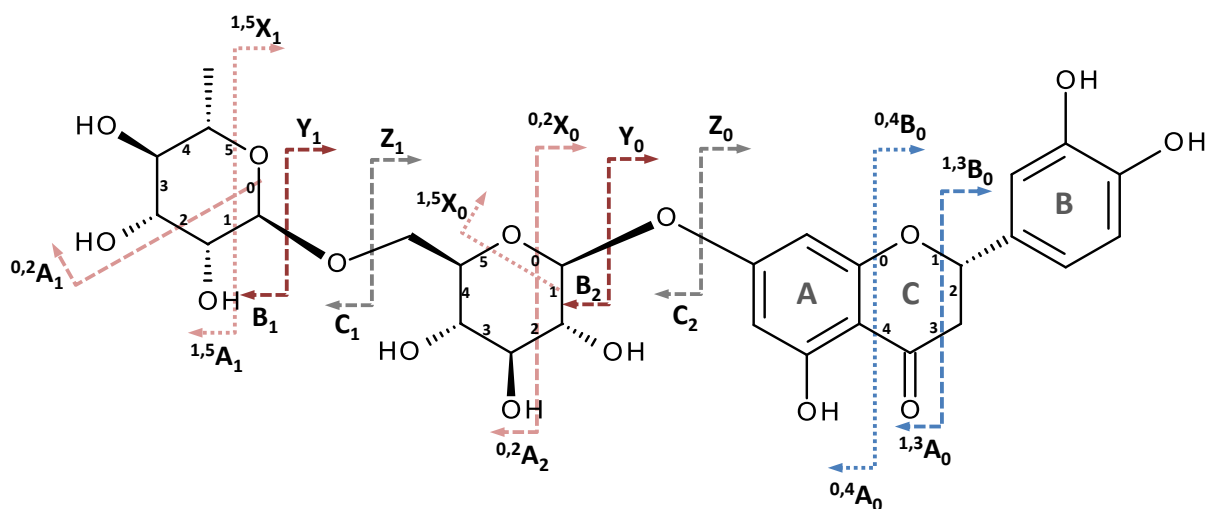


**Figure 18.** The fragmentation nomenclature of flavanone glycoside using eriocitrin as an example. Flavanones constitute one of the subsets of flavonoids.

Fragmentation patterns and relative abundances of given fragments depend on the mode of ionisation and type of flavonoid. In case glycosylated flavonoids, the most common fragments are of  $Z_0$  and  $Y_0$  type in a positive ion mode [100, 101, 105, 107] and  $Y_0$  in a negative ion mode [99, 108], since the glycosidic bond is the most prone to cleavage. Fragmentation of *O*-glycosylated hesperidin, which is formed by attachment of two sugar units to flavanone aglycone, hesperetin, yields both  $[Z_1+H]^+$  and  $[Y_1+H]^+$  fragments in a positive ion mode [105]. *C*-glycosylated flavonoids, due to C-C bond between aglycone and the sugar unit are much more difficult to fragment than and *O*-glycosylated counterparts. In case of this group of compounds we can expect disruption of the sugar ring, e.g. luteolin-6-*C*-glucoside is cleaved to  $[{}^{1,5}X_0-H]^-$  fragment. Fragmentation of flavonoid aglycones leads mostly to various A and B fragments, both in a positive and negative ion mode. The cleavage points strongly depend on the type of flavonoid, e.g. fragmentation of hesperetin (flavanone) leads to  $[{}^{0,3}A+H]^+$  and  $[{}^{1,3}B+H]^+$  [105], cyanidin (anthocyanidin) to  ${}^{0,3}A^+$ ,  ${}^{0,2}A^+$  and  ${}^{0,2}B^+$  [109]. In a negative ion mode quercetin (flavonol) undergoes decomposition to  ${}^{1,2}A^-$  and  ${}^{1,2}A^-$  [99].

### III.2.3. An outlook of Bruker maXis™ UHR-Qq-TOF spectrometer

Bruker maXis™ ultra high resolution Qq-TOF mass spectrometer with electrospray ion source (**fig. 13, I**) was applied for all experiments involving MS measurements of liquid samples (frontal analysis, the

*Chapter II*, and selected experiments with magnetic nanoparticles, the *Chapter III*). Solvated analyte ions enter into the desolvation assembly (*II*) and then, as 'dry' ions, to dual ion funnel compartment (*III*). Ion funnels efficiently and selectively separate ions from uncharged solvent molecules and focalise them at the entrance to the following stage of the mass spectrometer [110]. An outlet of the first ion funnel is shifted downwards in relation to an outlet of the desolvation capillary to avoid accidental ingestion of expanding solvent jet to further compartments of MS.

Hexapole (*IV*) transmits ions against the vacuum gradient. Afterwards, ions enter into the quadrupole (*V*) that may transmit all ions in 'full scan' mode or act as ion filter. Quadrupole consists of four parallel metal rods. The rods within one pair localized diagonally are connected together to the same electrical source. Each pair of rods is connected to static (DC) potential with an opposite value for each pair and, in addition, to the source of time-variable potential (AC). The combination of these two values determines the  $m/z$  value (and its range) of ions that can pass through the quadrupole.

In the following stage ions pass through quadrupole-like CID fragmentation chamber (*VI*) that may transmit all ions in 'full scan' mode or fragment of the ion of interest in  $MS^2$  mode. The ions then enter into an ion cooler (*VII*) that slows them down and inject them subsequently into an orthogonal accelerator (**fig. 19, VIII** and the TOF diagram: **fig. 20**). This unit accelerates ions at the entrance to time-of-flight (TOF) mass detector (**fig. 19, IX** and **fig. 14**). The TOF works in a reflection mode thanks to a dual stage reflectron (**fig. 19, X**). An acceleration plate forms the gradient of the electric potential (**fig. 20**) that interacts with the charged species providing them with the potential energy ( $E_{pot}$ , **equation 2**). The charge of chemical species may be expressed as the elementary charge multiplied by their charge number (**equation 3**). Ion's potential energy is converted into kinetic energy ( $E_{kin}$ ) (**equation 4**) and ions travel through field-free TOF tube with the constant speed (**equation 5**). If we combine all of these equations, we can express the value of  $m/z$  as directly proportional to the square of the flight time (**equation 6b**). Finally, ions hit the surface of an electron multiplier detector (**fig. 19, XI**) that registers their flight time (convertible to  $m/z$ ) and their abundance.

$$\left[ \begin{array}{l} E_{pot} = U \cdot q \quad (2) \\ q = z \cdot e \quad (3) \end{array} \right.$$

$$\left[ \begin{array}{l} E_{kin} = \frac{1}{2} m \cdot v^2 \quad (4) \\ v = \frac{d}{t} \quad (5) \end{array} \right.$$

$$\frac{m}{z} = \frac{2U \cdot e}{d^2} \cdot t^2 \quad (6a)$$

$$\frac{m}{z} = constant \cdot t^2 \quad (6b)$$

Where:  $E_{kin}/E_{pot}$  – kinetic/potential energy,  $U$  – electric potential;  $q$  – charge of the chemical species,  $z$  – charge number,  $e$  – elementary charge,  $v$  – speed,  $m$  – mass of charged species,  $d$  – length of the TOF tube.

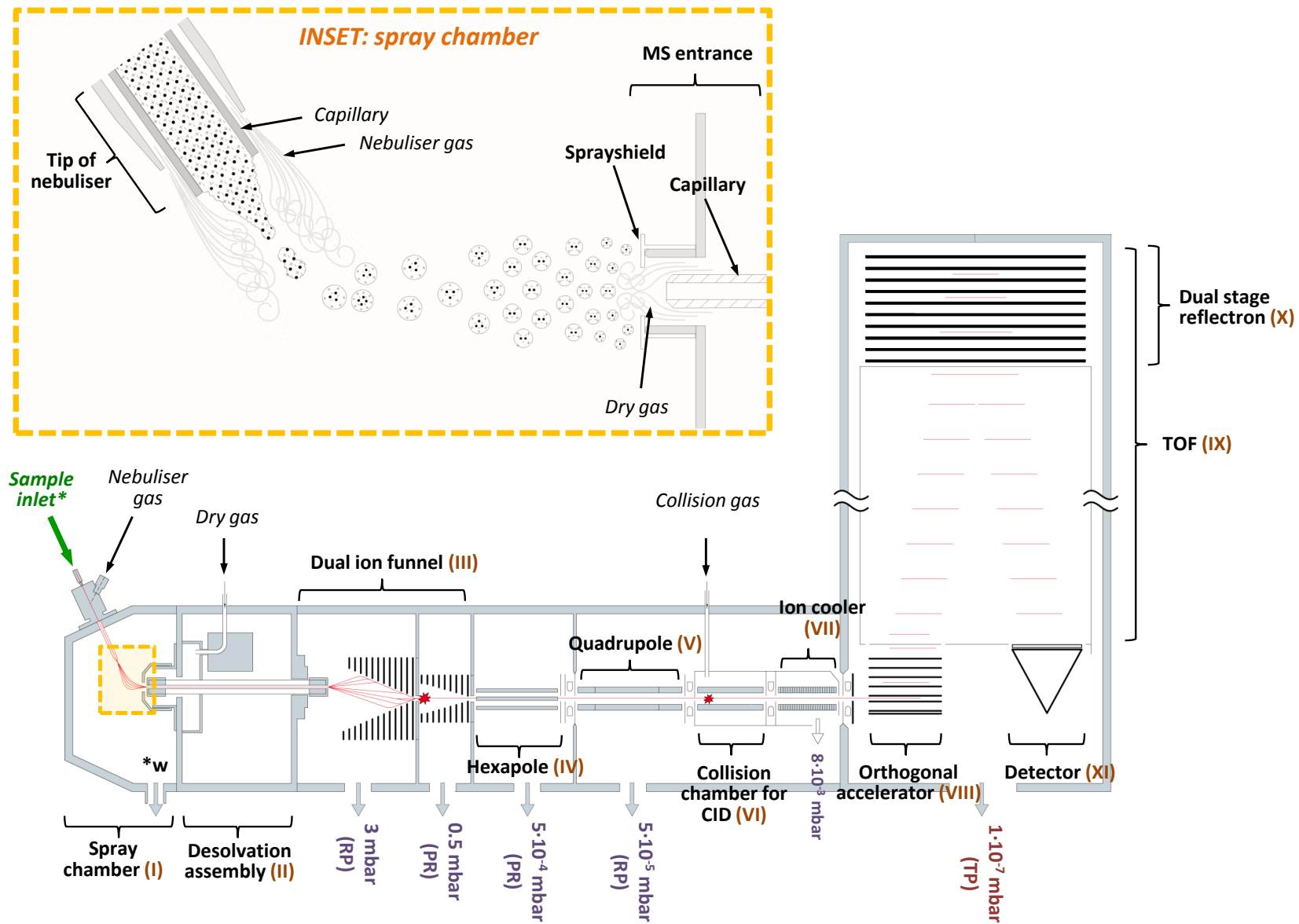


**Figure 19.** General layout of Bruker maXis™ UHR-Qq-TOF spectrometer. Illustration adapted with thorough modifications from promotional materials of Bruker Daltonik. RP - rough pump; TP - turbo pump.

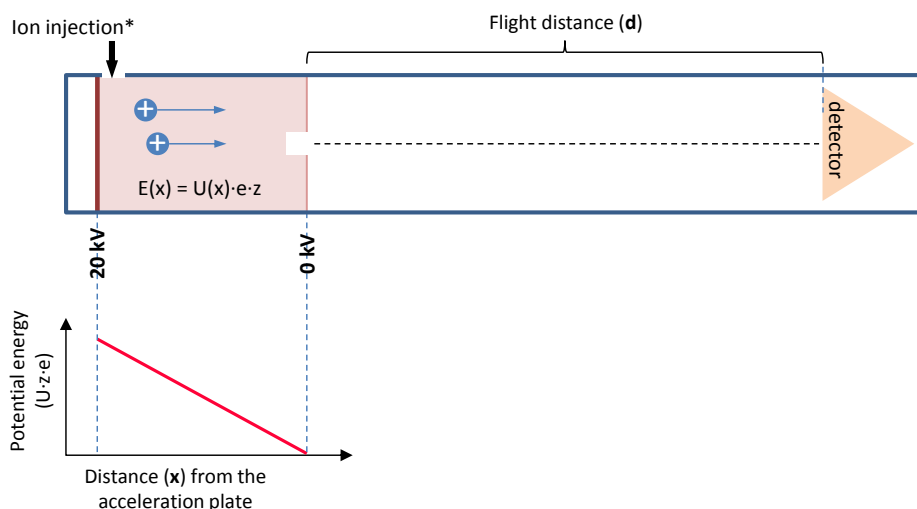


**Figure 20.** The layout of TOF assembly working in linear ion mode. (\*) - the geometry of ion injection depicted above was applied in Bruker maXis UHR qQ-TOF MS series. In case of MALDI-TOF MS ions are usually injected along the axe of the TOF tube.

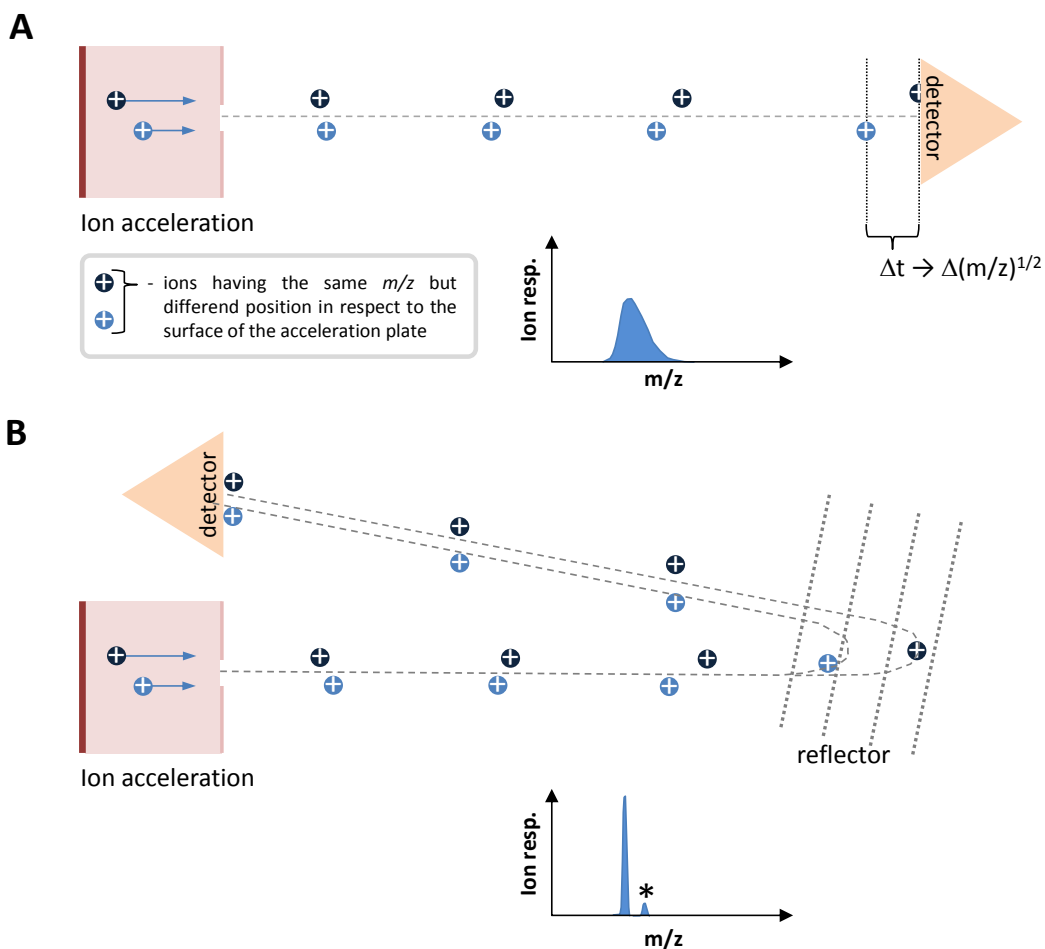


**Figure 21.** The comparison of TOF arrangement in linear (A) and reflector (B) mode. The first isotopic ion in the mass spectrum (B) was marked with an asterisk (\*).

The TOF may be operated in linear or in reflectron mode (MALDI-TOF) or be permanently arranged in the reflectron mode (Bruker maXis UHR qQ-TOF MS) (**fig. 19**). Ions entering to orthogonal accelerator may have an initial speed or have a certain spatial distribution. The value of the potential energy provided by the acceleration plate to the charged species depends on the distance from this plate (**fig. 20**). For this reason, the slight differences in the kinetic energy among ions of the same  $m/z$  may be observed leading to decrease of MS resolution. The function of ion reflector is to reduce these differences. Ions of the same  $m/z$  but higher  $E_{kin}$  will enter into the reflector unit deeper than those having lower  $E_{kin}$  (**fig. 21**). It will increase the flight time of faster ions through the reflectron leading to normalization of the total flight time and, at the same time, an increase of MS resolution.

### **III.3. Matrix-assisted laser desorption/ionisation and related techniques**

The term matrix-assisted laser desorption/ionisation (MALDI) was proposed for the first time by the group of Professor Franz Hillenkamp in 1985 [111]. They found that the laser energy required for ionisation of alanine may be reduced approximately ten times if laser wavelength-absorbing tryptophan is added to the sample. Laser desorption/ionisation technique used for ionizing intact proteins having molecular masses up to 35 kDa was shown for the first time by Koichi Tanaka *et al.* in 1988. To avoid laser-induced fragmentation of analyzed proteins they applied a cobalt powder of about 30 nm diameter finely dispersed in glycerol [112]. Later in 1988, Hillenkamp published the first true organic matrix-assisted laser desorption/ionisation of high-mass proteins (up to 67 kDa) using nicotinic acid as the laser-absorbing matrix [113]. Since then MALDI-MS has been successfully applied for studying wide range of small and large molecules (**table 3**), including their intact non-covalent complexes [75, 76, 80]. MALDI-TOF-MS is characterized by low sample requirement, an excellent sensitivity (reaching the picomole range [114]) and the potential of full automation.

Sample deposition on a target plate (usually made of polished steel) may be accomplished in many different ways. The most common methods are: *i*) 'dried droplet' method, when the analyte and matrix are mixed together the plastic eppendorf and its subsequent deposition on the spot and *ii*) 'thin layer', when the analyte is deposited on the layer of pre-spotted matrix.

The principal role of matrix is to act as the 'antenna' of laser energy that can then be used to ionize the analyte molecules (**fig. 16**). Matrix is in a great excess in relation to the analyte (even 1000-fold) what plays an important protective role for the analyte. Matrix ionisation mechanism is not fully understood and is postulated to be caused by the transfer of proton to analyte molecules by photo-excited matrix molecules. Direct ionisation of matrix molecules is postulated to be caused by the combination of two photon excitation accompanied by the absorption of thermal energy released upon the laser shot [115].

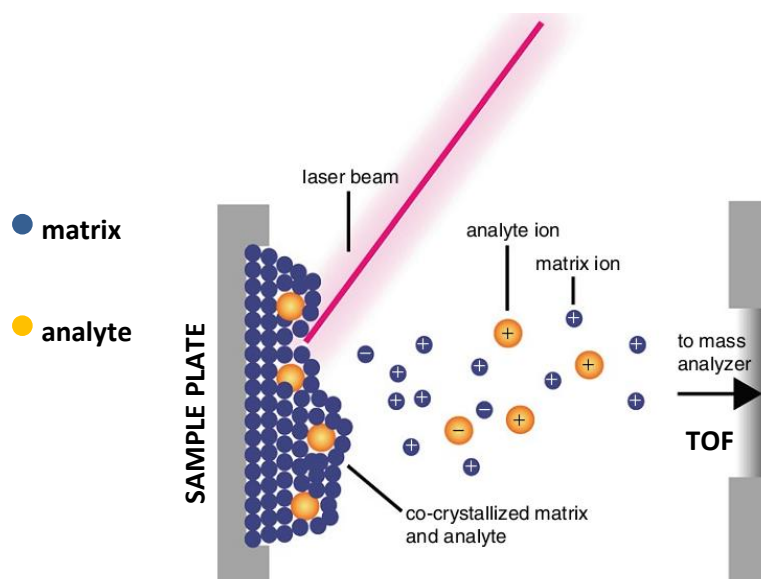


**Figure 22.** The scheme of MALDI ionisation process [116, 117]. The energy of laser beam is absorbed by matrix molecules that undergo desorption from the sample plate and ionisation of an analyte.

Organic matrices were successfully applied for studying small molecules, *e.g.* metal-phthalocyanines [118], 9-aminoacridine alone [119] or in a form of binary matrix with  $\alpha$ -cyano-4-hydroxycinnamic acid [120] or a 'proton sponge' (1,8-bis(dimethyl-amino)naphthalene) [121]. Nevertheless, a uniform surface of the mixture of organic matrix and the analyte is difficult to obtain what results in so called 'sweet spots' and poor spot-to-spot repeatability. Moreover, organic matrices may cause the interferences in the low-mass range (<500 Da). The latter drawback is acceptable when the mass of the studied ligands is above 500 Da, but it would impose the serious complications on screening of extracts for low-mass inhibitors or ligands without thorough optimization of a sample preparation. To address this issue, non-organic nanoparticles were applied in the role of ion emitter for the analysis of low-molecular compounds (**table 4**) [122, 123]. This approach is known as surface-assisted laser desorption/ionisation (SALDI), since the surface of the nanoparticles is responsible for energy adsorption and its transfer to the analyte. Since the first application of graphite particles as a SALDI matrix in 1995 [124], many developments and new types of nanomaterials have been successfully applied for studying small molecules without low-mass background, *e.g.* nanoparticles made of gold [125], silver [126], platinum [127],  $\text{TiO}_2$  [128, 129], ZnO [130], diamond [128] or  $\text{Fe}_3\text{O}_4$  coated with silica [131], nanowires [132] or fullerenes [133] (more examples in **table 4**).

The transfer of energy from the surface of nanomaterial to the analyte is believed to be a thermally driven process [132, 134]. The peak temperature of the nanomaterial surface upon laser shot ( $\Delta T$ ) depends on many factors related both with geometrical (size and shape) and intrinsic physical properties of the raw material: density ( $\rho$ ), heat capacity ( $C_p$ ), heat conductivity ( $\kappa$ ) and the laser wavelength absorption coefficient. In isolated environment the superficial peak temperature ( $\Delta T$ ) of nanomaterial is given by **equation 7** and – in fixed experimental conditions – it depends on density and the heat capacity of the nanomaterial. Laser-absorbing materials with low  $\rho$  and  $C_p$  are thus good

candidates for SALDI matrix. Yonezawa *et al.* demonstrated that nanoparticles made of copper (CuNP) are not suitable as SALDI matrix for peptides and proteins due to too low  $\Delta T$  (mostly due to high  $C_p$ ), despite their high UV absorption. Simultaneously, nanoparticles made of gold, having 1.38-times higher  $\Delta T$  than CuNP turned out to be an excellent SALDI matrix [134].

$$\Delta T = \frac{H_{LP}}{\rho d C_p} = \frac{const}{\rho C_p} \quad (7)$$

where:  $H_{LP}$  - laser fluence defined as laser pulse energy/spot surface;  $C_p$  - heat capacity;  $\rho$  - density;  $d$  - diameter of the irradiated area

The peak temperature upon the laser shot (expressed using **equation 7**) does not take into account the heat transport between nanomaterial and the steel LDI plate which is proportional to the material's heat conductivity ( $\kappa$ ). The higher  $\kappa$ , the lower peak temperature due to high heat dissipation [134].

The size of nanomaterial is also of key importance for the results of SALDI experiment. Shin *et al.* studied an impact of the length of ZnO nanowires on the yield of ionisation of small organic molecules [132] and showed that ZnO nanowires shorter than depth of conductive heating ( $D_{diff}$ , **equation 8**) do not provide an effective ionisation. The possible reason explaining this phenomenon is the flow out of absorbed thermal energy through the substrate and, consequently, a negative impact on the level of superficial peak temperature ( $\Delta T$ ).

$$D_{diff} = 2 \sqrt{\frac{\tau \kappa}{\rho C_p}} \quad (8)$$

where:  $\tau$  - duration of the laser pulse;  $\kappa$  - heat conductivity;  $C_p$  - heat capacity;  $\rho$  - density

In summary, an optimal SALDI matrix should effectively convert laser energy into thermal energy and retain it long enough to provide an efficient desorption and ionisation.

In this work an extensive development of SALDI-TOF MS approach for high-throughput screening of inhibitory properties of small molecules of plant origin was described (*Chapter III*).

**Table 3.** The examples of an application of MALDI-TOF MS.

	Target analyte	Matrix	Deposition type	Laser wavelength	Ion mode	Remarks	Ref.
1	DNA (stabilized, double-stranded)	6-aza-2-thiothymine, 3-hydroxypicolinic acid	dried droplet	337 nm	negative		[135]
2	Low molecular acids detected as matrix adducts	metal-phthalocyanines	dried droplet	355 nm	negative	Low matrix/analyte ratio	[118]
3	Small molecules	Polythiophene	dried droplet*	337 nm	negative	Polymeric matrix; *-matrix remained solid, sample dried with nitrogen flow	[136]
4	Small molecules	9-AA	dried droplet	337 nm	negative		[119]
5	Small molecules	$\alpha$ -CHCA in the mixture with 9-AA	dried droplet	337 nm	negative, positive		[120]
6	Small molecules	DHB	thin layer	NA	positive	Matrix deposition by piezoelectric inkjet printer	[137]
							[121]
7	Oligonucleotides, peptides	ionic liquids	dried droplet	337 nm	positive		[138]
8	Peptides	$\alpha$ -CHCA	dried droplet	NA	positive		[139]
9	Peptides	DHB	dried droplet	337 nm	positive		[140]
10	Peptides	$\alpha$ -CHCA; DHB; HABA; dithranol	dried droplet	NA	positive		[141]
11	Peptides	$\alpha$ -CHCA	dried droplet	NA	positive		[142]
12	Proteins	Ferulic acid; SA	dried droplet	337 nm	positive	Direct analysis of whole bacteria cells	[143]
13	Proteins	$\alpha$ -CHCA	thin layer	355 nm	positive		[144]
14	Proteins	$\alpha$ -CHCA	dried droplet	355 nm	positive		[145]

$\alpha$ -CHCA:  $\alpha$ -cyano-4-hydroxycinnamic acid

DHB: 2,5-dihydroxy benzoic acid

HABA: 2-(4-hydroxyphenylazo)benzoic acid

9-AA: 9-aminoacridine

SA: sinapinic acid

**NA: information not available**



**Table 4.** The examples of an application of SALDI-TOF MS.

	<b>Analyte</b>	<b>Matrix</b>	<b>Deposition type</b>	<b>Laser wave-length</b>	<b>Ion mode</b>	<b>Ref.</b>
1	Peptides, proteins, small molecules	Graphite nanoparticles	Glycerine mixed with the analyte solution; graphite nanoparticles drop-placed on top of the liquid	337 nm	positive	[124]
2	Steroids	Fullerene C <sub>70</sub>	Analyte deposition onto dry layer of fullerene	337 nm	negative, positive	[133]
3	Small organic molecule (propranolol)	Graphitized carbon black nanoparticles	Analyte deposition onto pre-spotted target plate	337 nm	positive	[146]
4	Benzylpyridinium halide	Carbon nanotubes; fullerene C <sub>60</sub> ; nanoporous/non-porous graphitic carbon; nanodiamonds; highly oriented pyrolytic graphite	Analyte deposition onto dry matrix layer	337 nm	positive	[147]
5	Aminothiols	Gold nanoparticles	dried droplet	337 nm	positive	[125]
6	Small molecules	Zinc oxide nanoparticles	dried droplet	337 nm	positive	[130]
7	Small molecules	Magnetic silica nanoparticles (hydrophobic and hydrophilic)	dried droplet	NA	negative, positive	[148]
8	Low-molecular explosives	Magnetic silica-based sub-micron particles	dried droplet	NA	negative, positive	[149]
9	Peptides	$\alpha$ -CHCA-bound gold nanoparticles	dried droplet	337 nm	negative, positive	[150]
10	Small molecules	Polystyrene particles coated with gold	dried droplet	NA	positive	[151]
11	Low-mass peptides	Silica nanoparticles	Analyte deposition onto pre-spotted target plate	355 nm	positive	[152]
12	Peptides and synthetic polymer (PEG)	Ag, Au, Cu and Pt nanoparticles	Analyte deposition onto pre-spotted target plate	337 nm	positive	[134]
13	Proteins, protein-protein complexes	HgTe nanostructures	dried droplet	337 nm	positive	[153]
14	Low-mass phenolic compounds	Titanium dioxide nanoparticles	dried droplet	337 nm	negative	[129]
15	Small molecules	Zinc oxide nanowires	Analyte deposition onto ZnO nanowire substrate	355 nm	positive	[132]
16	Peptides and proteins	Magnetic Fe <sub>3</sub> O <sub>4</sub> -silica core-shell nanoparticles	dried droplet	337 nm	positive	[131]
17	Estrogens	Ag nanoparticles	dried droplet	337 nm	negative	[126]
18	Peptides and proteins	Titania nanotube array	Analyte deposition onto dry matrix layer	NA	positive	[154]
19	Small molecules	Nanostructured silicon substrates	Analyte deposition onto silicon substrates	337 nm	negative, positive	[155]

#### IV. The strategies for protein immobilisation

Immobilised enzymes are widely used on industrial scale [156] and on a laboratory scale, including analytical chemistry [157, 158], diagnostics [159] or drug screening [160, 161]. In many cases immobilised enzymes are used to determine enzymatic and kinetic parameters: maximal enzymatic velocity,  $V_{max}$ , and Michaelis–Menten constants,  $K_M$ , for novel substrates or for an evaluation of the inhibitory properties of leading drug molecules [162, 163]. Enzymes may be retained within dedicated area either by *i*) immobilisation based on specific interactions with the solid support; by *ii*) covalent attachment by means of one or multiple proteic superficial reactive residues (usually  $-NH_2$ ) or by *iii*) non-covalent entrapment within the three-dimensional polymer network or simple adsorption to the surface. The optimal immobilisation method depends on the specified needs and will be shortly reviewed in the following paragraphs.

##### IV.1. Non-covalent protein immobilisation

###### IV.1.1. Immobilisation based on specific protein-ligand interactions

Protein immobilisation based on specific protein-ligand interactions may require pre-treatment of the biological target (e.g. biotinylation) to make it compatible with commercially-available affinity stationary phases or simply take an advantage of the intrinsic properties of given group of biological targets (e.g. His-tag).

The immobilisation process using streptavidin/avidin-biotin linkage takes an advantage of extremely strong non-covalent interaction between one of two homotetrameric proteins: avidin (66 kDa) or streptavidin (approximately 60 kDa) and biotin, the low-mass organic molecule ( $K_d$  constant for avidin-biotin interaction is on the level of 1 fM ( $10^{-15}$  M) [164]), **fig. 23**.

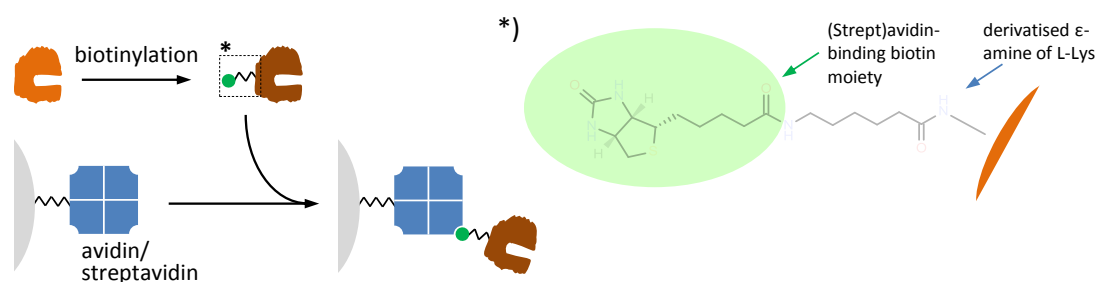


**Figure 23.** An immobilisation procedure using streptavidin/avidin-biotin specific interaction. Biotinylated biological target is directly coupled with commercially available streptavidin/avidin-bound solid support; \*- an example of the outcome of biotinylation of one of protein superficial L-Lys residues using biotinamido hexanoic N-hydroxysuccinimide ester (NHS-LC-biotin), the reagent used by e.g. Chan et al. [165] and Schriemer et al. [166].

This approach consists of two steps: *i)* biotinylation of the biological target, usually conducted by attachment of biotin derivative to the terminal  $\epsilon$ -amine groups of L-Lys residues on the surface of the biological target; *ii)* contacting the solution of biotinylated target with avidin (or streptavidin)-bound stationary phase [166, 167]. Various types of this kind of stationary phases are commercially available (e.g. avidin-agarose, Sigma-Aldrich product: A9207) and are relatively expensive (> 100 €/mL). However, this solution is suitable for laboratories seeking for a quick and well-established immobilisation method with minimal developments in the domain of surface functionalisation which is usually required for covalent protein immobilisation.

Many recombinant proteins expressed in bacteria organisms, e.g. in *Escherichia coli* possess a short polypeptide composed of several histidine residues, either at C- or N-terminus of the polypeptide chain. This poly-histidine moiety, called His-tag, poses high affinity to a metal chelate adsorbents, they can be used for selective separation and purification of given recombinant protein from remaining ingredients of homogenized expression cells [168]. The immobilised metal affinity chromatography (IMAC) utilises stationary phases decorated with cobalt or nickel cations [169-171]. The stationary phase consists of metal chelating moieties, such as iminodiacetic acid (IDA) or tris(2-ethylaminoethyl) amine (TREN), e.g. columns BioFox 40 IDA/TREN commercialized by KNAUER, Berlin, Germany. When all unbound proteins are washed out from the column, His-tag protein can be desorbed using buffered solution of imidazole, for the reason that this compound competes with His-tag for binding with the metal chelate adsorbent. His-tag may also be used as an anchoring point for protein immobilisation when anti-His-tag antibody-covered stationary phase is applied (**fig. 24**) [62].

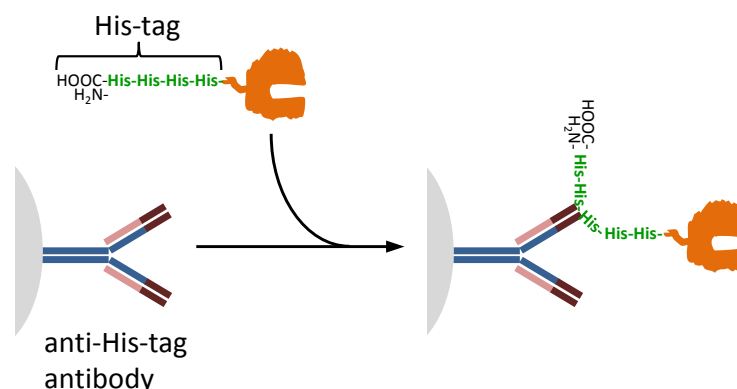


**Figure 24.** A direct immobilisation of His-tagged recombinant protein to anti His-tag antibody-covered stationary phase [62].

The latter approach may be particularly interesting in all laboratories where high-throughput screening of the inhibitors towards a **wide range** of recombinant proteins is conducted. A single-point anchoring of the recombinant protein reduces the risk of immobilisation-related protein inactivation. The main drawback of this approach is tremendously high cost of anti-His-tag antibodies both alone and in agarose-

immobilised form (*e.g.* agarose-bound monoclonal anti-His-tag costs more than 1000 €/1 mL, Sigma-Aldrich product: A5713).

#### *IV.1.2. Immobilised artificial membranes*

Immobilised artificial membranes (IAM) may be used to immobilize membrane-bound proteins such as receptors or transporters [172]. A solid support for IAM is composed of beads (*e.g.* made of silica) covered by a monolayer of phospholipid analogues. It may be obtained by derivatisation of the silica surface with organosilanes containing phospholipid moieties (*e.g.* phosphatidylcholine attached to the organosilane via one of its two aliphatic chains [173]) and the alkoxy groups responsible for coupling the organosilane molecule to the silica surface (further details concerning this pathway of silica derivatisation may be found in the *Chapter II, p. II.2.2*, page 63). During the first step, cells containing the membrane protein of interest are solubilised using dedicated detergent (responsible for the lipid membrane disruption) and contacted with the IAM beads. The mixture is then dialysed to remove the detergent. Thanks to the presence of superficial phospholipid monolayer on IAM beads, the target protein may be retained on their surface. This immobilisation approach is restricted to the membrane proteins exclusively and is not applicable to soluble biological targets existing in the cells in a free form.

#### *IV.1.3. Enzyme immobilisation by entrapment within a polymer network*

Enzyme molecules may be entrapped within the polymer network. Polymerisation is usually conducted *in situ* in the presence of the target enzyme [174]. Up to now numerous enzymes were retained within solid support using various entrapment approaches, *e.g.* alcalase within silica-based polymer [175], lipase within PVA/crosslinked chitosan film [176],  $\alpha$ -amylase within beads made of anionic polysaccharide [177]. The main advantage of the entrapment is the lack of mechanical constraints on protein molecules present in the case of covalent immobilisation. However, low loading capacity of common entrapment supports (and thus low ratio of the amount of enzyme per support surface unit) makes this approach not compatible with affinity-based screening methods (*e.g.* frontal affinity chromatography), since it favours the presence of high non-specific interactions between the analyte and the entrapment support (reader will find more information on this subject in the *Chapter II*).

### **IV.2. Covalent protein immobilisation**

#### **IV.2.1. General outlook**

Covalent immobilisation of the biological targets to the solid support is the most common way for the preparation of the stationary phases intended for affinity-based methods involving antibodies and

enzymes. Most of the immobilisation pathways are based on coupling of the terminal  $\epsilon$ -amino groups of lysine exposed on the surface of the proteic target (**fig. 25**). There is a wide variety of activated stationary phases prepared for one-step amine coupling (**fig. 25-A-F**). One of the most common solutions are aldehyde-based stationary phases (**fig. 25-A**) that can be prepared by simple derivatisation of amine-based supports with glutaraldehyde [68, 94, 178-180]. Superficial aldehyde groups may also be obtained by acid-catalysed opening of epoxide ring followed by oxidative cleavage of resulting diol [181-183]. In addition, amine covered stationary phases may be activated using an agent containing two acyl chloride groups, *e.g.* phthaloyl chloride [184] (**fig. 25-B**). Similarly to glutaraldehyde, one acyl chloride group reacts with superficial amines of the stationary phase, while the second is ready to bind the target protein. Agarose gel may be easily activated using cyanogen bromide to yield amine-reactive superficial cyanate ester groups (**fig. 25-C**) [185]. Stationary phases bearing superficial epoxide groups may be coupled directly with proteic target by amine-epoxide nucleophilic addition [186] (**fig. 25-D**). This type of stationary phase may be obtained by activation of agarose gel by epichlorohydrin. The reaction of protein coupling requires high pH of a coupling buffer and thus may not be suitable for all proteic targets.

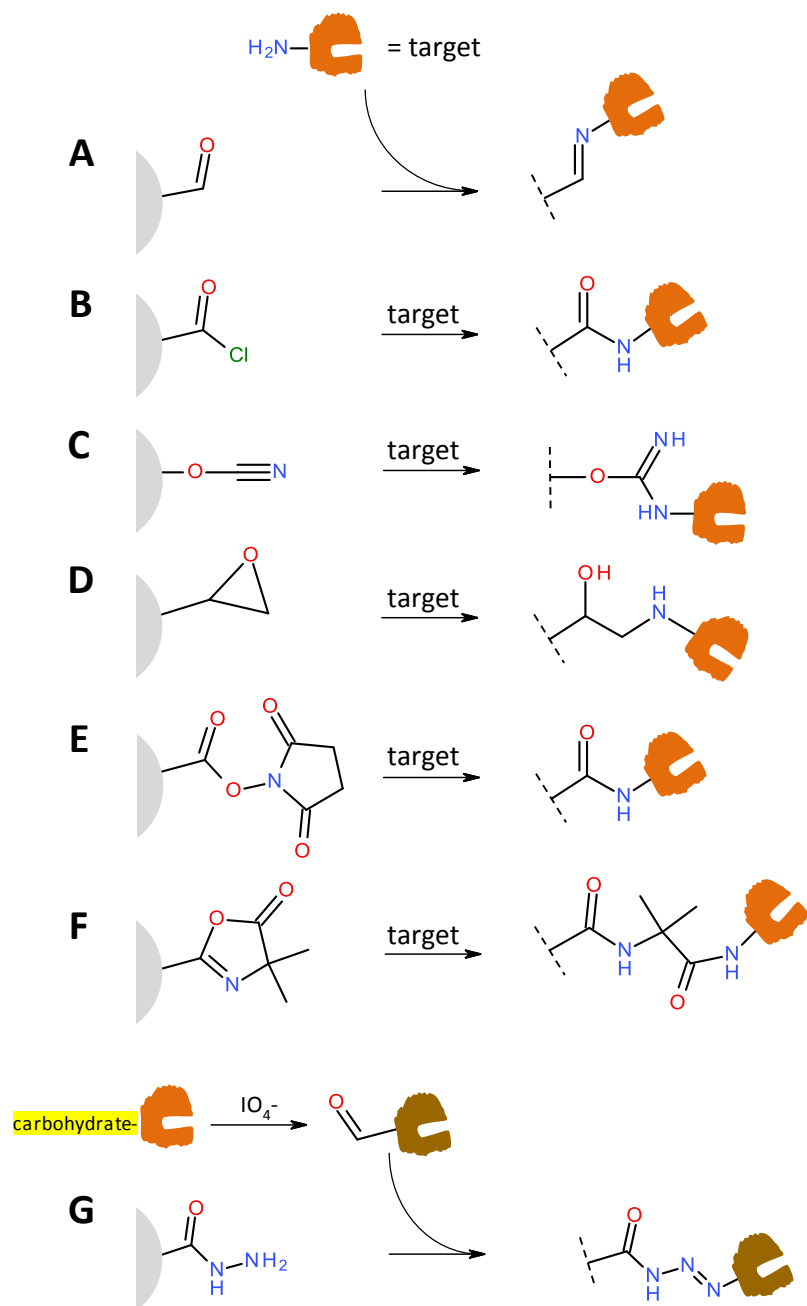


**Figure 25.** Covalent methods of protein immobilisation using superficial amine residues of the native protein (A-F) and aldehyde group obtained in a process of oxidative cleavage of superficial carbohydrates of glycoprotein (G).

*N*-hydroxysuccinimide-activated stationary phases may be coupled with the target protein in one-step reaction resulting in highly stable amide bond [187] (fig. 25-E). Polymeric stationary phases may be based on reactive monomers, such as *N*-hydroxysuccinimide-activated acrylic acid. Another example of reactive monomer compatible with the popular (meth)acrylate-based monomers and cross-linkers is poly(2-vinyl-4,4-dimethylazlactone) yielding superficial reactive azalactone groups [188, 189] (fig. 25-F). Unfortunately, the availability of this monomer on the global market is very limited.

An alternative immobilisation pathway may be applied to glycoproteins. Superficial carbohydrate moieties may be oxidised to aldehyde using periodate, in a process of diol oxidative cleavage, and then coupled to hydrazide-activated stationary phase [190-192] (**fig. 25-G**).

Numerous papers report increased thermal stability and improved storage life of covalently immobilised proteins [117, 193-196], possible due to stabilization of their three-dimensional structures.

#### IV.2.2. Impact of protein immobilisation on its kinetic parameters: $K_M$ and $V_{max}$

Protein immobilisation induces certain structural changes that can have a negative impact on its activity and substrate affinity to its active site [117]. In many cases the protein surface contains numerous amine functional groups, each of which can be used as an anchoring point of enzyme to the solid support (Reader will find more information on this subject in the *Chapter IV*). The localization of this anchoring point is random and cannot be controlled. It may cause an improper geometry of protein immobilisation (**fig. 26-A**). These factors usually increase an apparent  $K_M$  of immobilised enzyme (because of lower affinity of substrate to enzyme's active site) [117, 197] comparing to the free enzyme and decrease its specific activity (activity per enzyme mass unit) [117]. Peterson *et al.* showed that  $K_M$  of immobilised trypsin increased in parallel with an increase of a concentration of azalactone groups (**fig. 25-F**) on the surface of the immobilisation supports [189]. Increased amount of azalactone groups could lead to the growth of loading density of enzyme impeding an access of the substrate to enzyme's active site or could cause a multisite binding of the trypsin molecule affecting enzyme's geometry [189].

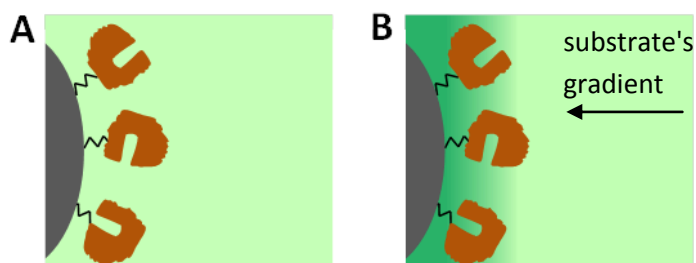


**Figure 26.** An example of possible geometries of protein immobilisation on the solid support non-interacting (**A**) and interacting with the substrate (**B**).

If enzyme's substrate interacts with the solid support used for immobilisation, it may be adsorbed on its surface. It leads to an increase of substrate's local concentration (pre-concentration) in the neighbourhood of enzyme molecules (**fig. 26-B**) what can induce a higher conversion rate and decrease the apparent  $K_M$  value [198].

## **CHAPTER II**

# **Frontal affinity chromatography**





L'analyse frontale (FA) est une approche basée sur le couplage LC-MS en mode d'infusion continue permettant le criblage de ligands ou d'inhibiteurs selon leur affinité à une cible biologique telle qu'une enzyme, qui dans notre cas sera soit la trypsine (enzyme modèle) ou la tyrosinase (enzyme d'intérêt dans le cadre de l'hyperpigmentation de la peau). La réponse est donnée par un profil d'élution caractéristique de l'affinité plus ou moins importante des ligands avec le site actif de l'enzyme.

Après un paragraphe consacré à la description et aux concepts mathématiques de l'analyse frontale qui permettent de déterminer la quantité d'enzymes immobilisées ( $B_t$ ) dans la colonne et la constante de dissociation ( $K_d$ ) du complexe enzyme/inhibiteur, le choix du mode de détection le plus approprié y sera discuté. Parmi les modes de détection par UV, barrettes de diode (DAD) ou par scintillation, la spectrométrie de masse en mode ESI offre l'avantage de déterminer la présence simultanée de plusieurs inhibiteurs potentiels et d'en déterminer une formule chimique brute. Cette stratégie permet par ailleurs l'utilisation d'autres sources d'ionisation telles que l'APCI ou l'APPI.

Vient ensuite une démarche d'optimisation du support sur lequel seront immobilisées les enzymes. Cette démarche est essentielle, en particulier en chromatographie d'affinité frontale, afin d'éviter au maximum la présence « d'interactions non spécifiques » lors d'un test de criblage. C'est pourquoi, ce phénomène a été évalué à travers une étude globale sur l'influence de la nature des monolithes en fonction de la nature (charge et polarité) de composés modèles. Une première stratégie a consisté à synthétiser des monolithes de nature organique poly(SBMA-co-AEMA-co-EGDMA) ou poly(NAS-co-EGDMA) et inorganiques (silice) au sein de capillaires. Par la suite, une seconde approche a conduit à la synthèse de billes de silices (silica-APTES-GLA et silica-oxGPTMS) destinées à remplir des cartouches analytiques.

La comparaison des monolithes organiques poly(SBMA-co-AEMA-co-EGDMA) et poly(NAS-co-EGDMA) révèle une complémentarité entre les deux formulations. En effet, bien que nous observions en présence des deux monolithes des **interactions non spécifiques faibles** avec les composés polaires, les **interactions non spécifiques fortes** avec des composés hydrophobes tels que l'ibuprofène ou la 1-phenylethylamine peuvent être évitées. Dans le cadre du support à base de billes de silices, nous observons la même complémentarité. Cependant, la synthèse de silica-APTES-GLA semble retenir les analytes fortement ou modérément hydrophobes, ainsi que les analytes négativement chargés (l'ibuprofène, DHPA et warfarin) contrairement au support silica-oxGPTMS. De ce fait, à travers cette étude, un abaque a pu être mis en place, nous permettant ainsi de sélectionner la surface appropriée (monolithe ou billes de silice) pour la chromatographie d'affinité frontale en phase aqueuse.

Au cours de ce travail, il s'est avéré que le support monolithe présentant la meilleure performance pour l'analyse frontale avec la tyrosinase comme enzyme immobilisée était le poly(NAS-co-EGDMA). Dans le cadre des études menées sur les billes de silices, le support de silica-oxGPTMS ont été préférées pour l'immobilisation de l'enzyme modèle (la trypsine) alors que pour l'enzyme d'intérêt (la

tyrosinase) l'immobilisation sur billes de silica-APTES-GLA a donné les meilleurs résultats. Bien qu'il soit montré dans ce chapitre l'intérêt de l'analyse frontale en se basant sur la présence dans nos échantillons que d'un seul inhibiteur, il est certain que cette méthodologie peut s'appliquer à l'analyse de mélanges complexes dans lesquels seraient susceptibles d'être présents plusieurs inhibiteurs. L'analyse frontale couplée à la spectrométrie de masse ouvre ici la possibilité de trouver de nouveaux inhibiteurs dans les extraits de plantes et constitue ainsi une alternative au fractionnement bio-guidé.

Les avantages de l'analyse frontale, dans le cadre de nos recherches, mis en avant par comparaison aux essais enzymatiques classiques sont :

- une caractérisation simultanée, rapide et automatique des interactions enzymes/inhibiteurs spécifiques, sans avoir recours à des marqueurs d'activité enzymatique, à partir de mélanges complexes tels que les extraits de plantes,

- la détermination de la constante de dissociation  $K_d$  du complexe enzyme/inhibiteur en travaillant à concentration connue d'inhibiteur,

- de faire plusieurs cycles de criblage moléculaire avec les mêmes lots d'enzymes immobilisée et ce avec une consommation faible d'enzyme de l'ordre de la picomole pour un capillaire ou de la nanomole pour une colonne remplies (silice),

- de travailler avec un large éventail d'enzymes immobilisées.

## **Chapter II** – Frontal affinity chromatography

<b>I. Frontal affinity chromatography: from theory to practice.....</b>	<b>45</b>
<b>I.1. An introduction to frontal affinity chromatography.....</b>	<b>45</b>
I.1.1. The historical background of frontal affinity chromatography.....	45
I.1.2 The principle and mathematical description of frontal analysis.....	45
I.1.2.1. A 'single infusion' approach.....	46
I.1.2.2. Staircase frontal analysis.....	48
<b>I.2. Selection of appropriate detection method.....</b>	<b>51</b>
<b>I.3. Non-specific interactions of analyte with the stationary phases. Selection of appropriate immobilisation support.....</b>	<b>52</b>
<b>I.4. The pathways of protein immobilisation commonly applied for frontal affinity chromatography.....</b>	<b>53</b>
<b>II. Stationary phases for FAC: development and application of FAC for searching for the inhibitors of tyrosinase and trypsin.....</b>	<b>57</b>
<b>II.1. Aims and objectives.....</b>	<b>57</b>
<b>II.2. Stationary phases for FAC.....</b>	<b>57</b>
<b>II.2.1. Capillary-format monoliths.....</b>	<b>57</b>
II.2.1.1. Organic monoliths based on esters of acrylic and methacrylic acid.....	58
II.2.1.1.1 Preparation of amine-covered hydrophilic organic poly(SBMA-co-AEMA-co-EGDMA) monolith with the surface hydrophilized by zwitterionic moieties.....	59
II.2.1.1.2 Preparation of hydrophilic monolith based on N-acryloxysuccinimide.....	61
II.2.1.2. Silica monoliths.....	61
II.2.1.2.1 Preparation of organic-inorganic silica monolith based on APTES/TEOS using surfactant as a porogen.....	62
II.2.1.2.2 Preparation of organic-inorganic silica monolith based on APTES/TEOS using room-temperature ionic liquid as co-porogen.....	62
<b>II.2.2. Silica beads as an immobilisation support.....</b>	<b>63</b>
II.2.2.1. Chromatographic support for silica beads.....	64
<b>II.3. Protein immobilisation on the surface of monoliths and silica particles.....</b>	<b>64</b>
<b>II.3.1. Capillary-format monoliths.....</b>	<b>65</b>
II.3.1.1. Derivatisation and preparation of the capillaries for enzyme immobilisation.....	66
II.3.1.1.1. Amine-bearing monoliths.....	66
II.3.1.1.2. Poly(NAS-co-EGDMA) monolith.....	66
II.3.1.2. Enzyme immobilisation: capillary-format monoliths.....	67
<b>II.3.2. Silica beads.....</b>	<b>67</b>
<b>II.3.2.1. Derivatisation of silica beads.....</b>	<b>67</b>
II.3.2.1.1 Activation of silica-APTES beads.....	67
II.3.2.1.2 Activation of silica-GPTMS beads.....	68
<b>II.3.2.2. Enzyme immobilisation: silica beads.....</b>	<b>68</b>
II.3.2.2.1. Immobilisation of tyrosinase on silica-APTES-GLA beads.....	68
II.3.2.2.2. Immobilisation of trypsin on silica-oxGPTMS beads.....	68
<b>III. Evaluation of the stationary phases for FAC.....</b>	<b>69</b>
<b>III.1. Trypsin as a biological target for method validation.....</b>	<b>69</b>
<b>III.2 Configuration of the experimental system.....</b>	<b>70</b>
III.2.1. Silica-packed cartridges.....	70
III.2.2. Capillary-format FAC.....	70

<b>III.3. Assessment of the nature of non-specific interactions for developed stationary phases.....</b>	<b>71</b>
<b>III.3.1. Capillary-format stationary phase.....</b>	<b>72</b>
III.3.1.1. Organic monoliths.....	72
III.3.1.2. Silica monoliths.....	75
<b>III.3.2. Silica particle-based stationary phases.....</b>	<b>76</b>
<b>III.3.3. Selection of the stationary phase for FAC: conclusions.....</b>	<b>78</b>
<b>IV.1. FAC experiment using tyrosinase and trypsin as biological targets.....</b>	<b>78</b>
IV.1.1. Capillary-format organic monoliths.....	78
IV.1.2. Silica particles.....	81
<b>IV.2. FAC – conclusions.....</b>	<b>84</b>
<b>V. Continuous-flow step gradient mass spectrometry based method for the determination of kinetic parameters of immobilised mushroom tyrosinase in equilibrating conditions: comparison with free enzyme.....</b>	<b>84</b>
<b>Appendix I: Supplementary Information.....</b>	<b>91</b>

## ***I. Frontal affinity chromatography: from theory to practice***

### ***I.1. An introduction to frontal affinity chromatography***

#### *I.1.1. The historical background of frontal affinity chromatography*

The origin of modern frontal affinity chromatography (FAC), commonly known as frontal analysis (FA), dates back to the late 1960s, when the first chromatographic approach based on a specific protein-ligand interaction was used to purify avidin from eggs using stationary phase with superficial biotin moieties [199]. Since then, affinity chromatography has been accepted as a simple way of purification of wide range of biomolecules, *e.g.* serine proteases, using peptide-coupled stationary phases [200]; antibodies, using immobilised immunoglobulin-binding proteins A or G [201, 202]; recombinant proteins artificially tagged with cleavable terminal poly-histidine peptide (His-tag), using a metal chelate adsorbent [168] and many others. The quantitative potential of FAC was demonstrated for the first time in 1975 by Kasai *et al.* [203] on the basis of the experiment employing glycyglycyl-L-arginine-bound stationary phase to determine dissociation constant values for various trypsin isozymes. This work was a simple extension of the classic preparative affinity chromatography which employs immobilised ligand and 'free' biomolecule. Nevertheless, the true protoplast of contemporary FAC was a 'reverse' approach: an application of immobilised biomolecular target and the ligand solution, published for the first time by Kasai in 1986 (*p. I.4, table 1, entry 1, page 54*) [204].

#### *I.1.2 The principle and mathematical description of frontal analysis*

Frontal analysis (FA) experiment in its simplest form is based on the continuous infusion of the studied inhibitor/ligand into the analytical support with immobilised macromolecular target (enzyme, receptor or antibody). This experiment design entails the characteristic shape of the elution profile of each compound in studied mixture (**fig. 1**): baseline plateau (**a**); breakthrough area with the inflection point (**b**) and the upper plateau (**c**).

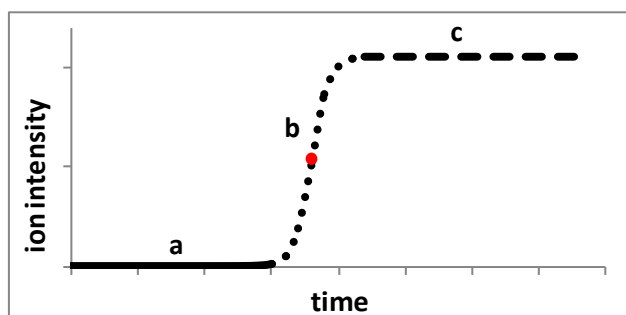


**Figure 1.** Breakthrough curve in frontal chromatography. Baseline plateau (**a**); breakthrough area with the inflection point (red) (**b**) and the upper plateau (**c**).

In case of the application of MS detection, we can follow ionisable ligands/markers independently by extracting their individual curves from the total ion current (*p. 1.4, table 2*, page 55).

### 1.1.2.1. A 'single infusion' approach

In further example we will take into consideration a mixture containing inhibitor and two non-interacting compounds infused into the column filled with solid support hosting immobilised enzyme (**fig. 2**), analysed by MS as the detector (selection of an optimal detector is discussed in *p. 1.2*). Additionally, we will assume that none of compounds within the test mixture interact non-specifically (*e.g.* by ionic, hydrophobic interactions) with the stationary phase<sup>†</sup>.

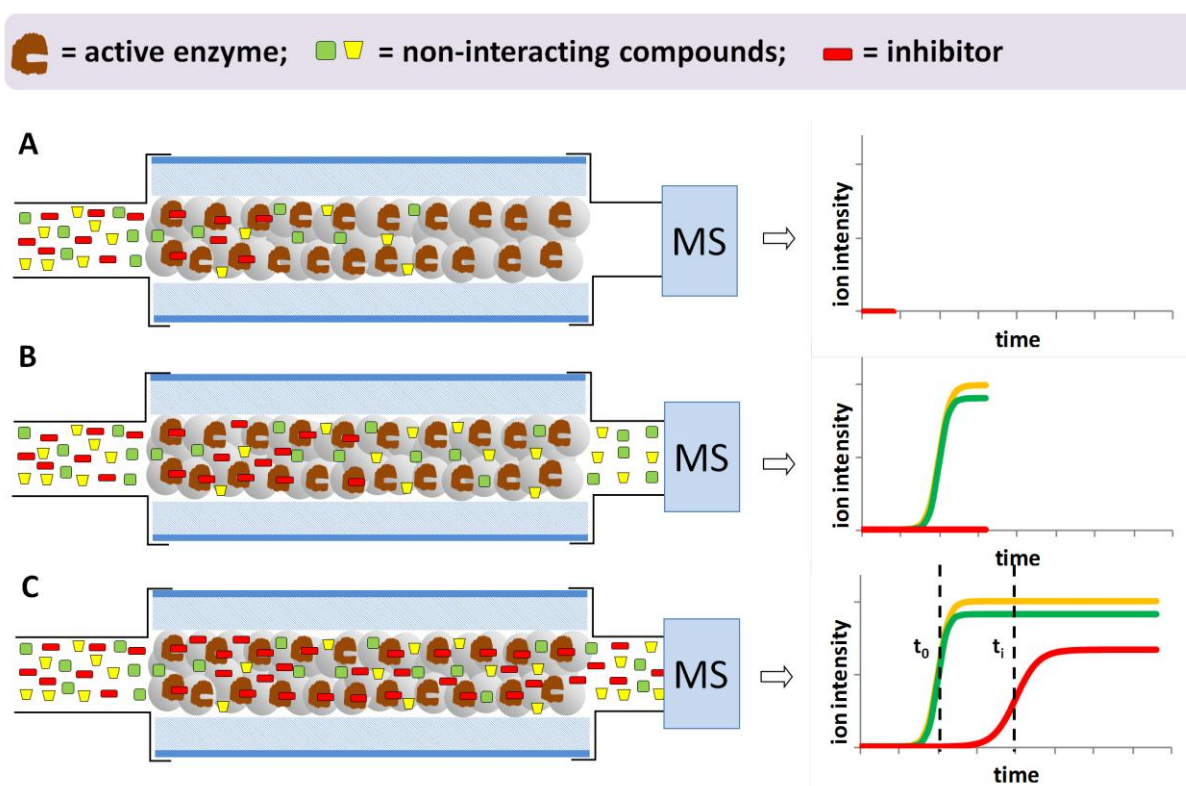


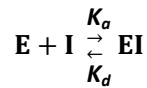
**Figure 2.** Schematic visualization of the interaction pattern of the components of the mixture of interacting and non-interacting compounds in the bioreactor (left) and the visualization of the EICs for each compound on various stages of frontal analysis experiment.

During the first stage of FA experiment (**fig. 2-A**) non-interacting compounds within infused plug pass freely through the bioreactor. Simultaneously, inhibitor molecules start to bind to immobilised enzyme molecules (**fig. 2-A**), and thus the front of extracted ion chromatogram (EIC) representing the inhibitor is delayed in respect to the fronts of non-interacting compounds (**fig. 2-B**). Finally, when the saturation level of the column is exceeded, inhibitor molecules start to appear in the mobile phase within the post-

<sup>†</sup> The issue of non-specific interactions in FAC is discussed in *p. 1.3* of present chapter.

bioreactor zone (**fig. 2-C**) and may be detected by mass spectrometer. The level of the column saturation for given inhibitor is strictly related with enzyme-inhibitor dissociation constant ( $K_d$ ): the lower  $K_d$  is, the stronger these interactions are and, consequently, the bigger delay of inhibitor-related EIC.

Let us take into consideration an inhibitor (I) that binds to enzyme (E) in reversible way to form an enzyme-inhibitor complex (EI), according to the following equation:



where:  $K_a$  - association constant [ $M^{-1}$ ];  $K_d$  - dissociation constant [ $M$ ]

Dissociation constant of the enzyme-inhibitor complex may be expressed as the following equation:

$$K_d = \frac{[\text{I}][\text{E}]}{[\text{EI}]} \quad (1)$$

Let us consider a column with immobilised enzyme having the volume  $v$ , (L), and the inhibitor **I** posing no non-specific interactions to the solid immobilisation support. If one infuses continuously a mobile phase containing the inhibitor having a concentration of **[I]**, ( $\mu\text{M}$ ), then we can conclude that the amount of inhibitor **I** specifically bound to the enzyme is equal to **[I]( $V_{\text{inh}}-V_0$ )**, ( $\mu\text{mol}$ ), where  $V_0$ , (L). is a volume of the mobile phase required for elution of the inhibitor from the control column devoid of the enzyme (or, alternatively, hosting denatured enzyme), which, in considered experimental conditions, is equal to the elution volume of a void volume marker;  $V_{\text{inh}}$  indicates a volume of the mobile phase required for elution of the inhibitor. The value **( $V_{\text{inh}}-V_0$ )**, (L), represents the volume of the mobile phase containing the inhibitor **I** at the concentration **[I]** which would pass through the column in the event of lack of the specific enzyme-inhibitor interaction. In other words, the value **( $V_{\text{inh}}-V_0$ )** represents the volume of **I** solution containing the amount of **I** that was specifically bound to the column. All values of 'volumes' mentioned above may be obtained by multiplying the **flow rate**, (L/min), of the mobile phase by **time**, (min), representing the inflection points of breakthrough curves, **fig. 2-C**. Consequently, the expression **[I]( $V_{\text{inh}}-V_0$ )/ $v$** , ( $\mu\text{M}$ ), describes the total concentration of the inhibitor specifically trapped in the column. The latter value is equal to the concentration of enzyme-inhibitor complex in the column. We can also notice that the total concentration of the enzyme in the column, **[E]<sub>tot</sub>**, ( $\mu\text{M}$ ), may be described as the amount of enzyme immobilised in the column divided by its volume  $v$ :  **$B_e/v$** , ( $\mu\text{M}$ ). Finally, we can conclude that the total concentration of unoccupied enzyme in the column may be expressed as **[E]<sub>tot</sub>** minus the concentration of EI complex, **[EI]**, formed in the experimental conditions. Taking into account the **equation 1** and all remarks above, we obtain the following equation describing an equilibrium state of the system:



$$K_d = \frac{[I]\{[E]_{\text{tot}} - [EI]\}}{[I] \frac{(V_{\text{inh}} - V_0)}{v}} = \frac{[I] \left\{ \frac{B_t}{v} - [I] \frac{(V_{\text{inh}} - V_0)}{v} \right\}}{[I] \frac{(V_{\text{inh}} - V_0)}{v}} = \frac{[I] \frac{B_t}{v} - [I]^2 \frac{(V_{\text{inh}} - V_0)}{v}}{[I] \frac{(V_{\text{inh}} - V_0)}{v}}$$

$$K_d = \frac{B_t}{(V_{\text{inh}} - V_0)} - [I] \quad (2)$$

The **equation 2** can be also converted into the following form ('FA' equation):

$$\frac{1}{[I](V_{\text{inh}} - V_0)} = \frac{K_d}{B_t} \cdot \frac{1}{[I]} + \frac{1}{B_t} \quad (3)$$

The values  $1/[I](V_{\text{inh}} - V_0)$  obtained for few various inhibitor concentrations plotted against  $1/[I]$  should give a linear relation and allow to determine  $B_t$  and  $K_d$  directly from the graph (**fig. 3**).

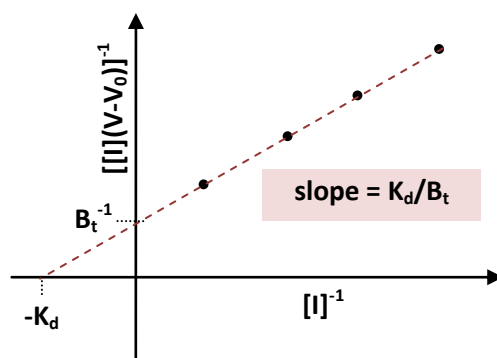


**Figure 3.** Graphical representation of the **equation 3** for the series of inhibitor infusions.

#### 1.1.2.2. Staircase frontal analysis

If FA experiment is aimed at a simple screening or ligand ranking, a single infusion of studied mixture is enough (**table 2**, entries **1-12**). The complete experiment includes determination of  $K_d$  value for given inhibitor or ligand requires a series of infusions of the inhibitor solutions differing in its concentration (**fig. 3**). This procedure might be time-consuming because it requires very thorough wash of the column after each infusion to remove all inhibitor molecules to liberate all active sites inside the column [166, 167]. The length of required washing time depends on the strength of the inhibitor's affinity and may last hours. If one fails to wash the column properly, some fraction of enzymes' active sites is blocked and an apparent breakthrough time for given run is lower. A staircase FA may help to address this issue by eliminating the need of incorporation of washing steps in-between the individual runs (**fig. 4**). It is based on application of the stairs-like gradient generated by two HPLC pumps: one of them is supplied by mobile phase and the second one with mobile phase containing studied inhibitor or ligand.

Since the first step of 'staircase' approach is identical to the classic frontal analysis run (**fig. 1**), we can rewrite the **equation 2** for this step (**fig. 4**) in the following form:

$$[I_1] = \frac{B_t}{(V_{inh,1} - V_{0,1})} - K_d \quad (4: 1^{st} \text{ step})$$

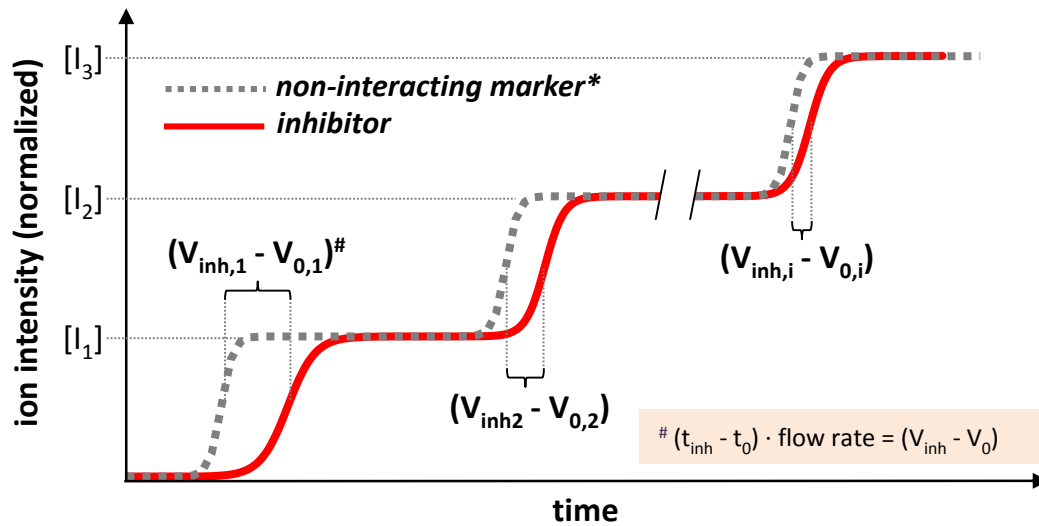


**Figure 4.** General outlook of the staircase FAC experiment. (\*) this experiment may be considered to be the final one only if the inhibitor does not pose any nonspecific interaction with the stationary phase.

When considering the second step of the staircase gradient, we have to take into account the fact that certain fraction of immobilised enzyme molecules had already been 'blocked' by the inhibitor when the first step was finished. As we stated in the first chapter, an amount of inhibitor specifically bound to our biological target is equal to  $[I](V_{inh}-V_0)$ , ( $\mu\text{mol}$ ), where  $[I]$ , ( $\mu\text{M}$ ), is the concentration of the inhibitor for which the delay  $(V_{inh}-V_0)$ , (L) was observed. The amount of the enzyme 'blocked' during the first step is thus equal to  $[I_1](V_{inh,1}-V_{0,1})$ , ( $\mu\text{mol}$ ). Consequently, we can write the following equation for the second step:

$$[I_2] = -\frac{[I_1](V_{inh,1} - V_{0,1})}{(V_{inh,2} - V_{0,2})} + \frac{B_t}{(V_{inh,2} - V_{0,2})} - K_d$$

$$[I_2] = \frac{B_t - [I_1](V_{inh,1} - V_{0,1})}{(V_{inh,2} - V_{0,2})} - K_d$$

$$[I_2] + \frac{[I_1](V_{inh,1} - V_{0,1})}{(V_{inh,2} - V_{0,2})} = \frac{B_t}{(V_{inh,2} - V_{0,2})} - K_d \quad (5: 2^{nd} \text{ step})$$

An augmentation of the inhibitor concentration from  $[I_1]$  to  $[I_2]$  increases the portion of 'blocked' enzyme sites by the value of  $([I_2]-[I_1])(V_{inh,2}-V_{0,2})$ . We can thus conclude that the overall amount of 'blocked'

enzyme sites after the second step of the staircase gradient is equal to  $[[I_1](V_{inh,1}-V_{0,1}) + ([I_2]-[I_1])(V_{inh,2}-V_{0,2})]$ . Consequently, we can write the following equation for the third step:

$$[I_3] = \frac{B_t - [I_1](V_{inh,1} - V_{0,1}) - ([I_2] - [I_1])(V_{inh,2} - V_{0,2})}{(V_{inh,3} - V_{0,3})} - K_d$$

$$[I_3] = \frac{-[I_1](V_{inh,1} - V_{0,1}) - ([I_2] - [I_1])(V_{inh,2} - V_{0,2})}{(V_{inh,3} - V_{0,3})} + \frac{B_t}{(V_{inh,3} - V_{0,3})} - K_d$$

$$[I_3] + \frac{[I_1](V_{inh,1} - V_{0,1}) + ([I_2] - [I_1])(V_{inh,2} - V_{0,2})}{(V_{inh,3} - V_{0,3})} = \frac{B_t}{(V_{inh,3} - V_{0,3})} - K_d \quad (6: 3^{rd} \text{ step})$$

The left sides of **equations 4, 5 and 6** are analogous. The general equation for the staircase frontal analysis may thus be summarized in a form of **equation 7** and expressed in a graphical form as it was shown in **fig. 5**.

$$[I_j] + y_j = \frac{B_t}{(V_{inh,j} - V_{0,j})} - K_d \quad (7)$$

$$\begin{cases} y_1 = 0 \\ y_2 = \frac{[I_1](V_{inh,1} - V_{0,1})}{(V_{inh,2} - V_{0,2})} \\ y_{j>2} = \frac{\sum_{i=1}^{j-1} ([I_i] - [I_{i-1}])(V_{inh,i} - V_{0,i})}{(V_{inh,j} - V_{0,j})} \end{cases}$$

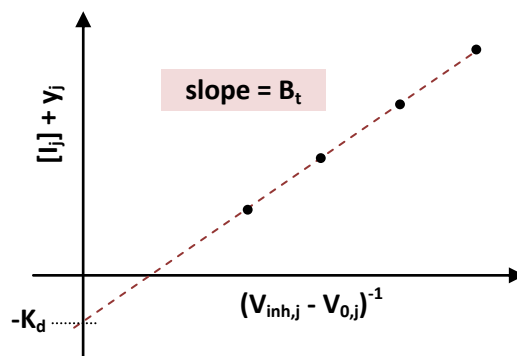


**Figure 5.** Graphical representation of the **equation 7** for a single run of staircase frontal analysis.

An application of staircase frontal analysis for studying immobilised molecules was published for the first time by Chan *et al.* in 2003 [165]. In quoted work, authors modified the graphical interpretation of the **equation 7**: the value  $(V_{inh,j} - V_{0,j})^{-1}$  was plotted against  $([I_j] + y_j)$ , and, consequently, the graph slope represented the reciprocal value of  $B_t$  (instead of  $B_t$  in **fig. 5**) and y-intercept represented  $K_d/B_t$  (instead of  $-K_d$  in **fig. 5**). The graphical representation shown in this manuscript was proposed for the first time by Slon-Usakiewicz *et al.* [62].

### 1.2. Selection of appropriate detection method

A detection method is of key importance for the range of possible applications of frontal affinity chromatography. FAC may be successfully applied as a tool for determining  $K_d$  of individual inhibitors even using simple UV or DAD detectors (**table 1**, entry **1-5**, page 54) [181-183, 192, 204]. In such cases, due to lack of selectivity of UV detector, only one molecule may be studied at the same time. Moreover, a control column without an active biological target must be applied to eliminate the risk of erroneous results caused by non-specific interactions of studied molecule and the stationary phase. Because of the lack of void volume marker, the flow rate must be accurate to ensure repeatable results.

Moaddel *et al.* published a series of papers devoted to the use of on-line scintillation detector for studying ligand-receptor interactions for several biological targets (**table 1**, entries **6-8**, page 54) [172, 205, 206]. This approach is based on application of known [ $^3\text{H}$ ]-labelled marker ligand of studied biological target that can be selectively tracked by the scintillation detector. If the marker-competitive ligands are present in the analyzed mixture, they will displace the marker from the receptor's binding site and thus shorten the inflection time of marker's breakthrough curve (the only one that can be monitored by scintillation detector). The main drawback of this approach is the need to apply target-specific radioactive marker. Moreover, in case of studying complex mixtures (*e.g.* plant extracts), it is not possible to elucidate which particular molecule within the mixture is responsible for the marker displacement.

To circumvent these drawbacks, mass spectrometry was used for the first time as FAC-coupled detection unit in 1998 by Schriemer *et al.* [166], leading to the popularisation of this approach in the domain of inhibitor/ligand screening (**table 2**, **fig. 6**).

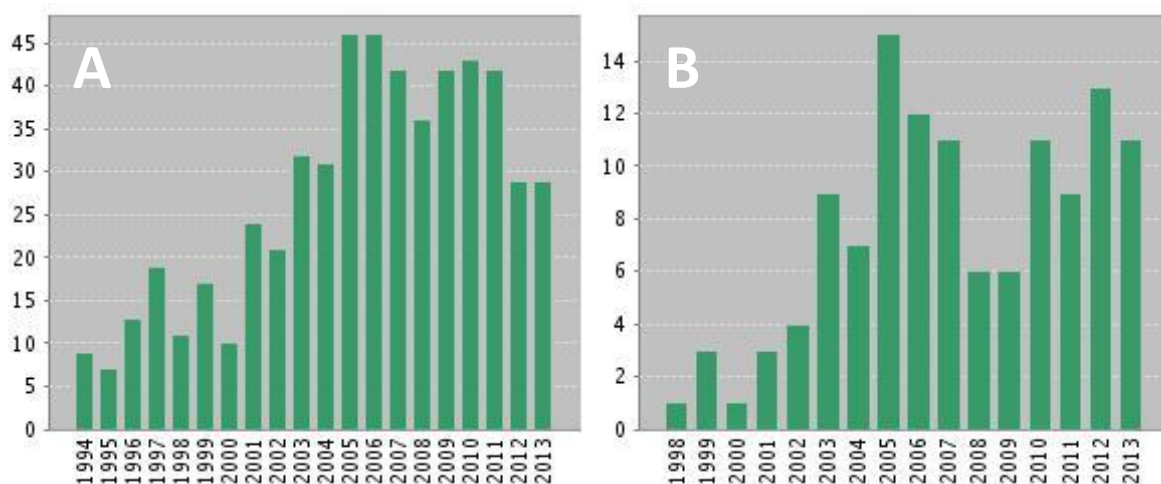


**Figure 6.** The number of papers containing the following expression within the topic: **A:** "frontal affinity chromatography"; **B:** "frontal affinity chromatography" AND "mass spectrometry" published within the last twenty years (according to Thomson Reuters, October 2013).

The major advantage of using mass spectrometry in coupling with FAC is the possibility to follow all (or most of) ions present in the studied mixture independently in a form of extracted ion chromatograms (EIC). It provides an additional dimension of the data analysis comparing to UV/Vis and allows to bypass

the limitations related with the use of scintillation detector described in the previous paragraph. Mass spectrometry offers an outstanding sensitivity (the analyte concentrations applied during the experiments described in further part of this manuscript were within the range of 0.5–1  $\mu\text{M}$ ). Contemporary mass spectrometers (e.g. Bruker *maXis* used in our laboratory) are compatible with a wide choice of ion sources enabling ionisation of various families of compounds, e.g. electrospray ionisation (ESI) is a suitable way to ionize polar molecules of a wide mass range, atmospheric-pressure chemical ionisation (APCI) may be applied to small polar to moderately hydrophobic, thermally-stable molecules, finally, atmospheric-pressure photoionisation (APCI) may be employed to ionize highly hydrophobic molecules, such as fullerenes [207]. The only limitation associated with the coupling of FAC/MS is the use of compatible buffers that must be composed of the volatile salts, such as ammonium formate or acetate. Ammonium salts are compatible with numerous immobilised proteins (**table 2**, column **C9**) and were successfully applied as a mobile phase and a storage buffer for all immobilised enzymes described in the present manuscript (tyrosinase, trypsin and TMPK kinases).

In conclusion, mass spectrometry is unrivalled selection for frontal affinity chromatography. Mass spectrometry, in contrast to UV/Vis or scintillation detectors, offers the possibility to track the constituents of complex mixtures independently.

### ***1.3. Non-specific interactions of analyte with the stationary phases. Selection of appropriate immobilisation support***

The choice of mobile phases used in FAC is in principle limited to highly aqueous solutions (**table 1** and **2**), to avoid the risk of denaturation of immobilised biological target. This environment highly promotes hydrophobic interactions between non-polar molecules and the stationary phase. Consequently, immobilisation supports should be as hydrophilic as possible. As can be seen in the **table 1** and **2**, **column C2**, immobilisation supports are made of highly hydrophilic materials, such as silica-based beads or crosslinked agarose (in beaded form known as Sepharose). Important to note is the fact that the global property of given stationary phase depends not only on the type of support but – even more significantly – on the type of superficial coating (e.g. few works listed in the **table 2** report the use of polystyrene-based beads, but with hydrophilized surface, on the other hand,  $\text{C}_{18}$ -coated silica beads are routinely applied as the hydrophobic stationary phase for reversed-phase chromatography [208]). As a result, even for hydrophilic support, one may observe a high degree of hydrophobic non-specific interactions if inappropriate immobilisation method is selected.

If the inhibitors of interest interact with the stationary phase in non-specific way, the overall shift of its breakthrough curve for an 'active' column (**fig. 7-A**, 'TI') will be the sum of the shifts related to specific ('SI') and non-specific ('NI') interactions (**fig. 7**). Consequently, to ensure that the results of FAC experiment are not altered by unexpected non-specific interactions, it is necessary to perform the control

run using 'blank' immobilisation support without the target enzyme or with denatured one (**fig. 7/B, table 1 and 2, column C7**).

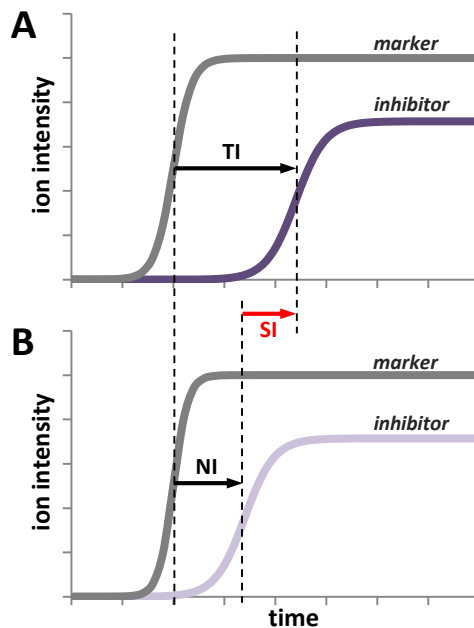


**Figure 7.** The comparison of frontal affinity experiments in the presence of non-specific interactions between the inhibitor and the immobilisation support, performed using 'active' column containing fully functional biological target (**A**) and the 'control' run obtained using 'blank' column without the target or with denatured (non-functional) one (**B**). **TI**: overall interaction between the inhibitor and the column; **NI**: non-specific interaction; **SI**: specific interaction between the inhibitor and the biological target.

#### **1.4. The pathways of protein immobilisation commonly applied for frontal affinity chromatography**

When considering the immobilisation methods employed to produce stationary phases dedicated to frontal analysis (**table 1 and 2, column C7**), we can distinguish three leading approaches: *i*) covalent immobilisation of the protein to the solid support (applicable for enzymes, antibodies, receptors); *ii*) immobilisation using streptavidin/avidin-biotin system (applicable for enzymes, antibodies, receptors), **fig. 8**; *iii*) and an application of immobilised artificial membrane (IAM) to immobilize membrane receptors.

**Table 1. Examples of application of FAC without coupling to mass spectrometry**

C1	C2	C3	C4	C5	C6	C7	C8	C9	C10	C11
Entr.	The type of solid immobilisation support	The total volume/ID of chromatographic bed	Biological target	The type of analysed molecules	The type of protein-surface attachment (p. 1.4)	Control (blank) experiment	Biological target pre-treatment	Buffer	Detection method	Source
1	Sepharose 4B	4300 $\mu\text{L}$ / not stated	Carboxymethylated ribonuclease T <sub>1</sub>	Guanosine	Not stated	No blank, adenosine as V <sub>0</sub> marker	NO	50 mM sodium acetate buffer, pH 5.5	UV/Vis	[204]
2	Hydrazide-activated silica beads	831 $\mu\text{L}$ /4600 $\mu\text{m}$	$\alpha$ 1-acid glycoprotein (AGP)	Carbamazepine	Beads–protein (hydrazide-activated beads reacted with aldehyde groups of oxidised AGP protein)	Naked immobilisation support	YES	Potassium phosphate buffer, 67 mM, pH 7.4		[192]
3	Diol-bonded silica beads	34.6 $\mu\text{L}$ /2100 $\mu\text{m}$	Monoclonal antibodies for 2,4-dichlorophenoxyacetic acid	2,4-dichlorophenoxyacetic acid	Superficial diol groups were oxidised to aldehyde and coupled with antibodies	Naked immobilisation support	NO	Potassium phosphate buffer, 100 mM, pH 7.0		[181]
4	Diol-bonded silica beads	3.46-69.3 $\mu\text{L}$ /2100 $\mu\text{m}$	human serum albumin (HSA)	Warfarin	Superficial diol groups were oxidised to aldehyde and coupled with HSA	Naked immobilisation support	NO	Potassium phosphate buffer, 67 mM, pH 7.4		[182]
5	Diol-bonded silica beads	346 $\mu\text{L}$ /2100 $\mu\text{m}$	Low-density lipoprotein (LDL)	Propranolol	Superficial diol groups were oxidised to aldehyde and coupled with LDL	Naked immobilisation support	NO	Potassium phosphate buffer, 67 mM, pH 7.4		[183]
6	IAM** silica beads	2945 $\mu\text{L}$ /5000 $\mu\text{m}$	Nicotinic receptor, $\gamma$ -Amino-Butyric Acid receptors, N-Methyl D-Aspartate receptor (co-immobilised)	Known ligands of studied receptors (small aromatic organic molecules)	IAM alone	None (ligand-displacement approach)	NO	Tris–HCl, 50mM, pH 7.4, containing 5 mM EDTA, 3 mM benzamidine, 0.2 mM phenyl methyl sulfonyl fluoride	on-line scintillation detector	[205]
7	IAM silica beads	2945 $\mu\text{L}$ /5000 $\mu\text{m}$	G-protein-coupled receptor	Histamine derivatives	IAM alone	None (ligand-displacement approach)	NO	Tris–HCl, 10mM, pH 7.5, containing 1 mM MgCl <sub>2</sub>		[206]
8	Open tubular silica capillary derivatised with APTES-GLA-avidin-biotin X***	1.96 $\mu\text{L}$ /100 $\mu\text{m}$	CB1/CB2 cannabinoid receptors	Small aromatic organic molecules	Solubilised cell membranes containing CB1/CB2 receptors immobilised on the surface of the IAM-like capillary wall	None (ligand-displacement approach)	NO	10 mM NH <sub>4</sub> OAc*, pH 7.4 /MeOH (90/10, v/v)		[209]

\* - NH<sub>4</sub>OAc: ammonium formate

\*\* - IAM: immobilised artificial membrane

\*\*\* - biotin-X: 6-[(Biotinoyl)amino]hexanoic acid

**Table 2. Examples of application of FAC coupled to mass spectrometry**

C1	C2	C3	C4	C5	C6	C7	C8	C9	C10
Entr.	The type of solid immobilisation support	The total volume/ID of chromatographic bed	Biological target (BT)	The type of analysed molecules	The type of protein-surface attachment	Control (blank) experiment	Biological target pre-treatment	Buffer	Source
1	Beads covalently linked with avidin	23 $\mu\text{L}/500 \mu\text{m}$	Carbohydrate-binding monoclonal antibodies	Carbohydrates	Beads–avidin–biotinylated antibody	None (ligand-displacement approach)	YES (biotinylation)	2 mM $\text{NH}_4\text{OAc}$ , pH 6.7	[166]
2	Polystyrene-based beads with hydrophilic surface linked with streptavidin	19.6 $\mu\text{L}/500 \mu\text{m}$	N-acetylglucosaminyltransferase V (GnT-V)	Trisaccharide analogs	Beads–streptavidin–biotinylated GnT-V	Immobilisation support end-capped with biotin	YES (biotinylation)	2 mM $\text{NH}_4\text{OAc}$ , pH 6.6	[210]
3	Sepharose CL-4B derivatised with epichlorohydrin (epoxy-activated)	104 $\mu\text{L}/2100 \mu\text{m}$	Polyclonal antibodies against EGFR inhibitor	Extract of <i>Cortaderia jubata</i>	Beads–antibody (coupled by amine-epoxide nucleophilic addition)	Immobilisation support end-capped with BSA	NO	2 mM $\text{NH}_4\text{OAc}$	[211]
4	Polystyrene-based beads with hydrophilic surface linked with streptavidin	2.90 $\mu\text{L}/250 \mu\text{m}$	N-acetylglucosaminyltransferase V (GnT-V)	Trisaccharide analogs	Beads–streptavidin–biotinylated GnT-V	Immobilisation support end-capped with biotin	YES (biotinylation)	25 mM $\text{NH}_4\text{OAc}$ , pH 6.6	[167]
5	IAM silica beads	102.6 $\mu\text{L}/6600 \mu\text{m}$	G-protein-coupled receptor (GPR17)	Nucleotide analogs	IAM	Unoccupied IAM	NO	5 mM $\text{NH}_4\text{OAc}$ , pH 7.4 /MeOH (90/10, v/v)	[212]
6	Open tubular silica capillary derivatised with APTES and GLA	3.14 $\mu\text{L}/100 \mu\text{m}$ (capillary)	Ligand binding domains of peroxisome proliferator-activated receptors (PPAR $\gamma$ )	Small aromatic organic molecules (carboxylic acids)	Capillary wall–APTES–GLA–PPAR $\gamma$	Naked immobilisation support	NO	10 mM $\text{NH}_4\text{OAc}$ , pH 7.4 /MeOH (90/10, v/v)	[180]
7	Diglycerylsilane-APTES monolith containing an entrapped transmembrane receptor	7.36 $\mu\text{L}/250 \mu\text{m}$ (capillary)	Nicotinic acetylcholine receptor (nAChR)	Epibatidine (low-mass alkaloid)	Microsomes containing nAChR entrapped within capillary-scale silica monolith	1) blank capillary (no microsomes); 2) heat-denatured nAChR column	NO	20 mM $\text{NH}_4\text{OAc}$	[95]
8	Cyanogen bromide-activated Sepharose 4B	~ 10 $\mu\text{L}/1613 \mu\text{m}$	Truncated peroxin (tPex5)	Peptides	Superficial cyanate ester groups react with the amine groups of protein	Naked immobilisation support	NO	4.5 mM 2,2-difluoroethylamine, 2.3 mM acetic acid, pH 7.0	[185]



## Chapter II – Frontal Affinity Chromatography

C1	C2	C3	C4	C5	C6	C7	C8	C9	C10
Entr.	The type of solid immobilisation support	The total volume/ID of chromatographic bed	Biological target (BT)	The type of analysed molecules	The type of protein-surface attachment	Control (blank) experiment	Biological target pre-treatment	Buffer	Source
9	IAM silica beads	102.6-307.9 $\mu\text{L}/6600 \mu\text{m}$	G-protein-coupled receptor (GPR17)	Nucleotide analogs	IAM	IAM prepared using membranes from the cell line without GPR17 expression	NO	10 mM $\text{NH}_4\text{OAc}$ , pH 7.4 /MeOH (90/10, v/v)	[213]
10	Open tubular silica capillary derivatised with APTES and GLA	3.14 $\mu\text{L}/100 \mu\text{m}$ (capillary)	Ligand binding domains of peroxisome proliferator-activated receptors (PPAR $\alpha/\gamma$ )	Small aromatic organic molecules	Capillary wall-APTES-GLA-PPAR $\alpha/\gamma$	None (for $K_d$ determination); ligand-displacement approach	NO	10 mM $\text{NH}_4\text{OAc}$ , pH 7.4 /MeOH (90/10, v/v)	[94]
11	Sepharose CL-4B derivatised with epichlorohydrin	104 $\mu\text{L}/2100 \mu\text{m}$	Polyclonal antibodies mimicking NS3 protease of HCV	<i>Phyllanthus urinaria</i> extract	Beads-antibody (coupled by amine-epoxide nucleophilic addition)	-	NO	2 mM $\text{NH}_4\text{OAc}$ , pH 6.7	[186]
12	Silica beads with streptavidin	1.22 $\mu\text{L}/250 \mu\text{m}$	EphB2 receptor tyrosine kinase	Small aromatic organic molecules	Beads-streptavidin-biotinylated anti-His-tag antibody-His-tagged EphB2	None (ligand-displacement approach)	NO	20 mM $\text{NH}_4\text{OAc}$ containing 1% DMSO	[62]
13	Silica beads with streptavidin	0.18 $\mu\text{L}/150 \mu\text{m}$ (capillary)	Cholera toxin B subunit	Cholera toxin B	Beads-streptavidin-biotinylated cholera toxin B	-	YES (biotinylation)	10 mM $\text{NH}_4\text{OAc}$ , pH 6.5	[165]

## **II. Stationary phases for FAC: development and application of FAC for searching for the inhibitors of tyrosinase and trypsin**

### **II.1. Aims and objectives**

The general aim of our work was to develop a novel approach to miniaturize the scale of the chromatographic bed for frontal affinity chromatography in order to reduce required amount of the biological target and allow to conduct rapid pre-selection of the inhibitor candidates of tyrosinase in plant extracts. The most common way to prepare low-volume chromatographic bed for frontal analysis is an application of PEEK microtubes or capillaries packed with the protein-bound particles (**table 2**, entries **4**, **12**, **13**, [62, 165, 167]) or protein immobilisation of the surface of the wall of silica capillary (**table 1**, entry **8**; **table 2**, entry **6** and **10**, [94, 180, 209]). The drawback of the first approach mentioned above is the necessity of application of the retaining frits and difficult process of packing the stationary phase into the tube or capillary. On the other hand, immobilisation of the biological target on the wall of silica capillary may be in certain cases not enough to obtain satisfactory binding capacity of the FAC system and may yield an odd 'ghost peaks' at the beginning of the EIC profile for given inhibitor [180]. Taking these conclusions into account, we decided to develop highly hydrophilic porous monoliths ready to bind the target enzyme in a covalent way<sup>‡</sup>.

As the flow rates applied for capillary-format chromatographic beds usually do not exceed 4-5  $\mu\text{L}/\text{min}$ , FAC experiment in this scale is basically limited to the 'single infusion' approach (**p. I.1.2.1**), due to the fact, that void volume of the classic HPLC apparatus is too high to provide the step gradient in a reasonable time. In our laboratory we developed the platform for 'staircase' frontal analysis (**p. I.1.2.2**) by evaluating the applicability of two ways of the covalent attachment of the target protein to the surface of silica beads. An advantage of using beads as the immobilisation support is that they can be used in larger chromatographic beds (cartridges) supporting higher flow rates (**p. II.2.2**).

### **II.2. Stationary phases for FAC**

#### **II.2.1. Capillary-format monoliths**

The term 'monolith' in the context of present work is understood as the continuous polymeric stationary phase prepared *in situ* inside silica capillary and covalently attached to the internal wall of its channel. Among the types of monolithic stationary phases there is a vast variety of the chemical compositions, methods of their preparation, physical properties and, finally, degree of their complexity [214, 215]. We limited our research interest to two most common families of monoliths:

---

<sup>‡</sup> i) the pathways of enzyme immobilization applied in this work are discussed in **p. II.3** of present chapter, page 64;

ii) the general review of strategies for protein immobilization are discussed in *Chapter I*, **p. IV**, pg 39.

acrylate/methacrylate ester-based organic polymers produced in a process of photoinitiated polymerization [216-218] and silica monoliths prepared in a sol-gel polymerisation process [69, 219-222].

### II.2.1.1. Organic monoliths based on esters of acrylic and methacrylic acid

Organic monoliths based on esters of acrylic and methacrylic acid (AA and MAA respectively) gained a high popularity due to the ease of their preparation and a widespread availability and diversity of commercially available monomers [189, 191, 218, 223-227]. They are usually prepared in a process of free-radical-driven polymerization. When UV-driven polymerisation is applied, the mixture containing monomer(s) (with one vinyl group), crosslinker(s) (two or more vinyl groups) and a free radical initiator dissolved in a porogen solvent is introduced into pre-treated silica capillary, which in turn is subjected to UV irradiation. The process of photoinitiated polymerisation requires an application of dedicated capillaries coated with UV-transparent teflon since polyimide – the classic capillary coating – strongly absorbs UV radiation.

The crosslinker is incorporated into the polymerisation mixture to obtain branched (crosslinked) and stable polymer. The properties of porogen solvent must be adjusted to solubilise monomers, crosslinkers and all other agents engaged in a process of polymerization and simultaneously precipitate the newly formed non-porous polymeric particles. These particles formed *in situ* inside the capillary act as the nuclei for further polymerisation for the reason that 'free' monomers/crosslinkers present in the polymerization mixture have higher affinity to solid nuclei than to one other [228]. This effect favours the superficial polymerization from kinetic point of view. Growing nuclei come into contact and sinter together forming rigid and porous microspheres (fig. 8).

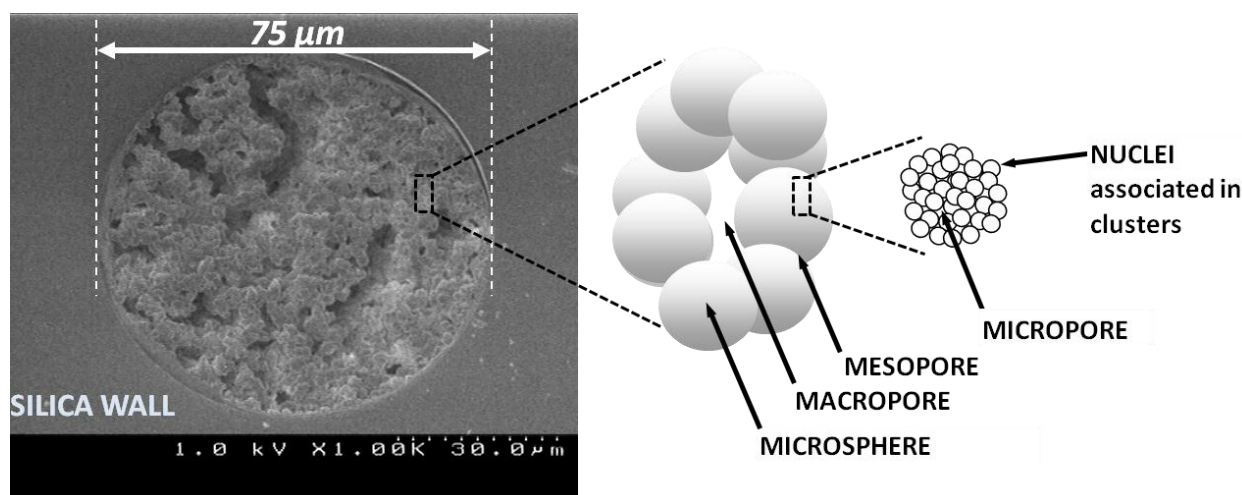


**Figure 8.** Scanning electron micrograph of a cross-section of the monolithic capillary and the hierarchical organization of organic porous monoliths. This poly(propargyl acrylate-pentaerythritol triacrylate-trimethylolpropane trimethacrylate) monolith fills the entire volume of the capillary channel and can be derivatised in a process of azide-alkyne Huisgen cycloaddition[218].

The interstices between nuclei within the microsphere are called micropores (widths up to 2 nm) and the gaps between the microspheres are known as mesopores (widths between 2 and 50 nm). Aggregates of microspheres fill the entire channel of the capillary (**fig. 8**). The channels between them are called macropores and have widths higher than 50 nm [228].

The polymerization of AA or MAA esters (**fig. 9**) is a process driven by free-radicals. It is thus necessary to apply an initiator – *e.g.* 2,2'-azobisisobutyronitrile (AIBN) – which initiates the formation of poly(meth)acrylate chains. A single molecule of AIBN undergoes decomposition into two free radicals when exposed to UV radiation or increased temperature (higher than 60°C).

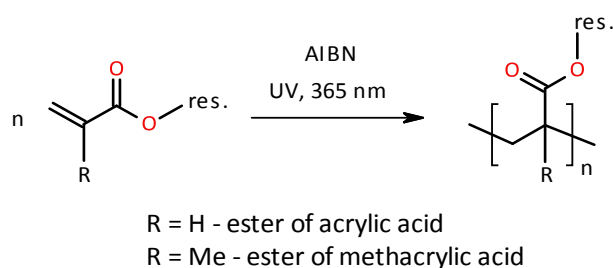


**Figure 9.** General schema of free-radical-generated polymerization of acrylate and methacrylate esters (monomers) in a presence of AIBN as the initiator.

A covalent attachment of the monolith to the capillary wall is of key importance to ensure stability, rigidity and durability of the polymer. To produce attachment points for AA or MAA ester-based polymer it is necessary to conduct vinylization of the capillary surface using *e.g.* 3-(trimethoxysilyl)propyl acrylate (**Appendix I, protocol S1, fig. S1**, page 91). An outlook of the silica surface derivatisation using organosilanes is shown in **p. II.2.2**.

Hydrophobic monoliths composed of esters of AA/MAA and aliphatic alcohols may find an application in reverse phase LC or in the separation of hydrophobic, neutral compounds by capillary electrochromatography [217, 229]. Hydrophilic monoliths were demonstrated to be useful *e.g.* in hydrophilic interaction chromatography (HILIC) [230] or for the separation of biomolecules [231].

#### II.2.1.1.1 Preparation of amine-covered hydrophilic organic poly(SBMA-co-AEMA-co-EGDMA) monolith with the surface hydrophilized by zwitterionic moieties

A starting point for the preparation of zwitterionic polymer was the protocol published by Viklund *et al.* who synthesized poly(SBMA-co-EGDMA)<sup>§</sup> polymer using MeOH as the only porogen [231] (the structures of methacrylates described in this paragraph may be found under the **fig. 10**). This polymer was shown to be stable and durable but reported size of microspheres (approximately 2-3 μm wide on the

<sup>§</sup> **EGDMA**: ethylene glycol dimethacrylate; **AEMA**: 2-aminoethyl methacrylate; **SBMA**: [3-(Methacryloylamino)propyl]dimethyl(3-sulfopropyl)ammonium, inner salt.

basis of the SEM image) was too large to make the polymer applicable for the characteristics of the narrow-bore capillary having 100  $\mu\text{m}$  in diameter. To decrease the size of microspheres and macropores (by delaying an onset of the polymer nucleation), the porogen solvent was enriched with cyclohexanol. Simultaneously, to incorporate AEMA into the mixture and keep the crosslinker/monomer ratio unchanged, the molar contribution of SBMA was reduced by 50%. An incorporation of AEMA into the structure of monolith is indispensable for further protein immobilisation (**p. II.3**).

The general procedure to prepare the polymerization mixture was following: AEMA (75  $\mu\text{mol}$ , 13.8 mg), SBMA (75  $\mu\text{mol}$ , 21.5 mg) and AIBN (6.1  $\mu\text{mol}$ , 1 mg) were added to the mixture of EGDMA (282  $\mu\text{mol}$ , 54.29  $\mu\text{L}$ ) and the porogen solvent: MeOH/cyclohexanol (295/40  $\mu\text{L}$ ). Mixture was sonicated for approximately 10 minutes until the complete dissolution of AIBN and then infused into pre-treated polytetrafluoroethylene-coated silica capillary (ID=100  $\mu\text{m}$ , OD=365  $\mu\text{m}$ ). The polymerisation procedure may be found in the **Appendix I, protocol S2**, page 91. After polymerisation, the capillaries were flushed with HPLC-grade acetonitrile for 15 h by means of external HPLC pump to remove unreacted monomers.

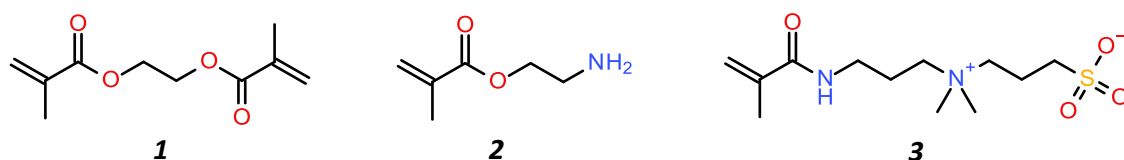


**Figure 10.** Monomers and crosslinker used for the preparation of poly(SBMA-co-AEMA-co-EGDMA) monolith. Crosslinker: **1**: ethylene glycol dimethacrylate (EGDMA), monomers: **2**: 2-aminoethyl methacrylate (AEMA), **3**: [3-(Methacryloylamino)propyl]dimethyl(3-sulfopropyl)ammonium, inner salt (SBMA).

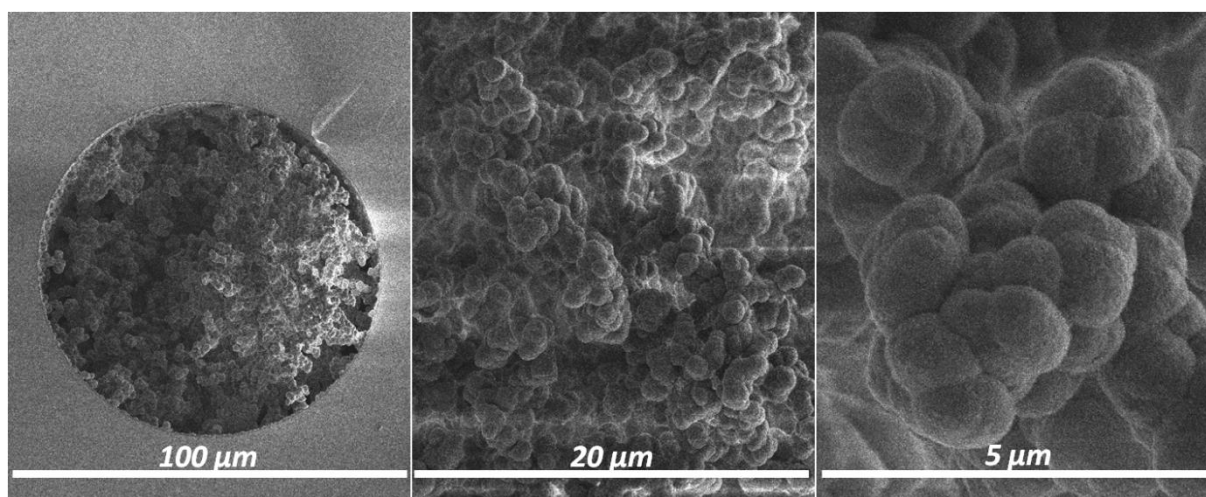


**Figure 11.** Scanning electron micrograph of the cross-section of poly(SBMA-co-AEMA-co-EGDMA) monolithic capillary under various levels of magnification.

Resulted monolith was shown to fill evenly the entire volume of the capillary channel (**fig. 11**). Moreover, no mechanical failures or cracks were observed during the classic exploitation of the poly(SBMA-co-AEMA-co-EGDMA) monolithic capillaries.

### II.2.1.1.2 Preparation of hydrophilic monolith based on N-acryloxysuccinimide.

N-acryloxysuccinimide (NAS)-based relatively hydrophilic\*\* monolith was prepared strictly according to the protocol published by Tjunelyte *et al.* who synthesized poly(NAS-co-EGDMA) monolith [216]. Briefly, NAS (139.4  $\mu\text{mol}$ , 26.2 mg, **fig. 12**) and EDMA (74.8  $\mu\text{mol}$ , 14.4  $\mu\text{L}$ ) were mixed with a volume of 91.7  $\mu\text{L}$  of AIBN solution in toluene (4.35 mg/mL). The concentration of AIBN in toluene was adjusted to obtain 1% (wt%) of AIBN in respect to all monomers in the final polymerization mixture. The mixture was alternately sonicated and vortexed for about 10 to 15 min to obtain homogeneous solution. The mixture was then infused into the capillary and subjected to polymerisation (**Appendix 1, protocol S2**). Capillary was then washed with HPLC-grade acetonitrile for 1 h and stored at 4°C until use.

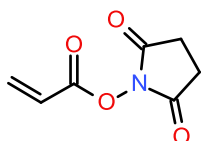


**Figure 12.** N-acryloxysuccinimide (NAS).

### II.2.1.2. Silica monoliths

Silica monoliths can be synthesized *in situ* inside the capillary using sol-gel process. The conventional silica monoliths are synthesized from tetraalkoxysilane precursor (e.g. tetraethoxysilane, TEOS, **fig. 13** [221]) that undergoes acid or base catalysed hydrolysis to alcohol and tetrahydroxysilane. The latter monomers condense and form a sol, the colloidal suspension of newly formed tetrahydroxysilane oligomers. The particles of oligomers undergo gradual polycondensation into clusters leading to gel formation and, at the end of an 'ageing' process, to stable silica network [232]. To obtain mesoporous silica material, an addition of through-pore templates to the polymerization mixture is required. The templating molecules, such as polyethylene glycol (PEG) of a high molecular mass (usually 10 kDa) [219-221], or micelle-forming surfactants, such as cetyltrimethyl ammonium bromide (CTAB) [69, 222], are removed from completed polymer by extraction with an organic solvent.

In present work we evaluated the applicability of two types of hybrid organic-inorganic silica monoliths in frontal affinity chromatography. These hybrid silica monoliths were produced by polycondensation of tetraalkoxysilanes and organosilanes, e.g. TEOS and (3-aminopropyl)triethoxysilane (APTES) respectively (**fig. 13**) [69, 195, 219, 220]. Amine-bearing silica monoliths (ASMs) may be modified to bind covalently the proteic target in the same way as poly(SBMA-co-AEMA-co-EGDMA) organic polymer (further details concerning the immobilisation process may be found in **p. II.3** in present chapter).

\*\* these formulations are relatively hydrophilic among easy to prepare polymers based on AA and MAA.

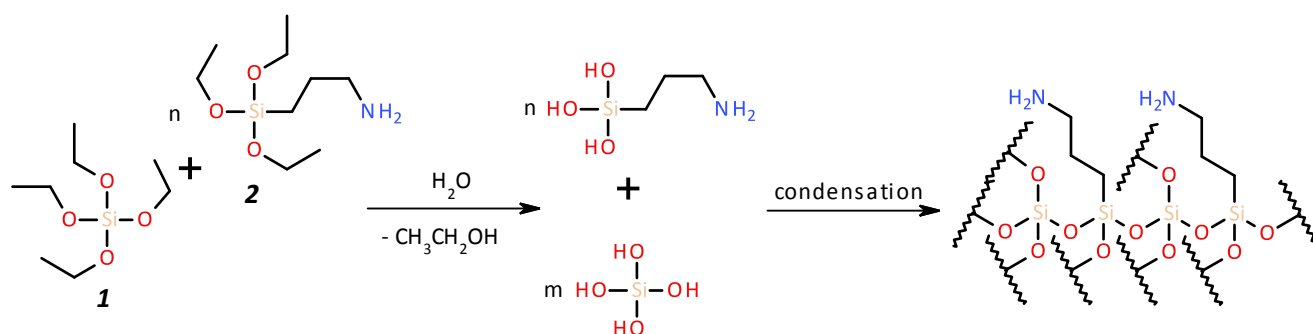


**Figure 13.** General schema of polycondensation of silica monolith precursors: **1**: tetraethoxysilane (TEOS), **2**: (3-aminopropyl)triethoxysilane (APTES). Both compounds undergo APTES-catalysed hydrolysis before polycondensation.

#### II.2.1.2.1 Preparation of organic-inorganic silica monolith based on APTES/TEOS using surfactant as a porogen

Capillary was cleaned and activated by flushing with 1 M NaOH (3 h at 200  $\mu$ L/h, 3h in static mode at 40°C), followed by water, 0.1 M HCl, water and methanol (in all cases 30 min, 200  $\mu$ L/h) in a sequence to render the surface with the silanol groups. Capillary was then dried in the stream of nitrogen for 1 h. Monolith was prepared strictly according to the protocol of Ma *et al.* [69]. Briefly, CTAB (13.56 mg) was mixed with ethanol (364.4  $\mu$ L) and water (54.2  $\mu$ L), then TEOS (189.8  $\mu$ L, 0.85 mmol) and APTES (200  $\mu$ L, 0.85 mmol) were added in a sequence. The mixture was vortexed for 1 minute. A sol obtained after this time was introduced into the capillary which was capped at both sites with the silicon rubber and placed at 40°C for 24 h. It was then rinsed with methanol (1.5 h) and water (30 min) at 5  $\mu$ L/min to remove the porogen and unreacted reagents.

In further part of the manuscript this monolith formulation will be referred to as **ASM-CTAB**.

#### II.2.1.2.2 Preparation of organic-inorganic silica monolith based on APTES/TEOS using room-temperature ionic liquid as co-porogen

The use of room-temperature ionic liquid (RTIL) as co-porogen and co-solvent in a process of the preparation of silica monoliths was described for the first time by Zhou *et al.* [233]. The main advantage of RTILs is their low vapor pressure which is believed to reduce the gel shrinkage phenomenon during the 'ageing' process [219, 234, 235]. Gel shrinkage phenomenon in a presence of organic or aqueous solvent process may be associated with the solvent evaporation before formation of a stable silica network [234]. Moreover, ionic liquids consisting of 1-butyl-3-methylimidazolium ([BMIM]BF<sub>4</sub>, **fig. 14**) may undergo self-assembly in the presence of silica oligomers and, consequently, act as pore template in sol-gel process (**fig. 14**) [219, 233, 235].

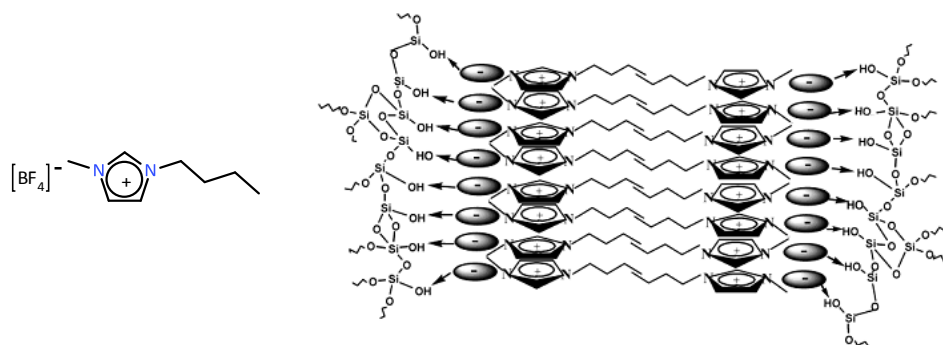


**Figure 14.** A structure of 1-butyl-3-methylimidazolium ( $[BMIM]BF_4$ ) and the way of self-assembly of  $[BMIM]BF_4$  in the presence of silica oligomers. Reproduced from [233].

Monolith was prepared according to the protocol of Chen *et al.* [219]. Briefly, polyethylene glycol (10 kDa, 10 mg) was dissolved in the mixture of 50  $\mu$ L of water and 200  $\mu$ L of EtOH. The following components were then added to resulting mixture in a sequence: BMIM-PF<sub>6</sub> (150  $\mu$ L), 200  $\mu$ L of TEOS (200  $\mu$ L, 0.9 mmol) and APTES (200  $\mu$ L, 0.85 mmol). The mixture of monomers was vortexed for about 1 min and charged into pre-treated silica capillary. Capillary was then placed at 60°C for 8h and washed as advised in the original protocol.

In further part of the manuscript this monolith formulation will be referred to as **ASM-RTIL**.

### II.2.2. Silica beads as an immobilisation support

We used Merck silica gel 60 (particle size: 40-63  $\mu$ m) as a support for enzyme immobilisation. A surface of silica particles must be modified to bind the proteic target in a covalent way. Derivatisation of the silica surface may be accomplished using organosilanes containing three alkoxy groups and the organic moiety, able to react with the protein molecules directly or to be a starting point for further activation (*p. II.3.2.1*). After hydrolysis of alkoxy groups, organosilane molecules condense with the superficial hydroxyl groups on the surface of the silica particles (**fig. 15**).

Prior to derivatisation, silica material must be activated. This process was conducted according to the protocol of Kahraman *et al.* with minor modifications [236]. Silica beads (3 g) were purified and activated by incubation in a mixture of 30% aqueous solution of NaOH/H<sub>2</sub>O<sub>2</sub> (30%)/H<sub>2</sub>O (1/1/4, v/v/v, 48 mL) for 15 minutes. Then, silica beads were washed with distilled water and then incubated for 80 minutes at 80°C in 48 mL of the following solution: 37% HCl/H<sub>2</sub>O<sub>2</sub> (30%)/H<sub>2</sub>O (1/1/4, v/v/v). Silica beads were then washed with distilled water and dried under vacuum using rotary evaporator.



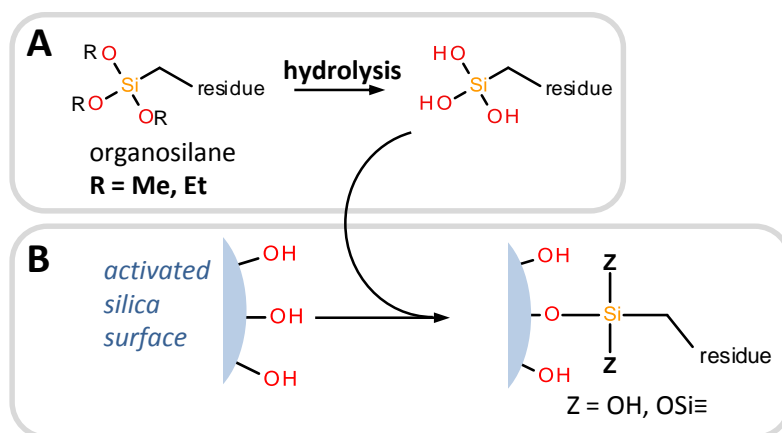


**Figure 15.** Outlook of the chemistry of silica derivatisation. **A:** hydrolysis of organosilanes to silica-reactive trihydroxysilanes; **B:** polycondensation of trihydroxysilanes with superficial silanol groups of previously activated silica-based surface (e.g. beads or capillary wall) [237-240].

### II.2.2.1. Chromatographic support for silica beads

Silica beads hosting immobilised target enzyme were slurry-packed into the cylindrical cartridge (internal diameter: 4.6 mm, length: 1.5 cm, 249  $\mu\text{L}$ ) and placed inside the cartridge host (**fig. 16**).



**Figure 16.** The support for silica particles with immobilised enzyme. **A:** cartridge, **B:** the cartridge nest.

### II.3. Protein immobilisation on the surface of monoliths and silica particles

The pathways of protein immobilisation for all protein supports applied in present work were summarized in **fig. 17**. Despite the same chemistry of protein immobilisation for amine-bearing monoliths and silica particles, the format of both types of supports impose significant practical differences in the activation and immobilisation process.

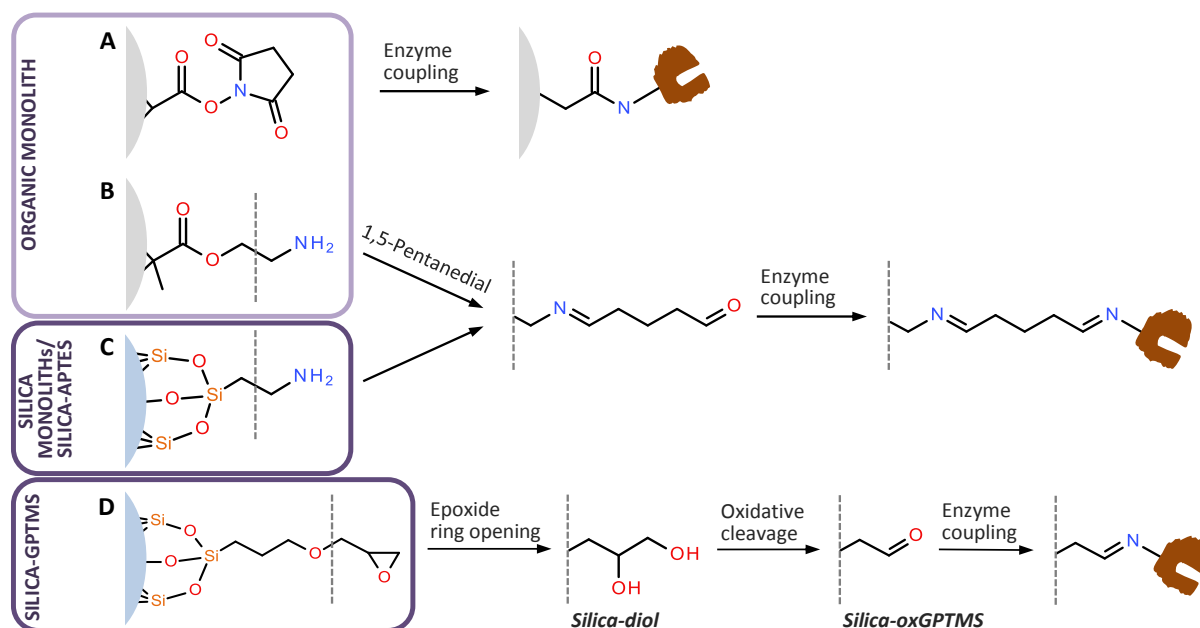


**Figure 17.** All of the pathways of protein immobilisation for all stationary phases and magnetic nanoparticles considered in the present manuscript. **A, B, C:** capillary monoliths; **C, D:** silica particles and magnetic nanoparticles. **A:** poly(NAS-co-EGDMA) monolith (p. II.2.1.1.2); **B:** poly(SBMA-co-AEMA-co-EGDMA) monolith (p. II.2.1.1.1); **C:** APTES-based silica monoliths (ASM-CTAB, p. II.2.1.2.1; ASM-RTIL, p. II.2.1.2.2) and silica particles/magnetic nanoparticles derivatised with APTES; **D:** silica particles/magnetic nanoparticles derivatised with GPTMS.

### II.3.1. Capillary-format monoliths

All silica monoliths described in this manuscript were synthesized in UV-transparent<sup>††</sup> teflon-coated fused silica capillaries having 100/360  $\mu\text{m}$  for internal/external diameter respectively (fig. 18). Monoliths described in p. II.2.1. may be divided into two groups: *i*) amine-bearing polymers requiring an activation before protein immobilisation (fig. 17-B/C) and *ii*) NAS-based monolith that may be used directly without any pre-treatment (fig. 17-A).

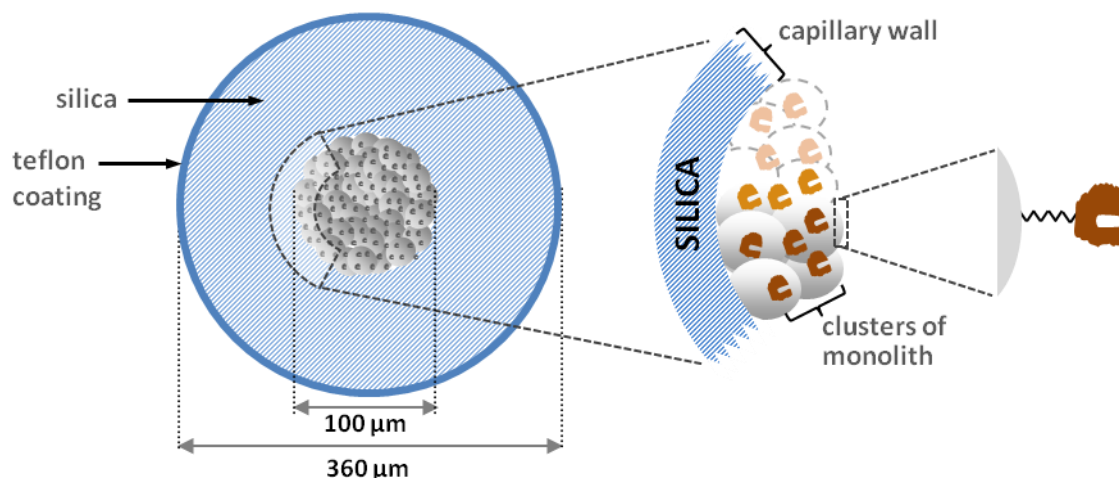


**Figure 18.** Schematic cross-section of a silica capillary containing an enzyme-linked polymeric monolith.

<sup>††</sup> Polyimide, commonly applied capillary coating, strongly absorbs UV radiation at 365 nm thus precluding UV-driven free radical polymerisation inside of the capillary channel (more details: **Appendix I, protocol S2**, pg 91).

### II.3.1.1. Derivatisation and preparation of the capillaries for enzyme immobilisation

#### II.3.1.1.1. Amine-bearing monoliths

Amine-bearing monoliths: poly(SBMA-co-AEMA-co-EGDMA), ASM-CTAB and ASM-RTIL (**fig. 17-B/C**) were derivatised in the same way. Briefly, a solution of 1,5-pentanedial (glutaraldehyde, GLA) (12.5% in 100 mM sodium phosphate buffer, pH 7.5) was pumped through the capillary at a flow rate of 1  $\mu\text{L}/\text{min}$  for 6 hours. Capillary was then rinsed with water for about 1 h and stored at 4°C until use. Capillaries activated in this manner are suitable for use directly as the immobilisation support.

Glutaraldehyde is covalently attached to the surface of monolith via carbon-nitrogen double bond which is formed in a process of nucleophilic addition of the superficial amine to one of aldehyde groups of GLA, followed by elimination of water from resulted hemiaminal yielding a secondary aldimine. Remaining aldehyde group may bind the proteic target according to the same mechanism. Imines, which are formed in a process of surface derivatisation, are chromophores and are usually yellow or orange [241]. This phenomenon may be used to visualise the activation step (**fig. 19**).

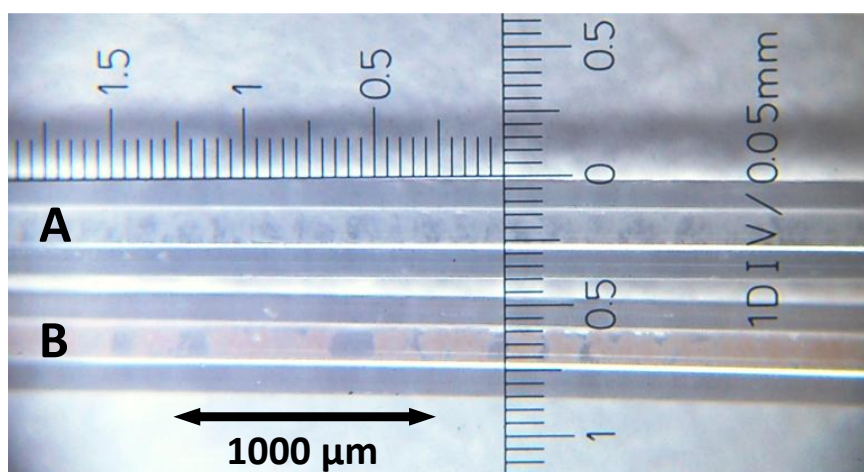


**Figure 19.** Amine-bearing capillary (ASM-RTIL) before (A) and after (B) activation with GLA. Imine groups formed in this process are responsible for orange colour of the monolith.

#### II.3.1.1.2. Poly(NAS-co-EGDMA) monolith

No derivatisation of poly(NAS-co-EGDMA) monolith is required. After preparation the monolith should be stored at 4°C in anhydrous conditions, since N-hydroxysuccinimide esters are susceptible to hydrolysis and after prolonged contact with aqueous solutions or moisture they lose the ability to bind proteins. Before protein immobilisation, capillary was flushed with HPLC-grade acetonitrile for 1 h to remove all impurities desorbed from the monolith during the storage and then with coupling buffer for 1-2 minutes to remove acetonitrile from the capillary to avoid protein denaturation upon contact with this organic solvent.

### II.3.1.2. Enzyme immobilisation: capillary-format monoliths

The immobilisation protocols for various types of capillaries are very similar. Briefly, an enzyme solution (usually 1 - 2.5 mg/mL) in sodium phosphate buffer, PHB (10 mM, pH 6.8 for mushroom tyrosinase; 50 mM, pH 7.5 for trypsin) was charged into 150  $\mu$ L injection loop which was then introduced between an HPLC pump and the capillary. Enzyme solution was infused into the capillary for 5 h. During this process, both capillary and the loop were stored in ice (**fig. 20**). In case of trypsin immobilisation, capillary was flushed with the coupling buffer to remove unbound enzyme and derivatised with 0.1 M glycine in 10 mM PHB (pH 6.8) for two hours. In case of tyrosinase immobilisation, capillary was disconnected from the source of enzyme solution and stored at 4°C for 16 h and subsequently derivatised with 1 mM glycine in 10 mM PHB (pH 6.8) for two hours.

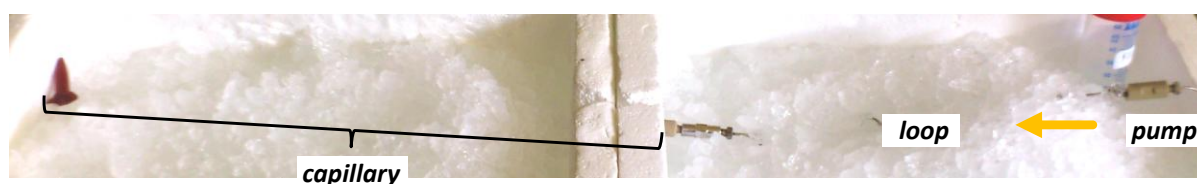


**Figure 20.** The process of infusion of enzyme solution into activated capillary.

In case of NAS-based monolith, superficial N-hydroxysuccinimide ester groups undergo in aqueous solutions gradual hydrolysis to N-hydroxysuccinimide and surface-embedded carboxylic acid. Accordingly, to improve column-to-column reproducibility, glycine was selected as an end-capping agent.

### II.3.2. Silica beads

#### II.3.2.1. Derivatisation of silica beads

Two types of silica-based stationary phases were prepared: *i*) amine-covered APTES-derivatised silica (**fig. 17-C**) and *ii*) epoxide-covered (3-Glycidyloxypropyl)trimethoxysilane (GPTMS)-covered silica (**fig. 17-D**). The coupling procedure of both organosilanes to the silica surface was the very similar. Briefly, a solution of organosilane (1.07 mmol/g of silica beads) in toluene was added to dry silica beads. The mixture was agitated under solvent reflux at 50°C for 13h and in 70°C for 2h for APTES and at 70°C for 16 h for GPTMS. Silica beads were then washed by MeOH and kept in an oven at 120°C for 1 h to promote the complete condensation of organosilane and the surface of silica beads.

##### II.3.2.1.1 Activation of silica-APTES beads

Amine-covered silica beads were activated using the same reactant as amine-bearing monoliths (**fig. 17-C**). A mass of 1 g of silica-APTES was added to 16.7 mL of 2.5% aqueous solution of GLA in 200 mM

sodium phosphate buffer, pH 7.5. and stirred at room temperature for 1 h. Activated silica particles were then dried in an oven at 40°C. The binding capacity of silica-APTES-GLA particles for bovine serum albumin (BSA) was determined to be on the level of 8.4 mg per 1 g of beads.

#### *II.3.2.1.2 Activation of silica-GPTMS beads*

Silica-GPTMS particles (**fig. 17-D**) were suspended in 40 mL of 0.1 M aqueous solution of HCl and agitated at room temperature for 3 h. Silica-diol particles were then washed with distilled water until neutral pH was obtained. An oxidative cleavage of superficial diol group was performed according to [183, 242]. Briefly, a volume of 40 mL of the periodic acid solution (0.22 M) in the mixture of 90/10 (v/v) acetic acid/water was added to approximately 3 g of silica-diol particles. The mixture was agitated in darkness for over 2 h. Silica-oxGPTMS beads were then washed with distilled water until neutral pH was reached.

### **II.3.2.2. Enzyme immobilisation: silica beads**

#### *II.3.2.2.1. Immobilisation of tyrosinase on silica-APTES-GLA beads*

A mass of 2.7 mg of mushroom tyrosinase (1715 U/mg) was dissolved in a volume of 3 mL of 10 mM sodium phosphate buffer, PHB (pH 6.8). Tyrosinase solution was added to 310 mg of derivatised particles. The coupling reaction was conducted for 6 h in ice under mild stirring. A solution of 1 mM glycine in PHB was used to quench unreacted aldehyde groups while the mixture was stored at 4°C overnight. Beads were loaded into the holders (cartridges) (**fig. 16**) without prior washing step. Both cartridges were flushed and equilibrated with MS-compatible buffer (details may be found in **p.III.3.2**) for at least 30 minutes at a flow rate of 0.2 mL/min.

#### *II.3.2.2.2. Immobilisation of trypsin on silica-oxGPTMS beads*

A mass of 6.3 mg of trypsin was dissolved in 1 mL of 50 mM sodium phosphate buffer, PHB (pH 8.0) containing  $MnCl_2$  and  $CaCl_2$  (both 1 mM). Trypsin solution was added to 350 mg of derivatised silica-oxGPTMS particles. The coupling reaction was conducted for 6 h in ice under mild stirring and then overnight in a static mode at 4°C. A solution of 100 mM glycine in PHB was used to quench unreacted aldehyde groups while the mixture was stored at 4°C for 2 h. The rest of a protocol is the same as in *p. II.3.2.2.1.*

### III. Evaluation of the stationary phases for FAC

#### III.1. Trypsin as a biological target for method validation

Development of any inhibitor screening method requires reliable reference biological system for method validation. In present work we applied easily accessible trypsin from bovine pancreas. Trypsin is a serine protease, belongs to the family of proteolytic hydrolases [243] and has a high specificity of protein cleavage - only at C-terminal site of arginine and lysine residues [244]. Trypsin is the basic enzyme used in proteomics and thus is widely commercially accessible at high purity and satisfactory specific activity. An active site of trypsin contains three key amino acids: Asp102, His57 and Ser195 (**fig. 21**). The latter residue poses the catalytic function and it is involved in all steps of the enzyme's proteolytic cycle, including the first and the most crucial one – a nucleophilic attack on the carbonyl carbon of the amino acid chain of the substrate protein. This nucleophilic attack of hydroxyl group of Ser195 is possible only due to its deprotonation by adjacent His57, stabilized spatially by Asp102 (**fig. 21-B**), since an 'isolated' alcohol group poses too weak nucleophile properties to be involved in the nucleophilic addition to carbonyl carbon.

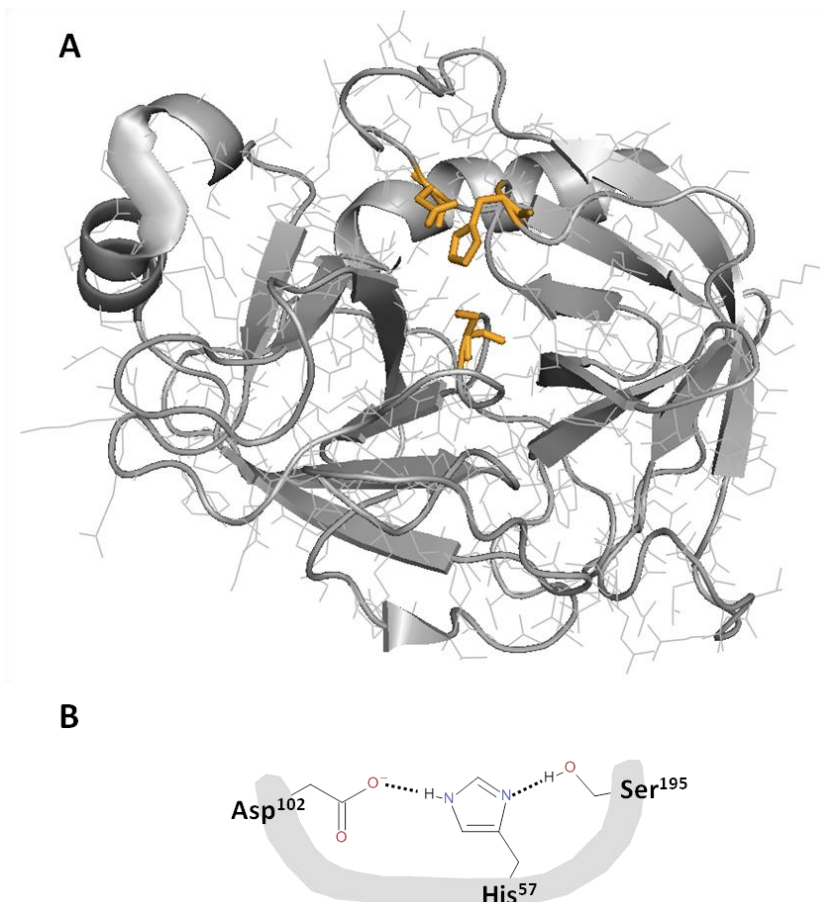


**Figure 21.** The structure of bovine trypsin (**A**, PDB: 2ptn [243] with Asp102, His57 and Ser195 residues marked in orange) and the way of activation of Ser195 within the catalytic triad, **B**. This figure was generated using PyMOL (<http://www.pymol.org/>).

To summarize, trypsin was selected as a validation target due to well defined spectrum of inhibitors, high stability, low cost of acquisition and its high availability in a pure form having high specific activity. Trypsin was successfully immobilised onto the solid support using its terminal  $\epsilon$ -amino groups [187, 245-247].

In present work, trypsin from bovine pancreas (TPCK treated,  $\geq 10000$  BAEE units/mg) was used for all experiments involving this enzyme.

### **III.2 Configuration of the experimental system**

MS experiments were performed on Bruker *maXis* UHR-Qq-TOF spectrometer (Bremen, Germany) with Bruker sprayer in positive and negative electrospray ionisation (ESI) mode (details will be discussed separately), working in a single-mass mode. MS was coupled in on-line mode with a Dionex UltiMate 3000 UHPLC system (binary pump, standard thermostated column compartment and DAD detector) (Germering, Germany). Since the way of dosage of the test mixtures depends on the scale of a chromatographic support, it will be summarized in the following paragraphs.

#### **III.2.1. Silica-packed cartridges**

Relatively high volume of the cartridge used to host silica particles with immobilised enzyme (**p. II.2.2.1**), equal to 249  $\mu\text{L}$ , makes possible to apply flow rates as high as 200  $\mu\text{L}/\text{min}$  during analysis. Binary pump LC system makes possible to form a step gradient of two mobile phases: **A** contains the buffer solution and **B**: an analysed mixture in the same buffer as the **A**. By changing the ratio of A to B one may modify an effective concentration of the analyte in the bioreactor. This configuration allows conducting 'staircase frontal analysis' (**p. I.1.2.2**). The main limitation of this approach is relatively long time needed to change the composition of studied mixture, since it requires a thorough wash of the HPLC channel.

#### **III.2.2. Capillary-format FAC**

A small volume of the capillary-format immobilisation support (approx. 2.36  $\mu\text{L}$  for 30 cm-long capillary) imposes limited flow rate during analysis (usually 3  $\mu\text{L}/\text{min}$ ). The dead volume of Dionex HPLC system is on the level of 200  $\mu\text{L}$  (including a mixing chamber), therefore the use of pump-driven step gradient would result in an initial delay of a  $t_0$  marker on the level of 67 minutes. Such a long analysis time (taking into account an additional delay caused by enzyme-inhibitor interactions) is not acceptable. Consequently, we applied software-controlled six-port valve (**fig. 22-A**) linking HPLC pump, capillary and the loop constituting a reservoir of the analysed mixture. It can be set in two positions: i) charging of the analyte loop; ii) sample run. In the first case the mobile phase from the pump is infused directly to the capillary and a syringe containing the analyzed mixture may be used to charge the loop. If we switch the

valve position to 'sample run', the pump will push the content of the sample loop into the capillary installed inside the thermostated 'column compartment' (**fig. 22-B**). Dead volume of the system between the sample loop and MS is about 15  $\mu\text{L}$  yielding an initial delay of a marker of about 5 minutes at a flow rate of 3  $\mu\text{L}/\text{min}$ .

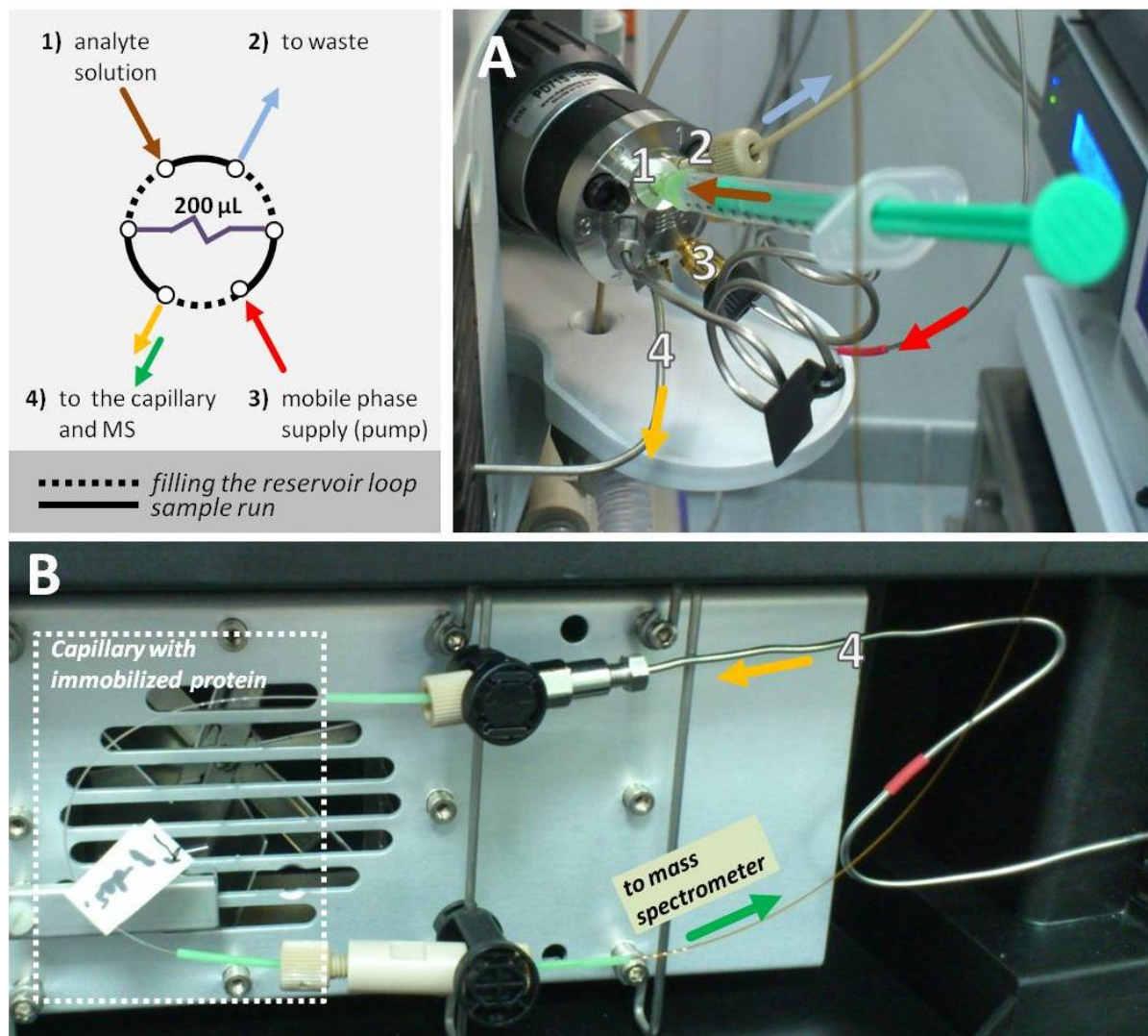


**Figure 22.** The system layout for capillary-format frontal affinity chromatography. **A:** software-controlled six-port valve, **B:** thermostated column compartment

### III.3. Assessment of the nature of non-specific interactions for developed stationary phases

To assess the scope of application of the stationary phases described in **p. II.2.1**, a test mixture containing standards covering a wide range of chemical properties (**fig. 23**) was used for evaluation of each stationary phase. To avoid an impact of the presence of surface-bound enzyme, each stationary phase was only subjected to end-capping in order to quench the superficial aldehyde groups. The end-capping procedure was identical for each type of the solid support.



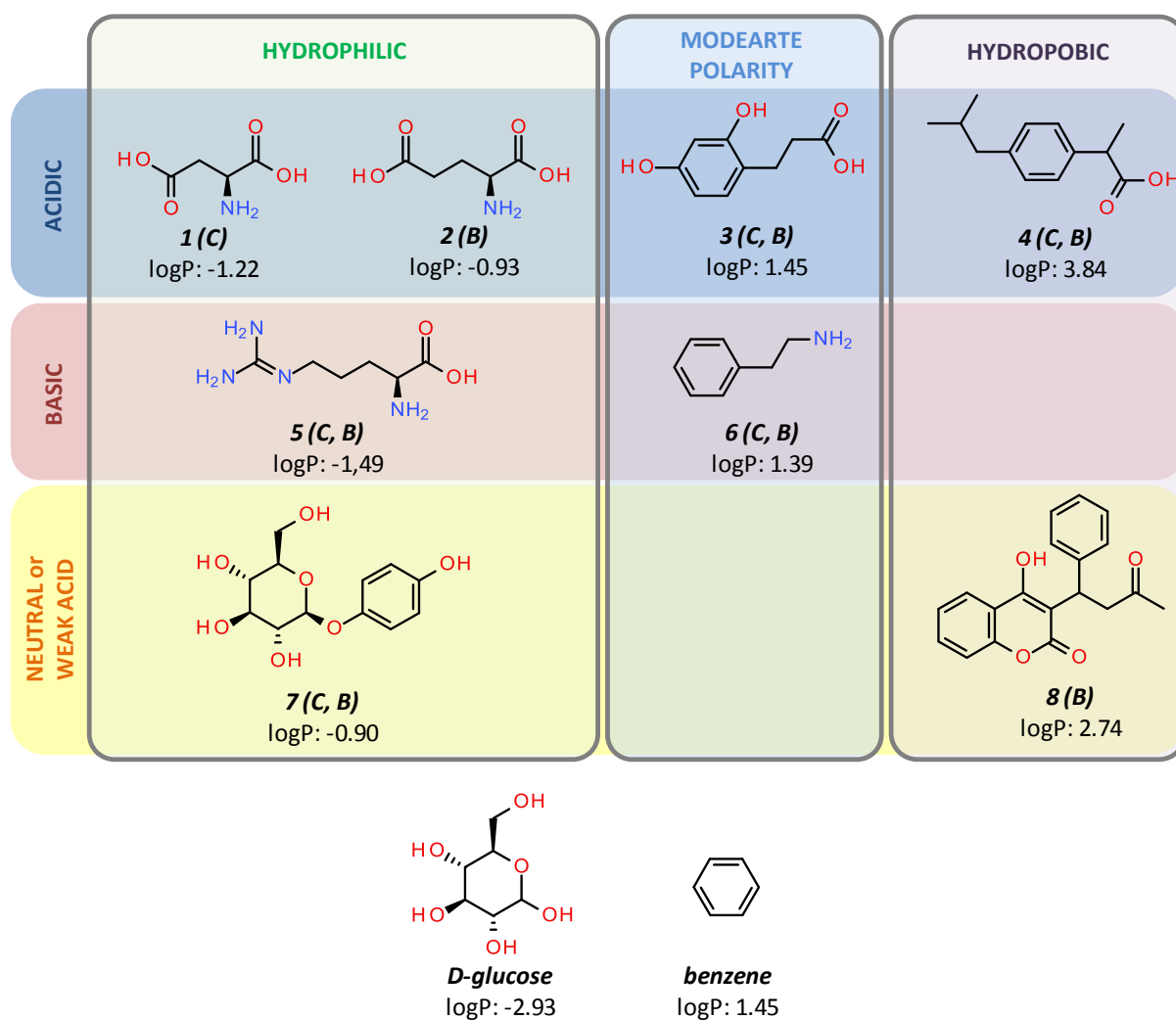


**Figure 23.** Compounds used for validation of the stationary phases for their applicability in FAC. Compounds assigned as 'C' were applied for assessment of capillary-format monoliths while 'B' for silica beads. **1:** L-Asp, **2:** L-Glu, **3:** 3-(2,4-Dihydroxyphenyl)propionic acid (DHPA), **4:** ibuprofen, **5:** L-Arg, **6:** 1-phenylethylamine, **7:** arbutin, **8:** warfarin. All logP partition coefficient values were generated by MarvinSketch 5.11.5 (ChemAxon) on the basis of KLOP, VG and PHYS algorithms to which the same 'weights' were attributed. Benzene and D-glucose were shown for the comparison.

### III.3.1. Capillary-format stationary phase

#### III.3.1.1. Organic monoliths

Capillaries containing poly(SBMA-co-AEMA-co-EGDMA) and poly(NAS-co-EGDMA) were prepared according to **p. II.2.1.1.1** and **p. II.2.1.1.2** respectively. Amine-covered poly(SBMA-co-AEMA-co-EGDMA) monolith was derivatised with glutaraldehyde according to **p. II.3.1.1.1**. To eliminate an impact of uncapped aldehyde or N-hydroxysuccinimide ester groups, both monoliths were quenched in identical way by contacting them with aqueous solution of glycine (100 mM) in 10 mM sodium phosphate buffer (pH 6.8) for 2 h. Each capillary was then flushed with MS-compatible buffer (10 mM ammonium formate, pH 6.8) for approximately 1 h until the total ion current (TIC) achieved full stability.

Mass spectrometer was operated in a positive mode of ionisation. Parameters of the ion source were adjusted to low flow rates, such as 3  $\mu\text{L}/\text{min}$ , applied during the analysis. To reduce the risk of ion fragmentation, the collision energy in the collision chamber was reduced to the minimal level enabling ions to pass through the collision chamber without visible loss of their intensity. The sample valve was switched from 'loading' to 'sample run' position after 15 seconds from the start of an acquisition. The data acquisition was conducted for 30 minutes for each capillary (**fig. 24**). Capillaries were thermostated at 25°C during the analysis.

<b>Method 1</b>	
Source Type:	ESI
Ion Polarity:	Positive
Nebulizer:	1.7 Bar
Dry Heater:	180°C
Dry Gas:	4.5 l/min
Scan Begin:	110 m/z
Scan End:	750 m/z
Capillary:	4500 V
Collision Energy:	6.0 eV

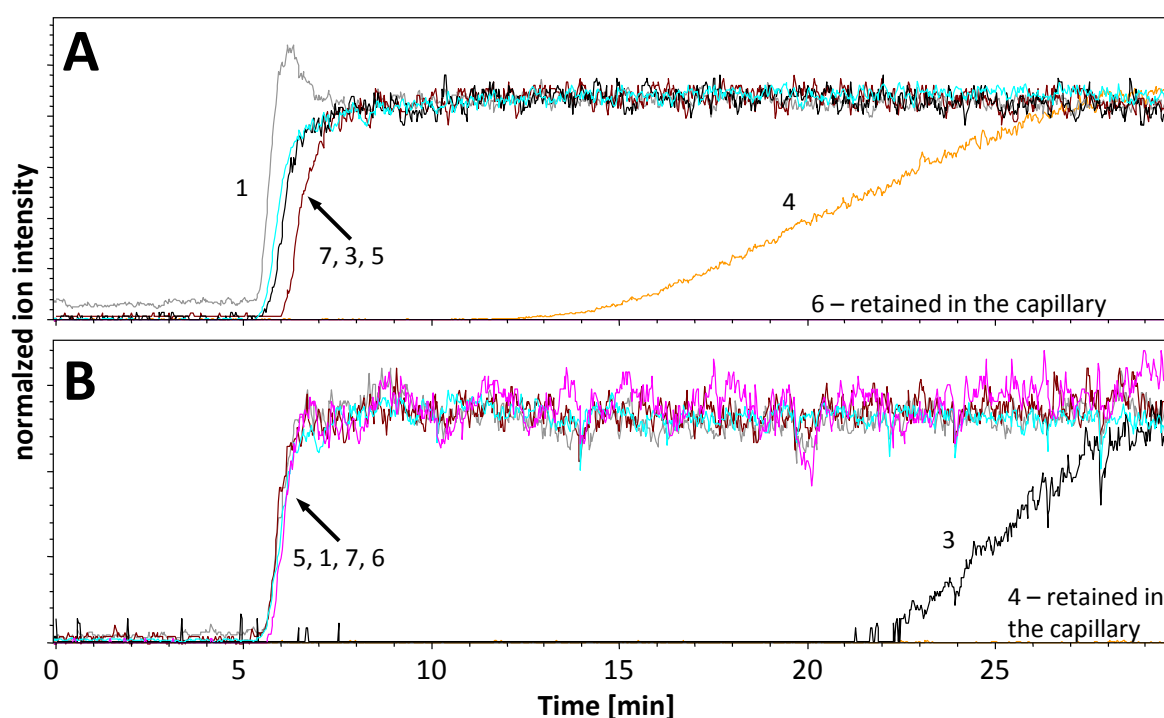


**Figure 24.** The series of extracted ion chromatograms representing the compounds infused into the test capillaries: **A:** poly(NAS-co-EGDMA) monolith; **B:** poly(SBMA-co-AEMA-co-EGDMA) monolith. **1:** L-Asp (grey,  $m/z$  134.045  $[M+H]^+$ ), **3:** 3-(2,4-Dihydroxyphenyl)propionic acid, DHPA (black,  $m/z$  183.065  $[M+H]^+$ ), **4:** ibuprofen (orange,  $m/z$  224.164  $[M+NH_4]^+$ ), **5:** L-Arg (brown,  $m/z$  176.122  $[M+H]^+$ ), **6:** 1-phenylethylamine (magenta,  $m/z$  123.10  $[M+1n+H]^+$ ), **7:** arbutin (cyan,  $m/z$  290.123  $[M+NH_4]^+$ ). Compound numbers correspond to the numeration in fig. 19. Data were acquired using the method 1.

The comparison of poly(SBMA-co-AEMA-co-EGDMA) and poly(NAS-co-EGDMA) monoliths revealed high complementarity between the two formulations. In case of both capillaries we can generally observe lack or low non-specific interactions with polar compounds of any charge and relatively high degree of non-specific interactions with hydrophobic compounds (ibuprofen or 1-phenylethylamine). For both capillaries, non-specific interactions of hydrophobic or moderately hydrophobic compounds seem to have a synergistic effect with their charge.

The surface of poly(SBMA-co-AEMA-co-EGDMA)-based monolith interacts preferentially with negatively charged compounds having moderate to high hydrophobicity (DHPA, ibuprofen), **fig. 24-B**. Non-specific interactions are completely suppressed for hydrophobic compounds bearing a positive charge (1-phenylethylamine). This effect may be explained in a following way: poly(SBMA-co-AEMA-co-EGDMA)-based monolith is charged positively due to the presence of a fraction of amine groups that were not modified by GLA during an activation process (**p. II.3.1.1.1**). At the same time, positively charged compounds are repulsed from the polymer surface what suppresses their retention inside the capillary.

The surface of poly(NAS-co-EGDMA)-based monolith interacts preferentially with hydrophobic compounds (ibuprofen, 1-phenylethylamine) of any charge, **fig. 24-A**. The surface of NAS-based monolith bears a negative charge generated by superficial carboxylic groups. It is manifested in reduced non-specific interaction of ibuprofen and completely suppressed interaction of moderately hydrophobic DHPA. On the other hand, a non-specific interaction of 1-phenylethylamine is greatly increased when compared to poly(SBMA-co-AEMA-co-EGDMA)-based monolith.

The comparison of both monoliths was summarised in **table 3**. The selection of appropriate monolith for frontal affinity chromatography in aqueous phase should be adjusted to the nature of the analyte.

**Table 3.** The summary of the degree of non-specific interactions for organic monoliths.

Charge at pH 6.8 →	negatively charged			positively charged		neutral
Polarity →	hydrophilic	moderate	hydrophobic	hydrophilic	hydrophobic	hydrophilic
Name →	L-Asp (1)	DHPA (3)	ibuprofen (4)	L-Arg (5)	phenylethylamine (6)	arbutin (7)
poly(SBMA-co-AEMA-co-EGDMA)						
poly(NAS-co-EGDMA)						

- not significant non-specific interaction ( $\Delta t$  less than 2 min)
- moderate non-specific interaction ( $\Delta t$  between 2 and 15 min)
- significant non-specific interaction ( $\Delta t$  between 15 and 25 min)
- very significant non-specific interaction ( $\Delta t$  more than 25 min)

## III.3.1.2. Silica monoliths

Organic monoliths turned out to be unsuitable for coupling with ESI ion source due to extremely high ion suppression imposed by silica-related and porogen-related ions (**fig. 25**), e.g. suppression of L-tyrosine ion,  $m/z$  182.08  $[M+H]^+$ , during an infusion of 31  $\mu\text{M}$  solution of L-Tyr in 10 mM ammonium formate buffer (pH 6.8) was as high as 50-100% of the ion intensity acquired without the capillary in the system. For comparison, no ion suppression is observed for organic polymers.

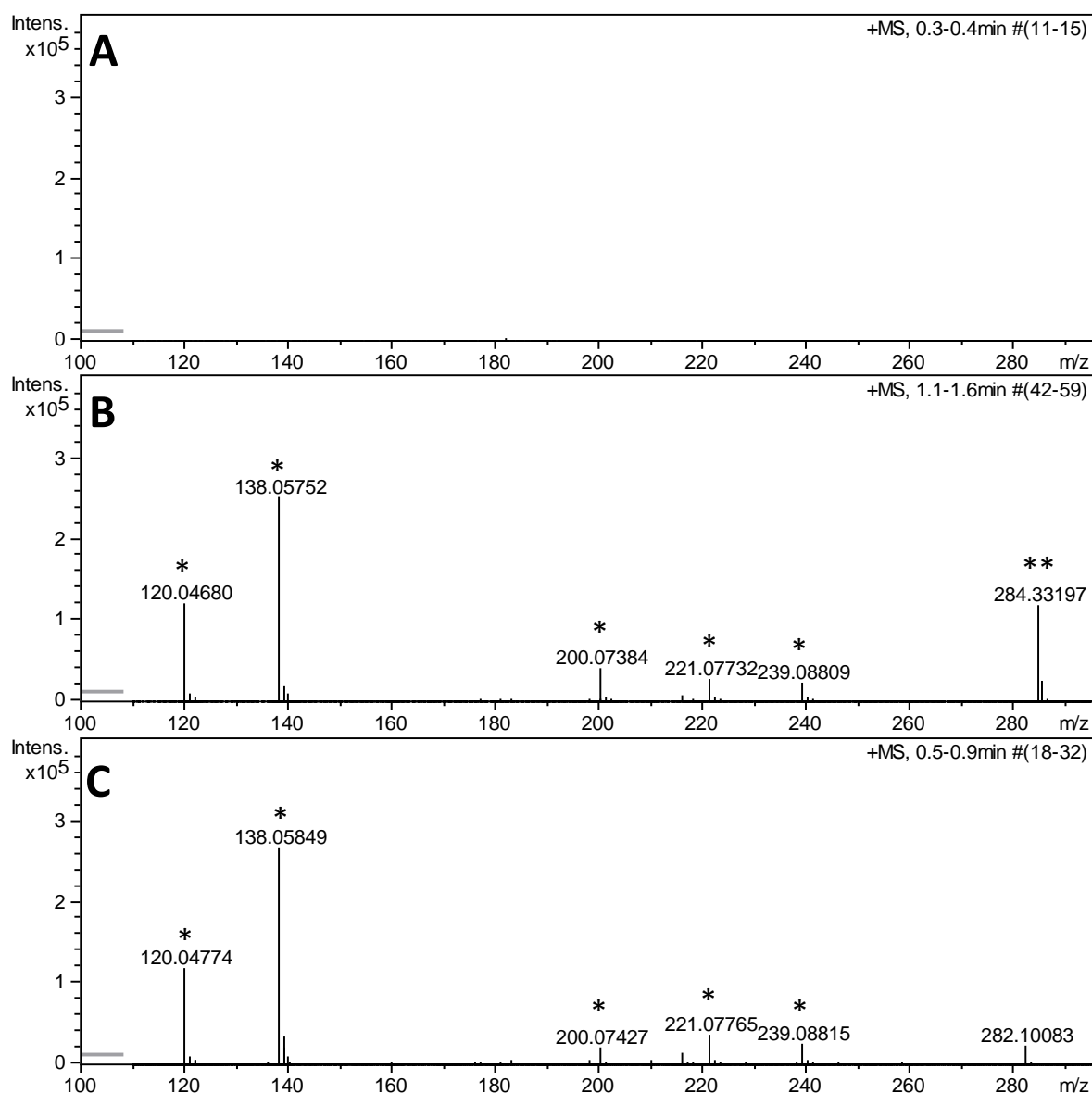


**Figure 25.** Exemplary mass spectra acquired in a positive mode of ionisation using 10 mM ammonium formate buffer. **A** – blank run without the capillary showing no buffer-related impurities; **B** – with ASM-CTAB monolithic capillary; **C** – ASM-RTIL monolithic capillary. Peaks marked with a single asterisk (\*) are related with silica monoliths. CTAB-related ion  $\text{C}_{19}\text{H}_{42}\text{N}^+$  was marked with two asterisks (\*\*).

Monolith-related impurities were impossible to remove using water or methanol, even after several hours of continuous washing. In case of the monolith prepared using CTAB as a porogen, CTAB-related ion  $\text{C}_{19}\text{H}_{42}\text{N}^+$  ( $m/z$  284.3320) was observed for certain time after the capillary was disconnected from the LC

system, possibly because it was stuck in the ESI ion source. Taking into account relatively difficult preparation procedure, we decided to focus our experimental efforts exclusively on organic polymers.

### ***III.3.2. Silica particle-based stationary phases***

Both types of silica particles, silica-APTES-GLA and silica-oxGPTMS, were prepared and activated according to **p. II.3.2.1**. Similarly to the protocol applied for capillary-format monoliths, silica particles were quenched by contacting them with aqueous solution of glycine (100 mM) in 10 mM sodium phosphate buffer (pH 6.8) for 2 h. Silica particles were then packed into the chromatographic support and washed with 10 mM ammonium formate buffer (pH 6.8) for approximately 30 minutes. The data acquisition was conducted for 11 minutes for each cartridge (**fig. 26**). Data were collected in a positive mode of ionisation using a MS method adjusted to high flow rate (increased flow rate of the nebulising gas and the curtain gas of the sprayshield and increased temperature of the sprayshield). Cartridges were thermostated at 25°C during the analysis.

#### ***Method 2***

*Source Type: ESI*

*Ion Polarity: Positive*

*Nebulizer: 3.0 Bar*

*Dry Heater: 200°C*

*Dry Gas: 11.6 l/min*

*Scan Begin: 100 m/z*

*Scan End: 600 m/z*

*Capillary: 4500 V*

*Collision Energy: 7.0 eV*

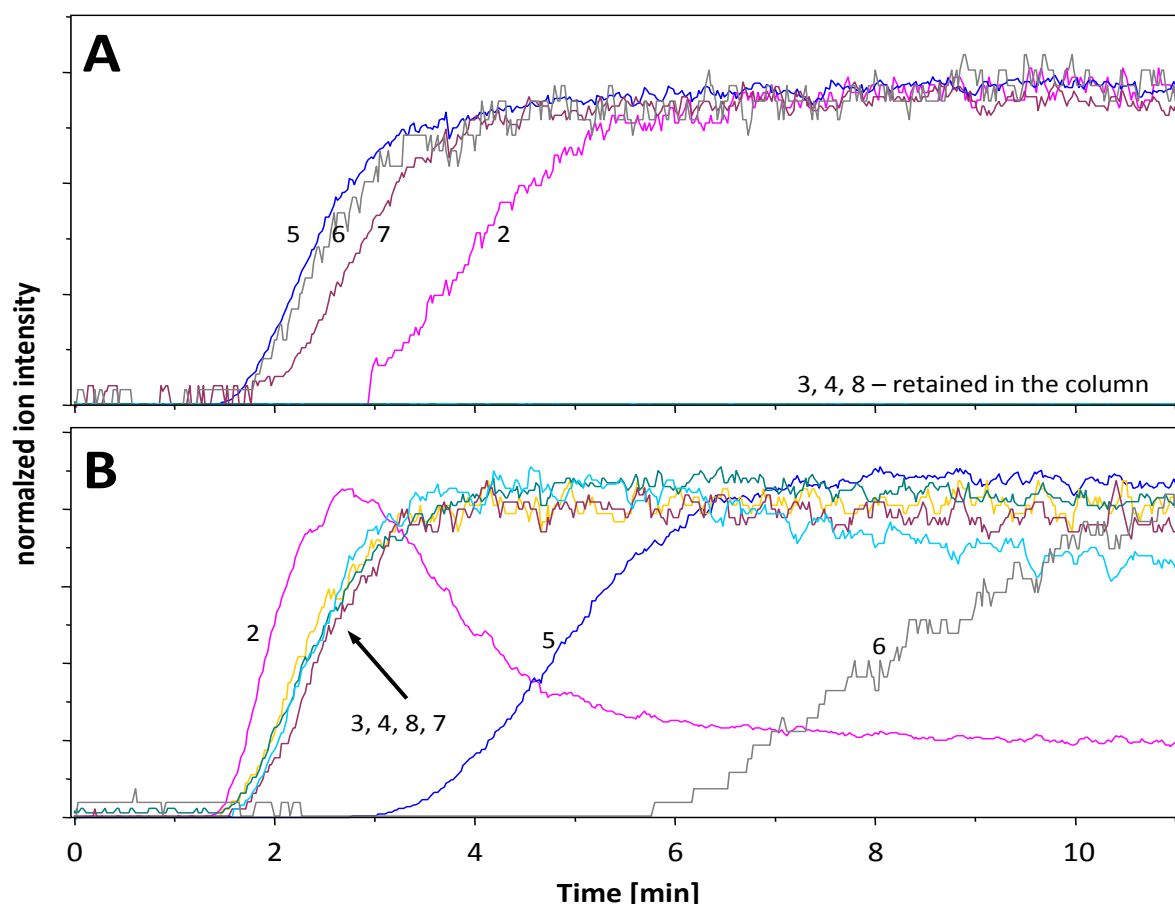


**Figure 26.** The series of extracted ion chromatograms representing the compounds infused into the test capillaries: **A:** end-capped silica-APTES-GLA beads; **B:** end-capped silica-oxGPTMS beads. **2:** L-Glu (magenta,  $m/z$  148.060  $[M+H]^+$ ), **3:** 3-(2,4-Dihydroxyphenyl)propionic acid, DHPA (yellow,  $m/z$  183.065  $[M+H]^+$ ), **4:** ibuprofen (darkgreen,  $m/z$  224.164  $[M+NH_4]^+$ ), **5:** L-Arg (blue,  $m/z$  176.122  $[M+H]^+$ ), **6:** 1-phenylethylamine (gray,  $m/z$  123.10  $[M+1n+H]^+$ ), **7:** arbutin (brown,  $m/z$  290.123  $[M+NH_4]^+$ ), **8:** warfarin (cyan,  $m/z$  311.117  $[M+2n+H]^+$ ). Compound numbers correspond to the numeration in fig. 19. Data were acquired using the method 2. Unusual shape of L-Glu EIC is caused by the suppression of this ion of other compounds within the mixture.

Similarly to amine-bearing poly(SBMA-co-AEMA-co-EGDMA)-based monolith, silica-ATPES-GLA particles strongly retain all hydrophobic or moderately hydrophobic, negatively charged compounds (ibuprofen, DHPA, warfarin). Hydrophobic 1-phenylethylamine is not retained, possibly due to repulsion from positively charged surface of modified silica.

In contrast to silica-ATPES-GLA particles, silica-oxGPTMS does not retain hydrophobic and negatively charged compounds but positively charged hydrophobic 1-phenylethylamine shows significant non-specific interactions.

The comparison of both monoliths was summarised in **table 4**. Similarly to the couple of organic monoliths, both types of silica particles are complementary to each other.

**Table 4.** The summary of the degree of non-specific interactions for silica particles.

Charge at pH 6.8 →	negative			partially negative	positive		neutral
Polarity →	hydrophilic	moderate	hydrophobic		hydrophilic	hydrophobic	hydrophilic
Name →	L-Glu (2)	DHPA (3)	ibuprofen (4)	warfarin (8)	L-Arg (5)	phenylethyl-amine (6)	arbutin (7)
Silica-APTES-GLA							
Silica-oxGPTMS							

- not significant non-specific interaction ( $\Delta t$  less than 2 min)
- moderate non-specific interaction ( $\Delta t$  between 2 and 5 min)
- significant non-specific interaction ( $\Delta t$  between 5 and 10 min)
- very significant non-specific interaction ( $\Delta t$  more than 10 min)

### III.3.3. Selection of the stationary phase for FAC: conclusions

Selection of appropriate base for protein immobilisation should be adjusted to expected nature of studied inhibitors. We showed that GLA-derivatised, amine-bearing stationary phases, both in capillary-format (poly(SBMA-co-AEMA-co-EGDMA)) and in the form of particles (silica-APTES-GLA) strongly interact with hydrophobic, negatively charged compounds. On the other hand, due to positively charged surface, these stationary phases may be successfully applied for studying cationic compounds. Poly(NAS-co-EGDMA)-based monolith and its high-scale counterpart, silica-oxGPTMS particles, may be used for screening libraries or extracts containing negatively charged compounds.

Capillary-format APTES/TEOS hybrid silica monoliths are not compatible with mass spectrometry equipped in ESI ion source due to enormous ion suppression, both in positive and negative mode of ionisation.

## IV.1. FAC experiment using tyrosinase and trypsin as biological targets

### IV.1.1. Capillary-format organic monoliths

Two biological targets were used to verify the usability of organic monoliths in FAC: tyrosinase and trypsin. Arbutin was applied as a model competitive inhibitor of tyrosinase [248] and leupeptin as a model competitive inhibitor of trypsin [249]. Capillaries were synthesized according to the protocol described in *p. II.2.1.1.* and the enzymes were immobilised as described in *p. II.3.1.2.* During all experiments capillaries were thermostated at 25°C. After the series of experiments involving an active enzyme, capillaries were flushed with MeOH for 1 h to denature the enzyme and were used as a negative control. This experimental design allows to use the same capillary for all set of tests thus eliminating the

impact of capillary-to-capillary differences on the parameters of the inflection curves for control and actual experiment.

A series of the 'single infusion' FAC experiments (*p. I.1.2.1*) using leupeptin as trypsin inhibitor standard gave satisfactory results for both types of trypsin-coupled monoliths. Poly(NAS-co-EGDMA)-based polymer interacts with leupeptin in non-specific way (*NI shift*, **fig. 27**), but the specific interactions, represented by *SI shift*, are significant enough to surpass this effect.

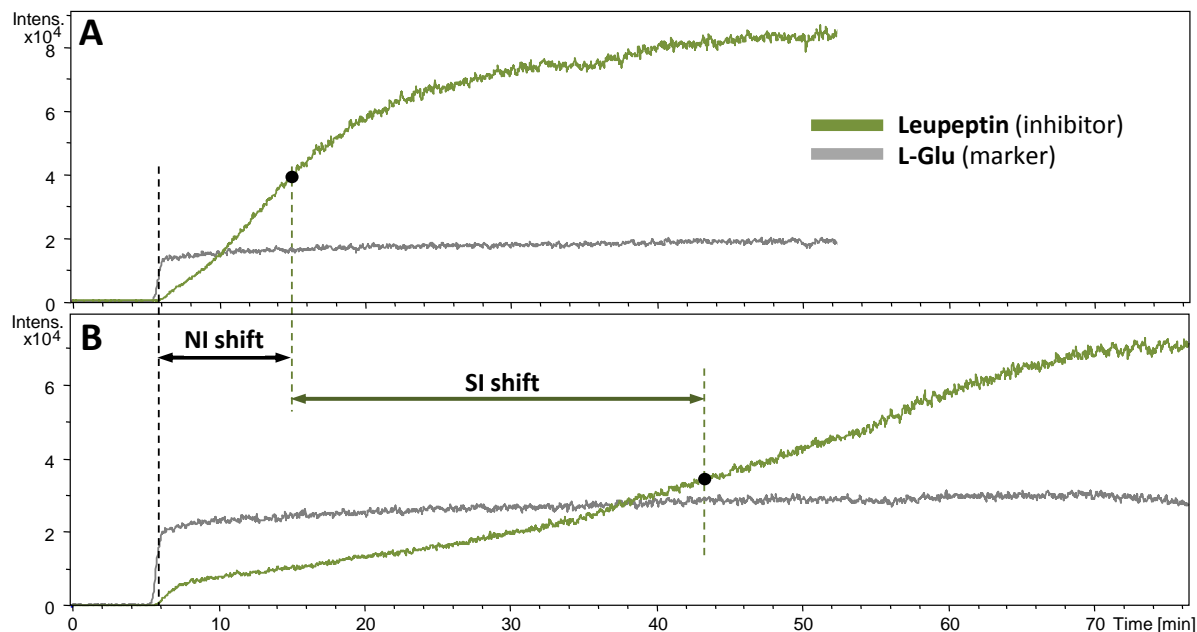


**Figure 27.** FAC experiment for trypsin immobilised on the surface of poly(NAS-co-EGDMA)-based monolith. **A:** capillary with denatured enzyme; **B:** capillary with active enzyme. **NI/SI shift:** the shift representing nonspecific/specific inhibitor–stationary phase interactions. Capillary length: 30 cm. Leupeptin, L-Glu, 0.5  $\mu\text{M}$  in 10 mM ammonium formate buffer (pH 8.1). Flow rate: 3  $\mu\text{L}/\text{min}$ , sample valve switch time: 15 seconds, temperature: 25°C. Leupeptin:  $m/z$  427.303  $[\text{M}+\text{H}]^+$ , L-Glu:  $m/z$  148.059  $[\text{M}+\text{H}]^+$ .

The time of analysis turned out to be very long (approximately 70 minutes). This issue may be addressed by shortening of the capillary length. It will not bring any damage to the monolith, since it is covalently attached to surface of the capillary channel along its entire length.

Comparing to poly(NAS-co-EGDMA)-based polymer (**fig. 28**), positively charged poly(SBMA-co-AEMA-co-EGDMA) polymer does not show almost any non-specific interactions with leupeptin (*NI shift*, **fig. 28**).



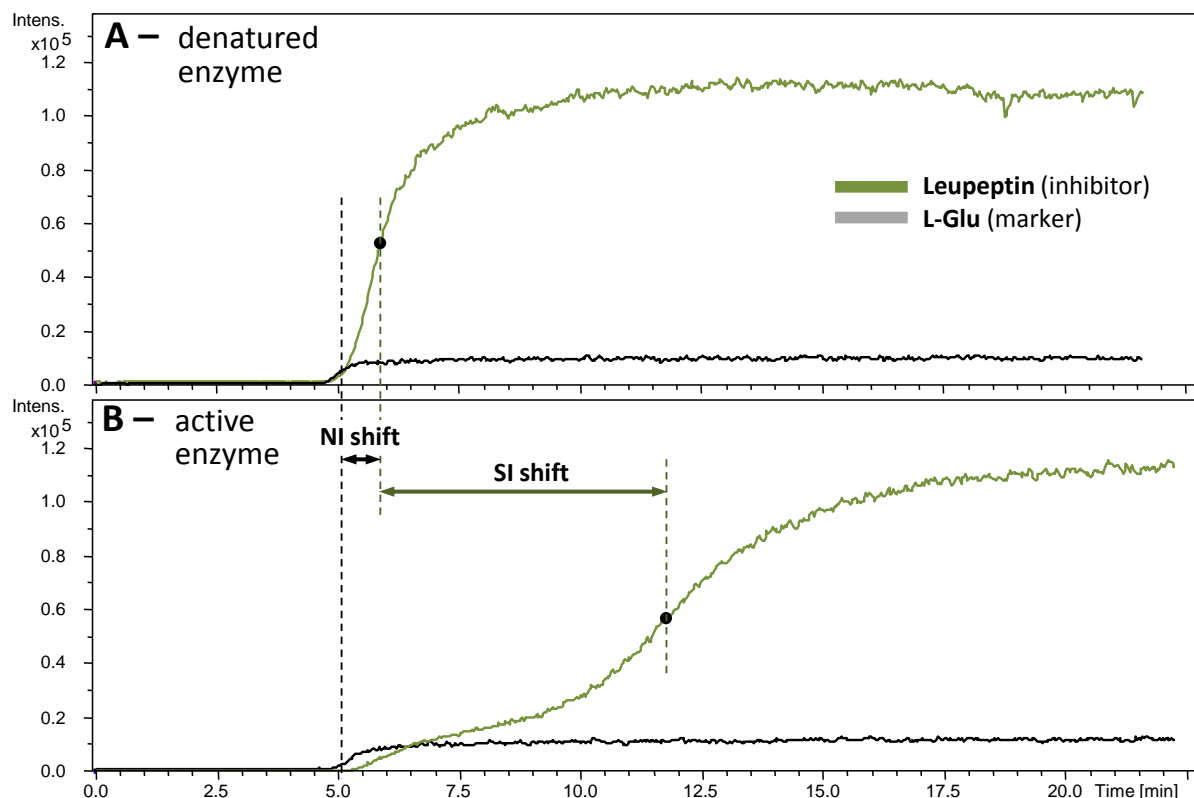


**Figure 28.** FAC experiment for trypsin immobilised on the surface of poly(SBMA-co-AEMA-co-EGDMA)-based monolith. **A:** capillary with denatured enzyme; **B:** capillary with active enzyme. **NI/SI shift:** the shift representing nonspecific/specific inhibitor–stationary phase interactions. Capillary length: 30 cm. Leupeptin, L-Glu, 0.5  $\mu$ M in 10 mM ammonium formate buffer (pH 8.1). Flow rate: 3  $\mu$ L/min, sample valve switch time: 15 seconds, temperature: 25°C. Leupeptin:  $m/z$  427.303  $[M+H]^+$ , L-Glu:  $m/z$  148.059  $[M+H]^+$ .

The strength of the specific interactions is lower than in case of poly(NAS-co-EGDMA)-based monolith, but the ratio of NI/SI shifts is much more significant (7.2 versus 3.1 for poly(NAS-co-EGDMA)-based monolith). The longer SI shift for poly(NAS-co-EGDMA)-based monolith (**fig. 27**) is possibly caused by lower protein binding capacity of the amine-bearing monolith.

Both polymer formulations were shown to be applicable for studying inhibitors of immobilised trypsin.

Poly(NAS-co-EGDMA)-based polymer was shown to be a perfect support for FAC approach employing mushroom tyrosinase as the biological target (**fig. 29**).

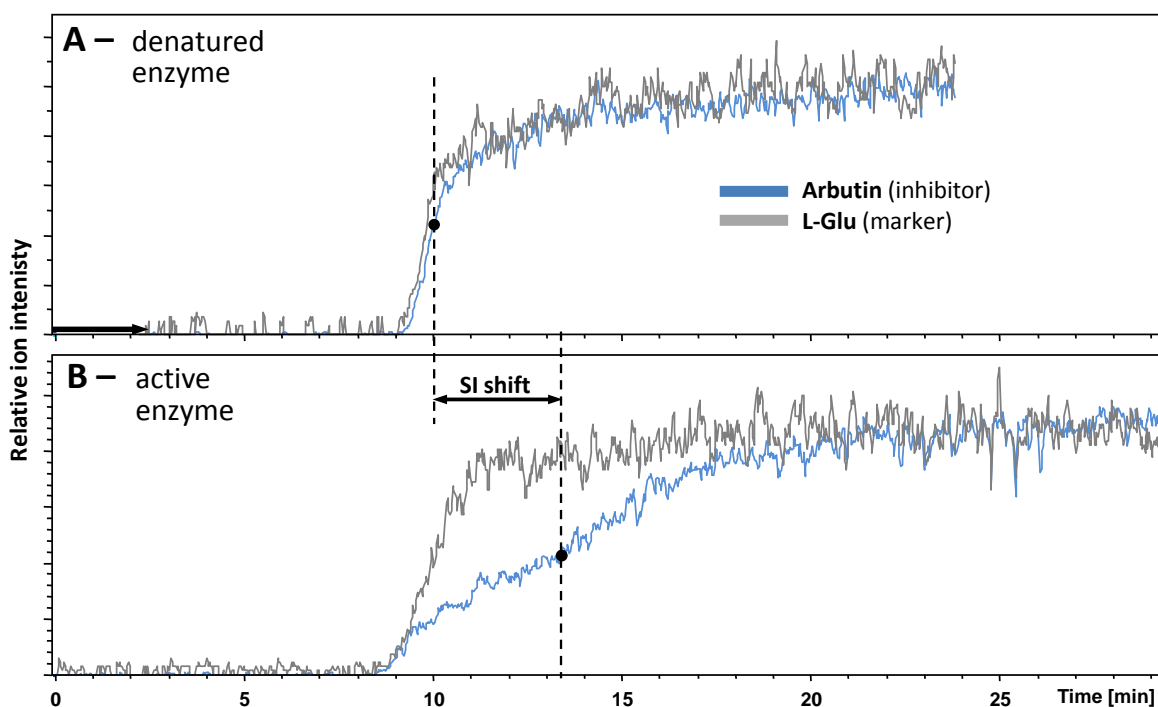


**Figure 29.** FAC experiment for tyrosinase immobilised on the surface of poly(NAS-co-EGDMA)-based monolith. **A:** capillary with denatured enzyme; **B:** capillary with active enzyme. **SI shift:** the shift representing specific inhibitor–stationary phase interactions. Capillary length: 25 cm. Arbutin, 0.5  $\mu\text{M}$ ; L-Glu, 1  $\mu\text{M}$  in 10 mM ammonium formate buffer (pH 6.8). Flow rate: 3  $\mu\text{L}/\text{min}$ , sample valve switch time was different for both runs therefore both curves representing denatured enzyme were shifted manually to overlay the void volume marker curve of the experiment employing an active enzyme. Temperature: 25°C. Arbutin:  $m/z$  290.123  $[M+\text{NH}_4]^+$ , L-Glu:  $m/z$  149.062  $[M+1n+H]^+$ .

Arbutin, used as the inhibitor standard, does not show any non-specific interactions with NAS-based polymer. It simplifies the data analysis, since the total shift of the inflection point for arbutin curve is related exclusively with the specific interactions of this inhibitor with tyrosinase.

#### IV.1.2. Silica particles

Silica-APTES-GLA particles were used as a support for tyrosinase immobilisation, silica-oxGPTMS for immobilisation of trypsin according to the protocols in p. II.3.2.2. Tyrosinase-bound beads were used for the 'single infusion' experiment while trypsin-bound beads to evaluate the 'staircase' frontal analysis (p. I.1.2.2).

The 'single infusion' experiment showed very significant delay of the EIC arbutin curve in the presence of an active mushroom tyrosinase (**fig. 30-B**). To shorten the time of analysis and, at the same time, the consumption of the biological target, one may reduce the volume of the chromatographic support.

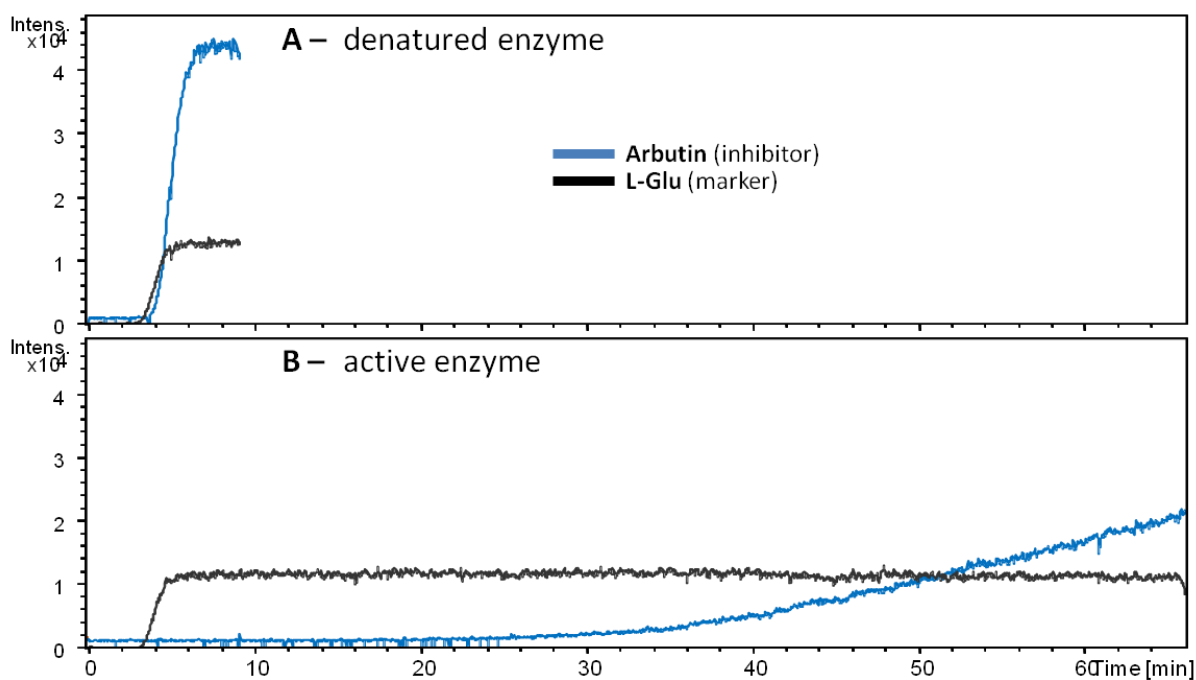


**Figure 30.** FAC experiment for tyrosinase immobilised on the surface of silica-APTES-GLA particles packed into the cartridge (p.2.2.1, fig. 14). **A:** cartridge with denatured enzyme; **B:** cartridge with active enzyme. Mobile phase: 60 mM ammonium formate (pH 7.8), flow rate: 0.2 mL/min, temperature: 25°C. Arbutin and L-Arg: 30  $\mu$ M each.

The 'staircase' frontal analysis approach was successfully conducted for leupeptin–trypsin couple (**fig. 31**). The step gradient applied in this experiment is very easily programmable within the HPLC method.

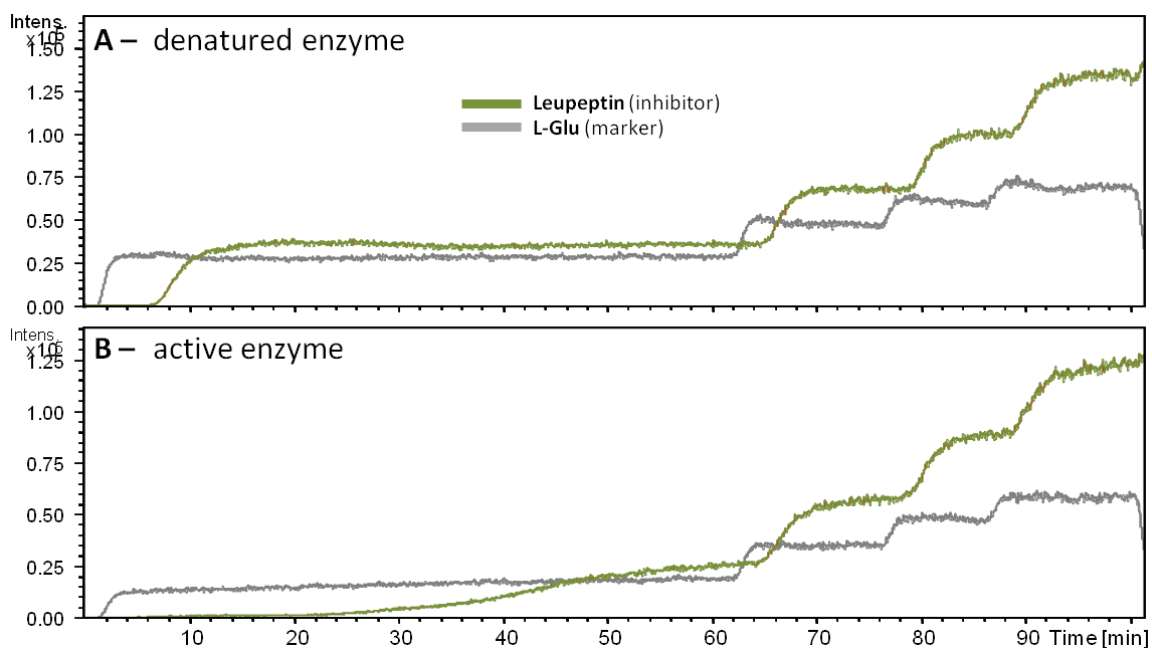


**Figure 31.** 'Staircase' FAC experiment for trypsin immobilised on the surface of silica-oxGPTMS particles packed into the cartridge (p.2.2.1, fig. 14). **A:** cartridge with denatured enzyme; **B:** cartridge with active enzyme. Mobile phase: 50 mM ammonium formate (pH 8.1), flow rate: 0.2 mL/min, temperature: 25°C. The concentration for leupeptin and L-Glu in the test mixture was 30 and 50  $\mu$ M respectively (annotated as  $c_{max}$ ). Gradient was composed of the following steps: 0-20-40-60-80% of the  $c_{max}$ .

The inflection points of the partial breakthrough curves were used to calculate the dissociation constant ( $K_d$ ) and the amount of immobilised target ( $B_t$ ) (**table 5**) on the basis of **equation 7** in *p. 1.1.2.2* of the *Chapter II<sup>##</sup>*. The graphical representation of the **equation 7** for the first three steps was shown in **fig. 32**.

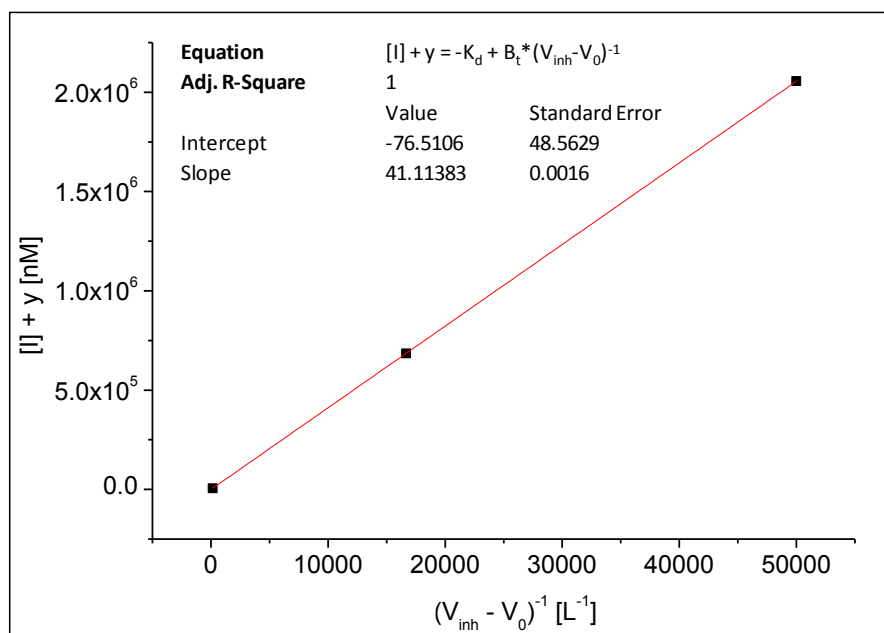


**Figure 32.** Graphical representation of the results obtained for a single run of staircase frontal analysis using leupeptin as a model inhibitor of immobilised trypsin.

The  $K_d$  value obtained in this experiment is within the same order of magnitude as the literature value for free enzyme.  $B_t$  value is in accordance with expected binding capacity of a similar beads – the binding capacity of silica-APTES-GLA for BSA was determined to be on the level of 8.4 mg/g of silica and a single cartridge may host up to 140 mg of dry silica, constituting an equivalent of 1.17 mg of BSA/cartridge (Reader will find the general protocol for the determination of BSA binding capacity of the solid support in the *Appendix I, protocol S3*).

**Table 5.**  $K_d$  and  $B_t$  parameters obtained from 'staircase FAC' the experiment

<b>Dissociation constant (<math>K_d</math>)</b>	<b>calculated: (76.5±48.6) nM</b>
	literature: 13.4 nM [250]
	<b>41.11 nmol/column</b>
<b>Amount of immobilised target <math>B_t</math>:</b>	<b>0.945 mg/column</b>

<sup>##</sup> **equation 7:**  $[I_j] + y_j = \frac{B_t}{V_{inh,j} - V_{0,j}} - K_d$

#### **IV.2. FAC – conclusions**

All immobilisation supports suitable for LC/MS coupling, namely organic monoliths and silica beads, were proven to be a successful base for frontal affinity chromatography. Both capillary-format monoliths used in this work (poly(NAS-co-EGDMA) and poly(SBMA-co-AEMA-co-EGDMA)) were shown to be an effective support for trypsin immobilisation and were proven to be an effective tool for frontal analysis using this enzyme as the biological target. The monolith based on poly(NAS-co-EGDMA) polymer was successfully applied for immobilisation of mushroom tyrosinase and FAC experiment using arbutin as its model inhibitor.

Organic monoliths may be applied in micro-scale experiments requiring an application of expensive biological targets. Their use is limited to 'single infusion' mode of FAC due to low flow rates supported by the capillaries. Cartridges packed with derivatised particles are suitable both for 'single infusion' and 'step gradient FAC'.

Both types of silica particles (silica-APTES-GLA and silica-oxGPTMS) were shown to constitute a stable support for enzyme immobilisation and frontal analysis using tyrosinase and trypsin respectively. Silica-oxGPTMS particles coupled with trypsin were successfully applied for demonstrating the applicability of the step-gradient FAC in our laboratory.

The selection of: *i*) the scale of the immobilisation support (capillary or column format); *ii*) the type of polymer or particles (**p. III.3**) and, finally, *iii*) the mode of FAC experiment depends on projected objectives of the research, availability of the biological target and expected chemical properties of studied inhibitors (polarity and charge).

#### **V. Continuous-flow step gradient mass spectrometry based method for the determination of kinetic parameters of immobilised mushroom tyrosinase in equilibrating conditions: comparison with free enzyme**

Rapid Commun. Mass Spectrom. 2011, 25, 3549–3554  
(wileyonlinelibrary.com) DOI: 10.1002/rcm.5268

# Continuous-flow step gradient mass spectrometry based method for the determination of kinetic parameters of immobilized mushroom tyrosinase in equilibrating conditions: comparison with free enzyme

Aleksander Salwiński, Raphaël Delépée\* and Benoît Maunit

Institute of Organic and Analytical Chemistry (ICOA), UMR CNRS 6005, University of Orleans, BP 6759, 45067 Orléans Cedex 2, France

A mass spectrometry (MS)-based methodology for enzymatic assay in equilibrium conditions was designed and evaluated. This on-line assay involves the introduction of a continuous-flow step gradient (CFSG) of a substrate solution in the column containing immobilized enzyme and the simultaneous tracking of the product formation. We showed that the constant concentration of substrate in the entire bioreactor for an appropriate duration ensures the equilibration of the studied enzyme (mushroom tyrosinase). Under these conditions, it was demonstrated also that the kinetic and enzymatic parameters (Michaelis-Menten constant,  $K_M$ , the maximal specific activity,  $SA_{max}$ ) are independent of the flow rate of the mobile phase. The feasibility of the mentioned approach for inhibitory tests was also investigated. The coupling of the mass spectrometer to the bio-reactor allows the selective monitoring of the enzymatic reaction products and increases their detection level. Very high sensitivity, 500 pmol/min/column, and selective monitoring of the products of the enzymatic reaction are allowed by MS detection. The methodology developed here constitutes a sensitive analytical tool to study enzymes requiring long equilibration times. Copyright © 2011 John Wiley & Sons, Ltd.

Immobilized enzymes are widely used on industrial scale<sup>[1]</sup> and on a laboratory scale, including analytical chemistry,<sup>[2,3]</sup> diagnostics,<sup>[4]</sup> drug screening,<sup>[5,6]</sup> etc. In many cases immobilized enzymes are used to determine enzymatic and kinetic parameters: maximal enzymatic velocity,  $V_{max}$ , Michaelis-Menten constants,  $K_M$ , for novel substrates or for the evaluation of the inhibitory properties of leading drug molecules.<sup>[7,8]</sup> The on-line kinetic assays of immobilized enzymes are normally conducted by injection of a known amount of substrate into an immobilized enzyme reactor (IMER) followed with detection of the product formed within the IMER.<sup>[7–11]</sup> In the single injection mode, both apparent  $K_M$  and  $V_{max}$  values depend drastically on the flow rate of the mobile phase<sup>[7–10]</sup>; in some cases, no specified trend of this relationship can be determined, even for the same enzyme.<sup>[9,10]</sup> A decrease in the flow rate leads to an increase in the contact time between enzyme and substrate. For very low flow rates the full conversion of given amount of substrate can be achieved that consequently leads to formation of plateau of the relation between product amount and flow rate.<sup>[11,12]</sup> Working within this range of flow rates makes it impossible to apply the Michaelis-Menten model (MM) to calculate kinetic parameters; thus the pre-optimization of the single injection assay is required. In the event of the use of long IMERs for single-injection assay

(e.g. capillaries), enzymatic conversion of each single substrate portion gradually lowers its local concentration during its migration towards the outlet of the IMER. This affects the apparent  $V$  value for each substrate injection and causes deviation from the MM model. Another phenomenon that may influence the results of a kinetic assay in single injection mode occurs when the studied enzyme shows a delay ('lag phase') in substrate conversion.<sup>[13–15]</sup> To circumvent these limitations, in this paper we propose a continuous-flow step gradient method (CFSG) for on-line kinetic tests of immobilized enzymes using mass spectrometry (MS) for selective detection of the product formation. The presented method is based on stepwise increase of the substrate concentration in continuous-flow mode and ensures full equilibration of the bioreactor compared to single injection experiments. The CFSG approach that is described here for the first time combined a continuous flow bioreactor,<sup>[16]</sup> and a frontal analysis of ligand–protein binding methodology.<sup>[17,18]</sup> The mushroom tyrosinase, used as a model enzyme (EC 1.14.18.1), catalyzes the oxygen-based oxidation of monophenols to *o*-diphenols and their subsequent oxidation to *o*-quinones.<sup>[19]</sup> Thus, we demonstrate that the apparent  $V_{max}$  measured by the CFSG method is independent of the flow rate, show applicability of the CFSG method to inhibition studies and compare obtained values to free enzyme. In addition, we show a temperature dependence on the kinetic parameters of mushroom tyrosinase. The feasibility of this approach for inhibition studies was presented using kojic acid as model tyrosinase inhibitor.<sup>[20]</sup> Thanks to the application

\* Correspondence to: R. Delépée, Institute of Organic and Analytical Chemistry (ICOA), UMR CNRS 6005, University of Orleans, BP 6759, 45067 Orléans Cedex 2, France.  
E-mail: Raphael.Delepee@univ-orleans.fr

of MS it became possible to monitor all products of the tyrosinase activity and achieve an outstanding 500 pmol/min/column level of quantitation.

## EXPERIMENTAL

### Instrumentation

MS experiments were performed on Bruker maXis UHR-Qq-TOF spectrometer (Bremen, Germany) with a Bruker sprayer in positive electrospray ionisation (ESI) mode, working in single-mass mode. The mass spectrometer was coupled in on-line mode with a Dionex UltiMate 3000 ultra-high-performance liquid chromatography (UHPLC) system (binary pump, standard thermostated column compartment and DAD detector) (Germering, Germany). For all experiments total ion chromatograms were recorded within the mass range of 110 to 400. Profiles of ions of interest (L-Tyr,  $m/z$  182.081 and  $M + 2$  isotopic peak of L-Tyr  $m/z$  184.084; L-DOPA, 198.079 and dopachrome 194.047) were generated as 'extracted ion chromatograms' within the  $\pm 0.01$   $m/z$  range. Subsequently, average mass spectra were generated for the steady-state for each step gradient and used to obtain final values of ion responses.

### Chemicals

Mushroom tyrosinase, L-tyrosine (>99%), (3-aminopropyl) triethoxysilane (APTES) (97%), glutaraldehyde (GLA) (25% in water) and kojic acid (KA) were purchased from Sigma Aldrich (Isle-d'Abeau, France), ammonia (28% solution in water) from Alfa-Aesar (Karlsruhe, Germany), formic acid (97%) and sodium hydroxide were obtained from Fluka (Isle-d'Abeau, France) and hydrogen peroxide (30%) from Fisher Scientific (Elancourt, France). Silica beads (Geduran Si 60, 40–63  $\mu\text{m}$ ) were purchased from Merck (Darmstadt, Germany). All experiments were conducted in ammonium formate buffer (11 mM, pH 6.8, verified before each experiment).

### Preparation of the bioreactor

Non-porous silica beads (3 g) were purified and activated by incubation in a mixture of a 30% aqueous solution of NaOH/30%  $\text{H}_2\text{O}_2/\text{H}_2\text{O}$ : 1/1/4, v/v/v (48 mL) for 15 min. Then, silica beads were washed with distilled water and then incubated for 80 min at 80 °C in 48 mL of the following solution: 37% HCl/30%  $\text{H}_2\text{O}_2/\text{H}_2\text{O}$ : 1/1/4, v/v/v. Silica beads were then washed with distilled water and dried under vacuum.

To an amount of 2 g of activated silica beads 10 mL of toluene and 0.5 mL of APTES were added. The mixture was agitated under solvent reflux at 50 °C for 13 h. Silica beads were then washed with distilled water and kept in an oven at 100 °C for 1 h to promote the complete condensation reaction with APTES. To the resulting silica beads coated with APTES, 30 mL of glutaraldehyde solution (1.67 mL of aqueous solution of GLA (25%) per 1 mg of derivatised silica) prepared in sodium phosphate buffer (0.2 M, pH 7.5) was added. The resulting mixture was allowed to react at room temperature for 2 h. Silica-beads<sub>APTES/GLA</sub> were then dried under vacuum.

A volume of 1 mL of a solution of mushroom tyrosinase (0.91 mg/mL) was added to a flask containing 0.121 g of dry silica-beads<sub>APTES/GLA</sub>. The mixture was allowed to react at 4 °C for 7 h. After completion of the reaction, the mixture was centrifuged, the supernatant was collected for assay purposes and the beads were packed into an empty HPLC column (30 mm length, 4.6 mm diameter). The empty space was filled with sand. The grafting yield was 90.2%.

### Kinetic studies of the free enzyme

All kinetic tests were performed at room temperature (25 °C). Both buffers and samples were thermostated in the water bath. In addition, the measuring cell was also temperature controlled. Kinetic tests were based on several the 'time course' measurements of L-dopaquinone formation (at 475 nm,  $\epsilon_{475\text{nm}} = 3716$  L·mol/cm), produced during the enzymatic reaction.<sup>[21]</sup> The assay was conducted in a 1 mL quartz cuvette filled with tyrosinase solution (corresponding to 2.73  $\mu\text{g}$  of enzyme) in 10 mM sodium phosphate buffer, pH 6.8. The reaction was started by addition of L-tyrosine solution in the same buffer (to obtain a final concentration between 70 and 600  $\mu\text{M}$ ). For the inhibition assay, the three following concentrations of kojic acid were used: 0, 11.57 and 21.21  $\mu\text{M}$ . Values of specific activity (SA) for each L-Tyr concentration (Eqn. (1)) were fitted to the Michaelis-Menten (MM) model to obtain the kinetic parameters. Contrary to enzymatic velocity ( $V_{\text{enz}}$ ), specific activity (SA) is an independent parameter describing enzymatic activity per unit of enzyme quantity; therefore, it will be used later on in this work.

$$\text{SA} [\mu\text{mol}/\text{min}/\text{mg}] = \frac{\Delta \text{Abs}_{475\text{nm}}}{\Delta t \times \epsilon_{475\text{nm}} \times C_{\text{enz}}} \times D \times 10^3 \quad (1)$$

where SA is specific activity;  $C_{\text{enz}}$  is the concentration of mushroom tyrosinase in the initial stock solution, mg/mL;  $\epsilon$  is the absorption coefficient of dopaquinone at 475 nm, L/mol/cm;  $\Delta \text{Abs}_{475\text{nm}}/\Delta t$  is the slope of the linear part of the time course curve,  $\text{s}^{-1}$ ;  $D$  is the dilution factor of the enzyme stock solution.

### Kinetic studies of immobilized enzyme by the CFSG method

The CFSG experiment requires a binary pump LC system to form a step gradient of two mobile phases: A contains the buffer solution and B: the substrate diluted into the buffer solution; this mobile phase is called the 'substrate phase'. By changing the ratio of A to B one may modify the effective substrate concentration in the bioreactor (Fig. 1).

Enzymatic specific activity (SA) is described as the amount of product generated per minute and per defined amount of enzyme ( $\mu\text{mol}/\text{min}/\text{mg}$ ). If we consider the bioreactor as the place of residence of the constant mass of enzyme (mg), we can write:

$$\text{SA} [\mu\text{mol}/\text{min}/\text{mg}] = \frac{n_{\text{pr}}}{\tau \times m} \quad (2)$$

where  $\tau$  is the time of contact between a substrate of a given concentration and enzyme (min);  $n_{\text{pr}}$  is the amount ( $\mu\text{mol}$ ) of product generated within the time  $\tau$ ;  $m$  is the total weight of immobilized enzyme in the bioreactor (mg).

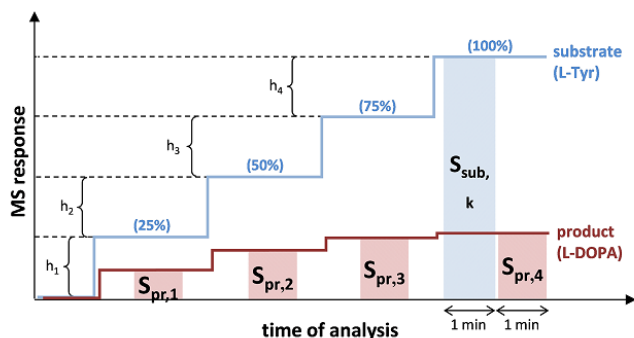


**Figure 1.** Schematic outlook of the methodology of continuous flow step gradient for analysis of enzymatic activity. Values in round brackets represent the contribution of the 'substrate phase' in the mobile phase.  $S_{pr,i}/S_{sub,k}$  is the surface below the product/substrate profile for the time equivalent of 1 min;  $h_i$  is the growth of L-Tyr ion response between successive levels of step gradient.

In respect to the continuous-flow method, in which the product is continuously drained from the bioreactor with a given flow rate  $Q$  (mL/min), an average time of the residence of non-retained substrate in the bioreactor is given by the void volume of bioreactor (mL) divided by  $Q$  (Eqn. (3)):

$$\tau[\text{min}] = \frac{V_0}{Q} \quad (3)$$

Thus, the apparent enzyme activity may be described as:

$$SA[\mu\text{mol}/\text{min}/\text{mg}] = \frac{n_{pr} \times Q}{m \times V_0} = \frac{C_{pr} \times Q}{m} \quad (4)$$

where  $V_0$  is the void volume of the bioreactor (mL),  $C_{pr}$  is the product concentration ( $\mu\text{mol}/\text{mL}$ ) in the system after passing through the bioreactor.

$C_{pr}$  is correlated to the amount of product of the enzymatic reaction ( $n_{pr}$ ) found in volume equal to the void volume of the reactor ( $V_0$ ) and generated within the time needed for  $V_0$  to pass through the bioreactor.

The concentration of product for each of step substrate gradient,  $C_{pr,i-4}$ , is directly proportional to the surface area under the product profile,  $S_{pr,i-4}$  (Eqn. (5), Figs. 1 and 2):

$$C_{pr,i-4}[\mu\text{mol}/\text{mL}] = \beta_{pr} \times S_{pr,i-4} \quad (5)$$

where index 'i' represents a given step of gradient;  $\beta$  is the response coefficient, which depends on the flow rate and settings of the mass spectrometer

From Eqns. (4) and (5), we obtain the following relationship describing the apparent enzyme activity for each concentration of substrate (Eqn. (6)):

$$SA_{i-4}[\mu\text{mol}/\text{min}/\text{mg}] = \frac{\beta_{pr} \times S_{pr,i-4} \times Q}{m} \quad (6)$$

The  $\beta$  coefficient depends highly on the current settings of the mass spectrometer such as ion transmission parameters, flow rate of drying gas, settings of the nebulizer, etc., and shows a linear relationship with the flow rate of the mobile phase. Therefore, an internal standard is required for the comparison of the subsequent analyses. If we introduce the ratio of product to substrate response coefficients,  $\alpha_{pr/sub}$  (Eqn. (7)):

$$\alpha_{pr/sub} = \frac{\beta_{pr}}{\beta_{sub}} \quad (7)$$

and apply Eqn. (5) for the substrate, then insert it and Eqn. (7) into Eqn. (6), we obtain the final relationship describing the enzymatic activity in the continuous flow mode (Eqn. (8)):

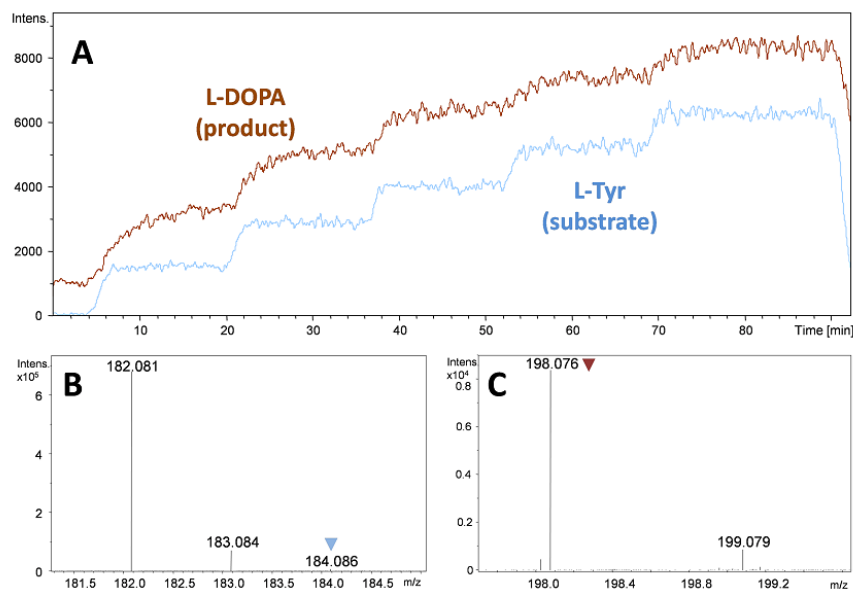


**Figure 2.** Practical profile of the substrate (L-Tyr) step gradient for exemplary assay. (A) The profile of ion intensities of L-Tyr (blue line,  $m/z$  184.086,  $M + 2$  isotopic peak) and L-DOPA (brown line,  $m/z$  198.076, monoisotopic peak); the  $M + 2$  isotopic ion is used for L-Tyr because the intensity of the monoisotopic ion of L-Tyr is too high to fit onto the same scale as L-DOPA. Mass spectra of (B) L-Tyr and (C) L-DOPA.



$$SA_{i_{1-4}} [\mu\text{mol}/\text{min}/\text{mg}] = \frac{\alpha_{pr} \times C_{sub_k} \times S_{pr,i_{1-4}} \times Q}{S_{sub_k} \times m} \quad (8)$$

where the index 'k' represents the reference level of the substrate gradient.

The response ratio (Eqn. (7)) may be determined experimentally on the basis of Eqn. (5) (for product and, analogically, for substrate) for mixtures of L-Tyr and L-DOPA measured together in the same buffer as applied during experiments with the bioreactor. The substrate can be considered as an internal standard only if its transformation during the enzymatic reaction is negligibly low (approximately 1–3%).

Experimental data were fitted to the MM model to obtain kinetic parameters and displayed as Lineweaver-Burk plots. The L-Tyr ion was monitored in the extracted ion chromatogram (*m/z* 182.081, [M + H]<sup>+</sup>, Fig. 2(B)) and L-DOPA as 198.079, [M + H]<sup>+</sup>, Fig. 2(C) (see next section). MS parameters were optimized to minimize formation of adducts of L-tyrosine and L-DOPA and fragmentation of these compounds.

## RESULTS AND DISCUSSION

### Practical description of the methodology

The experimental profile obtained from CFSG experiments (Fig. 2(A)) is very similar to the theoretical profile (Fig. 1). Differences between these profiles give information on enzyme behaviour. Indeed if the observed slope for the substrate profile can be attributed to apparatus dead volume, the long equilibration time observed on the product is the outcome of the complex enzyme cycle. The cycle of tyrosinase activity includes regeneration of enzyme from the most reduced (E<sub>deoxy</sub>) to fully oxidized form (E<sub>oxy</sub>). This comprises other products like dopaquinone or dopachrome.<sup>[13,14]</sup> Both dopaquinone (*m/z* 196.063, [M + H]<sup>+</sup>) and dopachrome (*m/z* 194.047, [M + H]<sup>+</sup>) ions were observed during the experiments but at negligible levels, approximately 9.5% of the total ion response for L-DOPA, within the range of 4–12% for the lowest step of gradient for dopachrome, and less than 1% for dopaquinone. Such a conversion of L-DOPA increases K<sub>M</sub> and lowers observed SA<sub>max</sub> values and is in all cases smaller than 10%. One should note that, in the same way, transformation of dopaquinone (into leukodopachrome and dopachrome) occurs also during assays of tyrosinase activity, both immobilized and in solution and is never taken into account during the data analysis.<sup>[8,9,15,19,20,24]</sup> This phenomenon is absent for enzymes catalysing one defined reaction. Full equilibration of the enzymatic system is only achievable by the CFSG approach. This shows the utility of the proposed methodology compared to the conventional single injection method.<sup>[7–10]</sup>

In the present work, L-Tyr was used as internal standard. Consumption of L-Tyr is on average at a level of 1.7% (0.3–3.3%). This means that the relationship between the substrate ion intensity (M + 2 isotopic peak of L-Tyr: *m/z* 184.084, [M + 2 + H]<sup>+</sup>) and its concentration both before and after passing through the bioreactor is linear (h<sub>1</sub> = h<sub>2</sub> = h<sub>3</sub> = h<sub>4</sub>, Figs. 1 and 2(A)). This linearity is also maintained for the second isotope of L-Tyr (its response is comparable to standard product ion response). In addition,

the use of L-Tyr as internal standard for L-DOPA is justified by the structural similarity of these compounds.<sup>[22,23]</sup> Due to linearity of the relationship of L-Tyr ion response to L-Tyr concentration, selection of the reference 'level' of the step gradient (Eqn. (8)) is fully unrestricted, and in the rest of this work will be called 'k'.

The response ratio of L-DOPA/L-Tyr (Eqn. (7)) was found to be 1.16 ± 0.07 (n = 5; measured for different ratios of L-DOPA/L-Tyr concentrations ranging from 0.3 to 2.3).

### Influence of the flow rate on the kinetic parameters of immobilized enzyme

Subsequent experiments for three flow rates at 25 °C (Fig. 3 and Table 1) showed lack of significant dependence of the maximal specific activity (SA<sub>max</sub>) and K<sub>M</sub> on the flow rate (Q) (Student's t-test, α = 0.05). Moreover, the error was homogeneous (according to Cochran's test). The non-significant variations obtained for these parameters are much smaller than the ones observed in the literature. For example, for tyrosinase: deviations of K<sub>M</sub> and V<sub>max</sub> are found up to 70%, 30% respectively for ΔQ = 0.1 mL/min and for acetylcholinesterase: K<sub>M</sub> and V<sub>max</sub> are up to 21%, 27% respectively for ΔQ = 0.2 mL/min.<sup>[7–10]</sup> The lack of influence of the flow rate on enzymatic parameters for the CFSG method is the result of reaching an equilibrium state

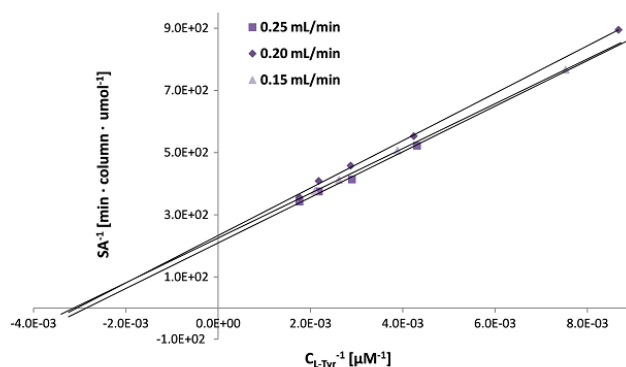


Figure 3. Influence of the flow rate on the Lineweaver-Burk plots representing experiments at 25 °C.

Table 1. Kinetic parameters of immobilized tyrosinase for various flow rates. For each flow rate one series consisting of four or five points (indicated in the table) was recorded.

Flow rate [mL/min]	SA <sub>max</sub> <sup>a</sup> [nmol/min/column]	K <sub>M</sub> <sup>a</sup> [μM]
0.25 (n = 5)	4.60 ± 0.13	324 ± 19
0.2 (n = 5)	4.43 ± 0.24	350 ± 39
0.15 (n = 4)	4.46 ± 0.06	323 ± 9
collective (n = 14)	4.49 ± 0.21	331 ± 32

<sup>a</sup>Non-significant difference between all values of a row checked by Student's t-test (α = 0.05). Deviations of SA<sub>max</sub> and K<sub>M</sub> are homogenous according to Cochran's test (α = 0.05).

and keeping the substrate concentration constant within the bioreactor. For all flow rates, the apparent substrate concentration for a given step in gradient is the same and is not subjected to dilution or diffusion as for the single-injection approach. An average  $K_M$  constant for immobilized enzyme ( $331 \pm 32 \mu\text{M}$ ) is higher than for the free enzyme ( $125.8 \pm 11.9 \mu\text{M}$ ) which is consistent with the literature.<sup>[24–26]</sup> In addition this results from the steric constraints caused by covalent attachment of the enzyme to the support. Day-to-day repeatability of  $K_M$  and  $SA_{\text{max}}$  is satisfactory and the standard deviation does not show any statistical significance (Student's *t*-test,  $\alpha = 0.05$ ). For example, an experiment with two values of flow rate, 0.20 and 0.15 mL/min (both  $n = 5$  points per run) conducted one day before the experiments summarized in Table 1, yielded collective  $K_M$  and  $SA_{\text{max}}$   $366 \pm 46 \mu\text{M}$  and  $4.38 \pm 0.28 \text{ nmol/min/column}$ , respectively. RSD% values for  $K_M$  and  $SA_{\text{max}}$  are 7% and 1%, respectively; however, we observed a gradual drop in enzyme activity, especially after aggravating tests at higher temperatures.

To confirm these results, a single switch of 'substrate phase' was conducted as follows: L-Tyr,  $\times\mu\text{M}$  (%): 0 (0) – 557 (100) – 0 (0) for five various flow rates. The observed growth of product/substrate amount ratio upon the decrease in flow rate is caused by longer contact time between substrate and enzyme. According to expectations, due to correction by the flow rate,  $SA_{\text{app}}$  (calculated by Eqn. (8) for one, fixed concentration of L-Tyr for all values of flow rate) remains unchanged despite the growth in relative product amount (Fig. 4). When the speed of product drainage from the IMER is the same as or higher than the conversion rate, product/substrate amount ratio is expected to reach a plateau, because the product dilution phenomenon is eliminated after the solvent evaporation in the ion source of the mass spectrometer.

#### Influence of the temperature on the kinetic parameters of immobilized enzyme

The relation between  $SA_{\text{max}}$  and temperature of enzymatic reaction is fully compliant with Arrhenius' equation (Fig. 5). The  $SA_{\text{max}}$  value may be used to plot the Arrhenius relationship, because the total amount of enzyme is unchanged

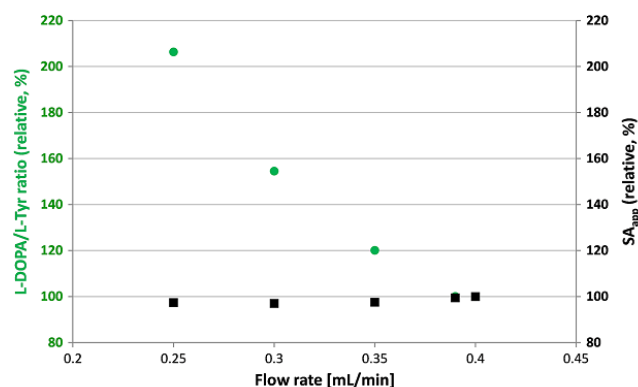


**Figure 4.** Comparison of L-DOPA/L-Tyr (product/substrate ratio (dots, ●) and apparent SA (squares, ■), calculated on the basis of Eqn. (8)) for fixed L-Tyr concentration.

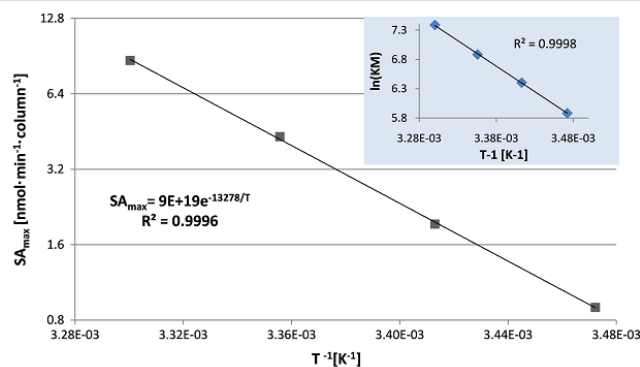


**Figure 5.** Arrhenius relation  $SA_{\text{max}}(T^{-1})$ , logarithmic scale was applied. Inset: relationship between  $K_M$  and reversed temperature.

during subsequent experiments. The activation energy of L-DOPA formation by immobilized tyrosinase calculated on the basis of the Arrhenius equation is 110.4 kJ/mol.

The linear relationship of  $\ln(K_M)$  versus inversed temperature (Fig. 5, inset) is consistent with the van't Hoff equation and shows that the Michaelis-Menten constant may be attributed to dissociation constant of the L-Tyr from the enzyme-substrate complex.<sup>[27]</sup>

#### Inhibitory studies of tyrosinase by the CFSG method

Kojic acid (KA) was selected as a model inhibitor of tyrosinase. It was shown to be a competitive inhibitor of monophenolase activity of mushroom tyrosinase towards L-Tyr.<sup>[20]</sup> For CFSG experiments, the concentration of inhibitor was maintained constant in the bioreactor during entire gradient duration. In the case of the free enzyme assay, the inhibition constant ( $K_I$ ) was found to be  $3.56 \pm 0.44 \mu\text{M}$ , while for the immobilized enzyme it was  $3.10 \pm 0.05 \mu\text{M}$  (Lineweaver-Burk plots are shown in Fig. 6).

#### CONCLUSIONS

The continuous-flow step gradient method for studying enzyme activity in on-line mode with MS detection is a very useful technique for bioreactors showing very low activity (e.g. 500 pmol/min/bioreactor, which is obtained for the highest concentration of KA recorded for this study). This is

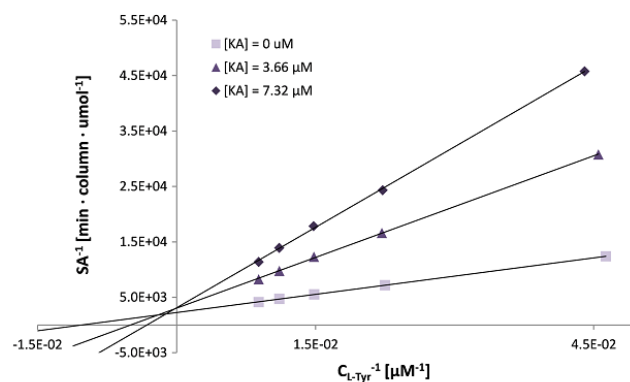


**Figure 6.** Lineweaver-Burk plots representing inhibitory properties of kojic acid towards immobilized tyrosinase.

especially valuable for screening purposes, where in many cases human enzymes have to be applied to avoid false positive or false negative results during the use of their animal or bacterial equivalents. Amounts of human-derived enzymes are usually very limited thus rendering the need to apply extremely sensitive analytical methods. The CFSG method eliminates the influence of flow rate on the kinetic parameters (activity,  $K_M$ ) and enables on-line inhibition assays. Simultaneously, application of a mass spectrometer as the detector enables the specific and sensitive monitoring of enzymatic products, which is often not possible in the case of UV-VIS spectroscopy.

### Acknowledgements

The authors would like to thank Dr. Cyril Colas (ICOA, Orleans, France) for his continuous and valuable technical assistance in LC/MS measurements. The authors also wish to thank Dr. Agnes Chartier for her valuable contribution to the linguistic part of the present work and instructive discussions concerning the factual content.

### REFERENCES

- [1] A. Gallifuoco, F. Alfani, M. Cantarella, G. Spagna, P. G. Pifferi. *Process Biochem.* **1999**, *35*, 179.
- [2] H. Henriksson, I. G. Muñoz, R. Isaksson, G. Pettersson, G. Johansson. *J. Chromatogr. A* **2000**, *898*, 63.
- [3] C. Yao, L. Qi, J. Qiao, H. Zhang, F. Wang, Y. Chen, G. Yang. *Talanta* **2010**, *82*, 1332.
- [4] J. Annie Ho, L. Wu, N.-C. Fan, M.-S. Lee, H.-Y. Kuo, C.-S. Yang. *Talanta* **2007**, *71*, 391.
- [5] R. Mallik, M. J. Yoo, C. J. Briscoe, D. S. Hage. *J. Chromatogr. A* **2010**, *1217*, 2796.
- [6] Y. Cheng, E. Ho, B. Subramanyam, J.-L. Tseng. *J. Chromatogr. B* **2004**, *809*, 67.
- [7] M. Bartolini, V. Cavrini, V. Andrisano. *J. Chromatogr. A* **2007**, *1144*, 102.
- [8] M. Bartolini, N. H. Greig, Q.-S. Yu, V. Andrisano. *J. Chromatogr. A* **2009**, *1216*, 2730.
- [9] A. M. Girelli, E. Mattei, A. Messina, D. Papaleo. *Sensor. Actuat. B* **2007**, *125*, 48.
- [10] A. M. Girelli, E. Mattei, A. Messina. *Sensor. Actuat. B* **2007**, *121*, 515.
- [11] C. L. Cardoso, V. V. Lima, A. Zottis, G. Oliva, A. D. Andricopulo, I. W. Wainer, R. Moaddel, Q. B. Cass. *J. Chromatogr. A* **2006**, *1120*, 151.
- [12] F. A. Bertolino, I. E. De Vito, G. A. Messina, H. Fernández, J. Raba. *J. Electroanal. Chem.* **2011**, *651*, 204.
- [13] T.-S. Chang. *Int. J. Mol. Sci.* **2009**, *10*, 2440.
- [14] M. Jimenez, F. García-Carmona. *Biochem. Biophys. Acta* **1996**, *1297*, 33.
- [15] J. C. Espín, R. Varon, L. G. Fenoll, M. A. Gilabert, P. A. García-Ruiz, J. Tudela, F. Garcia-Canovas. *Eur. J. Biochem.* **2000**, *267*, 1270.
- [16] R. S. Singh, G. K. Saini, J. F. Kennedy. *Carbohydr. Polym.* **2011**, *83*, 672.
- [17] E. Calleri, C. Temporini, G. Massolini. *J. Pharmaceut. Biomed.* **2011**, *54*, 911.
- [18] Z. Tong, K. S. Joseph, D. S. Hage. *J. Chromatogr. A* **2011**, DOI: 10.1016/j.chroma.2011.04.078.
- [19] L. G. Fenoll, J. N. Rodríguez-López, F. García-Molina, F. García-Cánovas, J. Tudela. *Int. J. Biochem. Cell Biol.* **2002**, *34*, 332.
- [20] J. S. Chen, C.-I. Wei, R. S. Rolle, W. S. Otwell, M. O. Balaban, M. R. Marshall. *J. Agric. Food Chem.* **1991**, *39*, 1396.
- [21] M. E. Marín-Zamora, F. Rojas-Melgarejo, F. García-Canovas, P. A. García-Ruiz. *J. Biotechnol.* **2006**, *126*, 295.
- [22] D. Richardson, C. A. Ortori, V. Chapman, D. A. Kendall, D. A. Barrett. *Anal. Biochem.* **2007**, *360*, 216.
- [23] N. Yamane, Z. Tozuka, Y. Sugiyama, T. Tanimoto, A. Yamazaki, Y. Kumagai. *J. Chromatogr. B* **2007**, *858*, 118.
- [24] M. Y. Arica, G. Bayramoğlu, N. Bıçak. *Process Biochem.* **2004**, *39*, 2007.
- [25] M. Y. Arica, S. Senel, N. G. Alaeddinoglu, S. Patır, A. Denizli. *J. Appl. Polym. Sci.* **2000**, *75*, 1685.
- [26] E. A. Ponomareva, V. E. Kartuzova, E. G. Vlach, T. B. Tennikova. *J. Chromatogr. B* **2010**, *878*, 567.
- [27] I. Hajdu, A. Szilagyi, J. Kardos, P. Zavodszky. *Biophys. J.* **2009**, *96*, 5003.

## Appendix I. Supplementary data

### **Protocol S1.** *Vinylisation of the silica wall for covalent attachment of the organic polymer*

UV-transparent fused silica capillary was first activated by flushing it with 1 M NaOH for 30 min at a flow rate of 200  $\mu\text{L/h}$  then treated by the solution of TMSPA (**fig. S1**) in 6 mM acetic acid (1/125, v/v) for 10 min at 300  $\mu\text{L/h}$  and afterwards derivatised in a static mode for 1 hour at room temperature. The capillary was then washed with water for 30 min at 200  $\mu\text{L/h}$ . Remaining water must be eliminated from the capillary by flushing it with the stream of air to avoid the precipitation of the hydrophobic monomers that are subsequently introduced into the capillary. The mechanism of the silica surface derivatisation is described in *p. II.2.2.* of present chapter.

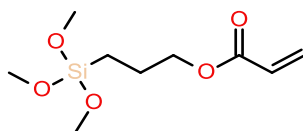


**Figure S1.** *The structure 3-(trimethoxysilyl)propyl acrylate (TMSPA).*

### **Protocol S2.** *Photoinitiated polymerisation of the organic monoliths*

The polymerisation of monoliths was photoinitiated by a standard UV light source (BLX E-365, 5x8W, 365 nm, BIO-LINK Vilber Lourmat, Marne-la-Vallée, France). The teflon-coated capillary filled with the mixture of monomers and capped at both sites with the silicon rubber was irradiated with UV light for approximately 55 minutes (the total energy emitted during the process of polymerisation was controlled by the light source and was equal to 6  $\text{J/cm}^2$ ).

### **Protocol S3.** *Bradford protein assay*

Bradford protein assay was used for quantification of bovine serum albumin (BSA) bound to the solid support (silica particles described in the *Chapter II* or magnetic nanoparticles described in the *Chapter III*). A standard assay was based on a comparison of the difference in BSA concentration before and after its immobilisation on the surface of a known mass of a solid support of interest. The binding capacity was calculated on the basis of this difference and was expressed as the mass unit of BSA bound to the mass unit of the solid support, usually (mg/g).

#### *Preparation of a Bradford solution*

Briefly, a mass of 3.95 mg of Coomassie Brilliant Blue was dissolved in 5 mL of EtOH. A volume of 10 mL of orthophosphoric acid was subsequently added to this solution and resulting mixture was diluted up to 100 mL by distilled water. It was then filtrated through a syringe filter (0.45  $\mu\text{m}$ ) and stored in a dark

and cold place until use. BSA calibration solutions were prepared in the same buffer as the one applied for the immobilisation process (sodium phosphate buffer, 10 mM, pH 6.8).

A single protein assay was conducted by mixing a volume of 20  $\mu\text{L}$  of the test protein solution with 990  $\mu\text{L}$  of the Bradford solution in an Eppendorf tube. The mixture was then incubated in the dark and then subjected to a measurement of absorption at 595 and 450 nm. The calibration curve was constructed by plotting the values of  $A_{595\text{nm}}/A_{450\text{nm}}$  ratio against the concentrations of BSA calibration solutions, according to Zor *et al.* [251].

# Modified 'staircase' frontal affinity chromatography for determination and characterization of the inhibitors of enzymes in the complex mixtures



Aleksander SALWIŃSKI, David DA SILVA, Raphaël DELÉPÉE, Benoît MAUNIT

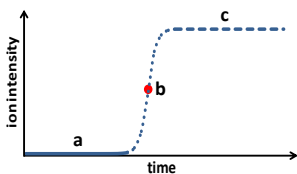
Université d'Orléans, CNRS, ICOA, UMR 7311, F-45067 Orleans, France

e-mail: aleksander.salwinski@univ-orleans.fr



## INTRODUCTION

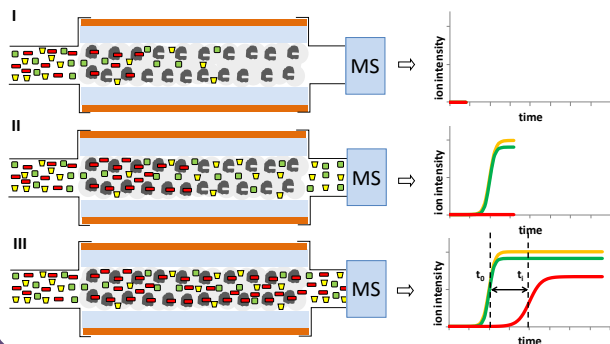
Frontal analysis (FA) is an approach based on LC-MS system enabling simultaneous ranking the ligands/inhibitors according to their affinities to biological target (enzyme/receptor). FA experiment is based on the constant infusion of the studied ligand/inhibitor (or their mixture) and void, non-interacting marker into the bioreactor with the immobilized target (enzyme or receptor). This experiment design entails the characteristic shape of the elution profile for each compound in the mixture baseline plateau (a); area of the growth of curve with the inflection point (b, ) and the upper plateau (c). In case of the application of MS detection, we can follow ionisable ligands/markers independently.



## FRONTAL ANALYSIS - FUNDAMENTALS

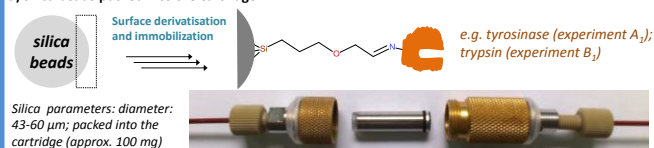
During infusion of the studied mixture into the bioreactor non-interacting compounds freely pass through it. The only possible interactions for this group of compounds are non-specific (e.g. ionic, hydrophobic) and may be resolved by applying blank (reservoir of e.g. inactivated enzyme prepared in the same way as bioreactor). Simultaneously, inhibitor molecules start to bind to the enzyme (I) and thus the front of the curve related to inhibitor is delayed in relation to the fronts of non-interacting compounds (II). Finally, after obtaining full saturation of the bioreactor, inhibitor molecules start to appear in the mobile phase in the post-bioreactor zone (III). For constant amount of immobilized enzyme (B<sub>0</sub>) and given concentration of inhibitor, [I]<sub>0</sub>, enzyme-inhibitor dissociation constant K<sub>d</sub> is inversely proportional to 'inhibitor delay', (t<sub>1</sub> - t<sub>0</sub>), (III), where t<sub>1</sub> and t<sub>0</sub> are times corresponding to the inflection points of inhibitor/non-interacting compounds. To obtain K<sub>d</sub> and B<sub>0</sub> values, several infusions of the test mixtures differing in the concentration of the interacting compound are needed.

■ = enzyme; □ = non-interacting compounds; ■ = inhibitor

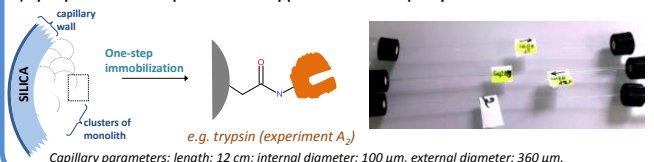


## The strategies of enzyme immobilization to MS compatible solid support

### a) silica beads packed into the cartridge



### b) hydrophilic monolithic porous stationary phase inside the capillary



## Literature

D.C. Schriemer, D. R. Bundle, L. Li, O. Hindsgaul, Angew. Chem. Int. Ed. **1998**, 37, 3383-3387  
L. Zhu, L. Chen, H. Luo, X. Xu, Anal. Chem. **2005**, 77, 6125-6133  
Enrica Calleri et al., J. Med. Chem. **2010**, 53, 3489-3501

## Acknowledgement

AS is grateful for the financial support of Région Centre.

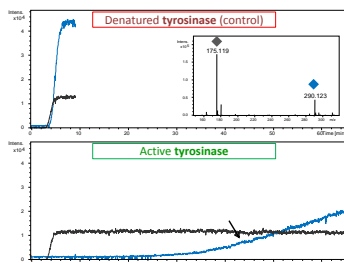


## RESULTS

### A) Single infusion experiment

#### A<sub>1</sub>) Tyrosinase, silica beads

The profiles of extracted ion chromatograms of L-arginine (void volume marker, [M+H]<sup>+</sup>: m/z 175.119) and arbutin (inhibitor, [M+NH<sub>4</sub>]<sup>+</sup>: m/z 290.123) for the columns with immobilized tyrosinase active/denatured.

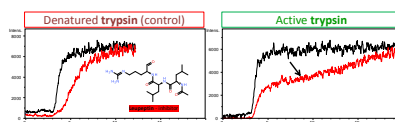


Significant delay of the extracted ion chromatogram of the inhibitor in case of the column with active enzyme. An immediate information about the prospective inhibitor candidates in the mixture

Conditions: Mobile phase: 60 mM ammonium formate, pH 7.8; flow rate: 0.2 mL/min; temp. 25°C. Arbutin/L-arginine: 30 μM each.

#### A<sub>2</sub>) Trypsin, monolithic capillary

The profiles of extracted ion chromatograms of L-aspartic acid (void volume marker, [M+H]<sup>+</sup>: m/z 134.041) and leupeptin (inhibitor, second isotope: [M+H]<sup>+</sup>: m/z 429.301) for the capillaries with immobilized trypsin (active/denatured).



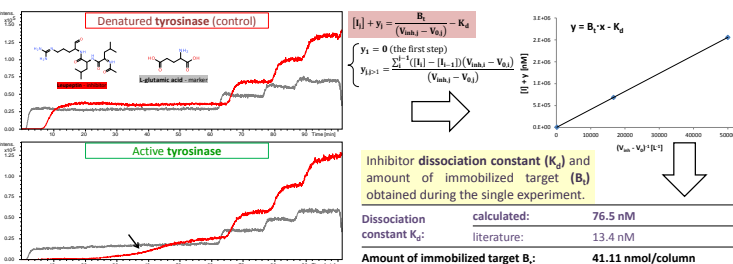
Significant delay of the inhibitor in case of the capillary with active enzyme.

Conditions: Mobile phase: 10 mM ammonium formate, pH 8.5; flow rate: 4 μL/min; temp. 25°C. Leupeptin/L-aspartic acid: 500 nM each. Capillary length: 12 cm each.

### B) Multistep gradient experiment

#### B<sub>1</sub>) Trypsin, silica beads

The comparison of multistep gradient profiles of extracted ion chromatograms of L-glutamic acid (void volume marker, [M+H]<sup>+</sup>: m/z 146.044) and leupeptin (inhibitor, [M+H]<sup>+</sup>: m/z 425.285) for the columns with immobilized trypsin active/denatured (approximately 100 mg of the solid support/column). On the basis of the values of inflection points for each step of the gradient for active/denatured enzyme it is possible to calculate K<sub>d</sub> and B<sub>0</sub>.



## A COMPARISON OF THE MULTISTEP GRADIENT AND THE SINGLE INFUSION APPROACHES

	Single infusion	Multistep gradient
The possibility to obtain K <sub>d</sub> and B <sub>0</sub> parameters during the single experiment	NO, several infusions of the series of test samples differing in the concentration are required	YES
The possibility of an automation of the assay	YES (more difficult)	YES
Immediate information about the inhibitor candidate in the sample	YES	YES
The risk of enzyme saturation after the first few steps by strong inhibitors	NO	YES
Complexity of data analysis	very low	moderate
Application of the capillary (reduces required quantity of enzyme)?	YES	NO
Proposed application:	Quick assay of the presence of inhibitors/simultaneous ranking of the library of various inhibitors at the same concentration	Characterization of the inhibitor

## CONCLUSIONS

Although only single-inhibitor examples were presented herein, frontal analysis may also be applied for multi-inhibitor mixtures. Thanks to the application of mass spectrometer as the detection unit, it is possible to track (and draw breakthrough curves) for each component of studied mixture independently. FA opened the possibility to find new inhibitors in the plant extracts and thus constitutes an alternative to bioassay-guided fractionation.

### The advantages of frontal analysis approach comparing to the classical enzymatic assay:

- automated, simultaneous determination of specific inhibitor-enzyme interactions in the complex mixtures;
- the possibility of determination of the dissociation constant with known concentration of given inhibitor;
- possible reutilization of immobilized enzyme;
- no need for any marker of enzymatic activity;
- simplicity of the analysis;
- low consumption of enzyme (amounts on the level of pmol/capillary or nmol/column with silica beads);
- extendible for various enzymes and receptors



## **CHAPTER III**

**Enzyme-coupled nanoparticles-assisted laser  
desorption ionisation MS for searching for low-mass  
inhibitors of enzymes in complex mixtures**





Cette partie du manuscrit traite de l'utilisation de nanoparticules magnétiques de silice sur lesquelles sont immobilisées les enzymes trypsine (enzyme modèle) ou tyrosinase (enzyme d'intérêt), appelée **Enzyme Magnetic nanoParticules (EMPs)**, comme outil de criblage primaire d'extrait naturel de plantes permettant d'identifier par spectrométrie de masse MALDI-TOF MS des inhibiteurs d'origine naturelle de différentes cibles (enzymes). Il s'avère que l'utilisation des nanoparticules magnétiques de silice ouvre la possibilité d'immobiliser un large panel d'enzymes et qu'elles participent à l'ionisation des analytes lors de l'analyse par MALDI-TOF MS, évitant ainsi d'appliquer sur la plaque d'échantillonnage une matrice organique sous pH contrôlé telle que la 9-aminoacridine seule ou en mélange avec l'acide  $\alpha$ -cyano-4-hydroxycinnamique ou bien la 1,8-bis(diméthylamino)naphthalène.

Cette méthodologie innovante a été baptisée « **Enzyme-coupled Nanoparticles-Assisted Laser Desorption Ionisation Mass Spectrometry (ENALDI-MS)** ». Celle-ci est basée sur l'utilisation de bille de silice magnétiques de diamètre compris entre 100 nm et 1  $\mu$ m sur lesquelles une fonctionnalisation par le (3-aminopropyl)triéthoxysilane (APTES)/Glutaraldéhyde (GLA) et par le (3-glycidioxypropyl)triméthoxysilane (GPTMS) va permettre le greffage des deux enzymes tyrosinase et trypsine.

L'application de l'ENALDI-MS s'est faite selon deux approches complémentaires : i) la première appelée « IF-MS » pour « Ion Fading Mass Spectrometry » qui consiste à permettre une détection par spectrométrie de masse MALDI-TOF des interactions spécifiques entre des molécules d'intérêt présentes dans l'extrait végétal brut et l'enzyme cible, ici la tyrosinase ; ii) la deuxième dénommée « IH-MS » pour « Ion Hunting Mass Spectrometry » permet de confirmer les résultats obtenus par la première à travers une pré-concentration de l'inhibiteur présent dans l'échantillon.

Cette méthodologie a été appliquée dans un premier temps sur des composés standards, décrits dans la littérature comme étant des forts inhibiteurs, tels que la glabridine, inhibiteur de la tyrosinase et la leupeptine inhibiteur de la trypsine afin de valider la faisabilité. Par la suite, ces mêmes travaux ont été effectués sur des extraits de plantes de racines de réglisse (*Glycyrrhiza glabra*) et de tiges et feuilles de *Sparrmannia discolor* afin d'identifier de potentiels candidats lors du criblage primaire de ces extraits.

Il s'avère que les analyses effectuées sur ces extraits en présence de l'enzyme tyrosinase ont permis de mettre en évidence la présence de 6 candidats potentiels (inhibiteurs) et de les identifier par spectrométrie de masse Haute Résolution (maXis Qq-TOF, Bruker) et dont l'un a été confirmé par Résonance Magnétique Nucléaire. Parmi ces inhibiteurs l'acide 2-[(4-Hydroxyphényl)méthyl]malonique ainsi que l'Apigénin-6-C-rha-8-C-glu (isoviolanthin) et, dans une moindre mesure, son isomère proche l' Apigénin-6-C-glu-8-C-rha (violanthin) ont été révélés dans le cadre de l'extrait de réglisse. En ce qui concerne l'extrait de *Sparrmannia discolor*, l'acide rosmarinique et le Kaempferol-3-O-(6'-E-p-coumaroyl)-glucoside ont, quant à eux, été identifiés comme inhibiteurs de la tyrosinase.

Ces études, nous ont permis également de mettre en évidence un phénomène peu décrit dans la littérature, soit la participation efficace de l'enzyme tyrosinase, en présence du substrat naturel L-Tyrosine ou la catéchine, à l'hydroxylation et l'oxydation d'inhibiteurs tels que la glabridine et de l'acide 3-(2,4-dihydroxyphenyl)-propionique (DHPA).

Les deux approches IF-MS et IH-MS apparaissent comme des approches innovantes de criblage primaire, rapides et efficaces, afin de mettre en évidence les interactions enzyme-ligand et/ou enzyme-substrat dans des mélanges complexes tels que des extraits de plantes et ainsi donner la possibilité d'identifier des molécules bioactives d'intérêt, en l'occurrence ici des inhibiteurs naturelles de la tyrosinase.

**Chapter III** – Enzyme-coupled nanoparticles-assisted laser desorption ionisation MS for searching for low-mass inhibitors of enzymes in complex mixtures

<b>I. Ion Fading/ Ion Hunting Enzyme-coupled nanoparticles-assisted laser desorption ionisation MS...</b>	<b>95</b>
<b>I.1. Introduction.....</b>	<b>95</b>
<b>I.2. Experimental.....</b>	<b>97</b>
<b>I.2.1. Extraction of plant material.....</b>	<b>97</b>
<b>I.2.2. Synthesis of functional magnetic nanoparticles.....</b>	<b>97</b>
I.2.2.1. Synthesis of raw magnetic nanoparticles.....	97
I.2.2.2. Derivatisation of raw MPs.....	98
I.2.2.2.1. Aldehyde-covered MPs-APTES-GLA.....	98
I.2.2.2.2. Aldehyde-covered MPs-oxyGPTMS.....	98
<b>I.2.3. Immobilisation of enzymes: trypsin and tyrosinase.....</b>	<b>99</b>
<b>I.2.4. Kinetic assay of free and immobilised tyrosinase.....</b>	<b>99</b>
I.2.4.1. Determination of kinetic parameters of free and immobilised tyrosinase.....	99
I.2.4.2. Stability of immobilised tyrosinase.....	100
<b>I.2.5. Mass spectrometry.....</b>	<b>100</b>
<b>I.3. IF/IH-ENALDI MS: results and discussion.....</b>	<b>101</b>
<b>I.3.1. Characterisation of MPs as a non-organic matrix and host for enzyme immobilisation.....</b>	<b>101</b>
I.3.1.1. Structural characterization of MPs.....	101
I.3.1.2. Magnetic nanoparticles as an immobilisation support.....	102
I.3.1.3. Application of EMPs as non-organic matrix.....	104
<b>I.3.4. 'Ion Fading' IF-ENALDI MS and 'Ion Hunting' IH-ENALDI MS - illustration of the experimental approach using standard inhibitors.....</b>	<b>104</b>
I.3.4.1. Experimental design and evaluation of IF-ENALDI MS.....	104
I.3.4.2. Experimental design and evaluation of IH-ENALDI MS.....	107
<b>I.3.5. An application of IF-ENALDI MS to the samples of plant extracts.....</b>	<b>109</b>
<b>I.3.6. The complement of IF-ENALDI MS: identification of inhibitor and substrate candidates by ESI-Qq-TOF MS.....</b>	<b>112</b>
I.3.6.1. Aqueous extract of liquorice roots.....	115
I.3.6.2. Methanol extract of Sparrmannia discolor leaves and stems.....	120
<b>I.4. IF/IH-ENALDI MS – conclusions.....</b>	<b>126</b>
<b>II. The use of enzyme-coupled magnetic particles to study the spectrum of unusual substrates of tyrosinase by direct surface-assisted laser desorption/ionisation and ESI-Qq TOF MS.....</b>	<b>128</b>
<b>II.1. Introduction.....</b>	<b>128</b>
<b>II.2. The rationale for this study.....</b>	<b>131</b>
<b>II.3. ESI-Qq-TOF MS evaluation of tyrosinase-driven oxidation of 2,4-resorcinol-containing tyrosinase inhibitors.....</b>	<b>131</b>
<b>II.4. The experiment design and results.....</b>	<b>132</b>
<b>II.5. Conclusions.....</b>	<b>135</b>
<b>Appendix II: Supplementary Information.....</b>	<b>137</b>



## Abstract

In this report, enzyme-coupled magnetic nanoparticles (EMPs) were shown to be an effective affinity-based tool for finding specific interactions between enzymatic targets and the low-mass molecules in plant extracts using MALDI-TOF spectrometer. EMPs used in this work act as non-organic matrix enabling ionisation of small molecules without any interference in the low-mass range: <500 Da (enzyme-coupled nanoparticles-assisted laser desorption ionisation mass spectrometry, ENALDI MS) and simultaneously carry the superficial specific binding sites to capture inhibitors present in a studied mixture. We evaluated ENALDI approach in two complementary variations: 'Ion Fading' (IF-ENALDI), based on superficial adsorption of inhibitors and 'Ion Hunting' (IH-ENALDI), based on selective pre-concentration of inhibitors. IF-ENALDI was applied for two sets of enzyme–inhibitor pairs: tyrosinase–glabridin and trypsin–leupeptin and for the real plant sample: *Sparrmannia discolor* leaf and stem methanol extract. The efficacy of IH-ENALDI was shown for the pair of trypsin–leupeptin. Both ENALDI approaches pose an alternative for bioassay-guided fractionation, the common method for finding inhibitors in the complex mixtures.

## I. Ion Fading/ Ion Hunting Enzyme-coupled nanoparticles-assisted laser desorption ionisation MS

### I.1. Introduction

Plants are a rich source of biologically active substances, mostly inhibitors/ligands of various proteic targets [252]. Owing to the complexity of plant extracts, finding the small molecules interacting with given biological target (imposing a biological effect) is always the most pronounced challenge. Commonly, plant extracts are subjected to bioassay-guided fractionation [253-255]. This process requires multistep fractionation of the extract and manual assay of desired biological activity of each fraction. This experimental effort is obviously justified in case of studying multifactor effect on tissues or organisms (*e.g.* antispasmodic activity [256]), but seems to be outdated for simple enzyme–molecule interactions. An ideal methodology of searching for biologically active compounds in complex mixtures should be rapid (minimal pre-treatment of the biological mixture), require low amount of biological target, and versatility for various types of biological targets (enzymes and receptors). Apart from FAC, described in the *Chapter II*, there is another methodology combining these criteria and is called intensity ion fading mass spectrometry (IF-MS). It was used for the first time by the scientific group of Professor Francesc X. Avilés for searching for the specific interactions between various proteases and their high mass peptidic inhibitors [257]. Despite being published 10 years ago, only a few studies have used IF-MS [83, 87, 257-268]. IF-MS is based on the formation of specific complexes between target proteins and their binding partners leading to removal of bound molecules from the solution of studied extract. It leads to disappearance of corresponding ions from the mass spectrum of the extract. The principal technique employed for IF-MS is MALDI-TOF MS, because of low sample requirement, an excellent sensitivity and the potential of full automation. The main disadvantages of the application of classic organic matrices for IF-MS include denaturing conditions of sample analysis making it ineffective for fragile enzymatic systems (*e.g.* tyrosinase), difficulties with obtaining homogenous surface resulting in 'sweet spots' and possible matrix interference in a low-mass range (<500 Da). The latter drawback is acceptable when the mass of the studied ligands is above 500 Da, but it would impose serious complications on screening extracts for low-mass inhibitors or ligands without thorough optimization of a sample preparation. Organic matrices were successfully applied for studying small molecules, *e.g.* metal-phthalocyanines [269], 9-aminoacridine alone [270] or in a form of binary matrix with  $\alpha$ -cyano-4-hydroxycinnamic acid [120] or 'proton sponge' (1,8-bis(dimethyl-amino)naphthalene) [271]. The latter two matrices have highly basic character which makes them incompatible with the enzymes requiring a strict pH control. Denaturing properties or adverse environment of the organic matrices for biological systems are not the only factors that may affect the results of 'ion fading'. For example, Yanes *et al.* showed the importance of the way of sample deposition on the target MALDI spot, concluding that 'thin layer' is not applicable for visualizing the biological complexes and only 'dried droplet' provides satisfactory results [266].

Herein, we describe for the first time an original method solving the organic matrices-related limitations of 'ion fading' by proposing small molecule-compatible extension of IF-MS based on surface-assisted laser desorption/ionisation (SALDI) approach. SALDI utilizes inorganic nanoparticles in the role of ion emitter [122, 272]. Since the first application of graphite particles as a SALDI matrix in 1995 [273], many developments and new types of nanoparticles have been successfully applied for studying small molecules without low-mass background, *e.g.* nanoparticles made of gold [274], silver [275], platinum [276], TiO<sub>2</sub> [277, 278], ZnO [279], diamond [277] or Fe<sub>3</sub>O<sub>4</sub> coated with silica [280] (more examples Reader will find in the *Chapter I, p.III.3*). The process of desorption of the analyte from the surface of non-organic particles and its subsequent ionisation are believed to be caused by the growth of particles surface temperature upon the laser shot [281].

In our laboratory we synthesized core-shell type silica-coated iron oxide magnetic nanoparticles (MPs). We selected this type of MPs because of high versatility in the ways of silica surface derivatisation. In the present work MPs have dual function: they are used as high-capacity solid support for immobilised protein yielding the specific superficial adsorption sites and they also provide laser-induced desorption/ionisation of the analyte. To underline the dual function of the protein-nanoparticle conjugates, we use the following definition of this approach: enzyme-coupled nanoparticles-assisted laser desorption ionisation mass spectrometry (ENALDI MS). Besides classic 'Ion Fading' approach (IF-ENALDI), we showed the applicability of EMPs for specific pre-concentration of inhibitors, which we called 'Ion Hunting' (IH-ENALDI).



## I.2. Experimental

### I.2.1. Extraction of plant material

Dried and ground stems and leaves of *Sparrmannia discolor* were extracted with methanol and grounded roots of liquorice with deionised water by means of Milestone MicroSYNTH microwave oven (Soriso, Italy). Finely grounded plant parts were loaded into a 12 mL reactor. A volume of 7.6 mL of MeOH for *Sparrmannia discolor* or water for liquorice per 1 g of plant material was added and resulting mixture was subjected to three extraction cycles (*Sparrmannia*: 30 s each, constant irradiation power: 1000 W; liquorice: 30 s each, maximal temperature: 140°C, maximal microwave power: 1000 W). Extraction reactor was cooled down to ambient temperature in ice between each cycle. The extract was then separated from solid plant residue by centrifugation and filtration using a syringe filter (0.45 µm) for adapted for organic or aqueous solutions depending on the plant extract.

### I.2.2. Synthesis of functional magnetic nanoparticles

#### I.2.2.1. Synthesis of raw magnetic nanoparticles

The protocol was based on previous protocols [280, 282] with changes. A volume of 6 mL of 2 M ferric chloride in 2 M hydrochloric acid was added to the volume of 44 mL of oxygen-free deionised water into a round-bottom flask (250 mL). A solution of sodium sulfite (0.08 M, 25 mL) was added to the flask upon vigorous stirring and bubbling with nitrogen. A volume of 24 mL of aqueous solution of ammonia (4.67%) was then added to the flask. After stirring the mixture for 25 min at 70°C, the particles of iron(II,III) oxide were separated from the mixture by centrifugation (8000 rpm, 10 min). Particles were washed several times with deionised water and water/ethanol mixture (2/1, vol/vol).

The particles were then suspended in the mixture of 40 mL of EtOH and 10 mL of deionised water. While the mixture was vigorously stirred, 2.5 mL of tetraethyl orthosilicate and 2.5 mL of 10% aqueous solution of ammonia were added in a sequence. The mixture was stirred at 40°C for 16 h to obtain polycondensation of hydrolysed TEOS around iron(II,III) oxide nanoparticles resulting in the formation of silica shell (**fig. 1/II**). Silica-coated Fe<sub>3</sub>O<sub>4</sub> (MPs) nanoparticles were washed with MeOH by centrifugation (8000 rpm, 10 min) and subjected to cleaning by 4 M HCl to eliminate unsilanized Fe<sub>3</sub>O<sub>4</sub>. MPs were washed with deionised water until neutral pH (measured by pH indicator strips) of supernatant was obtained and then dried overnight at 40°C.

## 1.2.2.2. Derivatisation of raw MPs

## 1.2.2.2.1. Aldehyde-covered MPs-APTES-GLA

A mass of 0.655 g of dry MPs was suspended in 10 mL of dry toluene. A volume of 2 mL of (3-aminopropyl)triethoxysilane (APTES) was added while the flask was being irradiated with ultrasounds. The reaction of amination of the silica surface was conducted overnight at 60°C under stirring. Amine-covered nanoparticles (**fig. 1/III<sub>1</sub>**) were then washed several times with MeOH and dried overnight at 40°C. A volume of 30 mL of 2.5% glutaraldehyde solution in sodium phosphate buffer (PHB) (100 mM, pH 7.4) was added to 0.500 g of aminated particles and irradiated with ultrasounds. The mixture was then agitated for 5 h at room temperature. MPs-aldehyde (**fig. 1/IV<sub>1</sub>**) were then washed by centrifugation several times with deionised water and dried at 40°C. If not mentioned otherwise, this type of MPs was applied for the experiments described in the section *III.3. Results and discussion*.

MPs were characterized with transmission electron microscopy (TEM) using Philips CM20 TEM . The apparatus was equipped with LaB6 filament cathode and was operated at an acceleration voltage of 200 kV.

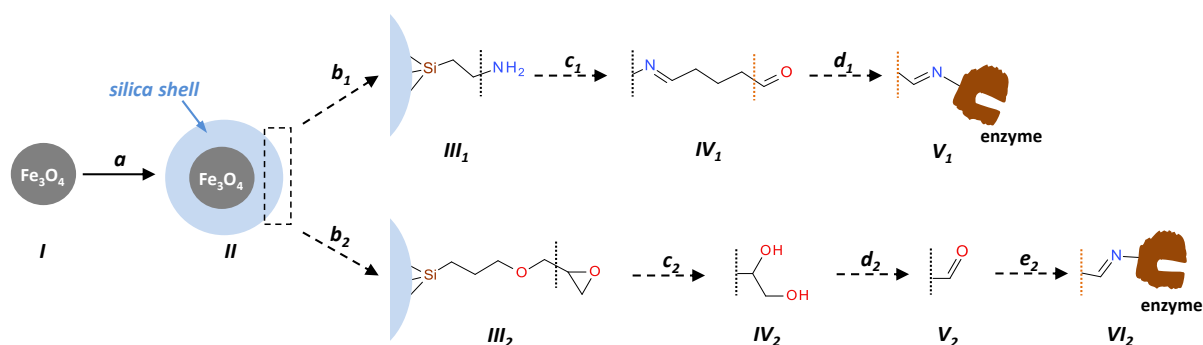


**Figure 1.** The pathway of EMPs preparation: *I* – iron(II,III) oxide magnetic nanoparticles; *II* – silica-coated nanoparticles (MPs); *III<sub>1</sub>* – aminated MPs; *IV<sub>1</sub>/V<sub>2</sub>* – aldehyde-coated MPs: MPs-APTES-GLA/MPs-oxyGPTMS; *V<sub>1</sub>/VI<sub>2</sub>* – enzyme-coupled MPs (EMPs); *III<sub>2</sub>* – epoxide-covered MPs; *IV<sub>2</sub>* – diol-covered MPs; (*a*) – silanization by TEOS; (*b<sub>1</sub>*) – surface amination by APTES; (*c<sub>1</sub>*) – derivatisation using glutaraldehyde; (*d<sub>1</sub>*) and (*e<sub>2</sub>*) – enzyme immobilisation; (*b<sub>2</sub>*) – silanization by GPTES; (*c<sub>2</sub>*) – acid-catalysed opening of epoxide ring; (*d<sub>2</sub>*) – diol oxidative cleavage

## 1.2.2.2.2. Aldehyde-covered MPs-oxyGPTMS

A mass of 0.640 g of dry MPs were suspended in 10 mL of dry toluene. A volume of 1.95 mL of (3-glycidyloxypropyl)trimethoxysilane (GPTMS) was added while the flask was being irradiated with ultrasounds for 10 minutes. The derivatisation of the silica surface was conducted overnight at 70°C under stirring. MPs-GPTMS (**fig. 1/III<sub>2</sub>**) were then washed several times with toluene and dried at 100°C for two hours. A volume of 25 mL of 0.1 M HCl was added to dry MPs-GPTMS to perform an opening of superficial epoxide rings. Reaction was performed during 3 h at room temperature. MPs-diol (**fig. 1/IV<sub>2</sub>**) were then

washed with distilled water until neutral pH of supernatant was obtained (measured by pH indicator strips) and then subjected to oxidative cleavage by periodic acid. A volume of 10 mL of the periodic acid solution (0.4 g) in the mixture of 90/10 (vol/vol) acetic acid/water was added to approx. 0.5 g of MPs-diol and irradiated by ultrasounds for 10 minutes in the darkness. The reaction mixture was then stirred at room temperature and darkness for over 2 h. MPs-aldehyde (MPs-oxyGPTMS) (**fig. 1/V<sub>2</sub>**) were then separated from the solution by magnet and washed with distilled water until neutral pH was obtained and dried overnight at 40°C.

### *1.2.3. Immobilisation of enzymes: trypsin and tyrosinase*

Trypsin/tyrosinase solution in PHB (pH 8.0/6.8, 50/10 mM respectively) was mixed with the solution of MPs-aldehyde (APTES-GLA for both enzymes, oxyGPMES for trypsin) dispersed in the same buffer and allowed to react under stirring for 6 h in ice. The reaction mixture was then stored at 4°C for 16 h. MPs-trypsin/tyrosinase particles were end-capped with glycine (100/1 mM in PHB, pH 6.8 respectively) at 4°C for 2/16 h respectively. Enzyme-coupled MPs (EMPs, **fig. 1/V<sub>1</sub>** and **VI<sub>2</sub>**) were then washed with 50 mM ammonium formate, pH 6.4 and diluted with the same buffer to obtain the final concentration of 1.7 mg/mL. When not used, EMPs were stored at 4°C in 50 mM ammonium formate buffer, pH 6.4.

### *1.2.4. Kinetic assay of free and immobilised tyrosinase*

#### *1.2.4.1. Determination of kinetic parameters of free and immobilised tyrosinase*

The procedure for free enzyme: a solution of free tyrosinase (1.5 µL, 1.0 mg/mL) in 10 mM sodium phosphate buffer (pH 6.8) was added in a sequence to a series of L-tyrosinase solutions (200 µL, 100-800 µM) in the same buffer, thermostated at 25°C. Enzymatic conversion of L-tyrosine (L-Tyr) to L-dopachrome was monitored at 420 nm using a microplate reader (µQuant, Fisher Scientific, Elancourt, France) (absorption coefficient of L-dopachrome at 420 nm is 2345 M<sup>-1</sup>·cm<sup>-1</sup>). The choice of this wavelength was determined by available choice of light filters compatible with µQuant apparatus and was set as the closest to the standard wavelength applied for L-dopachrome quantification: 475 nm.

Values of the specific activity (SA) for each L-Tyr concentration (**eq. 1**) were fitted to Michaelis–Menten model to obtain kinetic parameters (Michaelis–Menten constant,  $K_M$ , and maximal specific activity,  $SA_{max}$ ). SA is independent of the quantity of enzyme used, since it is expressed as the activity (*e.g.* in µmol/min) per mass unit of enzyme. It thus makes possible to compare directly activities of free enzyme and immobilised one, provided that a binding capacity of the enzyme carrier is known.

$$SA [\mu\text{mol} \cdot \text{min}^{-1} \cdot \text{mg}^{-1}] = \frac{\Delta\text{Abs}_{420 \text{ nm}}}{\Delta t \cdot \varepsilon_{420 \text{ nm}} \cdot C_{\text{enz}}} \cdot d \cdot D \cdot 10^3 \quad (\text{eq. 1})$$

where: *SA* – specific activity; *C<sub>enz</sub>* – concentration of mushroom tyrosinase in the initial stock solution, (mg/mL);  $\varepsilon_{420\text{nm}}$  – absorption coefficient of L-dopachrome at 420 nm, ( $M^{-1} \cdot \text{cm}^{-1}$ );  $\Delta\text{Abs}_{420\text{nm}}/\Delta t$  – slope of the linear part of time course curve of L-dopachrome formation, ( $\text{min}^{-1}$ ); *d* – length of the light path, (cm); *D* – dilution factor of enzyme solution

The procedure for immobilised enzyme: a series of L-tyrosine solutions (1450  $\mu\text{L}$ , 300-1800  $\mu\text{M}$ ) in 10 mM sodium phosphate buffer (pH 6.8) was thermostated at 25°C in the eppendorf thermomixer. A volume of 30  $\mu\text{L}$  of tyrosinase-bound EMPs (1.7 mg/mL) was added to each L-Tyr solution, which were then mixed at a rotation speed of 900 rpm to ensure homogenous distribution of nanoparticles in the solutions. The volumes of 100  $\mu\text{L}$  of each mixture were collected at the specified time points and scanned by microplate reader (at 420 nm). On the basis of the series of these measurements, time-course curves of L-dopachrome formation ( $\Delta\text{Abs}_{420\text{nm}}/\Delta t$ ) were constructed and the slopes of their linear parts were determined. The values of partial specific activities were calculated on the basis of the **eq. 1.**, with the exception that the concentration of enzyme, mg/mL, was calculated by multiplying the concentration of EMPs, mg/mL, by the value of MPs binding capacity for BSA. This standard protein was selected to determine MPs binding capacity for the reason that its molecular mass (66.4 kDa) is very close to the mass of a single unit of tyrosinase (62.5 kDa). Partial SA values were then fitted to Michaelis–Menten model to obtain  $K_M$  and  $SA_{\text{max}}$ .

Kinetic assay of free tyrosinase was conducted on the day of immobilisation, while EMPs were assayed on the next day after immobilisation. Experimental points obtained for both free and immobilised enzyme were fitted to Michaelis–Menten model of enzyme kinetics using OriginPro 8 software (OriginLab).

#### 1.2.4.2. Stability of immobilised tyrosinase

A volume of 490  $\mu\text{L}$  of 500  $\mu\text{M}$  solution of L-Tyr in ammonium formate buffer (25 mM, pH 6.4) was thermostated at 30°C for 10 min in the eppendorf thermomixer followed by addition of 10  $\mu\text{L}$  of the solution of tyrosinase-bound EMPs (1.7 mg/mL). The mixture was incubated for 20 minutes while shaking at the speed of 700 rpm. A volume of 500  $\mu\text{L}$  of EtOH was added to each eppendorf to stop the enzymatic reaction and EMPs were completely separated from the solution by centrifugation (6000 rpm, 5 min). L-dopachrome, formed in the enzymatic reaction, was quantified by measuring its absorption at 475 nm taking a mixture of the buffer/EtOH (50/50, v/v) as a blank.

#### 1.2.5. Mass spectrometry

The experiments with EMP-tyrosinase were conducted using Bruker Autoflex I MALDI-TOF MS and with EMP-trypsin using Bruker Ultraflex I MALDI-TOF/TOF MS (Bruker Daltonics, Bremen, Germany),

both equipped with a 337-nm nitrogen laser and controlled using Bruker FlexControl (version 3.3) software. Both devices were operated in reflectron negative-ion mode. In case of Auroflex I following settings were applied: 52-fold detector gain; ion source 1: 19 kV; ion source 2: 16.15 kV; lens: 8.25 kV; reflectron: 20 kV; laser frequency: 6.7 Hz. The settings of Ultraflex I were following: 52-fold detector gain; ion source 1: 20 kV; ion source 2: 16.7 kV; lens: 8.4 kV; reflectron 1: 21 kV; reflectron 2: 11.5 kV; laser frequency: 7.1 Hz.

Mass spectra were collected by accumulating a number of 300 laser shots in random places of the spot. The level of laser power was adjusted before each experimental session to provide sufficient ionisation and to avoid saturation of MS detector. All samples of denatured (blank) and active EMPs were always analysed on the same day by applying the same laser power. MS was calibrated using aqueous extract of liquorice roots containing known metabolites. The calibration list was based on known metabolites of liquorice described in the literature.

Bruker maXis™ ultra high resolution Qq-TOF mass spectrometer with collision-induced dissociation (CID) unit, equipped with electrospray ion source, working in negative ion mode was applied for all analyses of plant metabolites. The system was controlled using Bruker micrOTOFcontrol (version 3.0) software accompanied by DataAnalysis (version 4.0, SP4). The following settings of MS were applied: capillary voltage: 3.6 kV; nebuliser: 0.4 bar; dry gas: 2.0 L/min. Raw plant extract was diluted 100-fold in 50 mM ammonium formate buffer (pH 6.4) and infused into the mass spectrometer by a syringe pump at 600 µL/h. MS was calibrated using the tuning mix (G1969-85000, Agilent Technologies) employing enhanced quadratic mode. Molecular formulas of plant metabolites of interest were determined on the basis of  $m/z$  values and the isotopic patterns by means of Bruker *SmartFormula* software. Fragment ions were used for screening three compound databases: Chemspider, managed by Royal Society of Chemistry, METLIN Metabolomics Database, containing fragmentation data [283, 284] and the MassBank, hosted by the Institute for Advanced Biosciences, Keio University, Japan [285].

### **1.3. IF/IH-ENALDI MS: results and discussion**

#### *1.3.1. Characterisation of MPs as a non-organic matrix and host for enzyme immobilisation*

##### *1.3.1.1. Structural characterization of MPs*

Interconnected nanoparticles of a mean diameter of approximately 12 nm form numerous bigger clusters having a diameter ranging from 100 to 1000 nm (**fig. 2**). Each individual nanoparticle is composed of magnetic core coated with a layer of silica (approx. 1.5 nm).

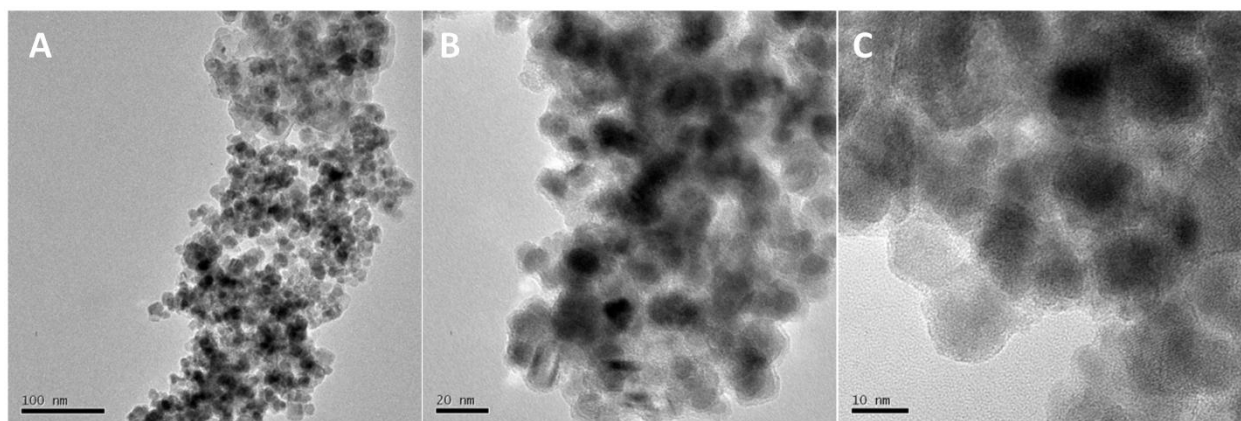


**Figure 2.** TEM images of magnetic nanoparticles under various levels of magnification: A - 38000-fold; B - 115000-fold; C - 250000-fold.

### 1.3.1.2. Magnetic nanoparticles as an immobilisation support

MPs were proven to have high protein binding capacity, approximately 180 mg of bovine serum albumin, BSA, or 80 mg of trypsin per gram of MPs (Reader will find the general protocol for determination of binding capacity in the *Appendix I, protocol S3*). BSA was used as a model protein for tyrosinase due to similar molecular dimensions. The kinetic assays of two batches of tyrosinase before and after immobilisation (**fig. 3**) revealed that the level of enzyme's specific activity conserved after its binding to MPs was within the range of 43-49%. This partial lose of activity may be caused by inappropriate binding geometry for some fraction of enzyme molecules and possible partial inactivation of free enzyme during the immobilisation process.  $K_M$  constant was 2.5-2.8 times higher for immobilised tyrosinase comparing to free enzyme. In practice it is caused by the decrease of L-Tyr affinity to immobilised tyrosinase, possibly due to limited L-Tyr accessibility to the enzymes' active sites.

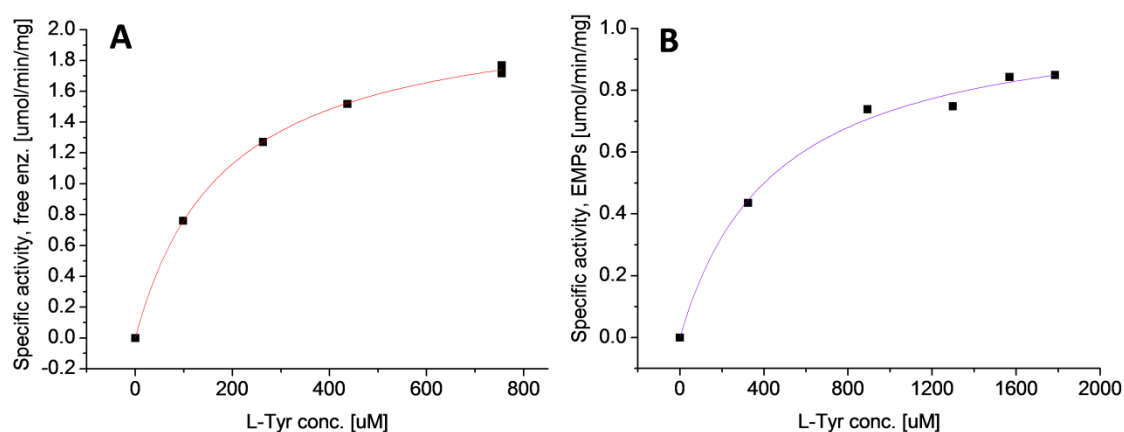


**Figure 3.** An example of the kinetic curves of free (A) and immobilised (B) tyrosinase. Both datasets were acquired for the same enzyme batch.

The stability of tyrosinase-bound EMPs stored at 4°C in 50 mM ammonium formate (pH 6.4) was shown to be significantly improved in comparison with the free enzyme stored in comparable conditions

(**fig. 4**). Free tyrosinase loses approximately 60% of the initial activity after 17-20 days of storage [286, 287]. The same degree of MPs-bound enzyme inactivation occurs after 60-71 days of storage.

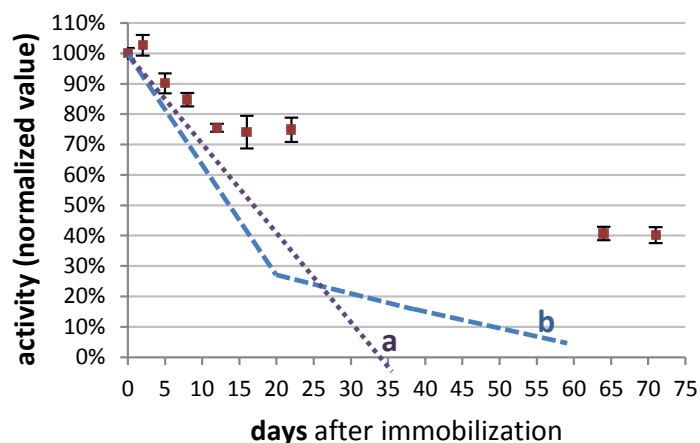


**Figure 4.** Storage stability of tyrosinase-bound EMPs in comparison with free tyrosinase: **a** – stored at 4°C in 50 mM sodium phosphate buffer (pH 6.5) [286]; **b** – 4°C in 10 mM sodium phosphate buffer (pH 7.2) [287]. Minimum two replicates were conducted for each time point.

#### An experiment demonstrating the stability of enzyme attachment

A volume of 10  $\mu\text{L}$  of MPs-tyrosinase (1736  $\mu\text{g}/\text{mL}$ ) was suspended in 290  $\mu\text{L}$  of 50 mM ammonium formate, pH = 6.4, (**fig. 5: I**) and mixed by means of a pipette. Beads were then attracted by magnet (**II**) to the vial wall. A volume of 150  $\mu\text{L}$  of the clear solution of supernatant (corresponding to 50% of the initial volume) was then transferred to second, empty vial. MPs trapped in the initial vial were re-suspended. A volume of 150  $\mu\text{L}$  of 1 mM aqueous solution of L-Tyr was added to both vials simultaneously, mixed and incubated at room temperature. After approximately 10 minutes from the moment of addition of L-Tyr solution, an orange coloration of L-dopachrome started to be well visible.

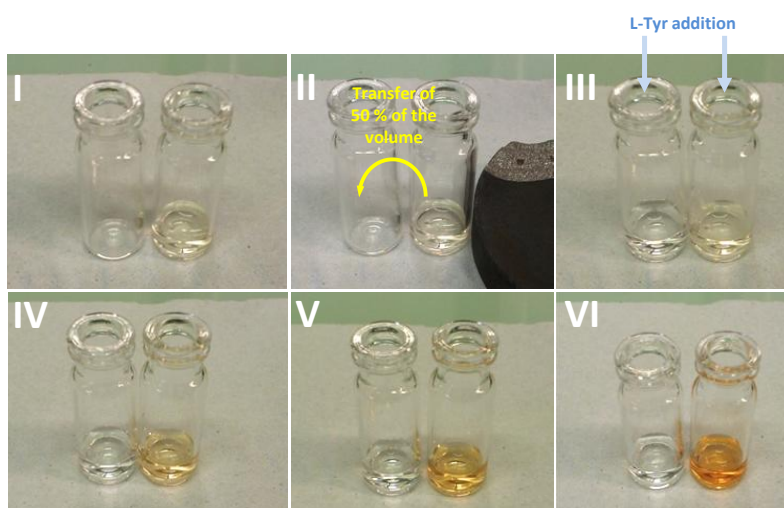


**Figure 5.** The following stages of the demonstration of the attachment stability of EMPs hosting immobilised tyrosinase.

The progress of L-Tyr conversion was depicted in **fig. 5** (III: t = 0; IV: t = 13 min; V: t = 23 min; VI: t = 71 min). This experiments clearly confirms that enzyme is firmly attached to the surface of MPs and no

storage-related enzyme desorption is observed. Moreover, this experiment demonstrates the simplicity of enzyme separation from the reaction medium just by using a simple magnet.

### 1.3.1.3. Application of EMPs as non-organic matrix

Preparation of a single ENALDI spot on the surface of polished steel plate includes the following steps: deposition of the analyzed mixture (e.g. plant extract), addition of EMPs solution and mixing resulting droplet using a pipette. After evaporation of the buffer solution (approximately 10-15 min), a uniform and even surface of EMPs is ready for laser irradiation (**fig. 6**). The time required to obtain stable vacuum level is not longer than in case of organic MALDI matrices. A summation of at least 100 shots (optimally 300 shots) collected in random places of the spot is required to obtain a single MS spectrum.

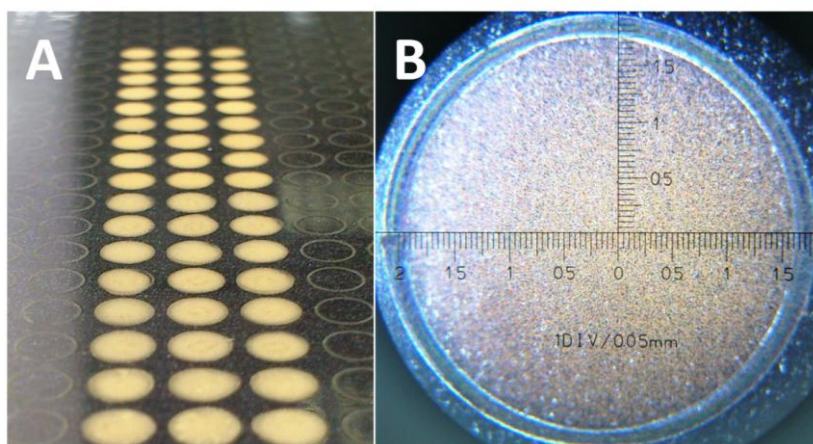


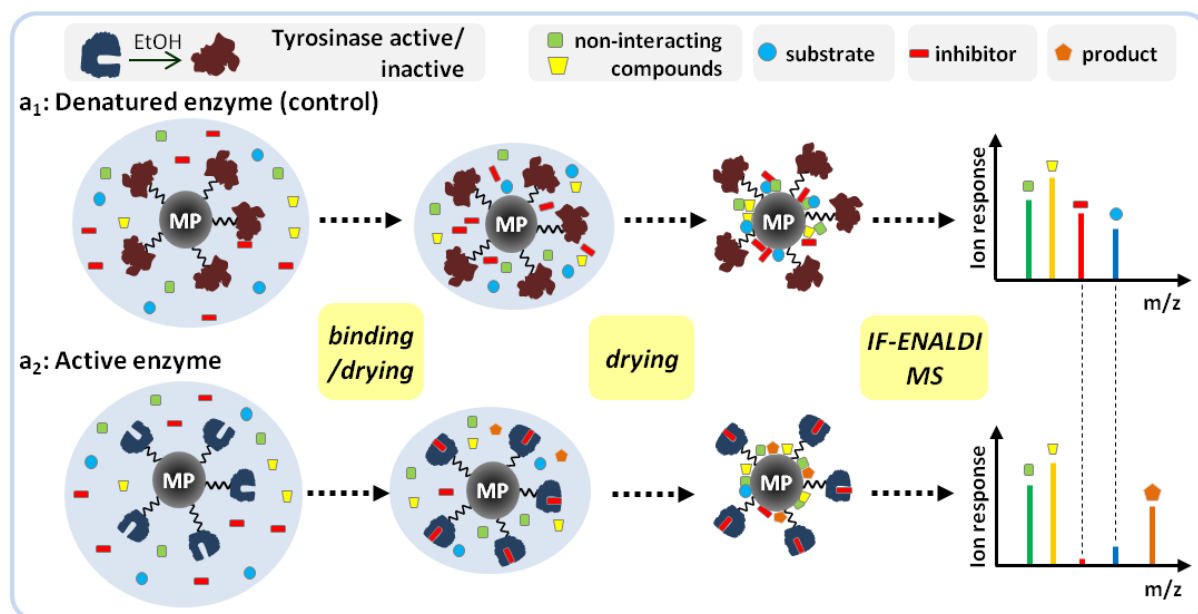
**Figure 6.** ENALDI spots on the polished steel MALDI plate. A - series of spots; B - a single ENALDI spot under 45-fold magnification.

### 1.3.4. 'Ion Fading' IF-ENALDI MS and 'Ion Hunting' IH-ENALDI MS - illustration of the experimental approach using standard inhibitors

#### 1.3.4.1. Experimental design and evaluation of IF-ENALDI MS

IF-ENALDI MS experiment is based on the application of MPs with immobilised enzyme (EMPs) as a specific target for the enzyme's binding partners (inhibitors) present in the analyzed solution, e.g. plant extract (**Scheme 1**). As it was stated previously, the process of desorption and ionisation of the analyte are believed to be caused by the growth of particles surface temperature upon the laser shot [281]. If the inhibitor of immobilised enzyme is present in the studied mixture, it will be selectively bound to enzyme's active site (**Scheme 1: a<sub>2</sub>**) and thus 'shielded' from the surface of MPs by enzyme itself and the linker. This 'shielding' of captured inhibitor is manifested in the decrease of the yield of its desorption and, in consequence, it can lower the response of the inhibitor ions comparing to the control experiment with EMPs hosting denatured enzyme (**Scheme 1: a<sub>1</sub>**).





**Scheme 1.** General outlook of the principle of 'Ion Fading' IF-ENALDI MS

For IF-ENALDI, a volume of 2  $\mu\text{L}$  of the sample solution in 50 mM ammonium formate (pH 6.4/8.5 for tyrosinase/trypsin respectively) was mixed with 2  $\mu\text{L}$  of MPs (1.7 mg/mL) in 50 mM ammonium formate (pH 6.4) directly on the target plate (Bruker MTP 384 polished steel) and allowed to dry. This way of sample deposition is a direct equivalent of 'dried droplet' method for MALDI MS.

Exemplary results of IF-ENALDI-MS (**fig. 8: IF-A, IF-B**) were obtained using standards (**fig. 7**): glabridin (*m/z* 323 in negative mode), an inhibitor of tyrosinase [288]; leupeptin (*m/z* 425), inhibitor of trypsin [289] and ibuprofen as an internal standard (*m/z* 205).

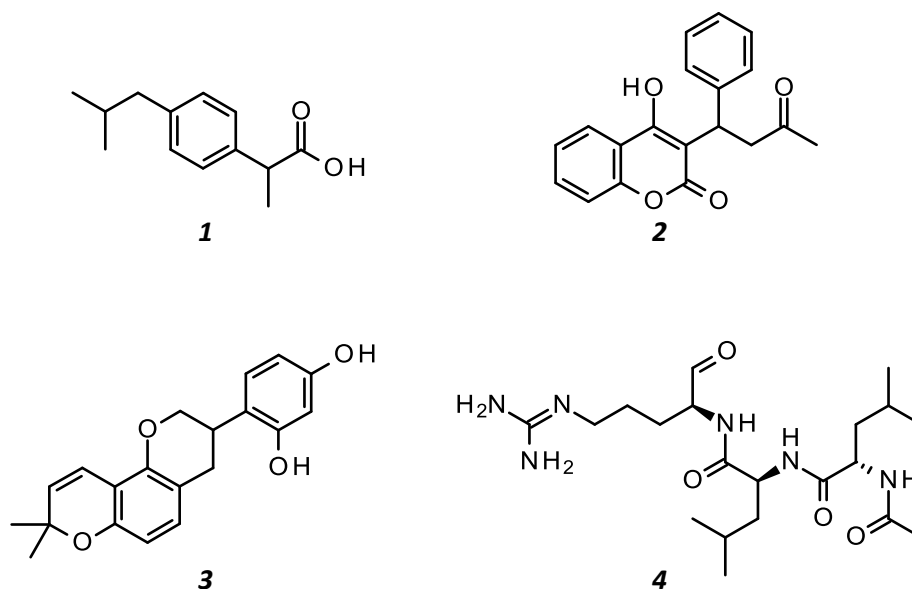


**Figure 7.** The structures of internal standards and model inhibitors used for validation of If/IH-ENALDI MS approach. Ibuprofen, MM: 206.1307 Da (**1**); warfarin, MM: 308.1049 Da (**2**); glabridin, MM: 324.1362 Da (**3**); leupeptin, MM: 426.2954 Da (**4**).

The stock solutions of EMPs (active and denatured as a negative control) and the solution of analyte were simply mixed directly on polished-steel MALDI plate and allowed to dry.

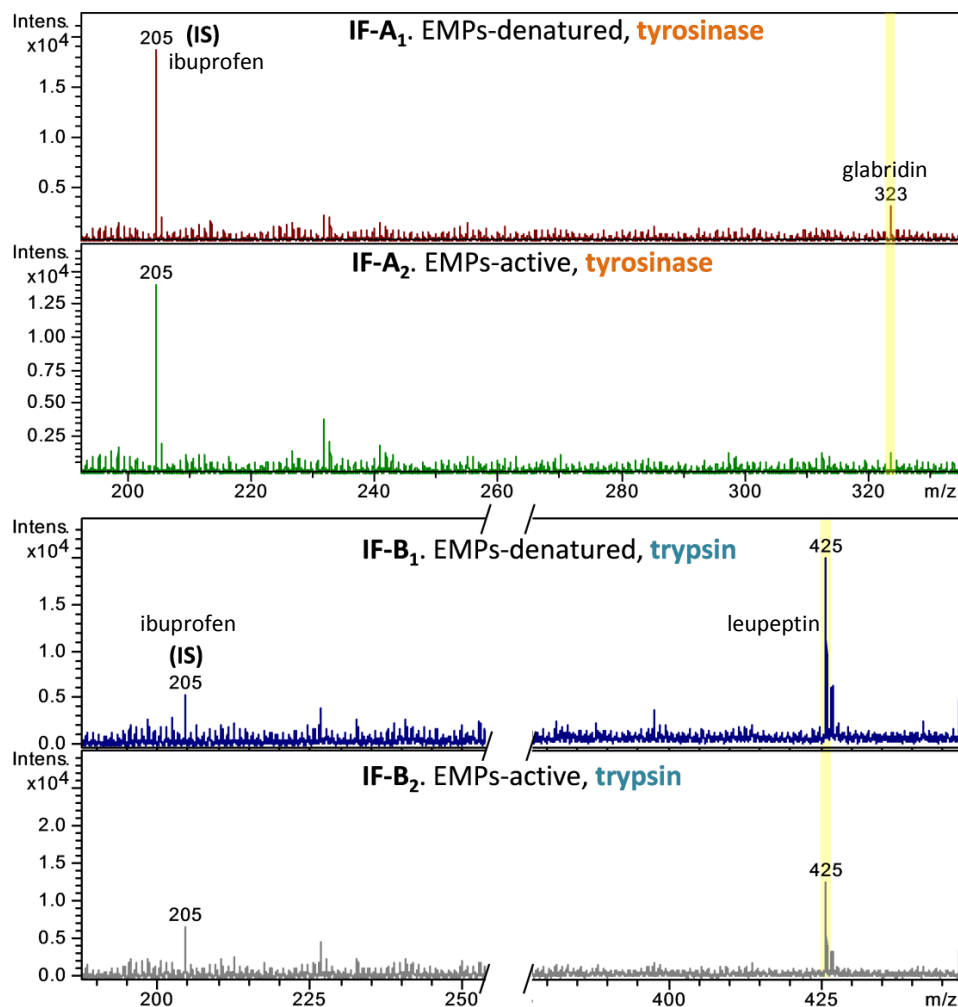


**Figure 8. IF-ENALDI approach** in the negative mode of ionisation: **IF-A**: the comparison of mass spectra of the test mixture of glabridin,  $m/z$  323 (5 pmol per spot) and ibuprofen as an internal standard  $m/z$  205 (IS, 75 pmol per spot) obtained using denatured (control) and active EMPs respectively. Data obtained using Bruker Autoflex; **IF-B**: the test mixture of leupeptin  $m/z$  425 (10 pmol per spot) and ibuprofen as internal standard  $m/z$  205 (60 pmol per spot), data obtained using Bruker Ultraflex. The scale of both sets of mass spectra were normalized to the intensities of ibuprofen ion, the internal standard.

The response of glabridin ion was reduced to the baseline level when active tyrosinase-bound EMPs were applied (**fig. 8: IF-A**). When active trypsin-bound EMPs were applied, the ion response of leupeptin was significantly reduced (by 39%) comparing to the control based on EMPs with denatured trypsin (exemplary ENALDI spectra: **fig. 8: IF-B**; the diagram: **fig. 9: A**) or by 34% when MPS-oxyGPTMS were used as the trypsin support (the diagram: **fig. 9: B**).

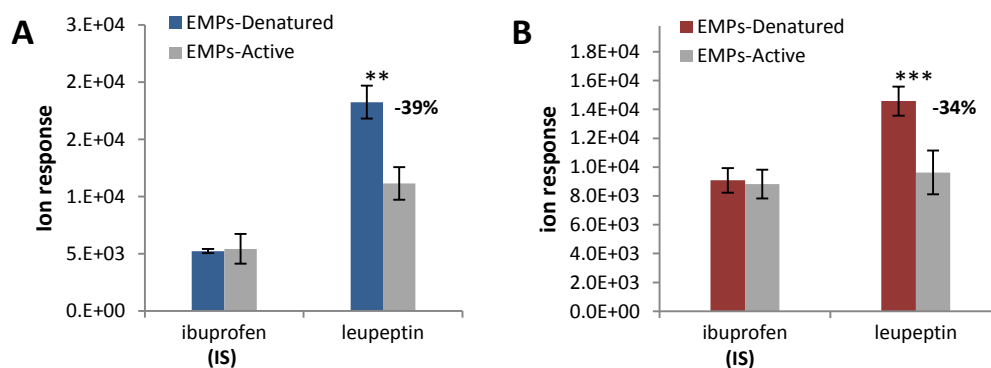


**Figure 9.** IF-ENALDI MS results for the mixture of ibuprofen/leupeptin and MPs-trypsin. Leupeptin (10 pmol per spot) and ibuprofen as IS (60 pmol per spot). **A** – MPs-APTES-GLA,  $n=3$ ; **B** – MPs-oxyGPTMS,  $n=4$ . Student *t*-test: \*\*/\*\* – significant/highly significant ( $P<0.05$ / $P<0.001$  respectively).

According to Kuramochi *et al.*,  $K_d$  of trypsin-leupeptin complex is equal to 13.4 nM [290]. If we assume that *i*) immobilisation-related loss of trypsin activity is the same as for tyrosinase and *ii*) that all enzyme molecules in the initial lyophilized powder were active, we should expect approximately 5.4 pmol of active enzyme per spot. If leupeptin is applied at the concentration of 10 pmol/spot, the total reaction volume is 4  $\mu$ L and  $K_d$  equal to 13.4 nM, we should expect ion fading on the level of 53% comparing to the control experiment. The value obtained using IF-ENALDI is lower possibly because a certain fraction of trypsin was inactivated during the immobilisation process because of trypsin auto-cleavage.

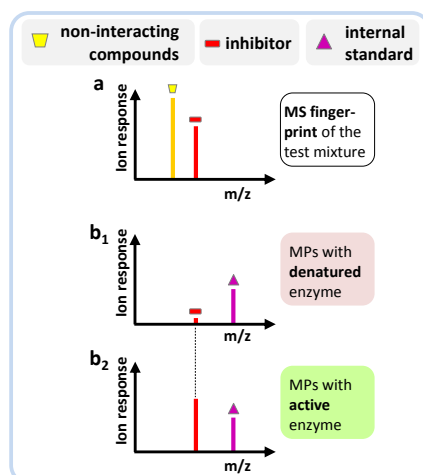
One should note very satisfactory spot-to-spot repeatability due to very uniform sample deposition and lack of so called 'sweet spots', very common for organic MALDI matrices. What is important to note, there is no statistically significant difference in the ionisation yield of non-interacting compounds between EMPs active and denatured. It shows that the target's conformation does not influence the general ionisation capacity of EMPs. It enables a direct comparison of 'blank' and 'active' EMPs.

Both immobilisation pathways (APTES-GLA and oxyGPTMS) of enzyme immobilisation to MPs were shown to be compatible with IF-ENALDI MS (IF diagrams: **fig. 9**). However, the superficial derivatisation has an impact on the ionisation yield of the components of analyzed solutions.

#### 1.3.4.2. Experimental design and evaluation of IH-ENALDI MS

The results of IF-ENALDI MS may be confirmed by the complementary 'Ion Hunting' (IH-ENALDI MS) approach (**Scheme 2**). It is based on the following steps: 1) acquisition of the general MS pattern of studied mixture (**Scheme 2: a**); 2) incubation of EMPs (active and denatured, **Scheme 2: b<sub>2</sub>/b<sub>1</sub>**) with studied mixture in the plastic *ependorf* tubes; 3) separation of the EMPs (with bound inhibitors in case of 'active' EMPs) from the mixture by magnet or centrifuge and removal of the supernatant; 4) re-suspension of the EMPs in denaturing solution containing an internal standard. This step is aimed at liberation of all specifically bound inhibitors from the enzyme by disruption of its globular structure. Warfarin, the internal standard ( $m/z$  307) is added for direct comparison of the mass fingerprints obtained by active and denatured EMPs; 5) deposition of the mixtures on MALDI plate followed by their analysis. In

contrast to IF-ENALDI-MS, in case of IH-ENALDI-MS one should observe higher intensity of inhibitor ions due to their selective pre-concentration by active EMPs (**Scheme 2: b<sub>2</sub>**).



**Scheme 2.** General outlook of the principle of 'Ion Fading' IH-ENALDI MS

For the typical IH-ENALDI experiment, a volume of 50  $\mu\text{L}$  of EMPs-trypsin (in ammonium formate, pH 6.4) was mixed with 50  $\mu\text{L}$  sample solution (10  $\mu\text{M}$  leupeptin in ammonium formate, pH 8.5, was applied as an example in the discussion below); after 45 min-long incubation supernatant was discarded and remaining EMPs were denatured by addition of 12.5  $\mu\text{L}$  of MeOH followed by addition of 12.5  $\mu\text{L}$  of 1  $\mu\text{M}$  solution of warfarin (internal standard, **fig. 7**, entry **4**). Deposition: 1  $\mu\text{L}$  of the resulting solution (3.4  $\mu\text{g}$  of MPs/spot) followed by 2.5  $\mu\text{L}$  of the solution after attraction of EMPs to the wall of *ependorf* to increase S/N ratio. An outcome of 'Ion Hunting' (IH-ENALDI) experiment with leupeptin as trypsin inhibitor (exemplary ENALDI spectra: **fig. 10** and the diagram: **fig. 11**) is fully complementary to 'Ion Fading' (**fig. 8: IF-B**) and shows statistically significant pre-concentration of leupeptin ( $m/z$  425) only by active EMPs. IH-ENALDI may thus be used to confirm the initial IF-ENALDI results (or replace it) using the same enzymatic platform and instrumentation.

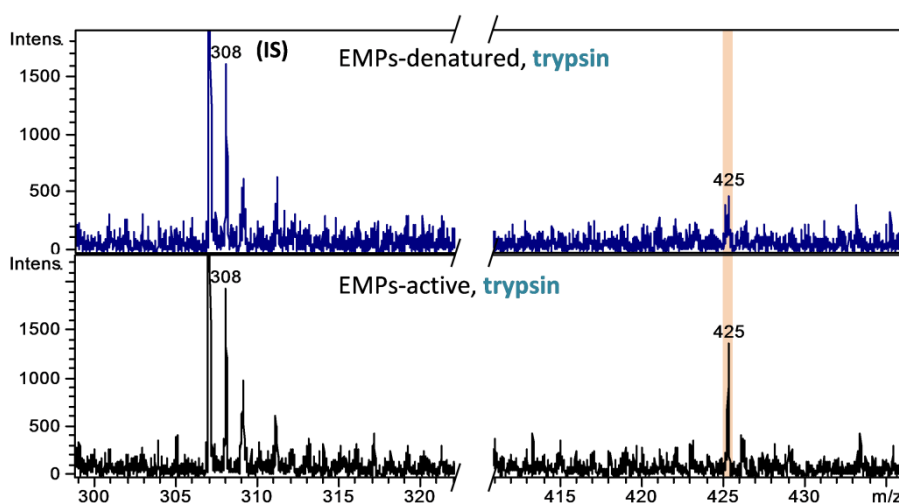


**Figure 10. IH-ENALDI approach:** mass fingerprints of 'ion hunting' using leupeptin as an example of trypsin inhibitor ( $m/z$  425) and warfarin,  $m/z$  307 (3 pmol/spot), as the internal standard. The first isotopic peak of warfarin was shown. In all cases an amount of EMPs was 3.4  $\mu\text{g}$ /spot, spectra were obtained using Bruker Ultraflex in the negative ion mode.

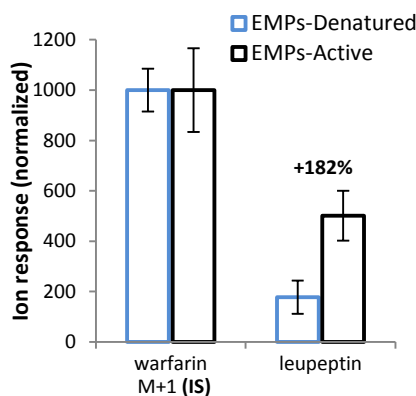


**Figure 11.** IH-ENALDI MS obtained for leupeptin, trypsin inhibitor, and warfarin as the internal standard,  $n=3$ .

Pre-concentration of leupeptin in the process of IH-ENALDI is more significant (**fig. 11**) than the decrease of ion intensity in case of IF-ENALDI (**fig. 9**). In the latter case, an amount of enzyme's active sites is limited strictly to the amount of MPs deposited on the spot (2  $\mu\text{L}$  of 10  $\mu\text{M}$  solution of leupeptin is mixed with 2  $\mu\text{L}$  of EMPs, 1.7  $\mu\text{g}/\mu\text{L}$ , resulting in 3.4  $\mu\text{g}$  of EMPs/spot). In case of IH-ENALDI, leupeptin/EMPs volumetric ratio is identical and equal to one (50  $\mu\text{L}$  of sample solution/ 50  $\mu\text{L}$  of EMPs, 1.7  $\mu\text{g}/\mu\text{L}$ ), but the total amount of leupeptin removed by active enzyme from the volume of 50  $\mu\text{L}$  of sample solution is then transferred to the volume of 25  $\mu\text{L}$  of the denaturing solution and thus pre-concentrated. This IH-ENALDI experimental design entails more significant difference of the inhibitor ion response between 'active' and control EMPs than for IF-ENALDI, but on the other hand, results in much higher EMPs consumption per analysis. Application of EMPs instead of free enzyme is advantageous because there is no need to use a ultrafiltration membrane to separate enzyme-inhibitor complexes from the studied mixture. Moreover, the immobilisation process eliminates all additional compounds found in the commercial enzyme solution (*e.g.* glycerine) that could contribute to MS interferences in the low-mass range.

### 1.3.5. An application of IF-ENALDI MS to the samples of plant extracts

An experiment with a real sample, the aqueous extract of liquorice roots, revealed four inhibitor candidates (exemplary ENALDI spectra: **fig. 12-A**, IF diagram: **fig. 14-A**):  $m/z$  209, 255, 549 and 577. In contrast to all other ENALDI results, ENALDI MS fingerprints for liquorice extract were quantified using signal to noise ratio (S/N) because of low ion responses of extract constituents. Due to instrument-related sinusoidal noises, the noise reference for given peak was set as the value  $[(m/z \text{ of peak of interest}) - 1]$ . The S/N ratio for given  $m/z$  value is thus expressed as  $(m/z)$  divided by  $(m/z-1)$ .

The experiment with the methanol extract<sup>55</sup> of *Sparrmannia discolor* leaves and stems revealed two inhibitor candidates:  $m/z$  177 and 359 (exemplary ENALDI spectra: **fig. 12-B**, the diagram: **fig. 14-B**), since the intensities of these ions were reduced without simultaneous emergence of possible products of their enzymatic conversion.

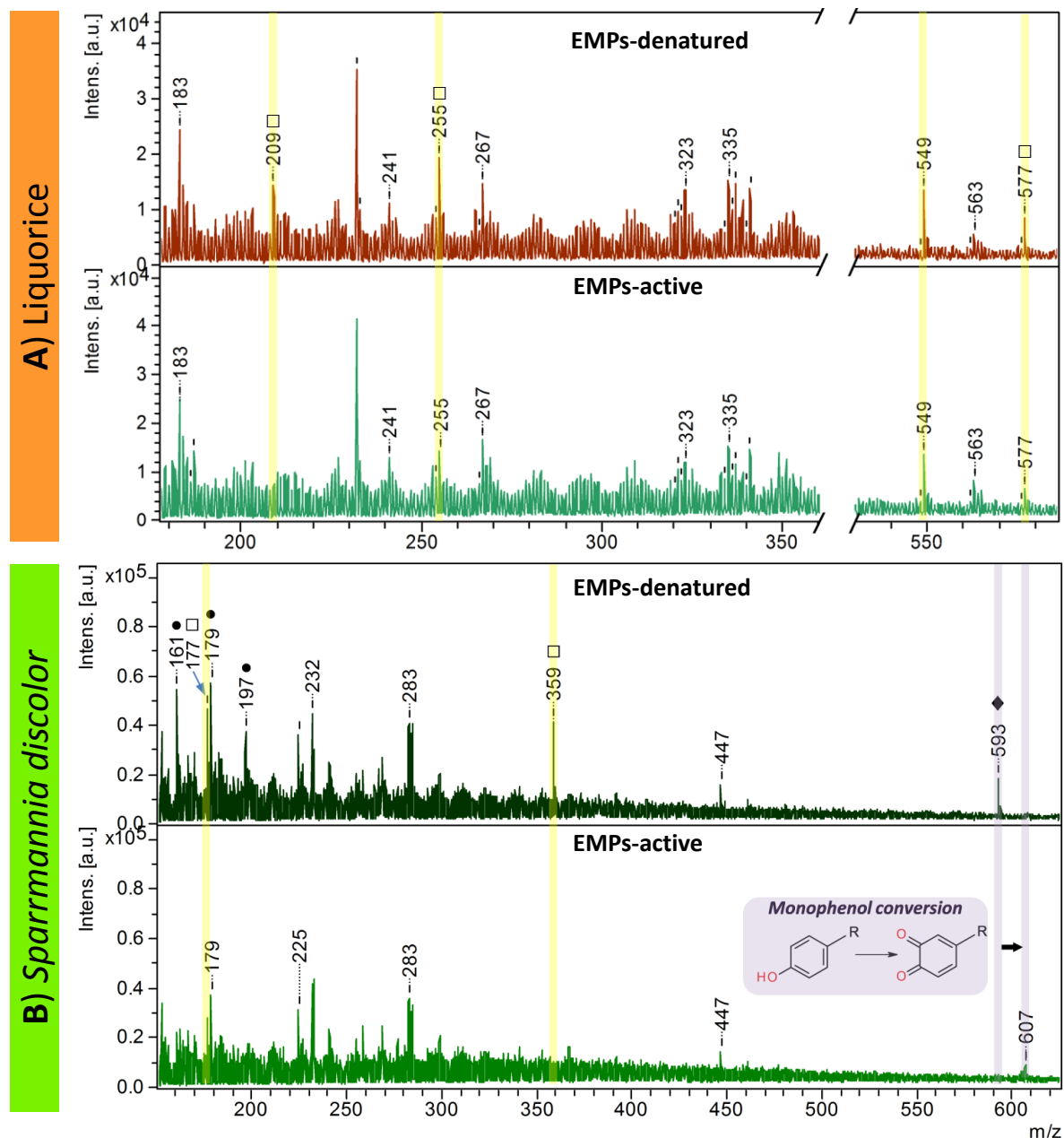


**Figure 12.** The mass fingerprints of: **(A)** the aqueous extract of liquorice roots, deposited amount: an equivalent of 450 ng of dry plant powder/spot; **(B)** the methanol extract of leaves and stems of *Sparrmannia discolor*, deposited amount: an equivalent of 600 ng of dry plant powder/spot. Inhibitor candidates were marked with open squares ( $\square$ ), monophenol substrate candidate with filled rhombus ( $\blacklozenge$ ) and the fragments of the compound with  $m/z$  359 were marked with filled dots ( $\bullet$ ). The inset: the pathway of tyrosinase-driven monophenol oxidation. In all cases an amount of EMPs was 3.4  $\mu\text{g}/\text{spot}$ .

<sup>55</sup> The use of methanol as the extraction solvent did not affect an enzymatic activity of tyrosinase, since the raw methanol extract (131 mg of dry plant powder/1 mL of MeOH) was diluted 500-fold in 50 mM ammonium formate.

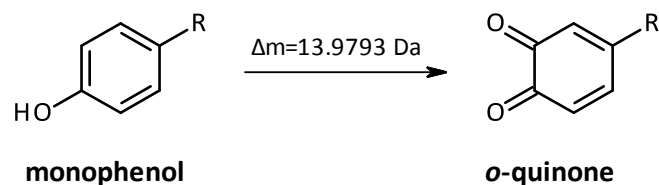


**Figure 13.** Tyrosinase-driven oxidation of *p*-phenol to corresponding *o*-quinone.

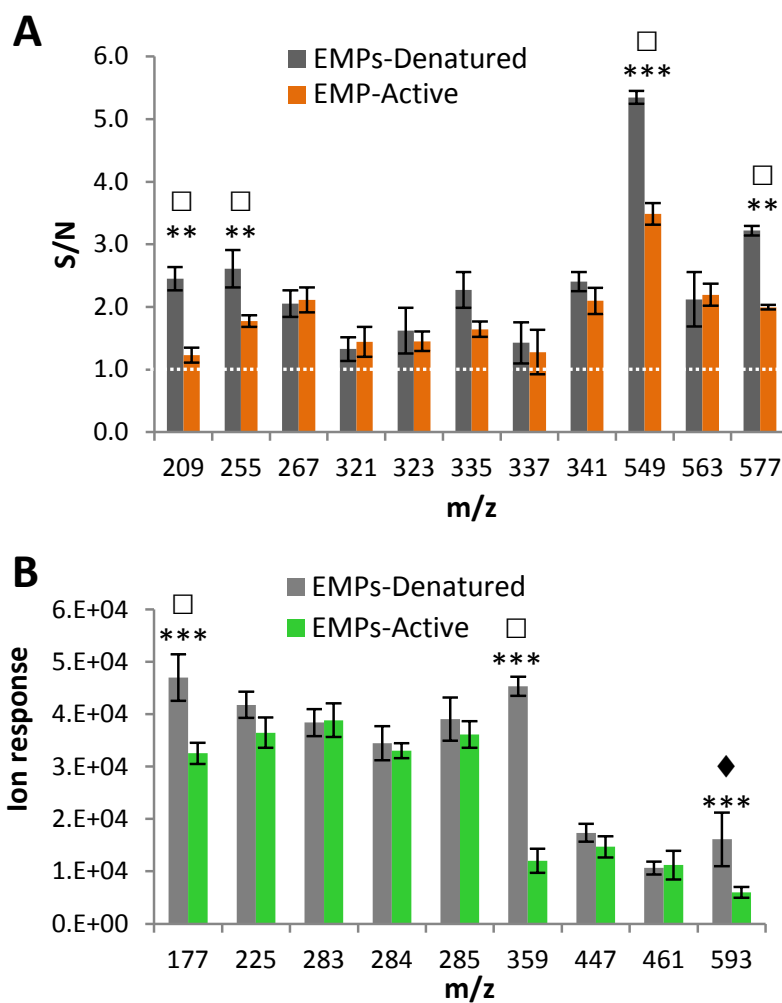


**Figure 14.** (A) the aqueous extract of liquorice roots,  $n=3$ , signal to noise (S/N) values were displayed,  $S/N=1$  describes the complete ion disappearance; (B) the methanol extract of leaves and stems of *Sparrmannia discolor*,  $n=4$ . All inhibitor candidates were marked with empty squares ( $\square$ ) and monophenol substrate candidate with black rhombus ( $\blacklozenge$ ). Student *t*-test:  $**/**$  – significant/highly significant ( $P<0.05/ P<0.001$  respectively) difference between MS fingerprints obtained using both types of MPs: active and denatured.

The latter inhibitor candidate having  $m/z$  359 was shown to be susceptible for fragmentation in a negative ion mode yielding three fragments:  $m/z$  197, 179 and 161 (more details in p. II.3.6.2). The third ion for which 'ion fading' is observed ( $m/z$  593) is conjugated with the 'new' peak at  $m/z$  607. The mass difference between them is equal to 14 Da what corresponds to tyrosinase-driven hydroxylation of monophenol and

its simultaneous oxidation to *o*-quinone (**fig. 13**). This example shows that ENALDI approach enables to observe enzymatic conversion of the substrates by visualization of the products of their enzymatic conversion.

### 1.3.6. The complement of IF-ENALDI MS: identification of inhibitor/substrate candidates by ESI-Qq-TOF MS

IF-ENALDI MS approach should be considered as the method for rapid pre-selection of inhibitor candidates without any pre-treatment of plant extract (*e.g.* separation or fractionation). These 'hits' – for the reason of low mass accuracy of MALDI mass spectrometer – should be subjected to more detailed analysis by high-resolution mass spectrometer, *e.g.* ESI-Qq-TOF instrument, providing mass accuracy lower than 5 ppm and the possibility to conduct fragmentation of selected ion(s).

During the metabolite identification process, we applied two common metabolite databases: METLIN and MassBank. The latter database, managed by the Institute for Advanced Biosciences, Keio University, Japan, contains MS spectra for all deposited compounds and CID fragmentation data for most of the records (in many cases a single compound is represented by few, independent sets of MS<sup>2</sup> spectra collected in different laboratories, conditions and using different mass spectrometers). METLIN database is a general library of metabolite information and only selected compounds are accompanied by low-resolution experimental mass spectra obtained on a 6510 Q-TOF (Agilent Technologies). Both databases may be browsed using either experimental *m/z* values (of the precursor or fragment ions) or using molecular formulas generated by the external software (*e.g.* Bruker SmartFormula™).

To illustrate an importance of the mass accuracy provided by MS instrument and the knowledge of the fragment ions, we conducted the simulation showing the number of possible 'hits' on the basis of measured *m/z* value and the fragmentation data as a function of mass accuracy (**table 1**).

**Table 1.** Number of the possible structures found for the precursor ions representing two different plant metabolites as a function of mass accuracy provided by the mass spectrometer.

Mass accuracy (ppm)	Mass accuracy calculated for <i>m/z</i> 580.0000 ( $\Delta m/z$ )	Number of the possible structures			
		METLIN		MassBank	
		<i>m/z</i> 577.1567*	<i>m/z</i> 593.1295**		
		(parent ion only)	(parent ion only)	(parent ion only)	(parent ion + fragment ions)
200	0.1160	362	303	14	
100	0.0580	196	166	14	
50	0.0290	108	151	12	3
30	0.0174	65	29	1	1
10	0.0058	65	28	1	1
5	0.0029	65	28	1	1

\* - an experimental *m/z* of the parent ion representing the metabolite of liquorice roots (**p. II.3.6.1**);

\*\* - an experimental *m/z* of the parent ion representing the metabolite of *Sparrmannia discolor* (**p. II.3.6.2**);



As it was indicated in **table 1**, the high mass accuracy significantly reduces the number of the possible structures retrieved by the search engines of the databases. If we add another dimension in a form of the fragment ions, we reduce the set of possible 'hits' even more.

In certain cases even very high mass accuracy may not be enough to distinguish the pair of close isobars. Let us consider the two following formulas:  $C_{30}H_{26}O_{13}$  (MM=594.13734 Da) and  $C_{28}H_{14}N_{14}O_3$  (MM=594.13733 Da). To resolve these two compounds we would require mass accuracy lower than 0.016 ppm and the resolution higher than 59 million. These values are not accessible for contemporary mass spectrometers. To address this issue, Bruker launched an innovative *SmartFormula*<sup>TM</sup> software enabling determination of the molecular formulas for small molecules on the basis of both *i*) accurate mass determination and *ii*) relative intensities of isotopic ions within the isotopic pattern (**fig. 15**). This feature may find an application in cutting the size of the set of database 'hits' containing the pair of the isobars having the difference in the exact masses falling below the mass accuracy of the mass spectrometer.

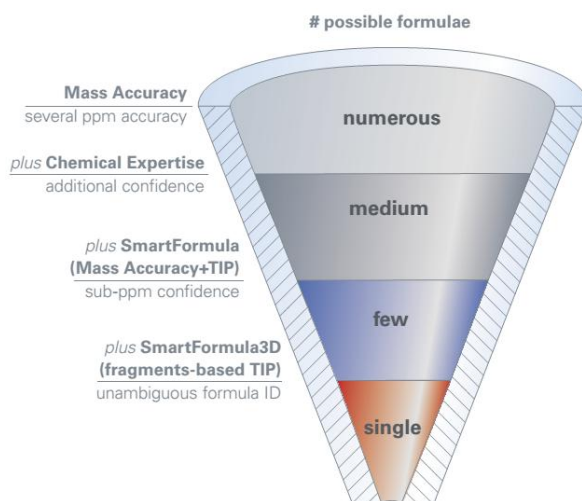


**Figure 15.** The diagram showing an impact of the knowledge of a precise isotopic pattern (taken into account by *SmartFormula* software) and the fragmentation pattern (*SmartFormula 3D* software) on the number of possible structures linked to  $m/z$  of the peak of interest. Illustration acquired from the promotional materials of Bruker.

An isotopic fit is expressed as *mSigma* value which is calculated for each molecular formula proposed on the basis of the  $m/z$  value of the peak of interest. The best fit is represented by the smallest *mSigma* value within the set of proposed formulas (Bruker Application Note #ET-26). An exemplary set of proposed molecular formulas for the compound having  $m/z$  593.1295 (one of the active metabolites of *Sparrmannia discolor*, p. II.3.6.2) was shown in **fig. 16**.

Meas. m/z	#	Formula	Score	m/z	err [mDa]	err [ppm]	mSigma	rdb	e <sup>-</sup> Conf	N-Rule
593.1295	1	C <sub>30</sub> H <sub>25</sub> O <sub>13</sub>	100.00	593.1301	0.5	0.9	5.7	18.5	even	ok
	2	C <sub>31</sub> H <sub>21</sub> N <sub>4</sub> O <sub>9</sub>	40.48	593.1314	1.9	3.1	10.8	23.5	even	ok
	3	C <sub>27</sub> H <sub>17</sub> N <sub>10</sub> O <sub>7</sub>	75.97	593.1287	-0.8	-1.4	12.4	24.5	even	ok
	4	C <sub>28</sub> H <sub>13</sub> N <sub>14</sub> O <sub>3</sub>	81.64	593.1301	0.5	0.9	16.7	29.5	even	ok
	5	C <sub>26</sub> H <sub>21</sub> N <sub>6</sub> O <sub>11</sub>	28.41	593.1274	-2.2	-3.6	17.2	19.5	even	ok
	6	C <sub>24</sub> H <sub>9</sub> N <sub>20</sub> O	25.49	593.1274	-2.2	-3.7	21.9	30.5	even	ok
	7	C <sub>14</sub> H <sub>5</sub> N <sub>30</sub>	9.90	593.1319	2.4	4.0	52.0	27.5	even	ok
	8	C <sub>16</sub> H <sub>17</sub> N <sub>16</sub> O <sub>10</sub>	9.38	593.1319	2.4	4.0	53.4	16.5	even	ok
	9	C <sub>39</sub> H <sub>13</sub> N <sub>8</sub>	5.88	593.1269	-2.7	-4.5	59.6	37.5	even	ok
	10	C <sub>18</sub> H <sub>29</sub> N <sub>2</sub> O <sub>20</sub>	6.73	593.1319	2.4	4.0	63.2	5.5	even	ok
	11	C <sub>13</sub> H <sub>9</sub> N <sub>26</sub> O <sub>4</sub>	17.22	593.1306	1.0	1.7	63.6	22.5	even	ok
	12	C <sub>15</sub> H <sub>21</sub> N <sub>12</sub> O <sub>14</sub>	16.98	593.1306	1.0	1.7	63.9	11.5	even	ok
	13	C <sub>43</sub> H <sub>17</sub> N <sub>2</sub> O <sub>2</sub>	21.56	593.1296	0.0	0.0	70.9	36.5	even	ok
	14	C <sub>14</sub> H <sub>25</sub> N <sub>8</sub> O <sub>18</sub>	16.38	593.1292	-0.3	-0.5	74.8	6.5	even	ok
	15	C <sub>9</sub> H <sub>5</sub> N <sub>32</sub> O <sub>2</sub>	7.01	593.1279	-1.7	-2.8	76.7	23.5	even	ok
	16	C <sub>12</sub> H <sub>13</sub> N <sub>22</sub> O <sub>8</sub>	14.98	593.1292	-0.3	-0.5	77.0	17.5	even	ok
	17	C <sub>13</sub> H <sub>29</sub> N <sub>4</sub> O <sub>22</sub>	4.85	593.1279	-1.6	-2.8	86.1	1.5	even	ok
	18	C <sub>11</sub> H <sub>17</sub> N <sub>18</sub> O <sub>12</sub>	4.59	593.1279	-1.7	-2.8	87.2	12.5	even	ok

**Figure 16.** The outcome of SmartFormula-based determination of the molecular formula of the ion having  $m/z$  593.1295, the parent ion representing the metabolite of *Sparrmannia discolor* (p. II.3.6.2);

The error of  $m/z$  determination for the entries **1** and **4**, namely C<sub>30</sub>H<sub>25</sub>O<sub>13</sub> and C<sub>28</sub>H<sub>13</sub>N<sub>14</sub>O<sub>3</sub>, is exactly the same, but the isotopic distribution of the latter formula – calculated by the *SmartFormula*<sup>TM</sup> on the basis of the abundances of all elements included in this structure – does not fit to the experimental pattern as good as the one for C<sub>30</sub>H<sub>25</sub>O<sub>13</sub>. For this reason, the most probable molecular formula assigned to the compound having  $m/z$  593.1295 is C<sub>30</sub>H<sub>26</sub>O<sub>13</sub> (the lowest mSigma value: 5.7).

## 1.3.6.1. Aqueous extract of liquorice roots

The molecular formula of the first compound annotated as an inhibitor (ENALDI  $m/z$  209, **fig. 12-A**, the diagram: **fig. 14-A**) was identified as  $C_{10}H_{10}O_5$  (experimental  $m/z$  209.0445, calculated  $m/z$  209.0450) using Bruker *SmartFormula* software. This compound was also mentioned in the bibliography describing the studies of various liquorice species: *Glycyrrhiza glabra*, *Glycyrrhiza uralensis*, *Glycyrrhiza inflata* and *Glycyrrhiza echinata*, but marked as 'unknown' [291]. Fragmentation of the precursor ion having  $m/z$  209.0445 revealed two parent ions:  $m/z$  165.0557 and 121.0665 representing the loss of one and two carboxyl groups respectively (**fig. 17**).

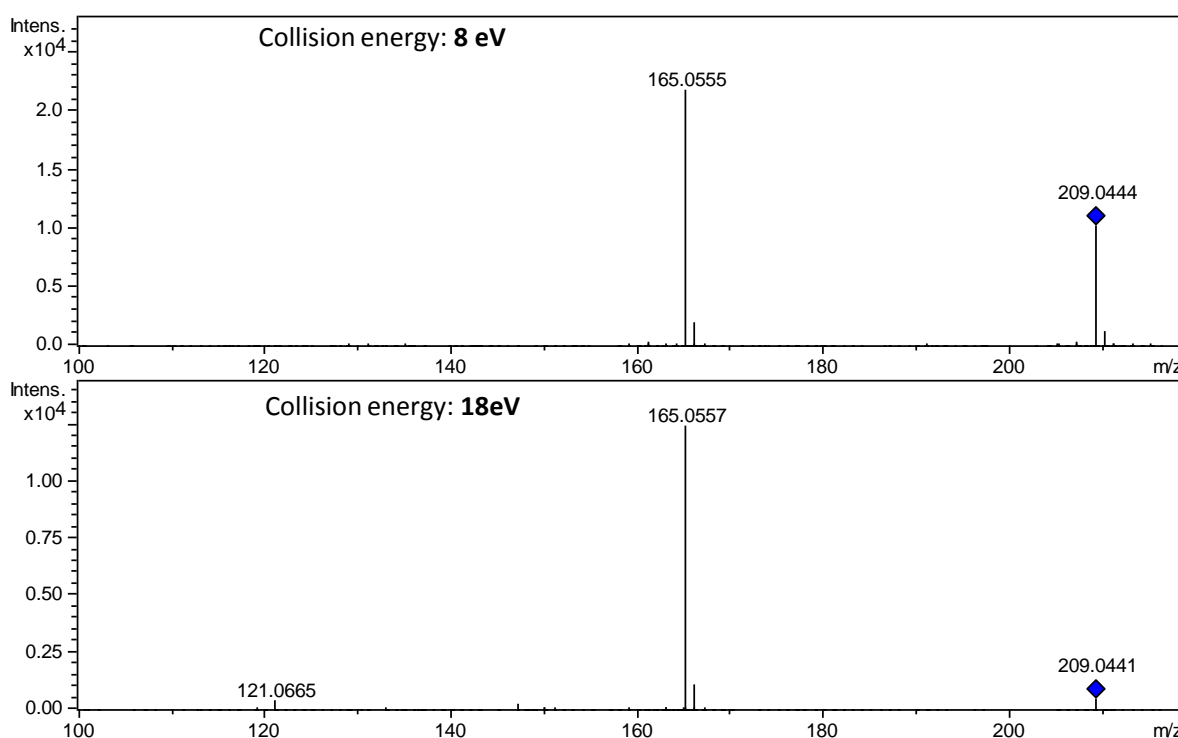


**Figure 17.** CID fragmentation pattern of liquorice metabolite identified as 2-[(4-Hydroxyphenyl)methyl]malonic acid in negative ion mode.

This compound was isolated from the extract using automated fractionation of liquorice aqueous extract (*Appendix II, p. 1, fig. S1*) and subjected to NMR analysis using two instruments (Bruker DPX 250 Avance, 250 MHz and Bruker Avance, 400 MHz).

<sup>1</sup>H NMR (250 MHz, Acetone) ppm: 3.11 (m, CH<sub>2</sub>), 3.59 (t, J=7.25 Hz, CH), 6.65 (m, 2H, Ar), 7.12 (m, 2H, Ar)

<sup>13</sup>C NMR (400 MHz, CD<sub>3</sub>OD) ppm: 170.13, 155.95, 129.88, 115.00, 53.21, 33.79

<sup>13</sup>C NMR (DEPT135, 400 MHz, CD<sub>3</sub>OD) ppm: 129.88 (pos, Ar), 115.00 (pos, Ar), 53.21 (pos, CH<sub>2</sub>), 33.79 (neg, CH)

$^1\text{H-NMR}$  showed unambiguously the presence of *p*-substituted aromatic ring. Two-dimensional proton-correlation NMR experiment revealed an aliphatic  $\text{CH}_2$  group (**fig. 18, (2)**) correlating with the *o*-hydrogens of aromatic ring and other CH aliphatic group. A DEPT  $^{13}\text{C-NMR}$  experiment confirmed the presence of aliphatic CH group other than aromatic (a negative peak at 33.79 ppm) and  $\text{CH}_2$  group (a positive peak at 53.21 ppm). On the basis of these findings we identified the compound of interest as 2-[(4-Hydroxyphenyl)methyl]malonic acid (**fig. 19, entry 1**).

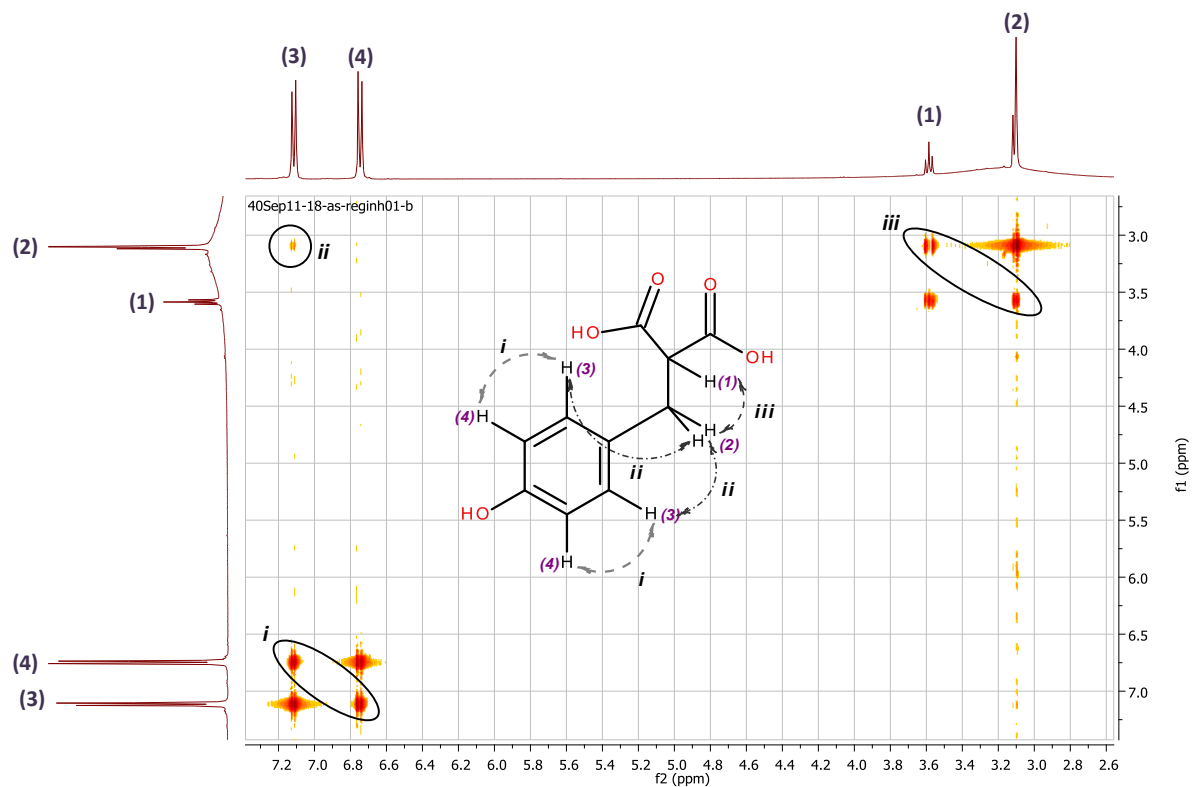


**Figure 18.** Proton-proton correlations of 2-[(4-Hydroxyphenyl)methyl]malonic acid.

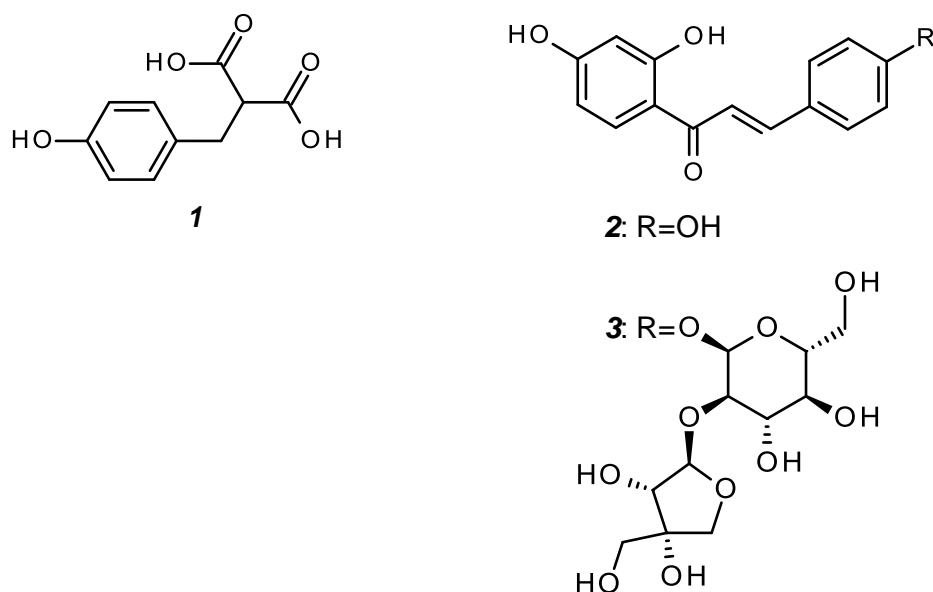


**Figure 19.** The structures of 2-[(4-Hydroxyphenyl)methyl]malonic acid (**1**) and isoliquiritigenin (2',4',4'-trihydroxychalcone) (**2**).

The second compound annotated as the inhibitor candidate ( $m/z$  255, **fig. 12-A**) cannot be indicated unambiguously, since in liquorice root extract there are at least three isomers corresponding to this mass: 5,7-dihydroxyflavanone (pinocembrin), 4',7-dihydroxyflavanone (liquiritigenin) and 2',4',4'-trihydroxychalcone (isoliquiritigenin) [291-293]. The latter compound, isoliquiritigenin (**fig. 19**, entry **2**), is a known tyrosinase inhibitor [37, 41]. The series of compounds having  $m/z$  549 is wide and is composed mostly on glycosylated compounds having  $m/z$  255, e.g. neolicuroside - glycosylated isoliquiritigenin or liquiritin apioside - glycosylated liquiritigenin (**fig. 19**, entry **3**) [292].

The inhibitor candidate having  $m/z$  577.1567,  $C_{27}H_{30}O_{14}$ , was tentatively identified as isoviolanthin (apigenin-6-C-rha-8-C-glu), shown to be present in various liquorice species [292]. In plants one can also find a close isomer of isoviolanthin, called violanthin (apigenin-6-C-glu-8-C-rha), which differs from isoviolanthin in the swapped positions of glucose and rhamnose attachment to the apigenin core. The fragmentation pattern of this inhibitor candidate (CID fragmentation: **fig. 20**, proposed fragmentation mechanism: **fig. 21**), in terms of fragment ions and their relative intensities, comply with the one for isoviolanthin and not for violanthin (**table 2**). Taking these findings into account we conclude that the major metabolite having  $m/z$  577.1567 was identified as isoviolanthin (**fig. 21**).

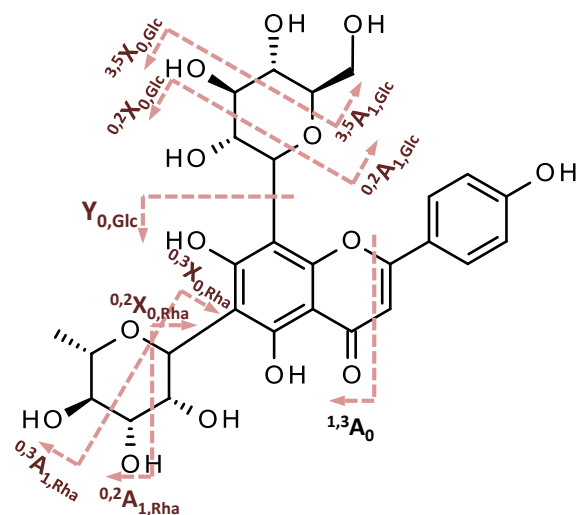


**Figure 20.** Proposed CID fragmentation pattern of isoviolanthin.

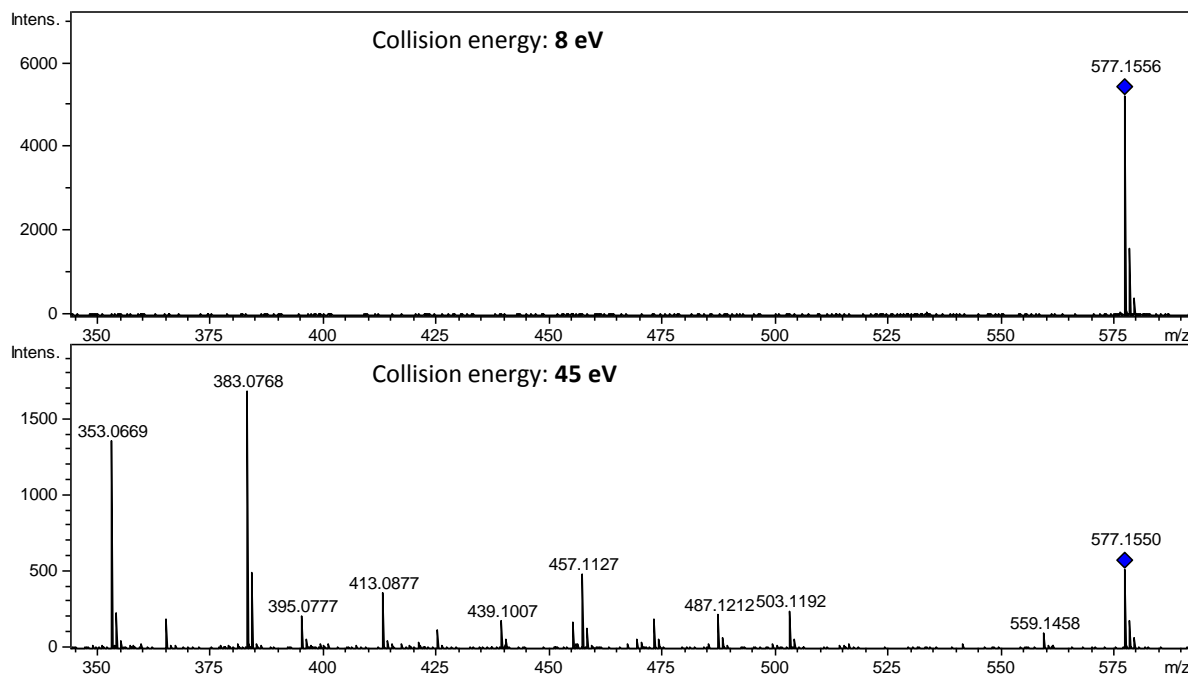


**Figure 21.** CID fragmentation pattern of liquorice metabolite identified as isoviolanthin in a negative ion mode.

**Table 2.** CID fragmentation pattern of liquorice metabolite having  $m/z$  577.1556 collected in a negative ion mode (A) and its comparison to the fragmentation patterns of isoviolanthin and violanthin (B) [291].

A: Fragmentation of ion having $m/z$ 577.1556 at 45 eV				B: The fragmentation pattern of:	
				Apigenin-6-C-rha-8-C-glu (isoviolanthin) [291]	Apigenin-6-C-glu-8-C-rha (violanthin) [291]
Experimental values $MS^2$ $m/z$ (% base peak)	Calculated $m/z$	Error (ppm)	Interpretation of the fragmentation pathway	$MS^2$ $m/z$ (% base peak)	
353.0669 (81)	353.0661	2.27	$[M^{-0,2}A_{1,Rha}^{-0,2}A_{1,Glc}]^-$	353 (100)	353 (47)
365.0627 (11)				365 (5)	not observed
383.0768 (100)	383.0766	0.52	$[M^{-0,3}A_{1,Rha}^{-0,2}A_{1,Glc}]^-$	383 (70)	383 (22)
395.0777 (12)				395 (12)	not observed
413.0877 (22)	413.0872	1.21	$[Y_{0,Glc-H}]^-$	413 (15)	not observed
425.0877 (7)				not observed	not observed
437.1007 (1)				437 (3)	not observed
439.0985 (11)				439 (14)	not observed
455.1028 (10)				not observed	not observed
457.1127 (29)	457.1134	1.53	$[^{0,2}X_{0,Glc-H}]^-$	457 (92)	457 (100)
458.1127 (7)	458.1060	14.63	$[^{1,3}A_0-H]^-$	not observed	not observed
469.1164 (3)				not observed	not observed
470.1116 (2)				not observed	not observed
473.1036 (11)	473.1083	9.93	$[^{0,2}X_{0,Rha-H}]^-$	473 (77)	473 (5)
487.1176 (13)				487 (8)	487 (49)
503.1192 (14)	503.1189	0.60	$[^{3,5}X_{0,Glc-H}]^-$ or $[^{0,3}X_{0,Rha-H}]^-$	503 (37)	not observed
533.1247 (1)				533 (5)	not observed
559.1458 (6)	559.1491	5.90	$[M-H-H_2O]^-$	559 (10)	559 (7)
577.1556	577.1557	0.17			

1.3.6.2. Methanol extract of *Sparrmannia discolor* leaves and stems

The two compounds annotated previously as inhibitor candidates ( $m/z$  177.0192 and 359.0765, ENALDI MS spectra: **fig. 12-B**, the diagram: **fig. 14-B**) or substrate candidate ( $m/z$  593.1297) were isolated in the quadrupole mass filter of ESI-Qq-TOF MS and subjected to collision-induced fragmentation. Experimental and calculated  $m/z$  values for all compounds of interest were provided in **table 3**, whereas experimental fragmentation patterns obtained in our laboratory and those deposited in METLIN or MassBank databases in **table 4**.

The inhibitor candidate having  $m/z$  177.0192 was identified as esculetin, 6,7-dihydroxycoumarin (**fig. 27**, entry **1**). The CID fragmentation pattern of esculetin in negative ion mode (**fig. 22**) in studied mass range is identical in terms of  $m/z$  values as the one of its isomer, daphnetin (7,8-dihydroxycoumarin). However, relative intensities of the fragment ions eliminated the latter candidate. Esculetin was proven to be a competitive inhibitor of tyrosinase and was isolated from *Euphorbia lathyris* L. [294].

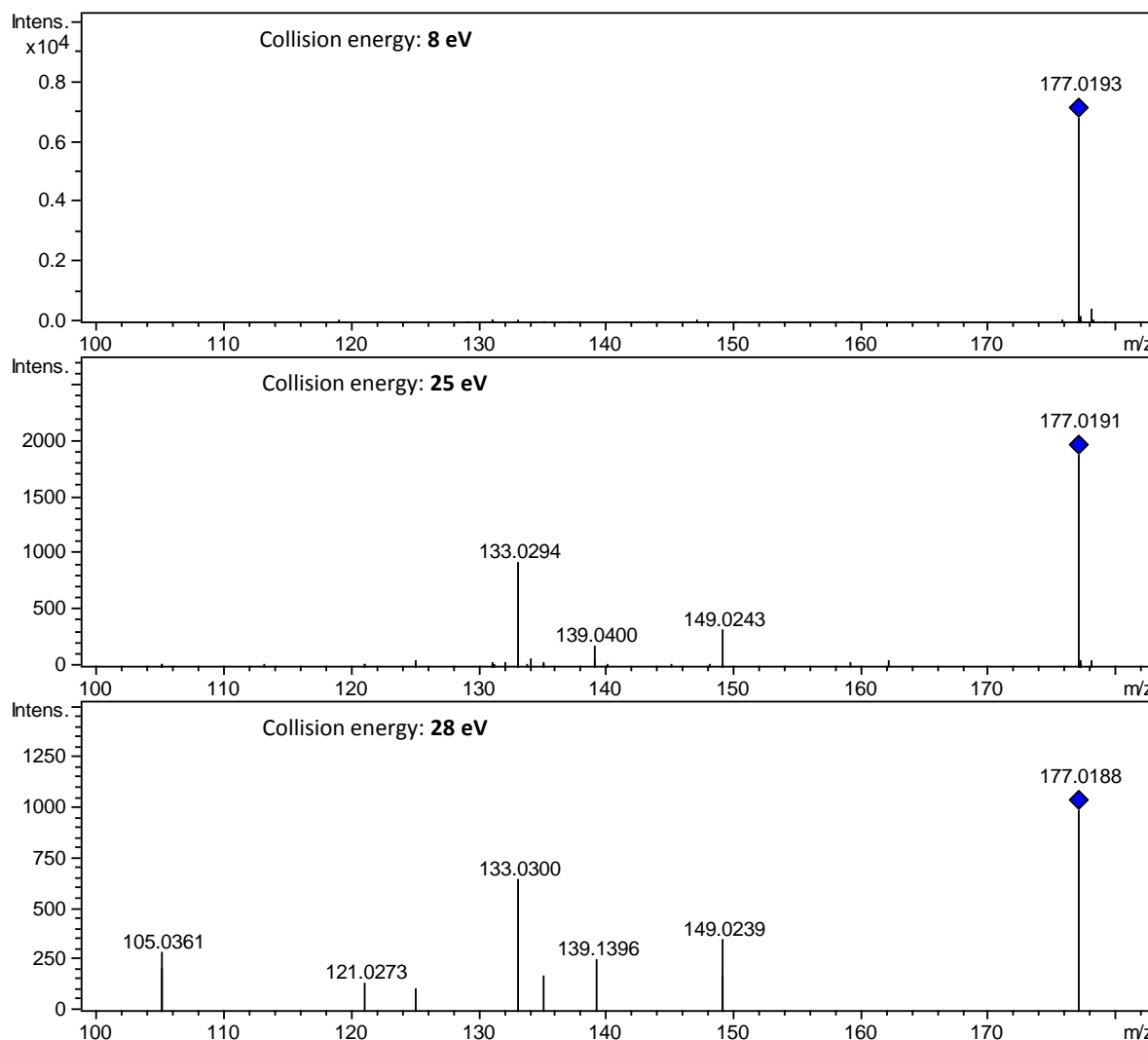


**Figure 22.** The fragmentation pattern of *Sparrmannia discolor* metabolite identified as esculetin in negative ion mode.



The inhibitor candidate ( $m/z$  359.0765) was unambiguously identified as rosmarinic acid (**fig. 27**, entry **2**). The fragmentation pattern of this compound from METLIN database (entry: 3504) fully complies with the results obtained in our laboratory (mass spectra in negative: **fig. 23** and positive ion mode: **fig. 24**). Rosmarinic acid is a known noncompetitive inhibitor of tyrosinase [295].

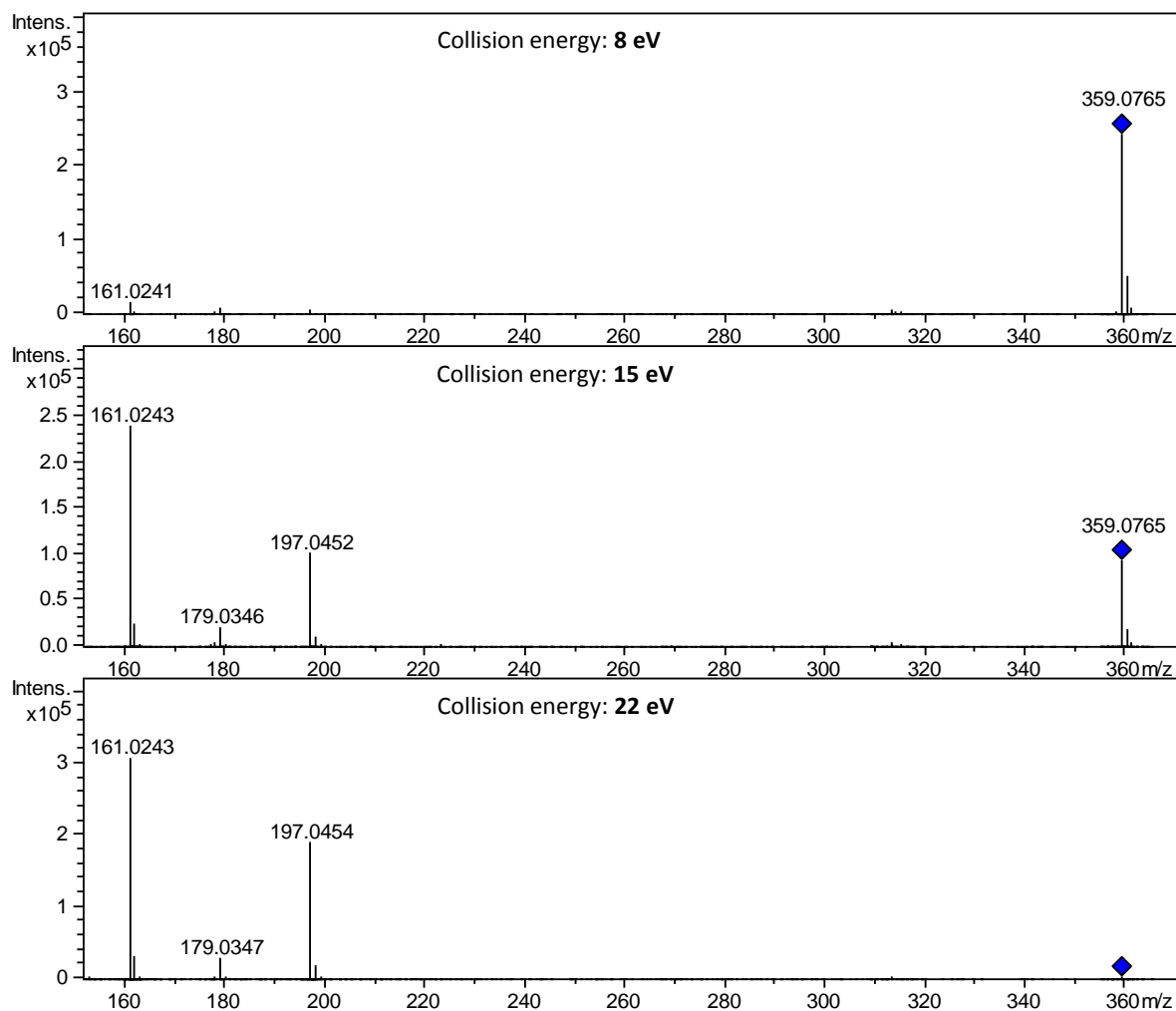


**Figure 23.** The fragmentation pattern of *Sparrmannia discolor* metabolite identified as rosmarinic acid in negative ion mode.

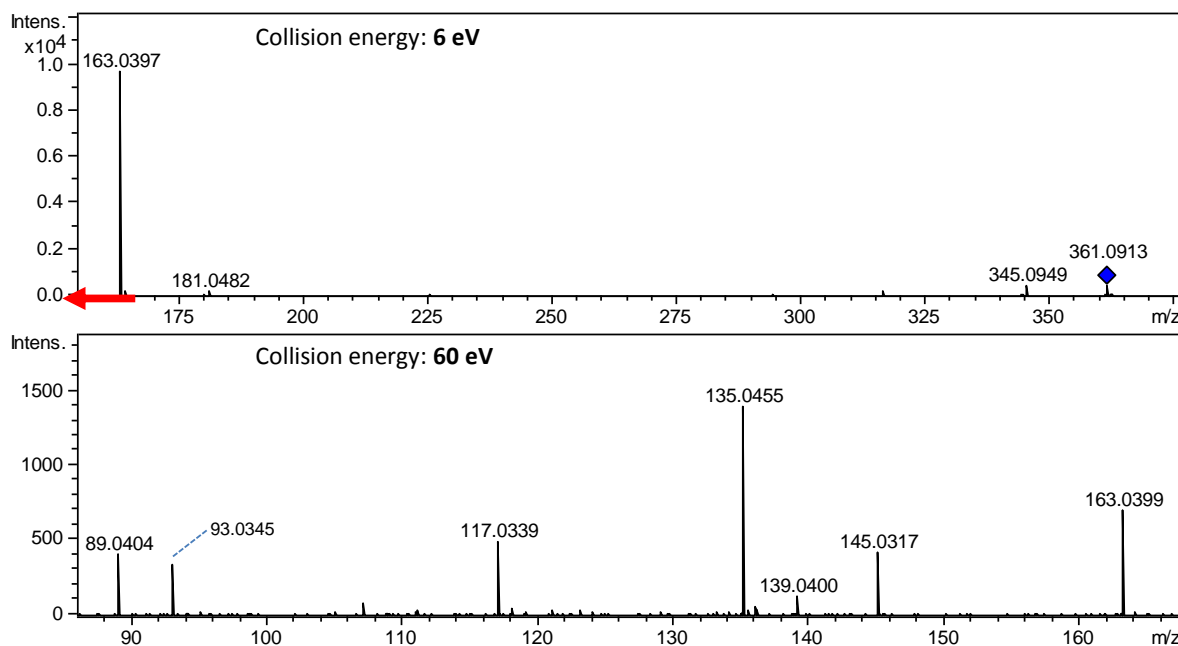


**Figure 24.** The fragmentation pattern of *Sparrmannia discolor* metabolite identified as rosmarinic acid in positive ion mode.

The substrate candidate with  $m/z$  593.1297 was identified as kaempferol-3-*O*-(6'-*E*-*p*-coumaroyl)-glucoside (**fig. 27**, entry **3**), on the basis of the fragmentation pattern deposited in MassBank database (entry: *PR100969*) and confirmed to be an analog of kaempferol-3-*O*-glucoside, naturally occurring flavonol (METLIN entry *3504*). Fragmentation pattern of its common isomer, kaempferol-7-*O*-glucoside, eliminated the possibility of its occurrence in the studied extract. Kaempferol-3-*O*-(6'-*E*-*p*-coumaroyl)-glucoside is known to be a tyrosinase inhibitor [296] but, according to our findings, one of its monophenol groups undergoes partial enzymatic oxidation to *o*-quinone (**fig. 13**). The experimental fragmentation pattern of kaempferol-3-*O*-(6'-*E*-*p*-coumaroyl)-glucoside can be found **fig. 25** (positive ion mode) and **fig. 26** (negative ion mode).

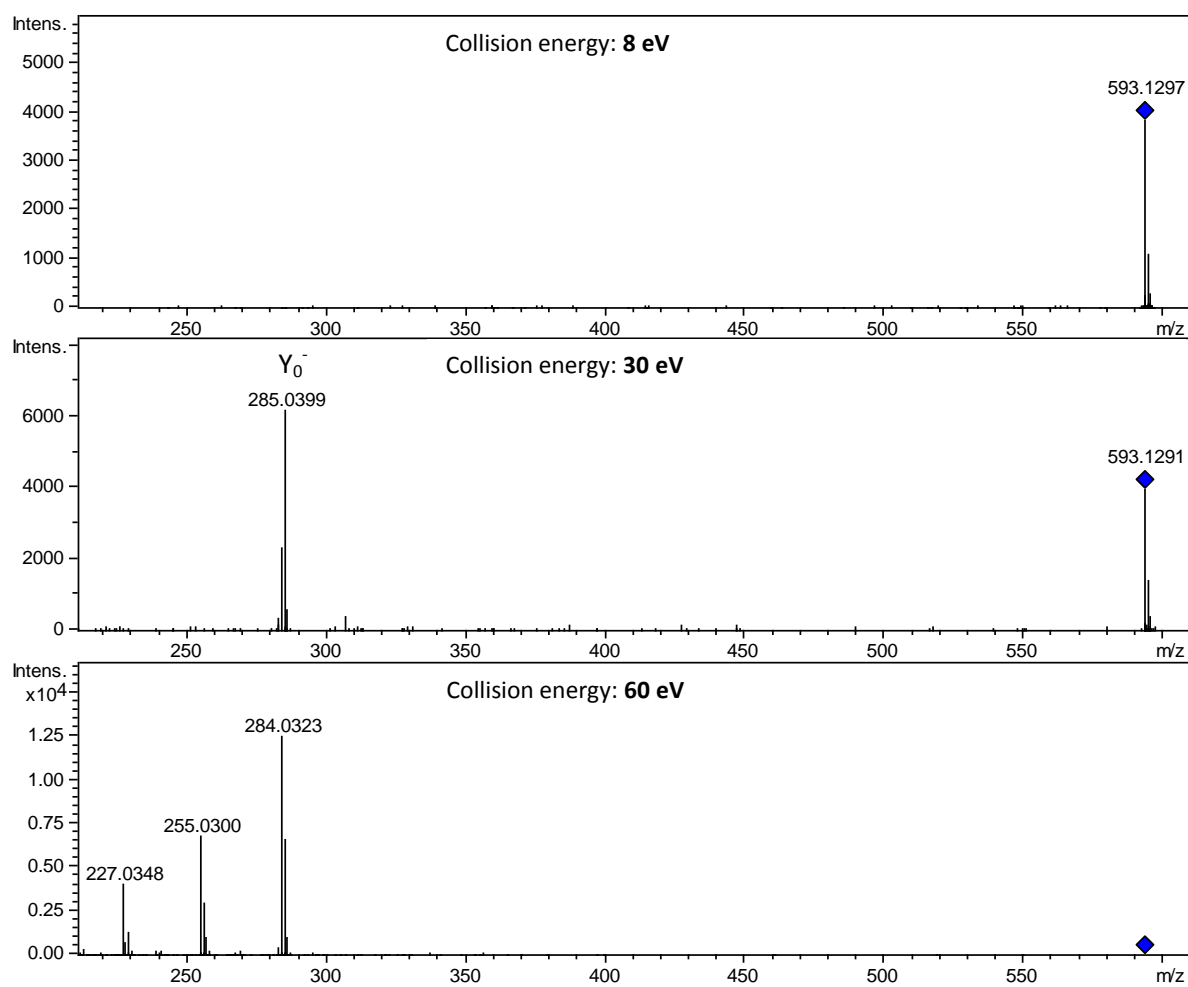


**Figure 25.** The fragmentation pattern of *Sparrmannia discolor* metabolite identified as kaempferol-3-O-(6'-E-p-coumaroyl)-glucoside in negative ion mode.

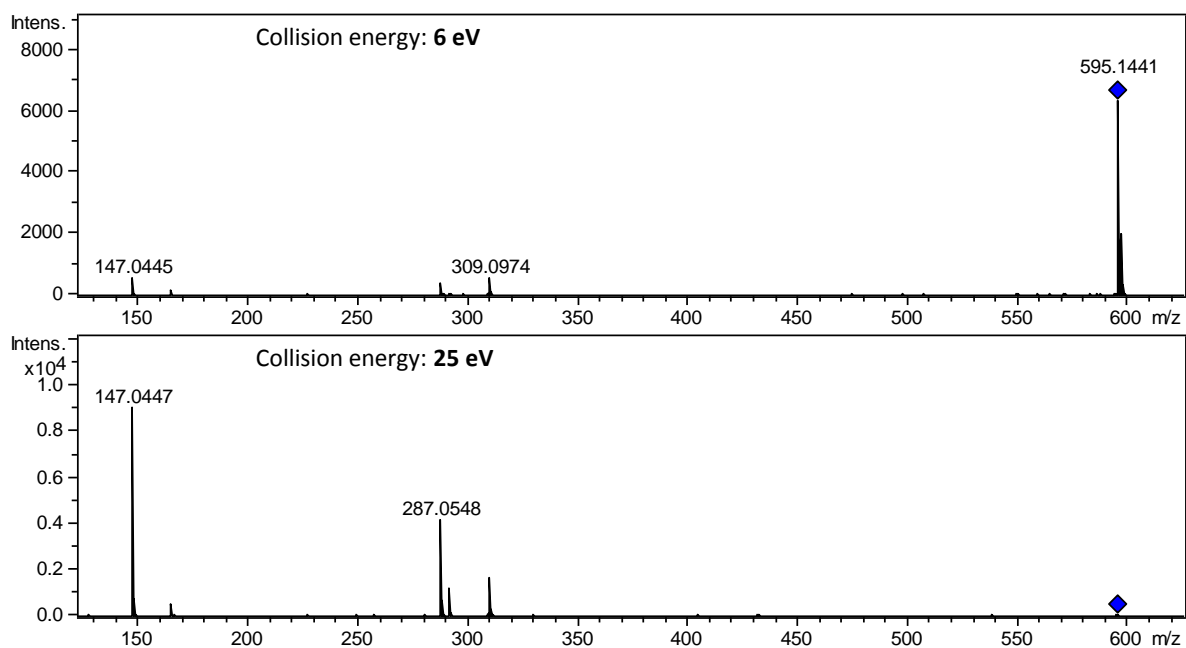


**Figure 26.** The fragmentation pattern of *Sparrmannia discolor* metabolite identified as kaempferol-3-*O*-(6'-*E*-*p*-coumaroyl)-glucoside in positive ion mode.

**Table 3.** Experimental and calculated values of  $m/z$  for identified active metabolites of *Sparrmannia discolor*

Name of compound	$m/z$ of $[M-H]^-$ ions			$m/z$ of $[M+H]^+$ ions		
	experimental	calculated	mass accuracy [ppm]	experimental	calculated	mass accuracy [ppm]
Esculetin	177.0192	177.01879	2.32	not measured	179.03444	-
Rosmarinic acid	359.0765	359.07668	0.50	361.0922	361.09233	0.36
Kaempferol-3- <i>O</i> -(6'- <i>E</i> - <i>p</i> -coumaroyl)-glucoside	593.1297	593.1295	0.34	595.1436	595.14515	2.60

**Table 4.** CID fragmentation patterns of active metabolites of *Sparrmannia discolor* collected in negative and positive ion mode. MELTIN and Massbank databases contain experimental fragmentation patterns of the standard compounds. Collision energies were given in the round brackets.

Negative ion mode							
Esculetin			Rosmarinic acid		Kaempferol-3-O-(6'-E-p-coumaroyl)-glucoside		
experimental	MELTIN, entry: 43936 (20 V)	MassBank, entry: FIO00084 (30 eV)	experimental	MELTIN, entry: 3504 (20 V)	experimental	MELTIN, entry: 45733* (40 V)	MassBank, entry: PR100969 (30 V)
105.0361 (28 eV)	105.0340	105.0350					
121.0304 (25 eV)	121.0288	121.0295	197.0456 (25 eV)	197.0447	307.0830 (30 eV)	not observed*	307.0822
125.0228 (28 eV)	not observed	125.0246	179.0348 (25 eV)	179.0348	285.0399 (30 eV)	285.0388	285.0390
133.0293 (25 eV)	133.0285	133.0294	161.0244 (25 eV)	161.0241	284.0323 (60 eV)	284.0314	284.0313
139.0402 (25 eV)	not observed	139.0403			255.0300 (60 eV)	255.0287	255.0293
149.0242 (28 eV)	149.0234	149.0245			227.0348 (60 eV)	227.0340	227.0347

\* - no fragmentation data were found for proposed compound in MELTIN database. Instead, fragmentation data for kaempferol-3-O-glucoside (non-coumaroylated analog) were shown.

Positive ion mode				
Rosmarinic acid			Kaempferol-3-O-(6'-E-p-coumaroyl)-glucoside	
experimental	MELTIN, entry: 3504 (20-40 V)	MassBank entry: PR040220 (5-60 V)	experimental	MassBank entry: PR101023 (5-60 V)
345.0949 (6 eV)	not observed	not observed	309.0974 (25 eV)	<b>309.0969</b>
181.0482 (6 eV)	181.0492	181.0491	291.0862 (25 eV)	291.0867
164.0439 (60 eV)	not observed	164.0432	287.0548 (25 eV)	<b>287.0545</b>
not observed	not observed	163.1067	165.0553 (25 eV)	165.0543
163.0397 (6 eV)	163.0339	<b>163.0395</b>	147.0447 (25 eV)	<b>147.0436</b>
not observed	not observed	145.0912	119.0492 (25 eV) low level	119.0492
145.0296 (40 eV)	<b>145.0269</b>	<b>145.0290</b>	109.0271 (25 eV) low level	109.0284
139.0400 (40 eV)	139.0373	139.0395	91.0532 (15 eV) low level	91.055
not observed	not observed	135.1050	not observed	81.0352
135.0455 (40 eV)	135.0434	<b>135.0445</b>		
not observed	not observed	117.0903		
117.0339 (60 eV)	<b>117.0337</b>	<b>117.0336</b>		
111.0451 (50 eV)	111.0432	111.0441		
107.0478 (50 eV)	107.0499	107.0490		
93.0345 (60 eV)	<b>93.0328</b>	93.0334		
not observed	not observed	89.0881		
89.0404 (60 eV)	<b>89.0401</b>	89.0387		

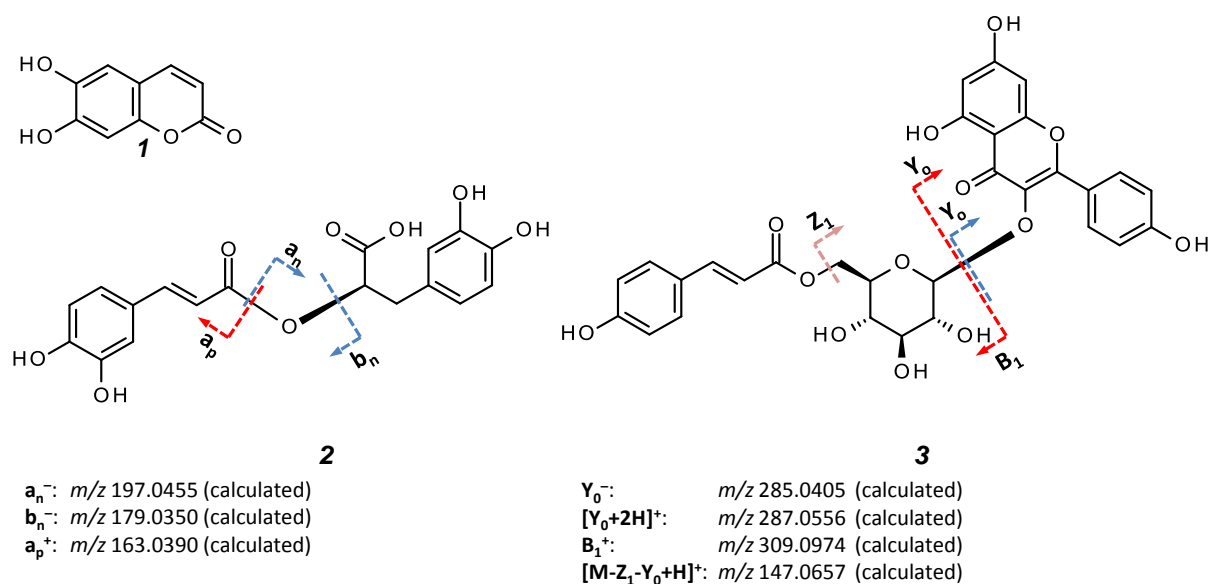


**Figure 27.** The structures of esculetin, MM: 178.02661 Da (1), rosmarinic acid, MM: 360.08452 (2) and kaempferol-3-O-(6'-E-p-coumaroyl)-glucoside, MM: (3). Underlined fragments were visualised on the mass spectra collected in the negative ion mode.

#### 1.4. IF/IH-ENALDI MS – conclusions

In summary, a novel approach that may help in finding low-mass inhibitors or substrate candidates in complex mixtures with minimal enzyme requirement (approximately 10 pmol/spot) has been developed. Tyrosinase-bound EMPs successfully indicated three inhibitor candidates in aqueous extract of liquorice roots. Only one identified peak ( $m/z$  209) was shown to represent a unique compound, 2-[(4-Hydroxyphenyl)methyl]malonic acid. The mass peak of  $m/z$  577 probably represents the mixture of apigenin-6-C-rha-8-C-glu (isoviolanthin) and, in lesser extent, its close isomer: apigenin-6-C-glu-8-C-rha (violetin). These compounds contain *p*-hydroxy substituted phenol groups in their structure, the moiety characteristic for a wide class of tyrosinase inhibitors (Chapter 1, table 1). Remaining mass peaks ( $m/z$  255 and 549) represent multiple compounds and – for this reason – it is not possible to draw any definitive conclusions about prospective identity of the compound responsible for 'ion fading' effect.

In case of methanol extract of leaves and stems of *Sparmannia discolor*, two compounds were pre-selected as inhibitor candidates ( $m/z$  177 and 359) and one as a substrate candidate ( $m/z$  593). All compounds were identified using ESI-qQ-TOF MS accompanied by two databases: METLIN and MaassBank. All identified compounds were already described as tyrosinase inhibitors, including the one pre-selected as a substrate.

EMPs were proven to be a versatile non-organic matrix capable of ionizing various types of small molecules (flavonoids, peptides, terpenes, saponins, nucleotides and nucleosides were tested in our lab) both in positive and negative ion mode. A single assay is very quick and simple (it is enough to mix the stock solution of EMPs and the analyte directly on MALDI plate and let to dry). Magnetic nanoparticles

provide a stable support for enzyme immobilisation extending its shelf life (up to 3-fold for tyrosinase), are cheap and simple to produce and easy to handle.

IF-ENALDI was shown to be extendible to various biological targets (trypsin and tyrosinase) and compatible with two different MALDI-TOF mass spectrometers. Since both variants of ENALDI are affinity-based methods, no marker of enzymatic activity is required. IF/IH-ENALDI approach poses an alternative for time-consuming and laborious bioassay-guided fractionation.

Because of limited mass accuracy of MALDI-TOF MS and lack of the capability of isolation and fragmentation of ions of interest, IF/IH-ENALDI MS can only be considered as a method for pre-selection of inhibitor candidates. All 'hits' should be subjected to further analysis using high resolution mass spectrometer.

## II. The use of enzyme-coupled magnetic particles to study the spectrum of unusual substrates of tyrosinase by direct surface-assisted laser desorption/ionisation and ESI-Qq TOF MS

### **Abstract**

Silica-coated magnetic particles pose high interest in the domain of surface-assisted laser desorption-ionisation (SALDI) as the non-organic matrix compatible with the low-mass compounds. MPs are cheap easy to produce, can be easily purified and separated from the solution and offer wide possibilities of surface derivatisation, including covalent coupling with various biomolecules. In this study we apply tyrosinase-coupled core-shell type silica-coated iron oxide magnetic particles (EMPs) in the simultaneous function of non-organic SALDI matrix and the enzyme carrier for studying the enzymatic conversion of unusual compounds containing the 2,4-diphenol moiety, known to be the strong inhibitors of tyrosinase: glabridin and 3-(2,4-dihydroxyphenyl)-propionic acid (DHPA). The reactions of enzymatic conversion were conducted directly on the spot of MALDI plate and, in addition, in solution for high-resolution ESI-Qq-TOF MS measurement. Both studied compounds: glabridin and DHPA were shown to be converted to corresponding quinones by tyrosinase only in the presence of the classic monophenol or *o*-diphenol substrate capable of regenerating the active site of enzyme.

### **II.1. Bibliographic introduction**

Numerous natural compounds containing the 2,4-diphenol (resorcinol) moiety were proven to be very efficient tyrosinase inhibitors, *e.g.* glabridin [37, 38], dalenin [16] or 3-(2,4-dihydroxyphenyl)-propionic acid (DHPA) [23] and often have several times stronger inhibitory activity than kojic acid, considered as a model tyrosinase inhibitor [34]. For this reason, the new approaches aimed at synthesising the novel tyrosinase inhibitors usually choose resorcinol-containing compounds as a starting point of synthesis [21, 45-47].

The mechanism of tyrosinase inhibition by resorcinol derivatives is not clear. For example, when the diphenolase activity of tyrosinase is taken into account, glabridin is found to be a non-competitive inhibitor; structurally similar dalenin was proven to be a mixed-type inhibition while synthetic 6''-hydroxy-2'',5'',7'',8''-tetramethylchroman-2''-yl)methyl 3-(2',4'-dihydroxy-phenyl)propionate is a competitive inhibitor. Chiari *et al.* showed that dalenin molecules form complexes with copper ions which could explain its inhibitory activity [16]. On the other hand, Khatib *et al.* reported in 2005 that 2,4,2',4'-hydroxychalcone, a very potent resorcinol-type tyrosinase inhibitor ( $IC_{50} < 20$  nM towards monophenolase activity), does not chelate copper ions and concluded that compounds having 2,4-dihydroxy substituted resorcinol moiety are much more potent tyrosinase inhibitors than their 3,5-dihydroxy or 3,4-dihydroxy-substituted analogs [24]. The ability of copper complexation cannot



therefore be considered as the major reason for the inhibitory activity of this group of compounds, but rather their characteristic moiety with 2,4-dihydroxy-substituted resorcinol. Chiari *et al.* conducted the docking of (2*R*)-dalenin to the model of tyrosinase active site and concluded that the 4-hydroxyl group of its resorcinol moiety interacts with peroxido ligand of oxy-tyrosinase [16]. Khatib *et al.* reported in 2007 that molecules obtained in a process of esterification of 3-(2,4-dihydroxyphenyl)-propionic acid (DHPA) with various alcohols (*e.g.* ethyl, isopropyl, octyl or 2,2-dimethylpropyl) are more potent tyrosinase inhibitors [23]. An addition of alkyl chains during the esterification process increased the hydrophobicity of the analogs in relation to the native DHPA and strengthened their interactions with the hydrophobic pocket surrounding the tyrosinase active site. These results show that 2,4-dihydroxy resorcinol moiety directly interacts with tyrosinase binuclear copper active site, while the remaining part of the inhibitor molecule is responsible for 'anchoring' it to the hydrophobic pocket around the active site.

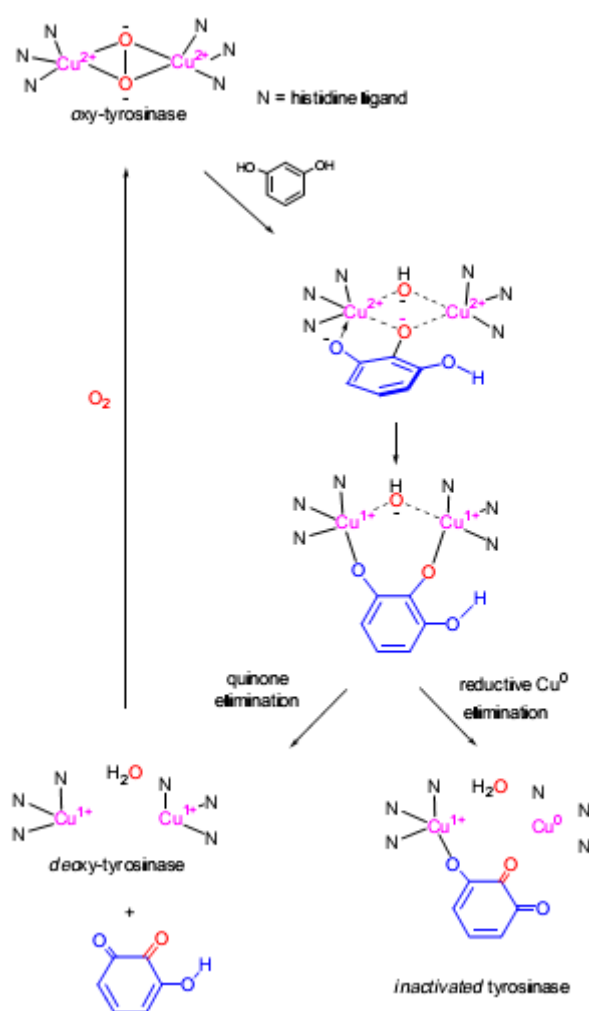


**Figure 28.** The mechanism of benzene-1,3-diol (resorcinol) conversion by tyrosinase with possible inactivation pathway proposed by Stratford *et al.* [297].

In January 2013, six months after results described in p. II.2 were obtained, Stratford *et al.* published results showing that benzene-1,3-diol (resorcinol) may be partially converted into

3-hydroxy-*o*-quinone and observed that pre-incubation of tyrosinase with resorcinol leads to enzyme inactivation [297]. According to the mechanism of tyrosinase inactivation (**fig. 28**), resorcinol is expected to bind to oxygenated *oxy*-tyrosinase. Moreover, the extent of enzyme inactivation was shown to be proportional to the time of its pre-incubation with resorcinol and reached a value as high as 95% after 8 minutes. Taking into account the fact that just a small fraction of tyrosinase is in the *oxy*- state (most of the native enzyme is in the *met*- form, even 85% [34, 297]), Stratford *et al.* proposed the mechanism of tyrosinase activation (*i.e.* its conversion from *met*- to *oxy*-form) assuming the formation of a new polyphenol (**fig. 29**, comp. **1**) from resorcinol and 3-hydroxy-*o*-quinone. Compound **1** can be subsequently oxidised to corresponding *o*-quinone (**2**) with simultaneous activation of tyrosinase (**fig. 29**).

The conclusions from these and other experiments presented in the ref. [297] are following: *i*) resorcinol leads to quick inactivation of tyrosinase; *ii*) resorcinol binds to *oxy*-tyrosinase exclusively; *iii*) resorcinol is hydroxylated in the *ortho* position in relation to both hydroxyl groups and then oxidised to 3-hydroxy-*o*-quinone (this reaction continues as long as enzyme is active); *iv*) the product of resorcinol and 3-hydroxy-*ortho*-quinone can activate tyrosinase by turning it from the *met*- to *oxy*-form.

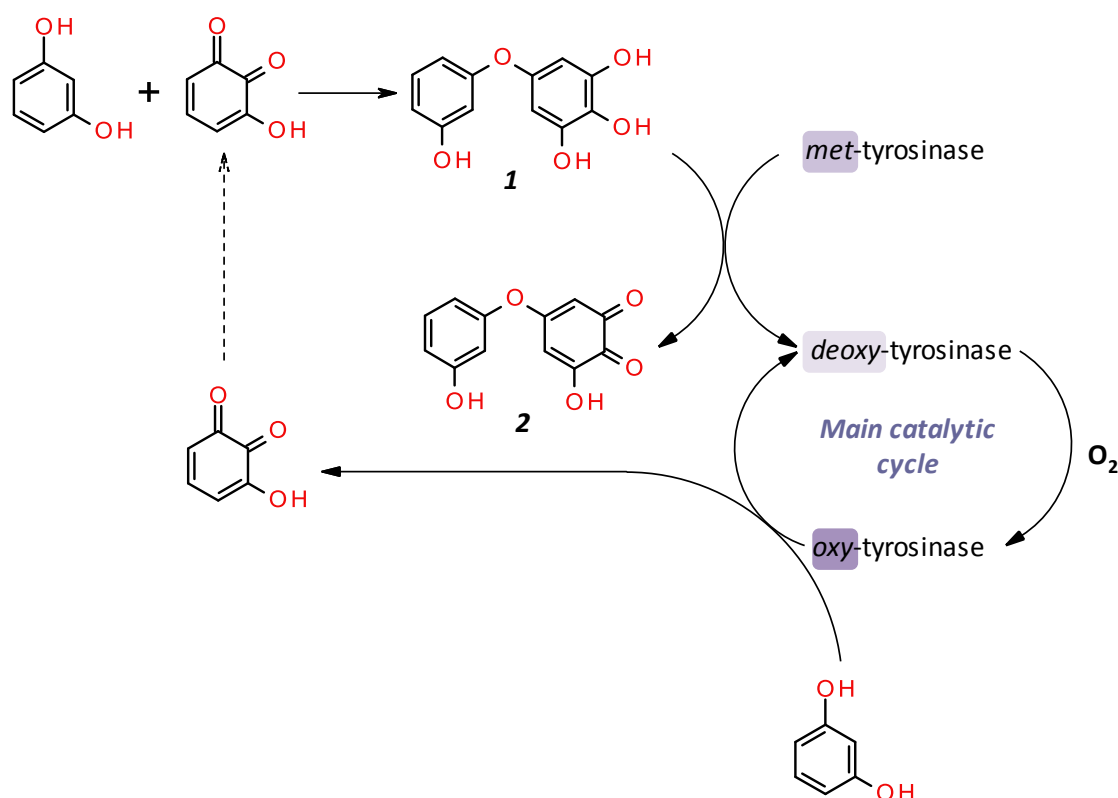


**Figure 29.** The mechanism of tyrosinase activation by the product **1** formed from resorcinol and 3-hydroxy-*o*-quinone. Illustration on the basis of the reference [297]. The number of 'main catalytic cycles' decreases gradually in time due to enzyme inactivation.

## II.2. The rationale for this study

During the initial tests of IF-ENALDI MS method we conducted numerous experiments with glabridin as an example of a strong tyrosinase inhibitor. During one of the experiments (conducted in May 2012) we decided to verify if activation of tyrosinase enzyme (*i.e.* generating *in situ* the oxy-form) would increase the onset of 'fading' of glabridin ion intensity. Surprisingly, we discovered that after application of L-Tyr as tyrosinase-activating agent, the intensity of the glabridin<sup>\*\*\*</sup> ion in the ENALDI mass spectrum obtained using EMPs with active tyrosinase was reduced by approximately 60% (**fig. 30-II**) compared to the one obtained using EMPs with denatured enzyme, along with an appearance of a new peak at *m/z* 337 (**fig. 30-I<sub>D</sub>**). The mass difference between this new peak and the glabridin ion (of about 14 Da, **fig. 30-I<sub>D</sub>**) suggests hydroxylation (+16 Da) followed by oxidation of two hydroxyl groups (-2 Da), the series of reactions characteristic for monophenolase cycle of tyrosinase (*Chapter I, fig. 3*). To verify the exact mass difference we conducted additional tests in solution using high resolution ESI-Qq-TOF-MS.

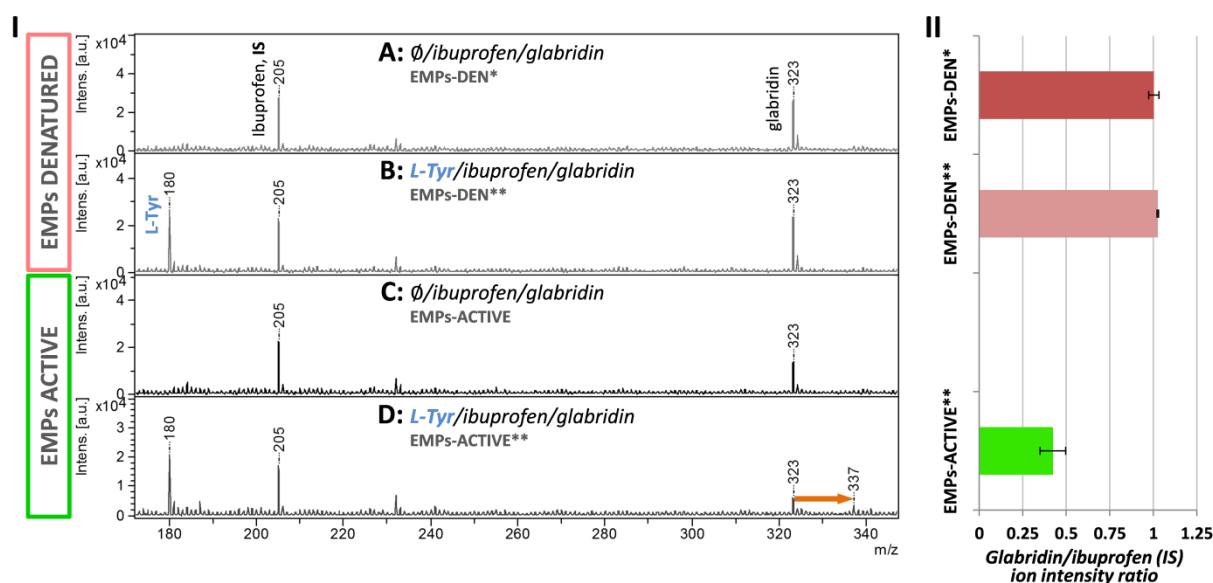


**Figure 30. I.** ENALDI-MS spectra of obtained in the following conditions: **A** - EMP<sub>s</sub>-tyrosinase\_denatured; ibuprofen (internal standard, IS), glabridin: 75/30 pmol per spot respectively; **B** - EMP<sub>s</sub>-tyrosinase\_denatured; L-Tyr, ibuprofen, glabridin: 30/75/30 pmol per spot respectively; **C** - EMP<sub>s</sub>-tyrosinase\_active; ibuprofen, glabridin: 75/30 pmol per spot; **D** - EMP<sub>s</sub>-tyrosinase\_active; L-Tyr, ibuprofen, glabridin: 30/75/30 pmol per spot respectively. In case of all samples, the amount of 3.4 μg of EMPs per spot was applied. L-Tyr ([M-H]<sup>-</sup>, *m/z* 180), ibuprofen ([M-H]<sup>-</sup>, *m/z* 205), glabridin ([M-H]<sup>-</sup>, *m/z* 323). **II.** Glabridin/ibuprofen (IS) ratio (*n*=2) for **I-A**, **I-B** and **I-D** ENALDI-MS spectra were shown on the right. The error bars show the range of ratio values (*n*=2) obtained in the experiment.

## II.3. ESI-Qq-TOF MS evaluation of tyrosinase-driven oxidation of 2,4-resorcinol-containing tyrosinase inhibitors.

We applied high-resolution ESI-Qq-TOF MS to verify the initial ENALDI MS results indicating tyrosinase-driven oxidation of glabridin in the presence of L-Tyr as the enzyme-activating agent. We extended the experimental sample set to 3-(2,4-dihydroxyphenyl)propionic acid (DHPA)<sup>\*\*\*</sup>, another

<sup>\*\*\*</sup> Structures of glabridin and DHPA Reader will find in the **table 1, Chapter I**, entries **2** and **5** respectively.

example of a resorcinol-containing tyrosinase inhibitor. Apart from L-Tyr, a monophenol tyrosinase substrate, we verified an ability of a diphenol substrate – catechin – to activate the active site of the enzyme in the presence of resorcinol-containing inhibitors.

#### II.4. The experiment design and results

The series of test solutions (A<sub>0</sub>, A<sub>1</sub>, A<sub>2</sub> containing glabridin; B<sub>0</sub>, B<sub>1</sub>, B<sub>2</sub> containing DHPA, **table 5**) were prepared in 50 mM ammonium formate. A volume of 100 µL of each working solution was mixed with 100 µL of the solution of MPs (denatured and active, 1700 µg/mL both). Each sample was incubated for 30 minutes at room temperature (approx. 21.6°C). EMPs were separated from the solutions by centrifugation and the supernatants were infused into mass spectrometer working in negative ion mode at a flow rate of 600 µL/h.

**Table 5.** Summary of test solutions. Each sample was incubated with both active and denatured EMPs.

Sample name	Internal standard	Resorcinol-containing tyrosinase inhibitor		Classic substrate (activator)	
	L-Arg (20 µM)	Glabridin (20 µM)	DHPA (20 µM)	L-Tyr (50 µM)	Catechin (50 µM)
A <sub>0</sub>	●	●	○	○	○
A <sub>1</sub>	●	●	○	●	○
A <sub>2</sub>	●	●	○	○	●
B <sub>0</sub>	●	○	●	○	○
B <sub>1</sub>	●	○	●	●	○
B <sub>2</sub>	●	○	●	○	●

● – presence; ○ – absence

#### MS parameters:

Source Type: ESI  
 Ion Polarity: Negative  
 Nebulizer: 0.4 Bar  
 Dry Heater: 180°C  
 Dry Gas: 2.0 l/min  
 Scan Begin: 100 m/z  
 Scan End: 1100 m/z  
 Capillary: 1900 V

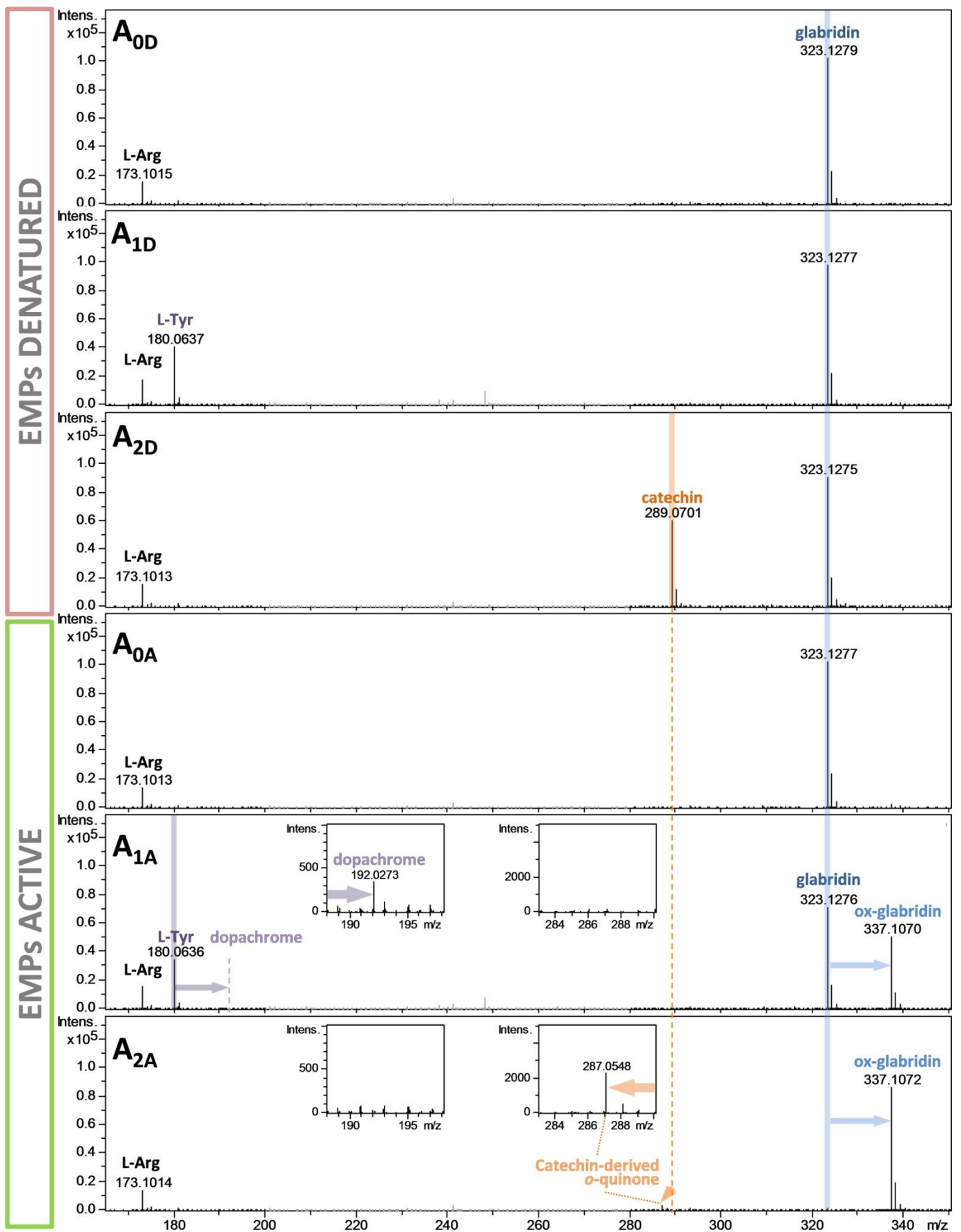


**Figure 31.** ESI-Qq-TOF-MS spectra of the solutions within A-series (**table 5**) after 30 min-long incubation with denatured/active EMPs (A<sub>D</sub>/A<sub>A</sub> respectively) at room temperature (approx. 21.6 °C). All ions were of [M-H]<sup>-</sup> type.

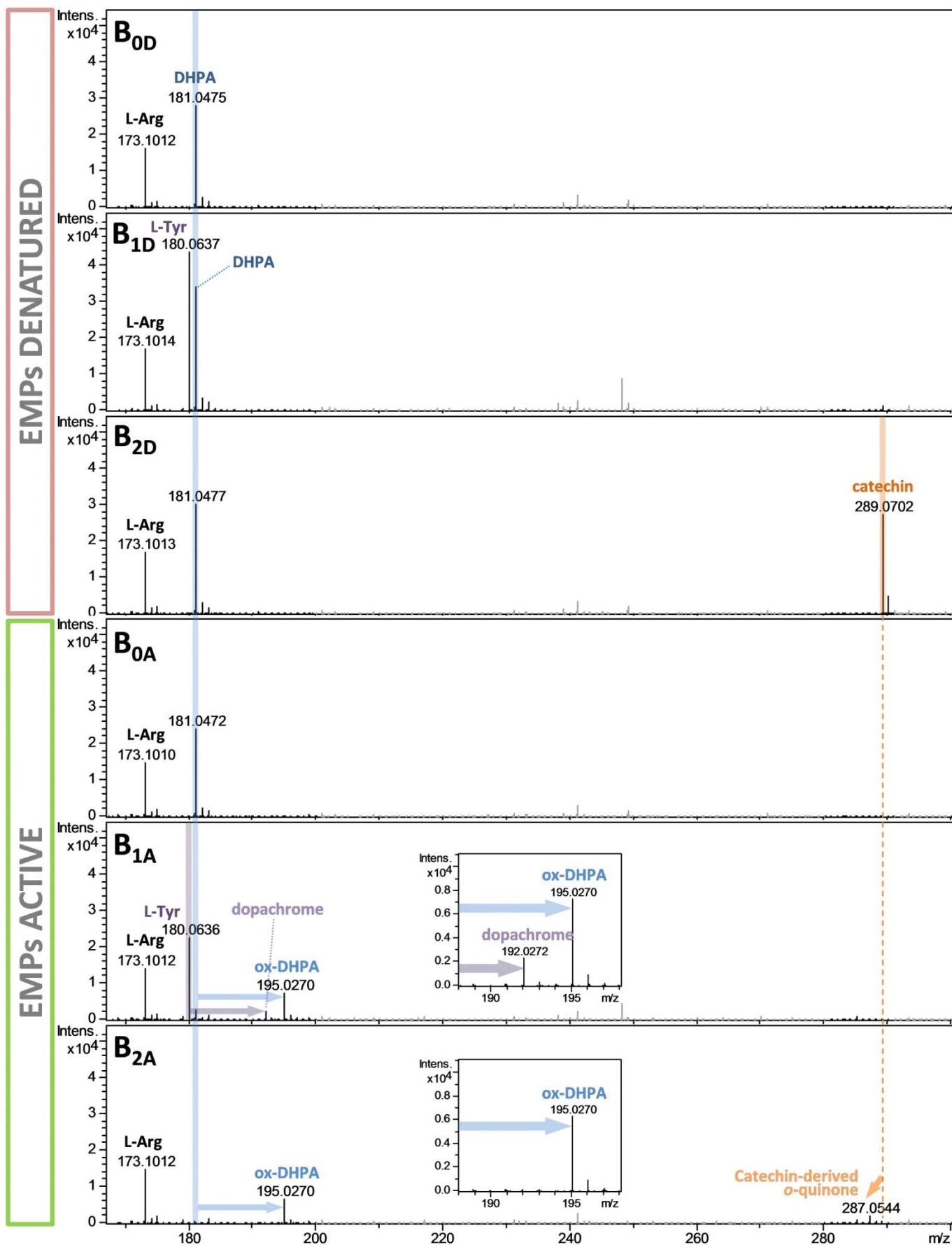


**Figure 32.** ESI-Qq-TOF-MS spectra of the solutions within B-series (table 5) after 30 min-long incubation with denatured/active EMPs (BD/BA respectively) at room temperature (approx. 21.6 °C). All ions were of  $[M-H]^-$  type.

The mass spectra of all samples **A** were depicted in **fig. 31**. In the case of denatured EMPs-tyrosinase (**A<sub>0D</sub>-A<sub>2D</sub>**), all compounds included within the test mixtures were successfully ionized and visualised in the spectra in the form of [M-H]<sup>-</sup> ions (L-Arg,  $m/z$  173.101; L-Tyr,  $m/z$  180.064; catechin,  $m/z$  289.070; glabridin,  $m/z$  323.128). When active EMPs (coupled with native tyrosinase) were applied to the mixture without the 'regular' tyrosinase substrate, **fig. 31-A<sub>0A</sub>**, no conversion of glabridin was noted and the mass spectrum was identical to the one obtained for denatured control EMPs (**fig. 31-A<sub>0D</sub>**). When tyrosinase substrates were added to the sample (L-Tyr, **A<sub>1A</sub>**, and catechin, **A<sub>2A</sub>**), for both of them the oxidation product of glabridin appeared ( $m/z$  337.1071 versus  $m/z$  323.1278 of glabridin, **A<sub>1A</sub>**). This yielded a mass difference equal to 13.9793 Da which perfectly corresponds to the calculated mass difference related to the sequential hydroxylation of monophenol and oxidation of its two hydroxyl groups to *o*-quinone ( $\Delta m = 13.97927$  Da). These results are consistent with the initial findings obtained by means of ENALDI MS (**fig. 30-I**).

The classic tyrosinase substrates were converted according to already well-known pathways. L-Tyr was hydroxylated and oxidised to the corresponding *o*-quinone (L-dopaquinone) that was immediately and spontaneously converted into L-dopachrome ( $m/z$  192.0273). The experimental mass difference between the substrate and the final product ( $\Delta m_{\text{exp}}=11.9636$ ) perfectly corresponds to the calculated one ( $\Delta m_{\text{calc}}=11.96361$ ). Catechin was oxidised to the corresponding *o*-quinone, stable under the experimental conditions. This process led to the elimination of two hydrogen atoms from the catechin molecule yielding a mass difference of 2.0153, well matching the calculated one ( $\Delta m_{\text{calc}}=2.01565$ ).

Analogous results were obtained for DHPA ( $m/z$  181.0477), the second resorcinol-containing tyrosinase inhibitor (**fig. 32**). Its oxidation product ( $m/z$  195.0270, the mass difference equal to 13.9793) appears only in the presence of one of the tyrosinase substrates considered in present studies (**fig. 32-B<sub>1A</sub>, B<sub>2A</sub>**).

It is important to note that the complete oxidation of resorcinol-containing molecules (both glabridin and DHPA) was achieved only for a diphenol tyrosinase substrate (catechin). When L-Tyr was applied, only a partial conversion of glabridin and DHPA was noted. A possible reason is a significant 'lag' phase for L-Tyr<sup>+++</sup> which is not the case for diphenols (*e.g.* catechin), converted with the maximal velocity from the first moment after contacting it with the enzyme. This effect could impede the onset of enzyme activation and lead to decreased yield of the conversion of studied resorcinol-containing inhibitors.

## II.5. Conclusions

We concluded that tyrosinase efficiently conducts hydroxylation and subsequent oxidation of glabridin and DHPA to corresponding hydroxy-*o*-quinones only if the regular substrates of the enzyme are provided in the sample (**table 6**). Both types of tyrosinase substrates (mono- or diphenol, L-Tyr and

---

<sup>+++</sup> the delay in the onset of the maximal velocity of monophenol conversion after the initiation of the reaction due to limited amount of *oxy*-tyrosinase in the reaction medium. The mechanism of tyrosinase activity was explained in the *Chapter I, p. 1.2*.

catechin respectively) can activate enzyme's active site in the presence of inhibitors. No visible conversion of glabridin and DHPA was noted in the absence of substrates, possibly because the oxidation products of both compounds cannot induce the 'activation cycle' (leading to oxy-tyrosinase) similar to the one characteristic for unsubstituted resorcinol (**fig. 29**). This confirms the observations of Stratford *et al.* that the *met*-form of the enzyme cannot oxidise resorcinol-containing substrates and that the outcome of the conversion of these compounds is the same as for monophenols (*o*-hydroxylation followed by oxidation of two adjacent hydroxyl groups to *o*-quinones).

Enzyme-bound magnetic nanoparticles were shown in *Chapter III* to be a useful tool for searching for low-mass tyrosinase inhibitors in the complex mixtures (such as plant extracts) using classic MALDI-TOF mass spectrometers with minimal enzyme requirement (approx. 6.5 pmol/analysis). Lack of any MALDI organic matrices added to the sample makes ENALDI-MS approach eligible for the analysis of compounds below 400 Da without any matrix-related interferences (**fig. 30-I**).

In this chapter an extension of EMPs applicability to follow tyrosinase-driven conversion of certain unusual substrates containing 2,4-diphenol (resorcinol) groups was described. Apart from the common application of EMPs as SALDI matrix, nanoparticles were used as the enzyme carrier for studying glabridin and DHPA conversion pathway 'in solution'. EMPs may be easily eliminated from the test mixture very quickly, minimizing the risk of sample contamination and enabling precise control of enzyme-substrate contact time.

**Table 6.** Summary of tyrosinase-driven conversion of its resorcinol-containing inhibitors

<b>Presence of a known substrate</b>	<b>Glabridin conversion?</b>	<b>DHPA conversion?</b>
YES (L-Tyr, monophenol)	YES, partial	YES, partial
YES (catechin, diphenol)	YES, full	YES, full
NO	NO	NO



## Appendix II: Supplementary Information

### 1. Purification of 2-[(4-Hydroxyphenyl)methyl]malonic acid

The purification was conducted by Dionex UltiMate UHPLC 3000 instrument equipped with the binary pump, automated injector integrated with fraction collector, standard thermostated column compartment and DAD detector (Germering, Germany), coupled with Bruker maXis ESI qQ-TOF MS (during an acquisition of the complete chromatogram only).

For a single run, a volume of 20  $\mu$ L of raw plant extract was injected to C18 HPLC column Alltima (150 $\times$ 4.6 mm ID, 5  $\mu$ m, Alltech, Deerfield, USA). The solvents and gradients were summarized in **table S1**. To collect sufficient amount of 2-[(4-Hydroxyphenyl)methyl]malonic acid required for the successful NMR experiment, a number of 100 injections was performed.

**Table S1.** Chromatographic parameters of the standard separation and a single run of fractionation

A: standard separation			B: shortened fractionation separation		
time [min]	water + 0.1% FA [%]	MeOH + 0.1% FA [%]	time [min]	water + 0.1% FA [%]	MeOH + 0.1% FA [%]
0	85	15	0	85	15
35	60	40	12	75	25
55	10	90	14	10	90
65	10	90	22	10	90
75	85	15	22	85	15
			30	85	15

The full chromatogram of liquorice extract was shown in **fig. S1**. The peak of interest (visualised by extracted ion chromatogram of target compound having  $m/z$  209.046) is eluted in the first order, therefore the gradient used for the purification process was modified to elute all remaining compounds as quickly as possible. Taking into account that required amount of injections reached one hundred, it drastically reduced solvent consumption.

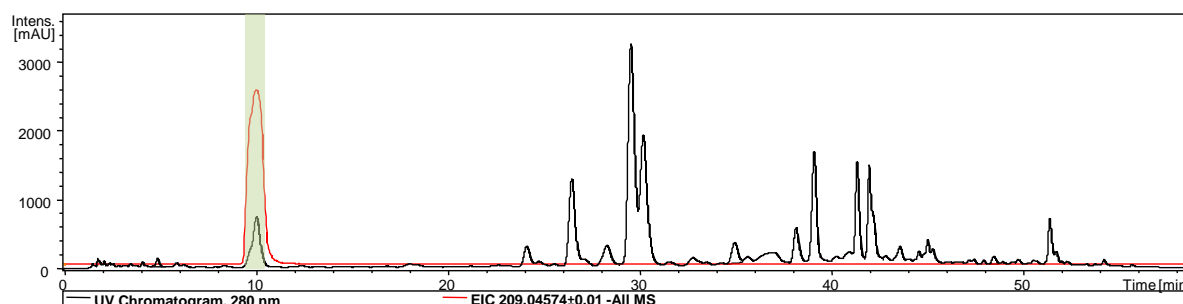


**Figure S1.** Typical chromatogram representing separation of liquorice raw extract, collected at 280 nm. The red extracted ion chromatogram shows the retention time of the target compound to be purified. Blue rectangle illustrates the collection 'window'.

## 2. Mass spectrometry

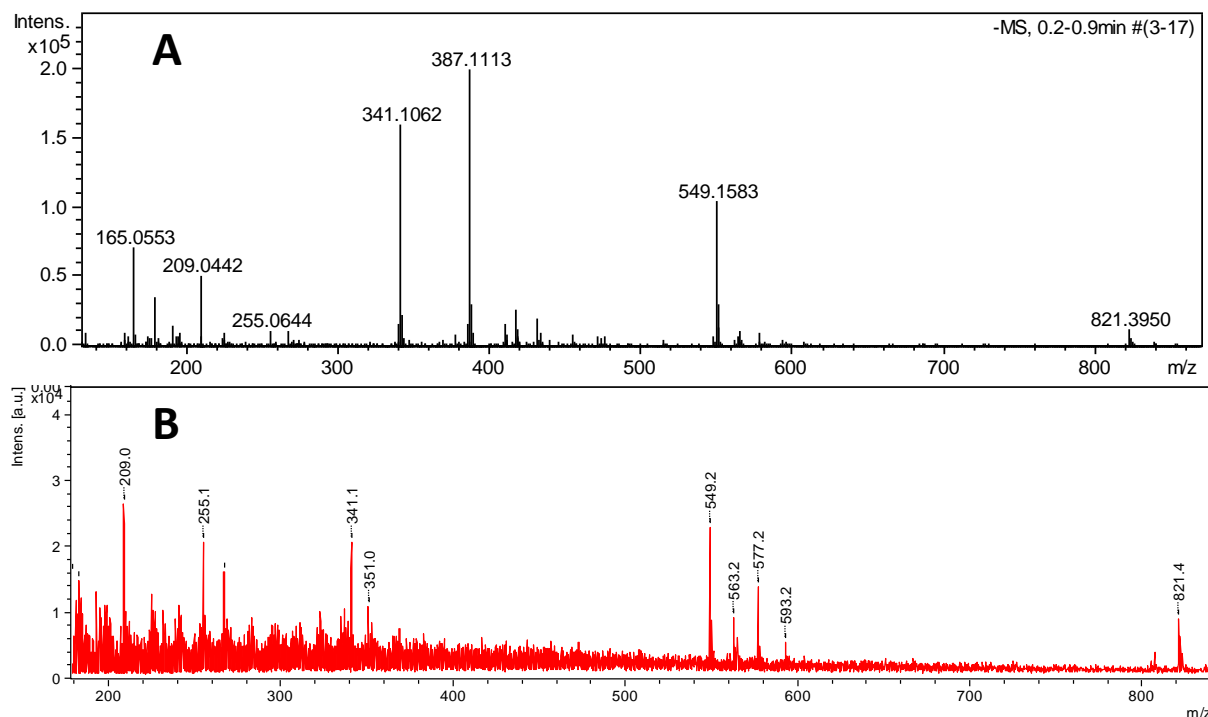


**Figure S2.** Comparison of mass spectra of an aqueous extract of liquorice roots obtained using ESI-Qq-TOF MS (A) and ENALDI-TOF MS, 600 ng of dry plant equivalent/spot (B). The conditions of spectra acquisition were described in the 'Mass spectrometry' section of the paper manuscript.

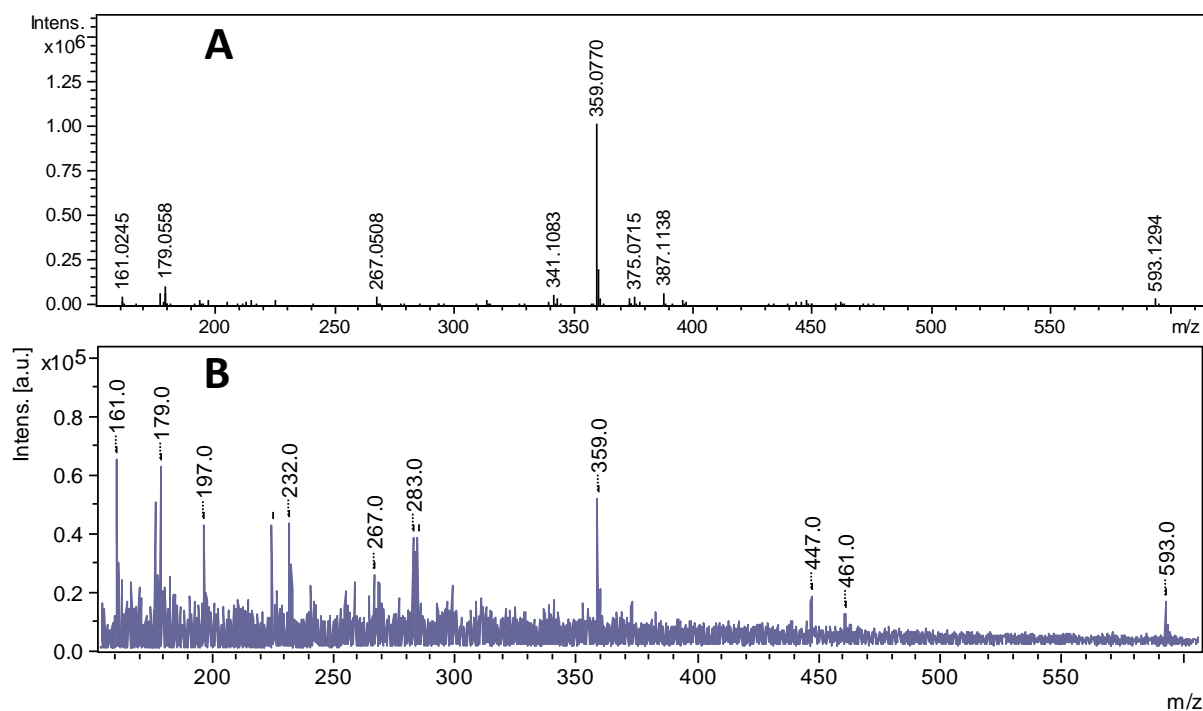


**Figure S3.** Comparison of mass spectra of a methanol extract of *Sparrmannia discolor* leaves obtained using ESI-Qq-TOF MS (A) and ENALDI-TOF MS, 600 ng of dry plant equivalent/spot (B). The conditions of spectra acquisition were described in the 'Mass spectrometry' section of the paper manuscript.



## **Chapter IV**

**I. An application of magnetic nanoparticles for evaluating the substrate specificity of human and viral thymidylate kinase using ESI-Qq TOF MS**

**II. Magnetic nanoparticles as non-organic matrix for SALDI-TOF coupled with thin layer chromatography**



Il a été démontré dans le chapitre précédent que les nanoparticules magnétiques de silice (MPs) sont à la fois un excellent support d'immobilisation d'enzymes (tyrosinase et trypsine) et qu'elles jouent un rôle efficace en tant que matrice non-organique dans les processus de désorption/ionisation laser des composés recherchés (inhibiteurs) par MALDI-TOF MS en milieu complexes (extraits de plantes), se rapprochant ainsi de la technique SALDI MS.

Ce chapitre IV est un chapitre d'ouverture permettant de valoriser l'utilisation de ces nanoparticules magnétiques de silice à la fois dans l'immobilisation de nouvelle cible (d'intérêt thérapeutique, enzyme « TMPK kinase ») et dans l'utilisation de celle-ci comme matrice non-organique dans le cadre d'un couplage HPTLC-MALDI-TOF MS.

Dans un premier temps, il a été évalué la faisabilité de l'immobilisation de nouvelles cibles telle que la Thymidylate Kinase (de souches humaine, hTMPK et virale, vvTMPK) ainsi que l'avantage de celle-ci dans le cadre de l'identification de substrats spécifiques (naturels ou de synthèses). Pour ce faire, les nanoparticules magnétiques immobilisées sont mises en contact directement dans un milieu réactionnel composé d'adénosine-5'-triphosphate (ATP, espèce donneuse de phosphates) en présence du 2'-deoxythymidine 5'-monophosphate (dTMP) décrit dans la littérature comme étant un substrat naturel de l'enzyme TMPK (humaine et virale). Après un temps d'incubation, les nanoparticules sont éliminées du milieu réactionnel à l'aide d'un aimant suivi d'une centrifugation. Le surnageant est alors analysé par spectrométrie de masse Haute Résolution Qq-TOF/MS. Cette méthodologie permet de mettre en évidence sur une même analyse à la fois la déphosphorylation (perte de 79.9658 Da) de l'ATP en ADP ( $m/z$  505.9874  $\rightarrow$  426.0216) et la conversion catalytique (phosphorylation) du substrat naturel dTMP en dTDP ( $m/z$  321.0482  $\rightarrow$   $m/z$  401.0151), prouvant ainsi la conservation de l'activité enzymatique et la spécificité du substrat envers les enzymes.

De futures recherches dans ce domaine permettront, d'une part d'évaluer l'efficacité de nouveaux substrats actifs vis-à-vis de notre cible thérapeutique en appui avec des développements en modélisation moléculaire et d'autre part, apporter une meilleure compréhension des cascades enzymatiques (activités successives des différentes enzymes kinases) impliquées dans diverses maladies.

Dans un second temps, ce même chapitre IV traite de la possibilité d'utiliser les nanoparticules magnétiques de silice « vierges » comme matrice non-organique dans le cadre du développement d'une méthode de couplage directe entre la technique de chromatographie sur couche mince de haute performance (en anglais High Performance Thin Layer Chromatography, HPTLC) et une technique de désorption/ionisation laser assistée par matrice (MALDI) couplée à un spectromètre de masse à temps de vol (TOFMS) permettant la caractérisation des différentes familles de flavonoïdes présentés dans un extrait de plante.

## CONFIDENTIAL

Pour ce faire, les études ont été effectuées sur les extraits de plantes utilisées lors des chapitres III, soit la réglisse et le *Sparrmannia discolor*. Il s'avère que l'utilisation des nanoparticules de silice « vierges » (par immersion) sur la plaque chromatographique n'induit aucun effet sur le rapport frontal (Rf) de chacun des composés ni sur l'utilisation des méthodes de révélations (densitomètre UV, révélateurs chimiques tels que NEU +PEG) en comparaison aux mêmes expériences réalisés sur plaque classique. Ce premier point validé, il a été essentiel d'évaluer l'apport de la présence de ces nanoparticules magnétiques lors de l'ionisation des différents spots Rf. Dans le cadre de ce travail, les résultats obtenus prouvent l'intérêt de la présence de cette matrice non-organique afin d'obtenir une ionisation efficace des différents analytes (flavonoïdes) et cela aussi bien en mode positif que négatif.

Ces travaux précurseurs, dans la mise en place et la validation de stratégie de criblage originale impliquant l'immobilisation de cible biologique ou bien du couplage de technique chromatographique telle que l'HPTLC avec la spectrométrie de masse comme technique de détection, vont ici nous permettre de répondre à de nouvelles problématiques développées au sein de l'équipe analytique « Extraction, Analyse de Molécules Bioactives » dirigée par Madame Claire Elfakir de l'Institut de Chimie Organique et Analytique (ICOA) de l'Université d'Orléans.

**Chapter IV** – An application of magnetic nanoparticles for evaluating the substrate specificity of human and viral thymidylate kinase using ESI-Qq TOF MS. Magnetic nanoparticles as non-organic matrix for SALDI-TOF coupled with thin layer chromatography

<b>I. An application of magnetic nanoparticles for evaluating the substrate specificity of human and viral thymidylate kinase using ESI-Qq TOF MS.....</b>	<b>140</b>
<b>I.1. Introduction.....</b>	<b>140</b>
I.1.1. Multidimensional potential of MPs as the carrier of enzymes.....	141
I.1.2. Nucleotide analogs as antiviral drugs.....	141
I.1.3. The importance of the selectivity of antiviral therapy.....	141
I.1.4. The design of selective antiviral therapy against poxviruses on the basis of the comparative study on substrate spectrum of viral and human TMP kinase (TMPK).....	142
<b>I.2. Materials and methods.....</b>	<b>143</b>
I.2.1 The chemistry of TMPK kinase immobilisation.....	143
I.2.2. The experiment design.....	144
<b>I.3. Experimental part.....</b>	<b>146</b>
I.3.1. Immobilisation of TMPK kinases.....	146
I.3.2. Typical assay of enzymatic activity by ESI-Qq-TOF MS.....	146
<b>I.4. Preliminary results.....</b>	<b>146</b>
I.4.1. Enzymatic activity of TMPK kinase in the context of mass spectrometry.....	146
I.4.2. Comparison of the two pathways of kinase immobilisation using vvTMPK as a model enzyme.....	146
I.4.3. Immobilisation of viral and human TMPK kinase to MPs-APTES-GLA nanoparticles.....	147
<b>I.5. The stability assay of viral/human thymidylate kinases.....</b>	<b>148</b>
<b>I. 6. Prospective applications of kinase-MPs in future experiments.....</b>	<b>149</b>
<b>I.7. General conclusions.....</b>	<b>149</b>
<b>II. Magnetic nanoparticles as non-organic matrix for SALDI-TOF coupled with thin layer chromatography.....</b>	<b>150</b>
II.1. Introduction.....	150
II.2. Experimental part.....	151
II.3. Results.....	151
II.3.1. Direct ionisation of plant metabolites. Comparison to an organic matrix, 9-aminoacridine.....	151
II.3.2. An impact of MPs deposition on separation and visualization of plant metabolites.....	154
<b>II.4. SALDI-TLC: conclusions.....</b>	<b>157</b>





## I. An application of magnetic nanoparticles for evaluating the substrate specificity of human and viral thymidylate kinase using ESI-Qq TOF MS

### Abstract

Magnetic nanoparticles were shown to be applicable as a solid support for immobilisation of thymidylate kinase, both of vaccinia virus and human origin. These EMPs with two types of kinases applied in parallel constitute a promising tool for verification of a selectivity of the antiviral drug candidates towards viral components of DNA replication system.

### I.1. Introduction

#### I.1.1. Multidimensional potential of MPs as the carrier of enzymes

In the *Chapter III* magnetic nanoparticles (MPs) were shown to be an excellent host for tyrosinase and trypsin immobilisation. In a form of enzyme-coupled MPs (EMPs) they were successfully applied as the non-organic matrix for surface-assisted laser desorption-ionisation MS (SALDI-MS) for searching for inhibitor candidates in complex mixtures, **fig. 1**. MPs can also be used as the enzyme host for the experiments in solution that can be subsequently analysed by ESI-Qq-TOF MS (*Chapter III, p. II.4*). The application of the target enzyme coupled with MPs is beneficial for direct assays by ESI-Qq-TOF MS since it eliminates the 'background' from the analysed sample: *i*) it allows to avoid all impurities accompanying the stock solutions of free enzymes (*e.g.* glycerol, TRIS, sugars) that may suppress ions of interest; *ii*) enzyme may be easily separated from the analysed solution by eliminating EMPs using magnet or centrifugation. Moreover, immobilised enzymes show higher stability over time comparing to their 'free' counterparts which seems to be particularly important for researchers working with expensive or rare enzymes of human origin.

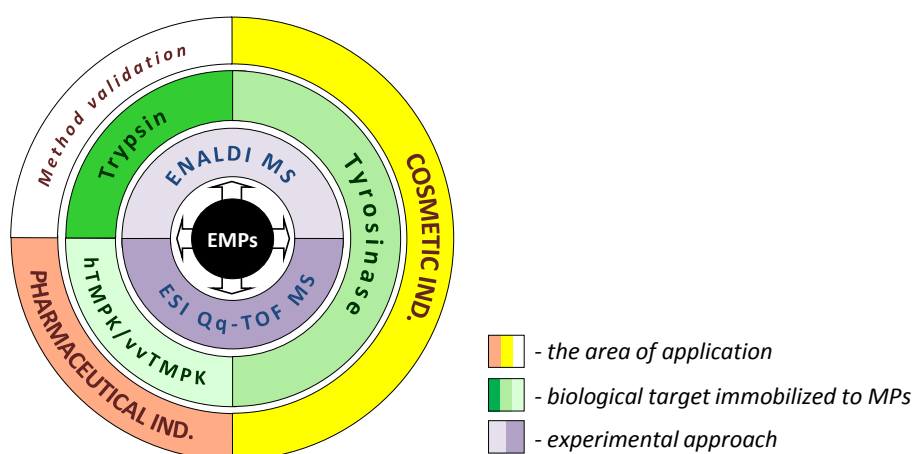


**Figure 1.** The variety of enzyme-coupled magnetic nanoparticles (EMPs) applications in the cosmetic and pharmaceutical industry described in present manuscript. ENALDI MS: Enzyme-Coupled Nanoparticles-Assisted Laser Desorption Ionisation Mass Spectrometry; TMPK: thymidylate kinase; hTMPK: human TMPK, vvTMPK: Vaccinia virus TMPK. ESI-Qq-TOF MS: mass spectrometer with electrospray ion source, time of flight analyser/detector and quadrupole as a mass filter (Q) and collision chamber (q).

This chapter describes the use of EMPs in the applications requiring the high mass accuracy and resolution inaccessible for ENALDI-TOF MS, particularly, a study of a substrate spectrum of human and viral thymidylate kinases. The applicability of MPs as the host for TMPK kinases was also evaluated.

### 1.1.2. Nucleotide analogs as antiviral drugs

Nucleotide analogs (NAs) constitute the important group of antiviral agents [298]. The therapeutic activity of their phosphorylated forms is based on the interruption of a viral DNA synthesis accomplished by two mechanisms: i) by blocking one of the elements of viral replication cycle: *e.g.* a viral DNA (RNA) polymerase or a viral reverse transcriptase [299, 300] or ii) by termination of a viral DNA elongation deriving from the properties of NAs (*e.g.* lack of 3'-hydroxyl group of deoxyribose prevents the formation of phosphodiester bond, the one used to conjugate nucleotides within the newly synthesized DNA strand)[300]. NA-TPs cannot be directly applied as drugs due to their limited stability and poor availability in the infected cells (for the reason of their polar nature and the lack of transmembrane transporter proteins, nucleoside triphosphates cannot pass through the cell membrane [300]). Instead, they are administered as nucleosides and undergo the activation by sequential phosphorylation to triphosphate (NA-TP) by the series of kinases inside the cell (**fig. 2**).

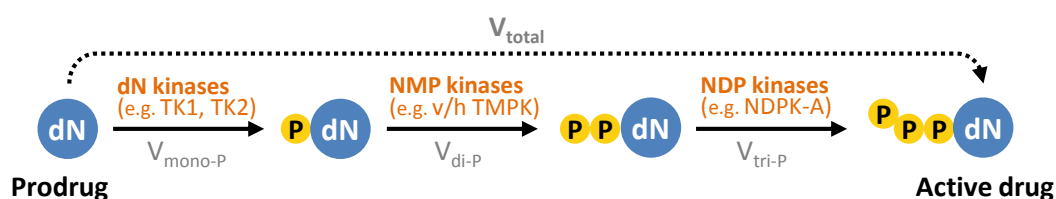


**Figure 2.** An illustration of full phosphorylation cascade. dN – deoxynucleoside; TK1/TK2 thymidine kinases 1/2; NMP – nucleoside monophosphate; NDP – nucleoside diphosphate; NDPK-A – nucleoside diphosphate kinase A; V – speed of reaction (*e.g.*  $\mu\text{mol}/\text{min}$ ).

### 1.1.3. The importance of the selectivity of antiviral therapy

Antiviral therapy targeting DNA replication mechanism should affect infected cells selectively to avoid systemic side effects [301]. One of the ways to design site-selective therapy is the use of viral kinases to convert non-toxic and non-active pro-drug into an active nucleotide triphosphate analog locally in the infected cells. The classic example of the therapeutic advantage of wider substrate spectrum of viral kinase comparing to the human counterparts is an application of acyclovir as a drug against herpes simplex virus (HSV), types 1 and 2, and varicella zoster virus [302]. It resembles the structure of guanosine and consists of guanine linked with hydroxyl-terminated non-branched chain instead of the sugar ring. Acyclovir is administered orally or topically as non-active prodrug. Selectivity of acyclovir towards infected cells derives from the fact that the first cycle of its phosphorylation to acyclovir-monophosphate can be

conducted almost exclusively by viral thymidine kinase [298, 301-303], having wider substrate spectrum than the human enzymatic counterpart. The two remaining phosphorylation cycles (to acyclovir-TP) are catalysed by the cellular kinases. Acyclovir-TP has higher affinity to the viral DNA polymerases and causes termination of the viral DNA chain. Although the conversion of acyclovir monophosphate to triphosphate is conducted by human kinases, uninfected cells lack the kinases capable to provide efficiently the first phosphorylation cycle and, therefore, the concentration of the active form of this drug is these cells very low. It reduces systemic adverse effect associated with acyclovir administration.

*1.1.4. The design of selective antiviral therapy against poxviruses on the basis of the comparative study on substrate spectrum of viral and human TMP kinase (TMPK)*

Vaccinia virus (vv) is the prototype member of poxviruses possessing double-stranded DNA genome [303, 304]. An emerging demand for novel agents targeting poxvirus-related infections (e.g. smallpox or monkeypox) is dictated by describing the new strains resistant to cidofovir, currently applied anti-poxvirus agent[301, 303, 305]. Replication of viral DNA occurs in the cytoplasm [304], therefore poxviruses encode their own enzymes responsible for the synthesis of nucleotides, including thymidine kinase (TK) and thymidylate kinase (TMPK), conducting the first two steps of thymidine phosphorylation [301, 303, 304]. Both kinases encoded by vaccinia virus (vvTK and vvTMPK) have wider substrate spectrum than the human equivalents, for example, vvTMPK can phosphorylate nucleoside monophosphates with larger bases such as dGMP or purine derivatives with bulky substituents, e.g. N<sup>2</sup>-ethyl-dGMP or 8-oxo-dGMP[301].

Tertiary structures of TMPK kinases of human and vaccinia virus are highly conserved (**fig. 3**). Both enzymes have a core composed of five parallel  $\beta$ -sheets surrounded by nine  $\alpha$ -helices[306, 307]. Degree of the amino acid sequence conservation between enzymes is lower: identity equals 42% (accomplished if the same amino acids is present in given position of the protein sequences) and similarity equals 64% (similar properties of amino acids in given position of the sequences)[303]. In **fig. 3** all L-Lysine residues were marked in green. The terminal  $\epsilon$ -amine groups of L-Lys side chains are responsible for covalent attachment of the protein to the surface of nanoparticles. Their distribution on the surface of both enzymes is uniform what increases the probability of the immobilisation without significant lose of the enzymatic activity.

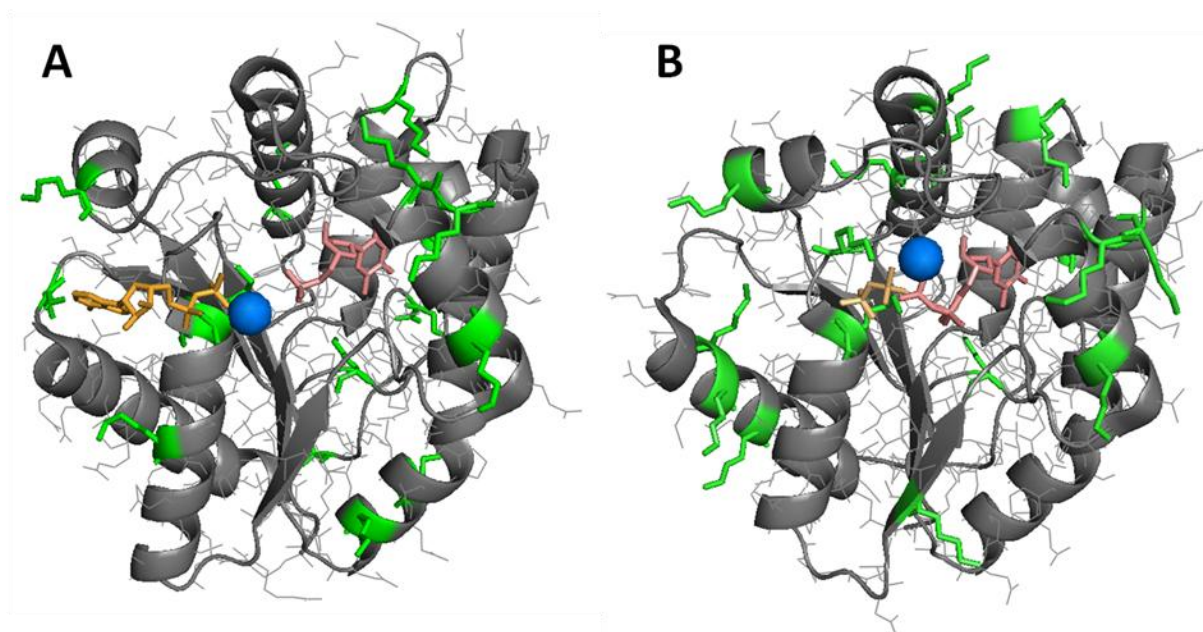


**Figure 3.** The comparison of human TMPK (A, PDB: 1E2D [307]) and vaccinia virus TMPK (B, PDB: 2V54 [306]). Both enzymes have similar molecular mass (24.05 kDa and 23.24 kDa respectively) and highly conserved fold. Phosphodonors were marked in orange, phosphoacceptors in red and magnesium ion in blue. Both structures were generated by PyMOL (Schrödinger, Inc.). These figures were generated using PyMOL (<http://www.pymol.org/>).

## 1.2. Materials and methods

### 1.2.1 The chemistry of TMPK kinase immobilisation

The two ways of immobilisation of tested kinases were the same as these described for trypsin in *Chapter III, p. III.2.2.2*: via imine linkage obtained in the reaction of  $\epsilon$ -amine groups of L-Lys on the surface of enzyme with superficial aldehyde groups covering MPs. The terminal aldehyde was obtained either by opening of the epoxide ring followed by subsequent oxidative cleavage of a diol or by modifying the surface-bound terminal amines with 1,5-pentanedial (commonly known as glutaraldehyde). These two ways of enzyme immobilisation were shown to be compatible with the 'Ion Fading' IF-ENALDI MS experiments and led to the comparable results concerning leupeptin-trypsin interactions (*Chapter III, p. III.3.4.1*). The aim of the experiment described in the following sections of the Manuscript was to check which immobilisation pathway allows to conserve a higher activity of kinase when assayed in solution.

## 1.2.2. The experiment design

The experiment consists of the following steps:

- incubation of the test mixture containing: *i*) ATP (phosphodonor), *ii*) dTMP (the primary substrate of both vTMPK and hTMPK, phosphoacceptor), *iii*) magnesium ions required for enzyme activity and *iv*) the studied substrate analog with MPs hosting vvTMPK and hTMPK (denatured/active) for one hour at room temperature;
- separation of MPs from the solution by centrifugation or attraction by magnet;
- injection of the supernatant into the mass spectrometer and the analysis of the conversion products.

The first step of the experiment involving MPs coupled with denatured enzyme ("*negative control*", **fig. 4**) is performed to acquire the mass pattern of the studied mixture and to verify whether the sample contains any contaminants which could interfere with the prospective phosphorylation products (**fig. 5-A**).

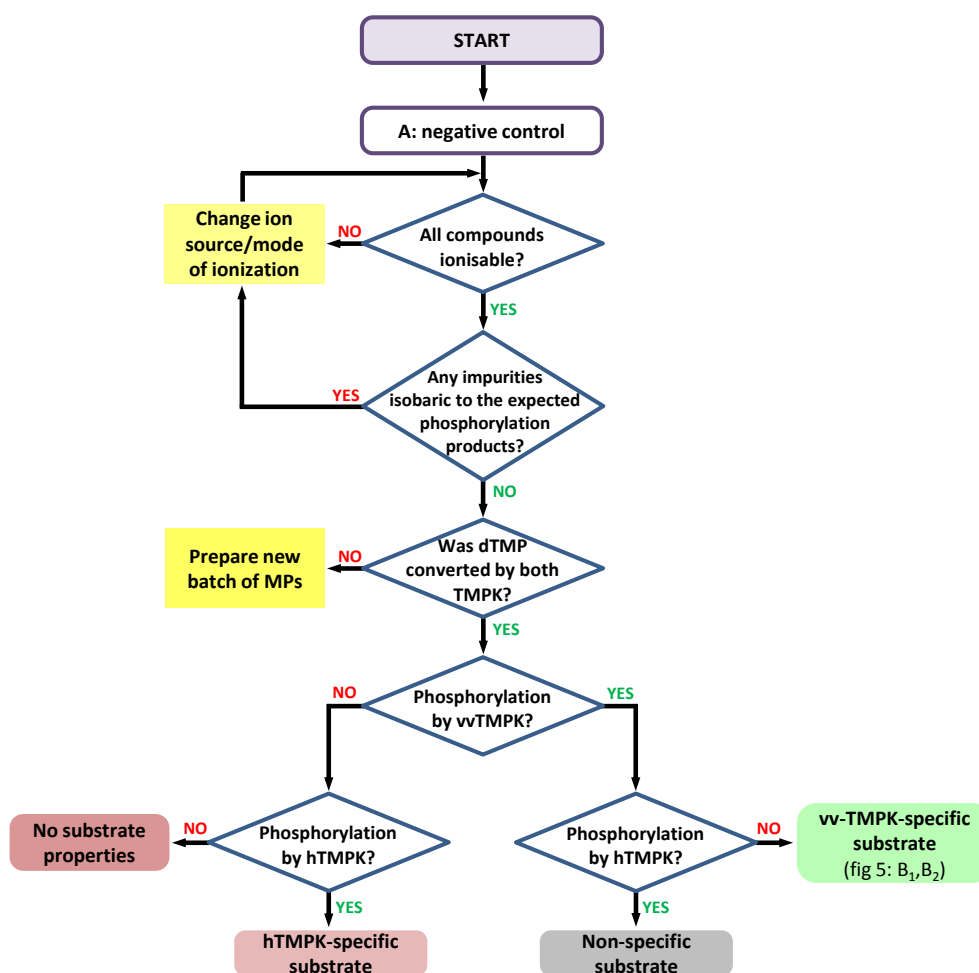


**Figure 4.** The algorithm of evaluating the substrate specificity of human and viral TMPK using magnetic nanoparticles. Simulation of the exemplary results for vvTMPK-specific substrate were shown in fig. 5.



### **1.3. Experimental part**

#### *1.3.1. Immobilisation of TMPK kinases*

The process of immobilisation of TMPK kinases was identical for both enzymes and both types of MPs (APTES-GLA and oxyGPTMS). MPs were dispersed in sodium phosphate buffer (10 mM, pH 6.8) to obtain the final concentration of 2 mg/mL. MPs solution was mixed with the appropriate amount of a stock solution of given kinase (dissolved in TRIS-HCl buffer with glycerol). An amount of kinase used for immobilisation was adjusted to obtain the proportion of 70 µg of enzyme per 1 mg of MPs (this binding capacity was determined for trypsin, the enzyme with similar molecular mass, approx. 23 kDa). Immobilisation was conducted for 5h in ice under stirring. The mixture without stirrer was then stored at 4°C overnight. EMPs were washed five times with cold ammonium formate buffer (50 mM, pH 6.4) and re-suspended in the same buffer to obtain the final concentration of 1.7 mg/mL. If not used, EMPs were stored at 4°C. A certain fraction of each batch of EMPs was denatured by incubating it in MeOH for 1 h, followed by one washing cycle with ammonium formate buffer (50 mM, pH 6.4) and re-suspension of the denatured EMPs in the appropriate volume of the same buffer to obtain the initial concentration of EMPs.

#### *1.3.2. Typical assay of enzymatic activity by ESI-Qq-TOF MS*

A volume of 25 µL of the test mixture (50 µM ATP, 50 µM dTMP; 200 µM MgCl<sub>2</sub> in 50 mM ammonium formate buffer, pH 6.4) is mixed with 25 µL of EMPs and incubated at 22°C. EMPs are then separated by magnet/centrifugation and the supernatant is injected into the mass spectrometer (injection: 10 µL, mobile phase: MeCN/water = 40/60, v/v, 200 µL/min). All MS spectra were collected in negative mode of ionisation.

### **1.4. Preliminary results**

#### *1.4.1. Enzymatic activity of TMPK kinase in the context of mass spectrometry*

TMPK kinase catalyses conversion of dTMP ( $m/z$  321.0482) to dTDP ( $m/z$  401.0151) with simultaneous dephosphorylation of ATP ( $m/z$  505.9874) to ADP ( $m/z$  426.0216) in the presence of magnesium ions. All  $m/z$  values provided above refer to  $[M-H]^-$  pseudo-molecular ions.

#### *1.4.2. Comparison of the two pathways of kinase immobilisation using vvTMPK as a model enzyme*

Vaccinia virus TMPK was immobilised on both types of MPs (APRES-GLA and oxyGPTMS) in the same way as described in *Chapter III, p. 1.2.2.2* on the same day and under identical conditions for both enzymes. All experiments were conducted according to *p. 1.3.2* of the present chapter with the incubation time of 135 min. The mass spectra acquired during the assay were shown in **fig. 6**.



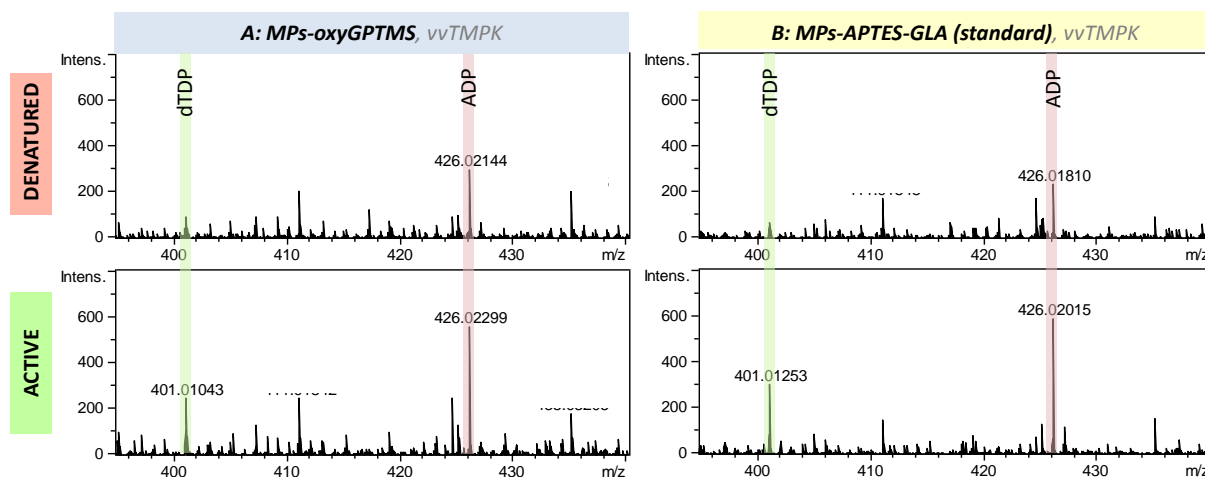


**Figure 6.** Comparison of the two immobilisation pathways on dTMP conversion. The level of dTDP ( $m/z$  401.0151,  $[M-H]^-$ ) is similar for both types of EMPs, but for MPs-APTES-GLA lower amount of impurities is observed. An assay was conducted eight days after the immobilisation process.

Phosphorylation of dTMP and dephosphorylation of ATP catalysed by viral TMPK kinase were conducted to the similar extent for both types of EMPs. However, an application of MPs-APTES-GLA (fig. 6, B) provides slightly better results in terms of dTDP intensity with reduced level of impurities. MPs-APTES-GLA were thus selected as a further base for kinases immobilisation.

#### 1.4.3. Immobilisation of viral and human TMPK kinase to MPs-APTES-GLA nanoparticles

MPs-APTES-GLA were selected as the basis for immobilisation of TMPK of human and viral origin.

All experiments were conducted according to p. 3.2. with the incubation time of 60 min.

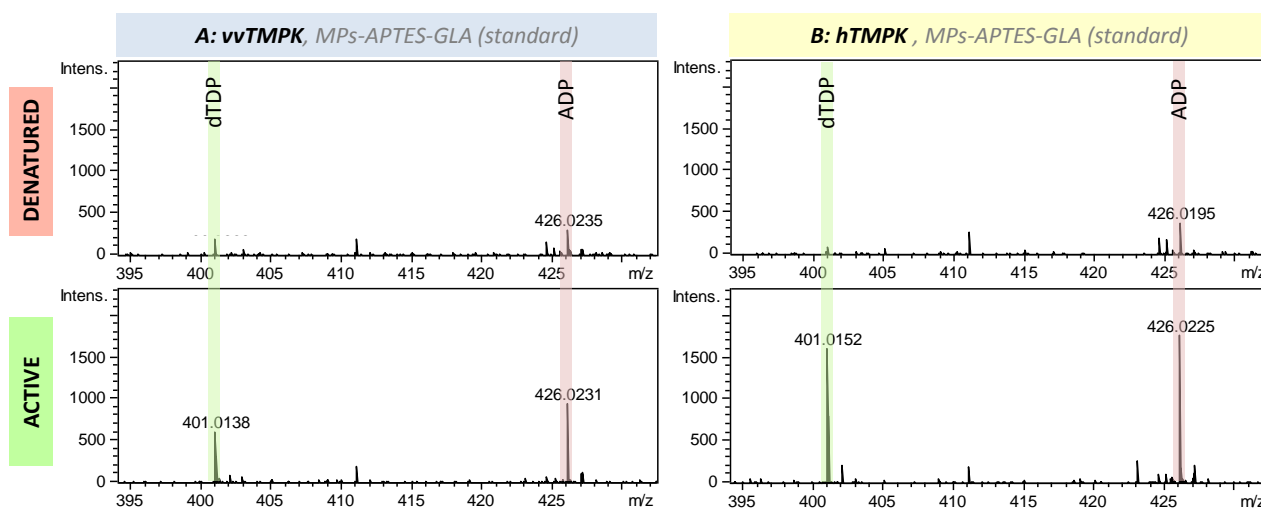


**Figure 7.** Comparison of an activity of two immobilised kinases: vvTMPK (A) and hTMPK (B), immobilised to MPs-APTES-GLA nanoparticles. An assay was conducted four days after immobilisation for both enzymes.

Both kinase enzymes (vv/h-TMPK) were successfully immobilised on MPs-APTES-GLA. Human TMPK shows significantly higher phosphorylation activity (**fig. 7-B**) than its viral counterpart (**fig. 7-A**). It is manifested by increased ion responses of both dTDP and ADP, the two products of TMPK kinase activity.

### 1.5. The stability assay of viral/human thymidylate kinases

The storage stability of immobilised kinases using MPs-GLA-APTES as the support was assayed on the basis of the fundamental reaction catalysed by both enzymes - conversion of dTMP to dTDP with simultaneous hydrolysis of ATP to ADP. The activity of both enzymes was followed for 17 days after immobilisation by monitoring the level of dTDP produced during the fixed reaction time (60 minutes). The assay was conducted as follows: a volume of 20  $\mu\text{L}$  of EMPs (v/h-TMPK, 1.7 mg/mL) was added to 20  $\mu\text{L}$  of a *test mixture* containing ATP/dTMP, 50  $\mu\text{M}$ , and  $\text{MgCl}_2$ , 200  $\mu\text{M}$ , in 50 mM ammonium formate. The mixture was incubated at 22°C for 60 min, EMPs were then separated and the supernatant infused into mass spectrometer working in negative ion mode.

The calibration curves of mass spectrometer were recorded on each day when the assay was conducted using the following calibration solutions: ATP/dTMP: 6.25, 12.5, 18.75, 25.0 and 50.0  $\mu\text{M}$ ;  $\text{MgCl}_2$ : 100  $\mu\text{M}$  (reflecting to an effective concentration of this salt after mixing EMPs and the *test mixture*) in 50 mM ammonium formate. The samples of the reaction mixtures were infused in-between the samples of the calibration curves.

The measured levels of dTDP were divided by the slope of given calibration curve and globally normalized to an initial point obtained on the first day after immobilisation (**fig. 8**).

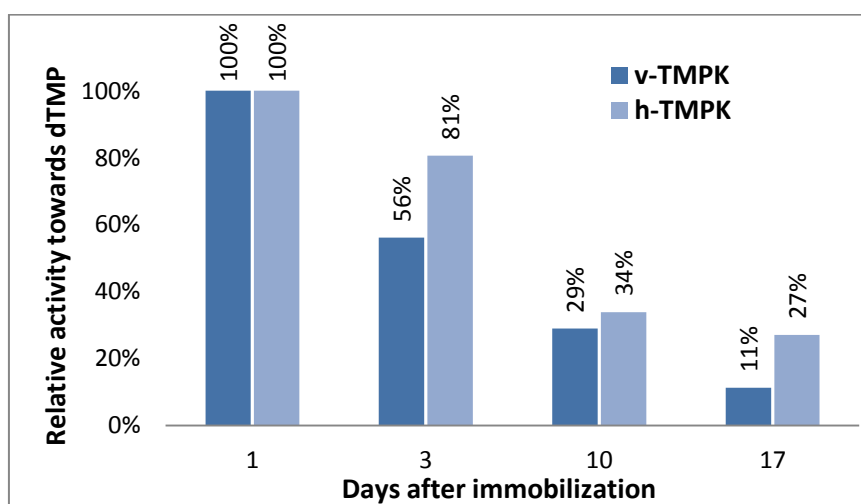


**Figure 8.** Storage stability of vv/h-TMPK-bound EMPs stored at 4 °C.

### ***1.6. Prospective applications of kinase-MPs in future experiments***

The main advantage deriving from the application of EMPs with immobilised kinases over the use of free enzyme is the lack of any interferences related with the enzymes' stock solutions. This EMPs-related benefit is even more pronounced when the full phosphorylation cascade is studied. The entire process of prodrug phosphorylation requires the successive contribution of three different enzymes (**fig. 3**) and the knowledge of the entire cascade is crucial for the global assessment of prodrug activation process. For example, if an apparent velocity of deoxynucleoside phosphorylation,  $V_{\text{mono-P}}$ , of human kinase is much lower than  $V_{\text{mono-P}}$  of its viral counterpart and if – at the same time – we observe reversed relation for the diphosphorylation step, namely  $V_{\text{di-P}}(\text{vv}) \gg V_{\text{di-P}}(\text{h})$ , the total apparent velocity of entire phosphorylation cascade may be comparable. One should also take into account that certain prodrug candidates may fail to pass one of cascade levels resulting in the lack of the active drug in the cell. It is thus not enough to study a single phosphorylation step to draw the definitive conclusions about site-selectivity of the prodrug activation process.

### ***1.7. General conclusions***

Magnetic nanoparticles may be used for the immobilisation of viral and human TMPK kinase. We showed that both immobilisation systems: through GLA-APTES or oxy-GPTMS linker are compatible with both kinases. The enzymatic activity of v/h-TMPKs is visible even two weeks after immobilisation if EMPs are stored at 4°C. During the course of these studies we successfully monitored the basic reaction of both enzymes: phosphorylation of dTMP to dTDP with simultaneous dephosphorylation of ATP to ADP.

## ***II. Magnetic nanoparticles as non-organic matrix for SALDI-TOF coupled with thin layer chromatography***

### **Abstract**

Magnetic Fe<sub>3</sub>O<sub>4</sub>-silica core-shell nanoparticles with immobilised enzymes were shown to be a useful non-organic matrix compatible with polished-steel target plate (*Chapter III and IV-A*). Herein we demonstrate that blank MPs (without derivatisation of the silica surface) deposited on the surface of silica TLC plate prior to separation of plant extract enable ionisation of the plant metabolites without any additions of organic matrices, both in positive and negative ion mode. Deposition of MPs onto TLC plate does not have any effect on the retention factors of the extract constituents and does not interfere with common methods of metabolite visualization (direct observation under UV, automated densitometry or revelation using staining reagents).

### ***II.1. Introduction***

TLC remains one of the cheapest and easiest methods of the preliminary analysis of the plant extracts [308] or monitoring of the progress of chemical reactions in the laboratories of organic chemistry. In connection with various staining methods, e.g. application of diphenylboric acid 2-aminoethyl ester to visualise flavonols [309] or primuline to visualise lipids [310-315], it allows to indentify the families of molecules present in studied extract sample. Because of the fact that the specificity of staining protocols is usually low, in case of lack of analytical standards, an application of mass spectrometry may turn out to be necessary for unambiguous identification of the compound present within the separation spot. The simplest way to accomplish on-line ionisation of the sample on the TLC plate is direct deposition of the organic matrix on the spot of analyte [310-312, 316, 317] or spray it uniformly on the entire surface of the TLC plate [313, 314, 318] or creating a hybrid TLC plate with the 'separation' zone made of silica and 'MALDI' zone composed of the matrix [319]. TLC plates may be analyzed also in the off-line mode involving scratching off the spot, extraction of the spot constituent and analyzing it in a classic way (e.g. using MALDI MS) [314, 315, 320]. Analyzing the small molecules extracted from the surface of the TLC plate using organic matrices may turn out to be very problematic due to significant matrix-related interferences in low-mass range (< 500 Da). To bypass this limitation, organic matrices may be replaced by nanoparticles in the role of ion emitters, an approach known as surface-assisted laser desorption/ionisation (SALDI). The first paper dealing with combination of SALDI with TLC was published in 1998 and described ionisation of peptides and selected pesticides with limited background noise using activated carbon [321]. In this chapter we present an example of a successful application of iron oxide-

silica core-shell magnetic nanoparticles as non-organic matrix capable of ionizing various plant extracts directly on the surface of the silica TLC plate.

## II.2. Experimental part

Methanol extract of leaves and stems of *Sparrmannia discolor* and aqueous extract of liquorice roots were used as the standards for the evaluation of SALDI-TLC MS based on superficial deposition of MPs on the surface of standard silica TLC plate.

MPs-based SALDI-TLC plate (5 x 7.5 cm) was prepared by 2-fold immersion (if not mentioned otherwise) of the TLC plate into methanol suspension of bare MPs (3 mg/mL). The extract samples (9 µL) were sprayed automatically onto both types of TLC plates (blank and MPs-covered) in a form of bands (band width: 7 mm). Separation of the plant extracts was conducted using a mobile phase as follows: EtOAc/MeOH/FA; 90/10/1; vol/vol/vol.

After separation of plant extract, both types of TLC plates were subjected to densitometric analysis at 254 nm using CAMAG TLC Scanner 3 (Moirans, France), controlled by CAMAG winCATS software (ver. 1.3.0).

Mass spectra were collected in the negative and positive ion mode by accumulating a number of 300 laser shots in random places of the spot.

After SALDI-TLC MS spectra were acquired, TLC plates (both blank and MP-covered) were contacted with Neu reagent to reveal the presence of the spots containing phenolic compounds. Neu reagent (1 g of 2-aminoethyl diphenylborinate in 100 mL of MeOH) and a solution of PEG 4000 (polyethylene glycol 4000 at 5% in EtOH) were sprayed in a sequence on the TLC plates [308]. After the plates were dried, spots were visualised at 366 nm.

## II.3. Results

### II.3.1. Direct ionisation of plant metabolites. Comparison to an organic matrix, 9-aminoacridine

An ionisation potential of (MPs)SALDI-TLC was compared with an efficient organic matrix – 9-aminoacridine (9-AA) – successfully applied for the ionisation of the small molecules<sup>\*\*\*</sup> [119].

The volumes of 4 µL of raw *Sparrmannia discolor* leaves and stems methanol extract and liquorice roots aqueous extract were deposited on the blank and MPs-covered TLC plates. After the spots were dried, the volumes of 4 µL of 100 mM 9-AA in MeOH were deposited on the extracts' spots on the raw TLC exclusively. Samples deposited on MPs-TLC plate were successfully ionized at the relative laser power equal to 23% (**fig. 9**). At the same laser power no ionisation of the samples covered with 9-AA was

---

<sup>\*\*\*</sup> More information on this subject Reader will find in the *Chapter I, p. III.3*.

observed. An increase of the laser power to 30% led to weak ionisation of selected liquorice metabolites (**fig. 9-A**), but did not improve the ionisation of the constituents of *Sparrmannia discolor* extract (**fig. 9-B**) in comparison with lower threshold of laser energy.

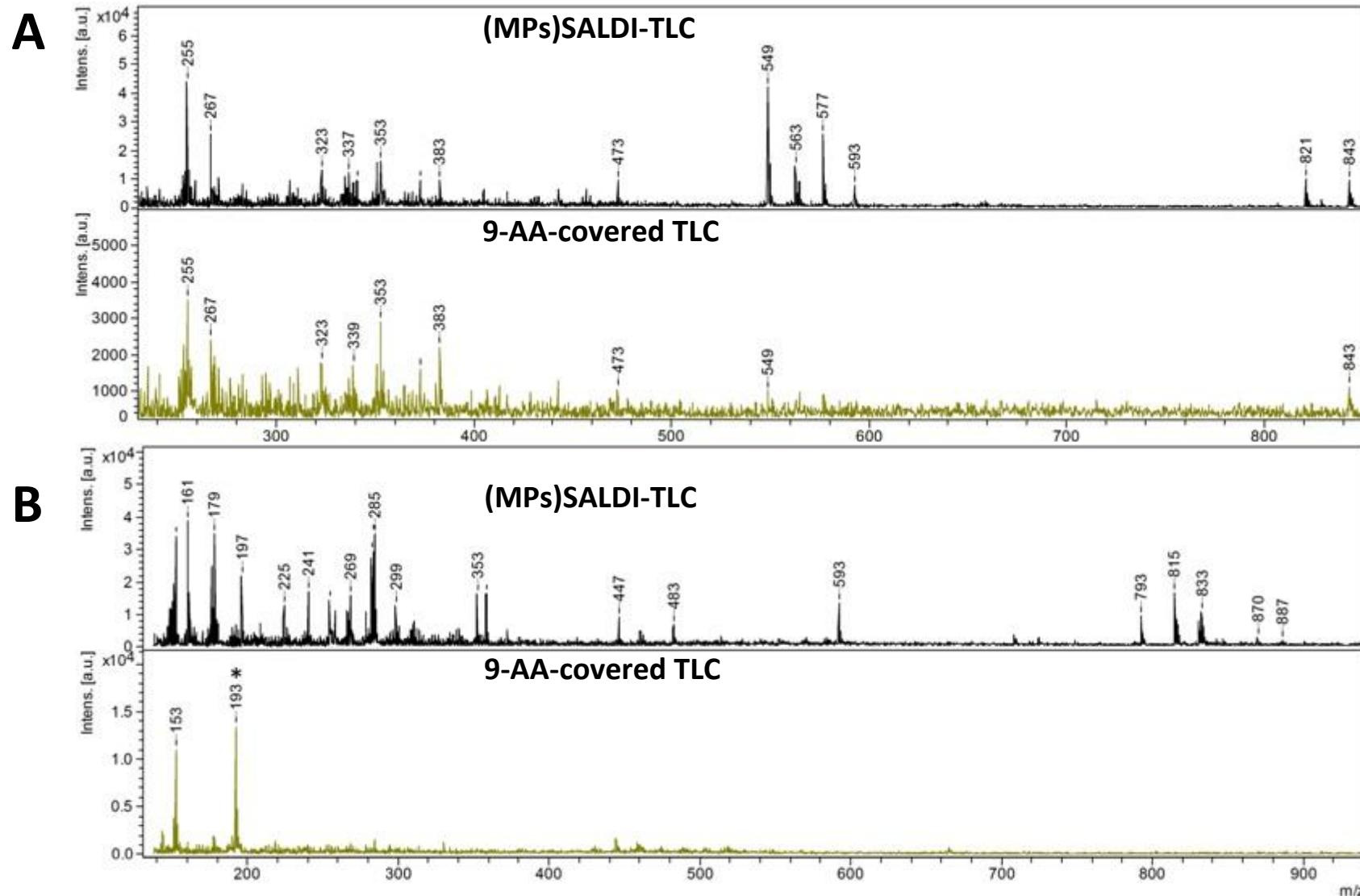


**Figure 9.** Comparison of the MS patterns of licorice roots extract (A) and *Sparrmannia discolor* leaves and stems methanol extract (B) obtained in the negative ion mode using MPs-based SALDI MS and 9-aminoacridine, the organic matrix compatible with negative ion mode. All spectra were collected on the same day by summing up the same amount of laser shots; the relative laser power applied for MPs-TLC: 23%, 9-AA-covered TLC: 30%. MPs-TLC was prepared by 3-fold immersion of the raw TLC plate into the suspension of MPs (3 mg/mL). Matrix-related ion was marked in asterisk (\*). Reader may compare (MPs)SALDI mass spectra of both plant extracts with ENALDI-MS mass spectra in the **Appendix II (figs. S2 and S3)**, page 138

### II.3.2. An impact of MPs deposition on separation and visualization of plant metabolites

MPs after deposition of silica TLC plate tend to accumulate in the gaps in-between porous silica particles (**fig. 10**), constituting a stationary phase in thin layer chromatography.

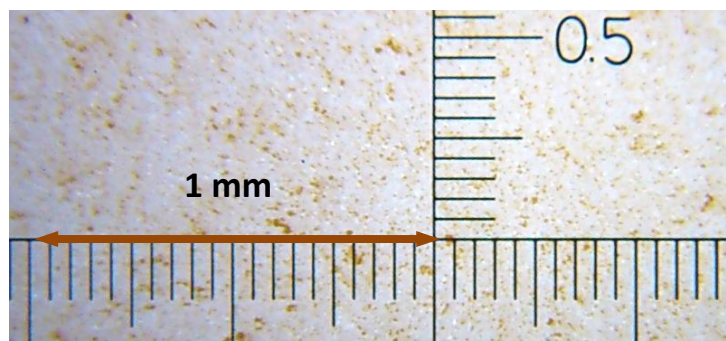


**Figure 10.** TLC plate covered with MPs under 45-fold magnification.

Bare, non-derivatised MPs have identical chemical nature as the TLC stationary phase<sup>§§§</sup>, and for this reason, superficially deposited MPs do not show any impact on the retention factors ( $R_f$ ) of *Sparrmannia discolor* metabolites (**fig. 11**). The presence of MPs does not interfere with the common ways of spots visualization: direct observation under UV light (**fig. 11-B**), revelation using Neu reagent followed by observation of the spots at 366 nm (**fig. 11-C**) or the characteristics of densitogram collected at 254 nm (**fig. 11-D**).

<sup>§§§</sup> The TLC stationary phases used in the present work were made of porous silica, as well as the coating of bare magnetic nanoparticles (MPs). More information concerning the synthesis of MPs Reader will find in the *Chapter III, p.I.2.2.1*.



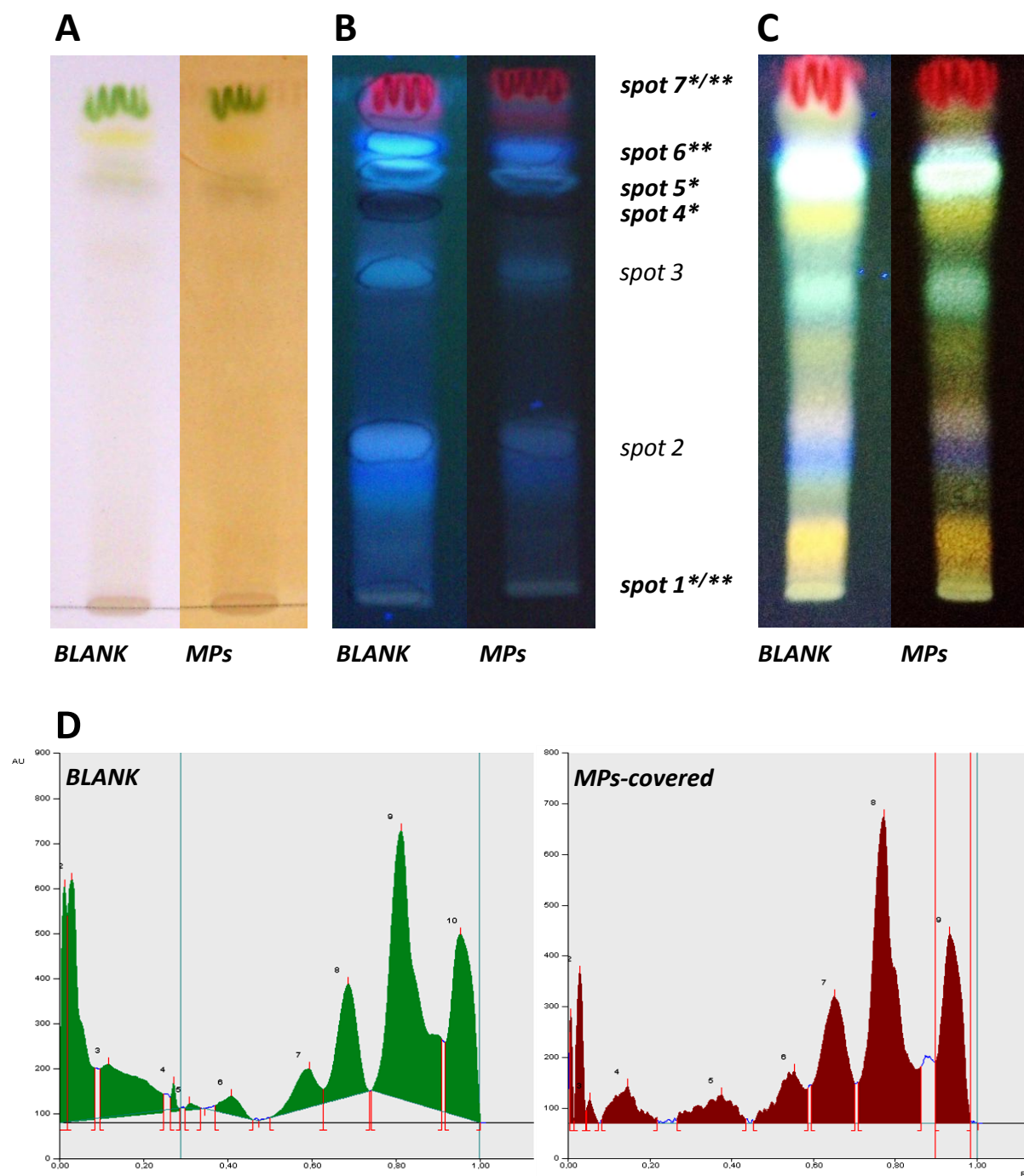


**Figure 11.** The comparison of blank and MPs-covered TLC plates after separation of methanol extract of stems and leaves of *Sparrmannia discolor*: **A** – under visible light; **B** – 366 nm, **C** – revelation system Neu + PEG reagent, 366 nm; **D** – densitometric analysis of TLC plates at 254 nm; <sup>\*/\*\*</sup> – ionized in the negative/positive ion mode respectively. Mass spectra of the spots marked in this figure are found in **figures 12 and 13**.

MPs were shown to be the efficient TLC-compatible non-organic matrix both in negative (**fig. 12**) and positive (**fig. 13**) ion mode. The mass spectra of the raw extract and those related with the most intense spots were shown in the subsequent lines. The TLC separation of the individual compounds leads to an increase in the intensities of their ions (e.g. **fig. 11, 1<sup>st</sup> spot**), possibly because of the reduced effect of saturation of the SALDI ion source.

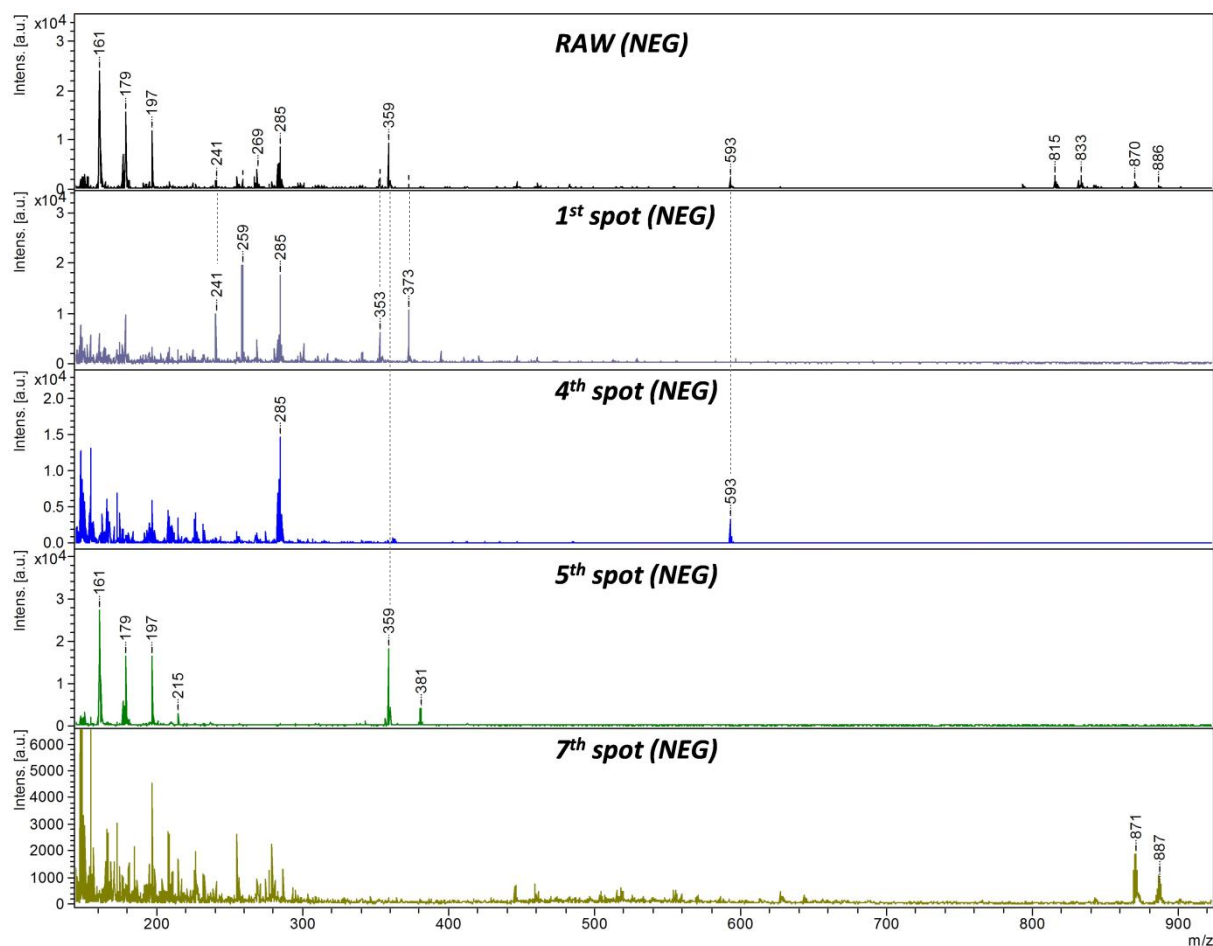


**Figure 12.** Mass fingerprint of the raw methanol extract of *Sparrmannia discolor* leaves and stems followed by mass spectra of the individual spots after separation. Mass spectra were collected in the negative ion mode using the same laser power. The numeration of the spots in this figure corresponds to the one shown in **fig. 11 A-C**.

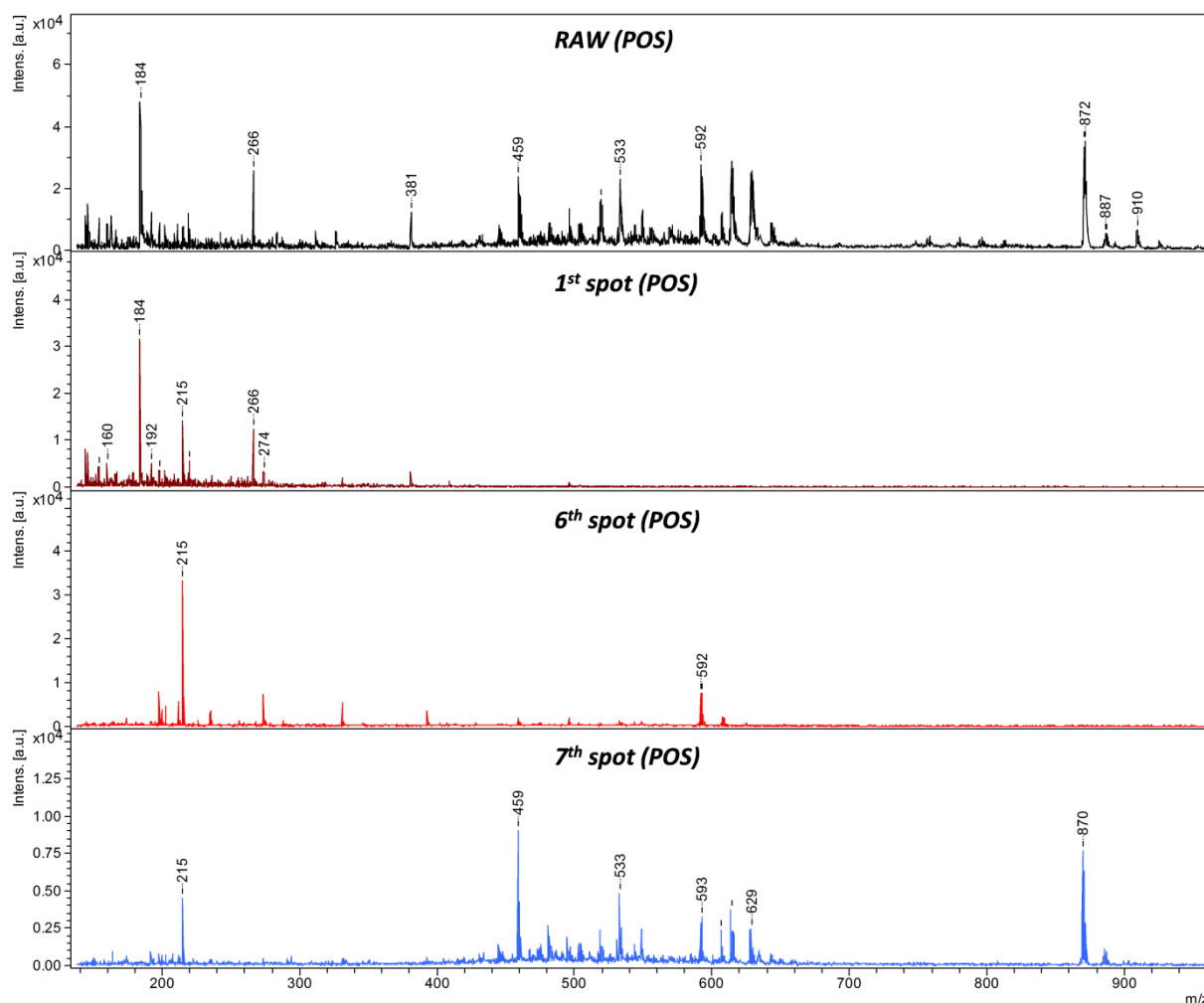


**Figure 13.** Mass fingerprint of the raw methanol extract of *Sparrmannia discolor* leaves and stems followed by mass spectra of the individual spots after separation. Mass spectra were collected in the positive ion mode, the numeration of the spots is the same as the one in **fig. 11 A-C**.

#### II.4. SALDI-TLC – conclusions

MPs-TLC hybrid plates were shown to be a perfect tool for direct MS-based analysis of the *Sparrmannia discolor* and liquorice extracts without any further pre-treatment of the TLC plate. MPs-TLC were shown to ionize plant metabolites in negative ion mode significantly more efficiently than 9-aminoacridine – well established matrix for the analysis of small molecules in negative ion mode – using lower laser power. MPs-TLC is the universal approach and may be used in both positive and negative ion mode. The preparation process of MPs-TLC plates is very simple and fast – it includes a double immersion of the raw TLC plate in the suspension of MPs in MeOH followed by drying the plate. The presence of MPs on the TLC plate does not interfere with the standard methods for visualization of the spots, including those based on applying the ultraviolet light at 254 or 366 nm. This compatibility is not the case for the common organic matrices, strongly absorbing UV light within this range of the spectrum.

Taking into account a high stability of MPs, (MPs)SALDI-TLC may find a commercial application as a ready-to-use TLC support for quick MS-based analysis of the plant extracts.

## GENERAL CONCLUSIONS

We devoted this work to two mass spectrometry-based approaches of high throughput pre-selection of tyrosinase inhibitor candidates contained in complex mixtures, such as plant extracts. The main industrial interest focused on tyrosinase inhibitors is their prospective application in the role of the skin whitening agents.

In the first part of this manuscript we described an improvement of existing state of art in frontal affinity chromatography (FAC) approach by evaluating the two new capillary-format polymeric stationary phases as the hydrophilic solid supports for protein immobilisation. We showed that amine-bearing stationary phases derivatised with glutaraldehyde strongly interact with hydrophobic, negatively charged compounds, both in capillary-format (poly(SBMA-*co*-AEMA-*co*-EGDMA)) and in the form of particles (silica-APTES-GLA). On the other hand, due to positively charged surface, these stationary phases may be successfully applied for studying cationic hydrophobic compounds for the reason of their limited nonspecific interactions caused by Coulombic repulsion from the stationary phase. Poly(NAS-*co*-EGDMA)-based monolith and its high-scale counterpart, silica-oxGPTMS particles, are suitable for screening of the libraries or extracts containing negatively charged compounds. Moreover we concluded that capillary-format APTES/TEOS hybrid silica monoliths are not compatible with mass spectrometry equipped in ESI ion source due to enormous suppression of the ions of analytes caused by impossible to remove material-related impurities, both in positive and negative mode of ionisation.

In conclusion, all immobilisation supports studied in this work, namely organic monoliths and silica beads, were proven to be a successful base for FAC. Selection of the scale of the immobilisation support, the type of polymer or particles or, finally, the mode of FAC experiment depends on the objectives of the research, availability of the biological target and expected chemical properties of studied inhibitors.

We have demonstrated that the polymeric stationary phases may be applied in micro-scale experiments requiring an application of expensive biological targets. Their use is limited to a 'single infusion' mode of FAC due to low flow rates supported by the capillaries. Cartridges packed with derivatised particles are suitable both for the 'single infusion' and the 'step gradient FAC what reduces the time of analysis.

The second part of this manuscript is dedicated to the development and application of a novel approach of pre-selection of tyrosinase inhibitors using enzyme-coupled magnetic nanoparticles (EMPs) used as non-organic matrix for surface-assisted laser desorption/ionisation MS. Tyrosinase-bound EMPs successfully indicated three inhibitor candidates in each studied plant extract: liquorice roots and leaves and stems of *Sparrmannia discolor*. Four out of six identified compounds were already described as tyrosinase inhibitors. Two remaining compounds contain *p*-hydroxy substituted phenol ring, the moiety characteristic for a wide class of tyrosinase inhibitors. EMPs were proven to be a versatile non-organic matrix capable of ionizing various types of small molecules (flavonoids, peptides, terpenes, saponins,

nucleotides and nucleosides were tested in our lab) both in positive and negative ion mode. A single assay is very quick and simple (it is enough to mix the stock solution of EMPs and the analyte directly on MALDI plate and let to dry). Magnetic nanoparticles provide stable support for enzyme immobilisation extending its shelf life (up to 3-fold for tyrosinase), are cheap and simple to produce and easy to handle. IF-ENALDI was shown to be extendible to various biological targets (trypsin and tyrosinase) and compatible with two different MALDI-TOF instruments. Since both variants of ENALDI are affinity-based methods, no marker of enzymatic activity is required. IF/IH-ENALDI approach poses an alternative for time-consuming and laborious bioassay-guided fractionation.

In addition to these findings we concluded that tyrosinase efficiently conducts hydroxylation and subsequent oxidation of glabridin and DHPA to corresponding hydroxy-*o*-quinones only if enzyme's regular substrates are provided in the sample. These 1,3-resorcinol moiety-containing compounds are considered as strong tyrosinase inhibitors. Both types of regular tyrosinase substrates (mono- or diphenol – L-Tyr and catechin respectively) can activate enzyme's active site (to *oxy*-tyrosinase) in the presence of inhibitors. No visible conversion of glabridin and DHPA was noted in the absence of the regular substrates, possibly because the oxidation products of both compounds cannot induce the 'activation cycle' similar to the one characteristic for unsubstituted resorcinol. It confirms the observations of Stratford *et al.* that *met*-form of enzyme cannot oxidise resorcinol-containing substrates and that the outcome of the conversion of these compounds is the same as for mono-phenols (*o*-hydroxylation followed by oxidation of two adjacent hydroxyl groups to *o*-quinones).

Magnetic nanoparticles were shown to be a versatile host for various enzymes. Besides of the two enzymes successfully immobilised to achieve the main objectives of this work (tyrosinase as the main biological target and trypsin as a validating target), we demonstrated a successful immobilisation of the viral and human TMPK kinases. We showed that both immobilisation systems: through GLA-APTES or oxy-GPTMS linkers are compatible with both kinases. Enzymatic activity is visible even two weeks after enzymes immobilisation if EMPs are stored at 4°C. During the course of these studies we successfully monitored the basic reaction of both enzymes: phosphorylation of dTMP to dTDP with simultaneous dephosphorylation of ATP to ADP. An application of the target enzyme coupled with MPs is beneficial for direct assays by ESI-Qq-TOF MS since it eliminates the 'background' from the analysed sample: *i*) it allows to avoid impurities accompanying the stock solutions of free enzymes (e.g. glycerol, TRIS, sugars) that may suppress ions of interest; *ii*) enzyme is separated from the analysed solution by eliminating EMPs using magnet or centrifugation. It opens the possibility of studying the subsequent steps of substrate phosphorylation cascade (what requires diverse kinases) without introducing any impurities present in the enzymes' stock solutions.

In previous sections of the manuscript we demonstrated that magnetic nanoparticles act as an efficient non-organic matrix for surface-assisted laser desorption ionisation MS. In the last paragraph of the manuscript we showed that MPs may be used as a matrix not only on the surface of polished steel plate, but also when deposited on the silica-based TLC plate. MPs-TLC hybrid plates were proven to be a perfect tool for direct MS-based analysis of the *Sparmannia discolor* and liquorice extracts without any further plate pre-treatment. MPs-TLC were shown to ionize plant metabolites in negative ion mode significantly more efficiently than 9-aminoacridine – well established matrix for the analysis of small molecules in negative ion mode – using lower laser power. MPs-TLC is universal and may be used in both positive and negative ion mode. The preparation process of MPs-TLC plates is very simple and quick – it includes a double immersion of the raw silica-based TLC plate in MeOH suspension of MPs followed by drying the plate. The presence of MPs on the TLC plate does not interfere with standard spot visualization methods, including those based on applying the UV light (254 nm), what is not the case for the common organic matrices, strongly absorbing within this range of the spectrum. Taking into account a high stability of MPs, (MPs)SALDI-TLC may find a commercial application as a ready-to-use TLC support for quick MS-based analysis of the plant extracts.

## PROSPECTS FOR THE FUTURE

The MS-based screening approaches described in present work constitute a set of complete tools enabling pre-selection of tyrosinase inhibitor candidates and were fully developed during this scientific project. However, there are certain points requiring further experiments and testing.

Frontal affinity chromatography approach was evaluated in two ways: *i)* the degree of possible non-specific interactions between the stationary phases of interest and the prospective analyte families was determined on the basis of the library of the test compounds; *ii)* specific protein-inhibitor interactions were shown for two biological targets: tyrosinase and trypsin. Nonetheless, in contrast to IF-ENALDI MS, FAC approach was not used in any experiment involving the real plant samples. This point requires further experiments and evaluation in the future.

IF-ENALDI MS successfully pre-selected several inhibitor candidates in the extracts of liquorice roots and *Sparmannia discolor* stems and leaves. Most of them were already described as the inhibitors of tyrosinase. The two hits, namely 2-[(4-hydroxyphenyl)methyl]malonic acid and isoviolanthin, found in the aqueous extract of liquorice roots, require further evaluation as tyrosinase inhibitors due to lack of bibliographic data. The future work in this domain includes the isolation of both compounds and subjecting them to the inhibition tests using mushroom tyrosinase as the target enzyme. If these compounds are found to be mushroom tyrosinase inhibitors, further testing involving a line of melanocyte cells is also required.

—◇◇◇—

## CONCLUSION GÉNÉRALE

Nos recherches dans le cadre de cette thèse ont consisté à développer deux approches analytiques basées sur la spectrométrie de masse afin d'identifier des inhibiteurs d'origine naturelle de l'enzyme tyrosinase à partir d'extrait de plantes.

En premier lieu, nous avons décrit l'optimisation faite sur l'utilisation de la chromatographie en analyse frontale notamment en ce qui concerne les phases monolithiques utilisées comme support hydrophile au sein de capillaire pour permettre l'immobilisation des enzymes tyrosinases et trypsine. Il a été montré que les phases stationnaires monolithes organiques poly(SBMA-co-AEMA-co-EGDMA) et inorganiques (silica-APTES-GLA) dérivatisées avec le glutaraldéhyde, toutes deux utilisées au sein d'un capillaire, interagissent fortement avec les analytes hydrophobes ou chargés négativement. Néanmoins, dû à la présence globale d'une charge positive à la surface de ces phases stationnaires, celles-ci semblent tout indiquées pour l'étude d'analytes hydrophobes cationiques en raison de la répulsion coulombienne existante. En ce qui concerne les monolithes organiques synthétisés en poly(NAS-co-EGDMA) et inorganiques à bases de particules silica-oxGPTMS, ils se sont avérés efficaces pour l'analyse de composés chargés négativement. Il faut également noter que l'utilisation de capillaires à base de monolithes constitués de silice APTES/TEOS n'est pas compatible avec l'utilisation de la source d'électronébulisation ESI de notre spectromètre de masse en raison d'une suppression d'ions importante et cela aussi bien en mode de détection positif ou négatif. Pour autant, que ce soit les supports monolithiques organiques ou inorganiques, ceux-ci ont montré leur efficacité lors des analyses par chromatographie en analyse frontale. Nous avons ainsi montré que ces phases monolithiques peuvent être utilisées à l'échelle d'un capillaire de faible longueur ce qui permet alors d'envisager une application de criblage moins onéreuse. Cependant, l'analyse n'est possible qu'en mode infusion simple compte-tenu des faibles débits supportés par les capillaires ce qui allonge les temps d'analyses. A contrario, l'utilisation de cartouches remplies de billes de silice (silica-APTES-GLA et silica-oxGPTMS) comme support d'immobilisation des enzymes permet à la fois de travailler en simple infusion mais également en gradient ce qui réduit alors le temps d'analyse. L'approche par chromatographie en analyse frontale a permis de déterminer les valeurs  $B_t$  relative à la quantité d'enzymes immobilisées sur les particules de silices employées dans les cartouches, ainsi que la constante de dissociation  $K_d$ .

Suite à ce premier développement de méthode basée sur la chromatographie en analyse frontale, nous avons élaboré une nouvelle stratégie analytique afin d'identifier des inhibiteurs de la tyrosinase basée sur l'utilisation d'enzymes immobilisées sur billes magnétiques de silice (Enzyme Magnetic nanoParticules (EMPs)) couplée à une analyse par spectrométrie de masse ionisation/désorption laser à Temps de Vol. Cette stratégie, que nous avons appelé « Enzyme-coupled Nanoparticles-Assisted Laser Desorption Ionisation Mass Spectrometry (ENALDI-MS) » a permis de mettre en évidence, la présence de 6 candidats potentiels (inhibiteurs) dans les extraits de racines de la Réglisse (*Glycyrrhiza glabra*) et de



tiges et feuilles de *Sparrmannia discolor*. Parmi ces inhibiteurs, l'acide 2-[(4-hydroxyphényl)méthyl]malonique ainsi que l'isoviolanthine (l'apigénin-6-C-rha-8-C-glu) (et, dans une moindre mesure, son isomère proche la violanthine (apigénin-6-C-glu-8-C-rha) ont été révélés dans le cadre de l'extrait de réglisse. En ce qui concerne l'extrait de *Sparrmannia discolor*, l'acide rosmarinique et le kaempferol-3-O-(6'-E-p-coumaroyl)-glucoside ont, quant à eux, été identifiés comme inhibiteurs de la tyrosinase. Un des avantages des nanoparticules magnétiques de silices concerne la facilité de leur production et de leur manipulation ainsi que la conservation de l'activité de l'enzyme qui en est multiplié par un facteur 3 suite à son immobilisation en comparaison à l'enzyme libre en solution. Cette nouvelle méthodologie est une alternative rapide et efficace à un fractionnement bioguidé d'extrait de plante plus chronophage.

Ces études, nous ont permis également de mettre en évidence un phénomène peu décrit dans la littérature, soit la participation efficace de l'enzyme tyrosinase, en présence du substrat naturel L-Tyrosine ou la catéchine, à l'hydroxylation et l'oxydation d'inhibiteurs tels que la glabridine et de l'acide 3-(2,4-dihydroxyphényl)-propionique (DHPA).

Dans le cadre de notre projet de recherche portant sur la mise en place de techniques innovantes permettant l'identification de candidats inhibiteurs naturels de la tyrosinase (intérêt cosmétique), l'utilisation des nanoparticules magnétiques de silice montre tout son potentiel en tant que support pour l'immobilisation d'enzymes. De ce fait, nous avons également démontré la possibilité d'immobiliser d'autre enzyme telle que l'enzyme TMPK kinase de souche virale ou humaine basée sur le greffage GLA-APTES ou oxy-GPTMS et cela afin d'ouvrir de nouveau champ d'action dans le domaine thérapeutique. De manière identique à l'immobilisation de la tyrosinase, l'activité catalytique des enzymes TMPK reste efficace après deux semaines de stockage à 4 degrés Celsius. De plus, cette méthodologie (immobilisation) permet de mettre en évidence sur une même analyse à la fois la déphosphorylation de l'ATP en ADP et la conversion catalytique (phosphorylation) du substrat naturel dTMP en dTDP. Une telle application basée sur les enzymes immobilisées permet i) de s'affranchir des tampons et autres adjuvants tels que le glycérol, le tampon TRIS qui peuvent conduire à des suppressions d'ions lors de l'analyse par spectrométrie de masse haute résolution et ii) d'obtenir une solution à analyser exempt d'enzymes. Ces résultats prometteurs ouvrent la perspective le développement de nouvelle méthodologie de criblage permettant la mise en évidence des étapes de phosphorylation pour un substrat donné spécifique à l'enzyme TMPK kinase et cela aussi bien de souche humaine que virale.

Enfin, nous avons montré la possibilité d'utiliser les nanoparticules magnétiques de silice vierges comme matrice non-organique dans le cadre du développement d'une méthode de couplage directe entre la technique de chromatographie sur couche mince de haute performance (High Performance Thin Layer Chromatography, HPTLC) et une technique de désorption/ionisation laser assistée par matrice (MALDI) couplée à un spectromètre de masse à temps de vol (TOF MS) permettant la caractérisation des

différentes familles de flavonoïdes présentent dans un extrait de plante. Il a été démontré que la présence des nanoparticules de silice vierges sur la plaque TLC n'a aucune incidence sur la migration des composés ainsi que sur la révélation sous lumière UV (254 nm). Cette approche innovante concernant la possibilité d'utiliser les nanoparticules de silice vierges comme matrices dans le domaine de la TLC-MALDI-TOF MS apparaît comme un atout majeur dans la mise au point de méthodes d'analyse d'extraits de plantes en particulier.

—◇◇◇—



## The list of chemical products and solvents

All chemicals used in this work were of analytical grade and were used without any further purification.

(3-Aminopropyl)triethoxysilane	Sigma Aldrich (Isle-d'Abeau, France)
(3-Glycidyoxypropyl)trimethoxysilane	Sigma Aldrich (Isle-d'Abeau, France)
[3-(Methacryloylamino)propyl]dimethyl(3-sulfopropyl)ammonium hydroxide	Sigma Aldrich (Isle-d'Abeau, France)
2,2'-Azobis(2-methylpropionitrile)	Acros Organics (Noisy-Le-Grand, France)
2-Aminoethyl methacrylate	Sigma Aldrich (Isle-d'Abeau, France)
3-(2,4-Dihydroxyphenyl)propionic acid	Sigma Aldrich (Isle-d'Abeau, France)
3-(Trimethoxysilyl)propyl acrylate	Acros Organics (Noisy-Le-Grand, France)
Adenosine triphosphate	Sigma Aldrich (Isle-d'Abeau, France)
All organic solvents (HPLC grade)	SDS (Val-de-Reuil, France)
Ammonia (28% solution in water)	Alfa-Aesar (Karlsruhe, Germany)
Arbutin	Sigma Aldrich (Isle-d'Abeau, France)
Bovine serum albumin	Sigma Aldrich (Isle-d'Abeau, France)
Catechin	Sigma Aldrich (Isle-d'Abeau, France)
Formic acid (97%)	Fluka (Isle-d'Abeau, France)
Glabridin	LVMH gift
Glutaraldehyde; 1,5-pentanedial	Sigma Aldrich (Isle-d'Abeau, France)
Hydrogen peroxide	Fisher Scientific (Elancourt, France)
Ibuprofen	Sigma Aldrich (Isle-d'Abeau, France)
Iron(III) chloride	Riedel-de Haën (Isle-d'Abeau, France)
Kojic acid	Sigma Aldrich (Isle-d'Abeau, France)
L-3,4-dihydroxyphenylalanine	Sigma Aldrich (Isle-d'Abeau, France)
L-arginine	Merck (Darmstadt, Germany)
Leupeptin hemisulfate salt	Sigma Aldrich (Isle-d'Abeau, France)
L-glutamine	Merck (Darmstadt, Germany)
L-tyrosinase (>99%)	Sigma Aldrich (Isle-d'Abeau, France)

Mushroom tyrosinase	Sigma Aldrich (Isle-d'Abeau, France)
N-acryloxysuccinimide	Sigma Aldrich (Isle-d'Abeau, France)
Orthophosphoric acid	Fluka (Isle-d'Abeau, France)
Periodic acid	Sigma Aldrich (Isle-d'Abeau, France)
Polytetrafluoroethylene-coated capillaries (ID=100 $\mu\text{m}$ , OD=365 $\mu\text{m}$ )	Polymicro Technologies (Phoenix, Arizona, USA).
Silica beads (Geduran Si 60, 40–63 $\mu\text{m}$ )	Merck (Darmstadt, Germany)
Silica-coated TLC	Merck (Darmstadt, Germany)
Sodium hydroxide	Fluka (Isle-d'Abeau, France)
Tetraethyl orthosilicate	Sigma Aldrich (Isle-d'Abeau, France)
Thymidine monophosphate	Fluka (Isle-d'Abeau, France)
Trypsin from bovine pancreas (TPCK treated, $\geq 10000$ BAEE units/mg)	Sigma Aldrich (Isle-d'Abeau, France)
Warfarin	Sigma Aldrich (Isle-d'Abeau, France)
Water (ultrapure)	obtained using a Millipore Elix UV system (Saint-Quentin-en-Yvelines, France)

–◊◊◊–

## List of Author's scientific papers

Papers related with this work were marked with red rectangles. The front pages of these papers were shown below.

1. Michalczyk, D.; Popik, M.; Salwinski, A.; Plonka, P. M., Extradermal melanin transfer? Lack of macroscopic spleen melanization in old C57BL/6 mice with de-synchronized hair cycle. *Acta Biochimica Polonica* **2009**, *56*, 343-353.
2. Salwinski, A.; Delepee, R.; Maunit, B., Continuous-flow step gradient mass spectrometry based method for the determination of kinetic parameters of immobilised mushroom tyrosinase in equilibrating conditions: comparison with free enzyme. *Rapid Communications in Mass Spectrometry* **2011**, *25*, 3549-3554.
3. Salwinski, A.; Roy, V.; Agrofoglio, L. A.; Delepee, R., In Situ One-Step Method for Synthesis of "Click"-Functionalized Monolithic Stationary Phase for Capillary Electrochromatography. *Macromolecular Chemistry and Physics* **2011**, *212*, 2700-2707.
4. Knack, D.; Hagel, C.; Szaleniec, M.; Dudzik, A.; Salwinski, A.; Heider, J., Substrate and Inhibitor Spectra of Ethylbenzene Dehydrogenase: Perspectives on Application Potential and Catalytic Mechanism. *Applied and Environmental Microbiology* **2012**, *78*, 6475-6482.
5. Szaleniec, M.; Salwinski, A.; Borowski, T.; Heider, J.; Witko, M., Quantum chemical modeling studies of ethylbenzene dehydrogenase activity. *International Journal of Quantum Chemistry* **2012**, *112*, 1990-1999.
6. Michalczyk-Wetula, D.; Salwinski, A.; Popik, M.; Jakubowska, M.; Plonka, P. M., Splenic melanosis during normal murine C57BL/6 hair cycle and after chemotherapy. *Acta Biochim Pol* **2013**, *60*, 313-321
7. Salwinski, A.; Delepee, R., Comparison of monolithic capillary electrochromatography and micellar electrokinetic chromatography for the separation of polycyclic aromatic hydrocarbons. *Talanta* **2014**, *122*, 180-186
8. Salwinski, A.; Da Silva, D.; Delepee, R.; Maunit, B., Enzyme-coupled nanoparticles-assisted laser desorption ionisation mass spectrometry for searching for low-mass inhibitors of enzymes in complex mixtures. *Journal of The American Society for Mass Spectrometry* **2014**, *25*, 538-547
9. Salwinski, A.; Da Silva, D.; Delepee, R.; Maunit, B., The use of enzyme-coupled magnetic nanoparticles for studying the spectrum of unusual substrates of mushroom tyrosinase by direct surface-assisted laser desorption/ionisation and high resolution ESI-Qq-TOF-MS. *Rapid Communications in Mass Spectrometry* **2014**, **accepted, in press**

Rapid Commun. Mass Spectrom. 2011, 25, 3549–3554  
(wileyonlinelibrary.com) DOI: 10.1002/rcm.5268

## Continuous-flow step gradient mass spectrometry based method for the determination of kinetic parameters of immobilized mushroom tyrosinase in equilibrating conditions: comparison with free enzyme

Aleksander Salwiński, Raphaël Delépée\* and Benoît Maunit

Institute of Organic and Analytical Chemistry (ICOA), UMR CNRS 6005, University of Orleans, BP 6759, 45067 Orléans Cedex 2, France

A mass spectrometry (MS)-based methodology for enzymatic assay in equilibrium conditions was designed and evaluated. This on-line assay involves the introduction of a continuous-flow step gradient (CFSG) of a substrate solution in the column containing immobilized enzyme and the simultaneous tracking of the product formation. We showed that the constant concentration of substrate in the entire bioreactor for an appropriate duration ensures the equilibration of the studied enzyme (mushroom tyrosinase). Under these conditions, it was demonstrated also that the kinetic and enzymatic parameters (Michaelis-Menten constant,  $K_M$ , the maximal specific activity,  $SA_{max}$ ) are independent of the flow rate of the mobile phase. The feasibility of the mentioned approach for inhibitory tests was also investigated. The coupling of the mass spectrometer to the bio-reactor allows the selective monitoring of the enzymatic reaction products and increases their detection level. Very high sensitivity, 500 pmol/min/column, and selective monitoring of the products of the enzymatic reaction are allowed by MS detection. The methodology developed here constitutes a sensitive analytical tool to study enzymes requiring long equilibration times. Copyright © 2011 John Wiley & Sons, Ltd.

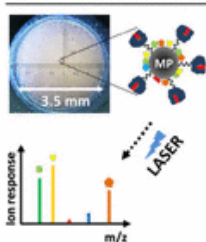
Immobilized enzymes are widely used on industrial scale<sup>[1]</sup> and on a laboratory scale, including analytical chemistry,<sup>[2,3]</sup> diagnostics,<sup>[4]</sup> drug screening,<sup>[5,6]</sup> etc. In many cases immobilized enzymes are used to determine enzymatic and kinetic parameters: maximal enzymatic velocity,  $V_{max}$ , Michaelis-Menten constants,  $K_M$ , for novel substrates or for the evaluation of the inhibitory properties of leading drug molecules.<sup>[7,8]</sup> The on-line kinetic assays of immobilized enzymes are normally conducted by injection of a known amount of substrate into an immobilized enzyme reactor (IMER) followed with detection of the product formed within the IMER.<sup>[7–11]</sup> In the single injection mode, both apparent  $K_M$  and  $V_{max}$  values depend drastically on the flow rate of the mobile phase<sup>[7–10]</sup>; in some cases, no specified trend of this relationship can be determined, even for the same enzyme.<sup>[9,10]</sup> A decrease in the flow rate leads to an increase in the contact time between enzyme and substrate. For very low flow rates the full conversion of given amount of substrate can be achieved that consequently leads to formation of plateau of the relation between product amount and flow rate.<sup>[11,12]</sup> Working within this range of flow rates makes it impossible to apply the Michaelis-Menten model (MM) to calculate kinetic parameters; thus the pre-optimization of the single injection assay is required. In the event of the use of long IMERs for single-injection assay

(e.g. capillaries), enzymatic conversion of each single substrate portion gradually lowers its local concentration during its migration towards the outlet of the IMER. This affects the apparent  $V$  value for each substrate injection and causes deviation from the MM model. Another phenomenon that may influence the results of a kinetic assay in single injection mode occurs when the studied enzyme shows a delay ('lag phase') in substrate conversion.<sup>[13–15]</sup> To circumvent these limitations, in this paper we propose a continuous-flow step gradient method (CFSG) for on-line kinetic tests of immobilized enzymes using mass spectrometry (MS) for selective detection of the product formation. The presented method is based on stepwise increase of the substrate concentration in continuous-flow mode and ensures full equilibration of the bioreactor compared to single injection experiments. The CFSG approach that is described here for the first time combined a continuous flow bioreactor,<sup>[16]</sup> and a frontal analysis of ligand–protein binding methodology.<sup>[17,18]</sup> The mushroom tyrosinase, used as a model enzyme (EC 1.14.18.1), catalyzes the oxygen-based oxidation of monophenols to *o*-diphenols and their subsequent oxidation to *o*-quinones.<sup>[19]</sup> Thus, we demonstrate that the apparent  $V_{max}$  measured by the CFSG method is independent of the flow rate, show applicability of the CFSG method to inhibition studies and compare obtained values to free enzyme. In addition, we show a temperature dependence on the kinetic parameters of mushroom tyrosinase. The feasibility of this approach for inhibition studies was presented using kojic acid as model tyrosinase inhibitor.<sup>[20]</sup> Thanks to the application

\* Correspondence to: R. Delépée, Institute of Organic and Analytical Chemistry (ICOA), UMR CNRS 6005, University of Orleans, BP 6759, 45067 Orléans Cedex 2, France.  
E-mail: Raphael.Delepee@univ-orleans.fr

## RESEARCH ARTICLE

# Enzyme-Coupled Nanoparticles-Assisted Laser Desorption Ionization Mass Spectrometry for Searching for Low-Mass Inhibitors of Enzymes in Complex Mixtures

Aleksander Salwiński,<sup>1</sup> David Da Silva,<sup>1</sup> Raphaël Delépée,<sup>2</sup> Benoît Maunit<sup>1</sup><sup>1</sup>University of Orléans, CNRS, ICOA, UMR 7311, 45067, Orleans, France<sup>2</sup>Present Address: Normandy University, UCBN, UR ABTE EA 4651, 14032, Caen, France

**Abstract.** In this report, enzyme-coupled magnetic nanoparticles (EMPs) were shown to be an effective affinity-based tool for finding specific interactions between enzymatic targets and the low-mass molecules in complex mixtures using classic MALDI-TOF apparatus. EMPs used in this work act as nonorganic matrix enabling ionization of small molecules without any interference in the low-mass range (enzyme-coupled nanoparticles-assisted laser desorption ionization MS, ENALDI MS) and simultaneously carry the superficial specific binding sites to capture inhibitors present in a studied mixture. We evaluated ENALDI approach in two complementary variations: 'ion fading' (IF-ENALDI), based on superficial adsorption of inhibitors and 'ion hunting' (IH-ENALDI), based on selective pre-concentration of inhibitors. IF-ENALDI was applied for two sets of enzyme-inhibitor pairs: tyrosinase-glucuronidase and trypsin-leupeptin and for the real plant sample: *Spartanum discolor* leaf and stem methanol extract. The efficacy of IH-ENALDI was shown for the pair of trypsin-leupeptin. Both ENALDI approaches pose an alternative for bioassay-guided fractionation, the common method for finding inhibitors in the complex mixtures.

**Keywords:** Enzyme immobilization, SALDI MS, Plant extract, Inhibitor, Nanoparticles

Received: 13 September 2013/Revised: 6 January 2014/Accepted: 6 January 2014

## Introduction

Plants are a rich source of biologically active substances, mostly inhibitors/ligands of various proteic targets [1]. Owing to the complexity of plant extracts, finding the small molecules interacting with given biological target (imposing a biological effect) is always the most pronounced challenge. Commonly, plant extracts are subjected to bioassay-guided fractionation [2–4]. This process requires multistep fractionation of the extract and manual assay of desired biological activity of each fraction. This experimental effort is obviously justified in case of studying multifactor effect on tissues or organisms (e.g., antispasmodic activity [5]), but seems to be outdated for simple enzyme-molecule interactions. An ideal methodology of searching for biologically

active compounds in complex mixtures should be rapid (minimal pretreatment of the biological mixture), require low amount of biological target, and versatility for various types of biological targets (enzymes and receptors). One methodology partially combining these criteria is called intensity ion fading mass spectrometry (IF-MS). It was used for the first time by the scientific group of Professor Francesc X. Avilés for searching for the specific interactions between various proteases and their high mass peptidic inhibitors [6]. Despite being published 10 years ago, only a few studies have used IF-MS [6–19]. IF-MS is based on the formation of specific complexes between target proteins and their binding partners, leading to removal of bound molecules from the solution of studied extract. It leads to disappearance of corresponding ions from the mass spectrum of the extract. The principal technique employed for IF-MS is MALDI-TOF MS, because of low sample requirement, an excellent sensitivity, and the potential of full automation. The main disadvantages of the application of classic organic matrices for IF-MS include denaturing conditions of sample analysis, making it ineffective for fragile enzymatic systems (e.g., tyrosinase), difficulties with obtaining uniform surface

**Electronic supplementary material** The online version of this article (doi:10.1007/s13361-014-0826-y) contains supplementary material, which is available to authorized users.

Correspondence to: Aleksander Salwiński; e-mail: aleksander.salwinski@univ-orleans.fr, Benoît Maunit; e-mail: benoit.maunit@univ-orleans.fr

Published online: 19 February 2014



Rapid Commun. Mass Spectrom. 2014, 28, 1–7  
(wileyonlinelibrary.com) DOI: 10.1002/rcm.6978

## The use of enzyme-coupled magnetic nanoparticles for studying the spectra of unusual substrates of mushroom tyrosinase by direct surface-assisted laser desorption/ionisation and high-resolution electrospray ionisation quadrupole-quadrupole-time-of-flight mass spectrometry

Aleksander Salwiński, David Da Silva, Raphaël Delépée<sup>†</sup> and Benoît Maunit<sup>\*</sup>

University of Orléans, CNRS, ICOA, UMR 7311, F-45067 Orleans, France

**RATIONALE:** Tyrosinase-coupled magnetic particles (EMPs) were used to demonstrate that resorcinol-containing tyrosinase inhibitors are oxidised by tyrosinase only in the presence of the enzyme's classic substrate. This shows the potential for the application of EMPs as a non-organic matrix for monitoring enzymatic conversion of a novel substrate family directly on-the-spot, principally due to minimal enzyme requirement per analysis.

**METHODS:** Tyrosinase was covalently coupled to core-shell-type silica-coated iron oxide magnetic nanoparticles (EMPs) that were applied as non-organic SALDI matrix suitable for studying low-mass compounds using a classic matrix-assisted laser desorption/ionisation time-of-flight (MALDI-TOF) mass spectrometer. Because of the dual function of the EMPs – enzyme host and non-organic matrix – we describe this ionisation method as Enzyme-coupled Nanoparticles-Assisted LDI-MS (ENALDI-MS). Supplementary studies of the enzymatic conversion of glabridin and 3-(2,4-dihydroxyphenyl)propionic acid (DHPA) were conducted by high-resolution electrospray ionisation quadrupole-quadrupole-time-of-flight mass spectrometry (ESI-QqTOF-MS).

**RESULTS:** The initial experiment involving EMPs as non-organic matrix (ENALDI-MS) showed enzymatic conversion of glabridin, a strong tyrosinase inhibitor, only in the presence of L-Tyr, the classic tyrosinase substrate. These findings were evaluated by ESI-QqTOF-MS proving that glabridin and DHPA are converted into the corresponding quinones by tyrosinase only in the presence of the auxiliary monophenol or *o*-diphenol substrates (L-Tyr and catechin, respectively) capable of regenerating the active site of tyrosinase.

**CONCLUSIONS:** EMPs were shown to be useful as a non-organic matrix to monitor enzymatic conversion of the novel tyrosinase substrate family directly on-the-spot with a minimal enzyme consumption (6.5 pmol/spot). Results obtained by ENALDI-MS were fully confirmed by ESI-QqTOF-MS demonstrating that resorcinol-containing tyrosinase inhibitors may be oxidised by the enzyme in the presence of its classic substrates. Copyright © 2014 John Wiley & Sons, Ltd.

Numerous natural compounds containing the 2,4-diphenol (resorcinol) moiety have been proven to be very efficient tyrosinase inhibitors, e.g. glabridin,<sup>[1,2]</sup> dalenin<sup>[3]</sup> or 3-(2,4-dihydroxyphenyl)propionic acid (DHPA),<sup>[4]</sup> and often have several times stronger inhibitory activity than kojic acid, considered as a model tyrosinase inhibitor.<sup>[5]</sup> For this reason, the new approaches aimed at synthesising the novel tyrosinase inhibitors usually choose resorcinol-containing compounds as a starting point of synthesis.<sup>[6–9]</sup>

The mechanism of tyrosinase inhibition by resorcinol derivatives is not clear. For example, when the diphenolase activity of tyrosinase is taken into account, glabridin is found

to be a non-competitive inhibitor; structurally similar dalenin was proven to provide a mixed-type inhibition while synthetic 6'-hydroxy-2'',5'',7'',8''-tetramethylchroman-2''-yl) methyl 3-(2',4'-dihydroxy-phenyl)propionate is a competitive inhibitor. Chiari *et al.* showed that dalenin molecules form complexes with copper ions which could explain its inhibitory activity.<sup>[3]</sup> On the other hand, Khatib *et al.* reported in 2005 that 2,4,2',4'-hydroxychalcone, a very potent resorcinol-type tyrosinase inhibitor (IC<sub>50</sub> < 20 nM towards monophenolase activity), does not chelate copper ions and concluded that compounds having a 2,4-dihydroxy-substituted resorcinol moiety are much more potent tyrosinase inhibitors than their 3,5-dihydroxy- or 3,4-dihydroxy-substituted analogs.<sup>[10]</sup> The ability of copper complexation cannot therefore be considered as the major reason for the inhibitory activity of this group of compounds, but rather their characteristic moiety with 2,4-dihydroxy-substituted resorcinol. Chiari *et al.* conducted the docking of (2R)-dalenin to a model of the tyrosinase-active site and concluded that the 4-hydroxyl group of its resorcinol moiety

<sup>\*</sup> Correspondence to: B. Maunit, University of Orléans, CNRS, ICOA, UMR 7311, F-45067 Orleans, France.  
E-mail: benoit.maunit@univ-orleans.fr

<sup>†</sup> Present address: Normandy University, UCBN, UR ABTE EA 4651, F-14032 Caen, France

## Bibliography

1. Fisk, W. A., Agbai, O., Lev-Tov, H. A., and Sivamani, R. K. The use of botanically derived agents for hyperpigmentation: A systematic review. *Journal of the American Academy of Dermatology* **2014**, *70*, 352-365.
2. Ortonne, J. P. [Normal and abnormal skin color]. *Ann Dermatol Venereol* **2012**, *139*, 70114-X.
3. Nicolaidou, E., and Katsambas, A. D. Pigmentation disorders: hyperpigmentation and hypopigmentation. *Clinics in Dermatology* **2014**, *32*, 66-72.
4. Seiberg, M., Paine, C., Sharlow, E., Andrade-Gordon, P., Costanzo, M., Eisinger, M., and Shapiro, S. S. The protease-activated receptor 2 regulates pigmentation via keratinocyte-melanocyte interactions. *Exp Cell Res* **2000**, *254*, 25-32.
5. Greco, G., Panzella, L., Verotta, L., d'Ischia, M., and Napolitano, A. Uncovering the Structure of Human Red Hair Pheomelanin: Benzothiazolylthiazinodihydroisoquinolines As Key Building Blocks. *Journal of Natural Products* **2011**, *74*, 675-682.
6. Olivares, C., Jiménez-Cervantes, C., Lozano, J. A., Solano, F., and García-Borrón, J. C. The 5,6-dihydroxyindole-2-carboxylic acid (DHICA) oxidase activity of human tyrosinase. *Biochem. J.* **2001**, *354*, 131-139.
7. Kim, Y. J., and Uyama, H. Tyrosinase inhibitors from natural and synthetic sources: structure, inhibition mechanism and perspective for the future. *Cell Mol Life Sci* **2005**, *62*, 1707-1723.
8. Yamada, T., Hasegawa, S., Inoue, Y., Date, Y., Arima, M., Yagami, A., Iwata, Y., Abe, M., Takahashi, M., Yamamoto, N., Mizutani, H., Nakata, S., Matsunaga, K., and Akamatsu, H. Comprehensive analysis of melanogenesis and proliferation potential of melanocyte lineage in solar lentigines. *Journal of Dermatological Science* **2014**, *73*, 251-257.
9. Han, Y. K., Park, Y. J., Ha, Y. M., Park, D., Lee, J. Y., Lee, N., Yoon, J. H., Moon, H. R., and Chung, H. Y. Characterization of a novel tyrosinase inhibitor, (2RS,4R)-2-(2,4-dihydroxyphenyl)thiazolidine-4-carboxylic acid (MHY384). *Biochimica et Biophysica Acta (BBA) - General Subjects* **2012**, *1820*, 542-549.
10. Germanò, M. P., Cacciola, F., Donato, P., Dugo, P., Certo, G., D'Angelo, V., Mondello, L., and Rapisarda, A. *Betula pendula* leaves: Polyphenolic characterization and potential innovative use in skin whitening products. *Fitoterapia* **2012**, *83*, 877-882.
11. Sendovski, M., Kanteev, M., Ben-Yosef, V. S., Adir, N., and Fishman, A. First structures of an active bacterial tyrosinase reveal copper plasticity. *J Mol Biol* **2011**, *405*, 227-237.
12. Olivares, C., and Solano, F. New insights into the active site structure and catalytic mechanism of tyrosinase and its related proteins. *Pigment Cell & Melanoma Research* **2009**, *22*, 750-760.
13. Olivares, C., García-Borrón, J. C., and Solano, F. Identification of Active Site Residues Involved in Metal Cofactor Binding and Stereospecific Substrate Recognition in Mammalian Tyrosinase. Implications to the Catalytic Cycle†. *Biochemistry* **2001**, *41*, 679-686.
14. Land, E. J., Ramsden, C. A., and Riley, P. A. Tyrosinase autoactivation and the chemistry of ortho-quinone amines. *Acc Chem Res* **2003**, *36*, 300-308.
15. Ismaya, W. T., Rozeboom, H. J., Weijn, A., Mes, J. J., Fusetti, F., Wichers, H. J., and Dijkstra, B. W. Crystal structure of *Agaricus bisporus* mushroom tyrosinase: identity of the tetramer subunits and interaction with tropolone. *Biochemistry* **2011**, *50*, 5477-5486.
16. Chiari, M. E., Vera, D. M., Palacios, S. M., and Carpinella, M. C. Tyrosinase inhibitory activity of a 6-isoprenoid-substituted flavanone isolated from *Dalea elegans*. *Bioorg Med Chem* **2011**, *19*, 3474-3482.
17. Liang, C., Lim, J. H., Kim, S. H., and Kim, D. S. Dioscin: a synergistic tyrosinase inhibitor from the roots of *Smilax china*. *Food Chem* **2012**, *134*, 1146-1148.
18. Delogu, G., Podda, G., Corda, M., Fadda, M. B., Fais, A., and Era, B. Synthesis and biological evaluation of a novel series of bis-salicylaldehydes as mushroom tyrosinase inhibitors. *Bioorg Med Chem Lett* **2010**, *20*, 6138-6140.

19. Yamazaki, Y., Kawano, Y., Yamanaka, A., and Maruyama, S. N-[(Dihydroxyphenyl)acyl]serotonins as potent inhibitors of tyrosinase from mouse and human melanoma cells. *Bioorg Med Chem Lett* **2009**, *19*, 4178-4182.
20. Lou, S. N., Yu, M. W., and Ho, C. T. Tyrosinase inhibitory components of immature calamondin peel. *Food Chem* **2012**, *135*, 1091-1096.
21. Cho, S. J., Roh, J. S., Sun, W. S., Kim, S. H., and Park, K. D. N-Benzylbenzamides: a new class of potent tyrosinase inhibitors. *Bioorg Med Chem Lett* **2006**, *16*, 2682-2684.
22. Chen, Q.-X., and Kubo, I. Kinetics of Mushroom Tyrosinase Inhibition by Quercetin. *Journal of Agricultural and Food Chemistry* **2002**, *50*, 4108-4112.
23. Khatib, S., Nerya, O., Musa, R., Tamir, S., Peter, T., and Vaya, J. Enhanced substituted resorcinol hydrophobicity augments tyrosinase inhibition potency. *J Med Chem* **2007**, *50*, 2676-2681.
24. Khatib, S., Nerya, O., Musa, R., Shmuel, M., Tamir, S., and Vaya, J. Chalcones as potent tyrosinase inhibitors: the importance of a 2,4-substituted resorcinol moiety. *Bioorganic & Medicinal Chemistry* **2005**, *13*, 433-441.
25. Haghbeen, K., and Wue Tan, E. Direct spectrophotometric assay of monooxygenase and oxidase activities of mushroom tyrosinase in the presence of synthetic and natural substrates. *Anal Biochem* **2003**, *312*, 23-32.
26. Fenoll, L. G., Rodríguez-López, J. N., García-Molina, F., García-Cánovas, F., and Tudela, J. Michaelis constants of mushroom tyrosinase with respect to oxygen in the presence of monophenols and diphenols. *The International Journal of Biochemistry & Cell Biology* **2002**, *34*, 332-336.
27. Selinheimo, E., Gasparetti, C., Mattinen, M.-L., Steffensen, C. L., Buchert, J., and Kruus, K. Comparison of substrate specificity of tyrosinases from *Trichoderma reesei* and *Agaricus bisporus*. *Enzyme and Microbial Technology* **2009**, *44*, 1-10.
28. Xie, J.-J., Song, K.-K., Qiu, L., He, Q., Huang, H., and Chen, Q.-X. Inhibitory effects of substrate analogues on enzyme activity and substrate specificities of mushroom tyrosinase. *Food Chemistry* **2007**, *103*, 1075-1079.
29. Espin, J. C., Varon, R., Fenoll, L. G., Gilabert, M. A., Garcia-Ruiz, P. A., Tudela, J., and Garcia-Canovas, F. Kinetic characterization of the substrate specificity and mechanism of mushroom tyrosinase. *Eur J Biochem* **2000**, *267*, 1270-1279.
30. Szaleniec, M., Salwiński, A., Borowski, T., Heider, J., and Witko, M. Quantum chemical modeling studies of ethylbenzene dehydrogenase activity. *International Journal of Quantum Chemistry* **2012**, *112*, 1990-1999.
31. Johnson, K. A., and Goody, R. S. The Original Michaelis Constant: Translation of the 1913 Michaelis-Menten Paper. *Biochemistry* **2011**, *50*, 8264-8269.
32. Chen, W. W., Niepel, M., and Sorger, P. K. Classic and contemporary approaches to modeling biochemical reactions. *Genes Dev* **2010**, *24*, 1861-1875.
33. Hajdu, I., Szilagyi, A., Kardos, J., and Zavodszky, P. A link between hinge-bending domain motions and the temperature dependence of catalysis in 3-isopropylmalate dehydrogenase. *Biophys J* **2009**, *96*, 5003-5012.
34. Chang, T. S. An updated review of tyrosinase inhibitors. *Int J Mol Sci* **2009**, *10*, 2440-2475.
35. Bentley, R. From miso, sake and shoyu to cosmetics: a century of science for kojic acid. *Nat Prod Rep* **2006**, *23*, 1046-1062.
36. Liu, J., Wu, F., Chen, L., Zhao, L., Zhao, Z., Wang, M., and Lei, S. Biological evaluation of coumarin derivatives as mushroom tyrosinase inhibitors. *Food Chem* **2012**, *135*, 2872-2878.
37. Nerya, O., Vaya, J., Musa, R., Izrael, S., Ben-Arie, R., and Tamir, S. Glabrene and isoliquiritigenin as tyrosinase inhibitors from licorice roots. *J Agric Food Chem* **2003**, *51*, 1201-1207.
38. Yokota, T., Nishio, H., Kubota, Y., and Mizoguchi, M. The Inhibitory Effect of Glabridin from Licorice Extracts on Melanogenesis and Inflammation. *Pigment Cell Research* **1998**, *11*, 355-361.

39. Shimizu, K., Kondo and, R., and Sakai, K. Inhibition of Tyrosinase by Flavonoids, Stilbenes and Related 4-Substituted Resorcinols: Structure-Activity Investigations. *Planta Med* **2000**, *66*, 11-15.
40. Suau, R., Cuevas, A., Valpuesta, V., and Reid, M. S. Arbutin and sucrose in the leaves of the resurrection plant *Myrothamnus flabellifolia*. *Phytochemistry* **1991**, *30*, 2555-2556.
41. Nerya, O., Musa, R., Khatib, S., Tamir, S., and Vaya, J. Chalcones as potent tyrosinase inhibitors: the effect of hydroxyl positions and numbers. *Phytochemistry* **2004**, *65*, 1389-1395.
42. Seo, S. Y., Sharma, V. K., and Sharma, N. Mushroom tyrosinase: recent prospects. *J Agric Food Chem* **2003**, *51*, 2837-2853.
43. Briganti, S., Camera, E., and Picardo, M. Chemical and Instrumental Approaches to Treat Hyperpigmentation. *Pigment Cell Research* **2003**, *16*, 101-110.
44. Stratford, M. R. L., Ramsden, C. A., and Riley, P. A. The influence of hydroquinone on tyrosinase kinetics. *Bioorganic & Medicinal Chemistry* **2012**, *20*, 4364-4370.
45. Germanas, J. P., Wang, S., Miner, A., Hao, W., and Ready, J. M. Discovery of small-molecule inhibitors of tyrosinase. *Bioorg Med Chem Lett* **2007**, *17*, 6871-6875.
46. Shimizu, K., Kondo, R., Sakai, K., Takeda, N., Nagahata, T., and Oniki, T. Novel vitamin E derivative with 4-substituted resorcinol moiety has both antioxidant and tyrosinase inhibitory properties. *Lipids* **2001**, *36*, 1321-1326.
47. Chung, K. W., Park, Y. J., Choi, Y. J., Park, M. H., Ha, Y. M., Uehara, Y., Yoon, J. H., Chun, P., Moon, H. R., and Chung, H. Y. Evaluation of in vitro and in vivo anti-melanogenic activity of a newly synthesized strong tyrosinase inhibitor (E)-3-(2,4 dihydroxybenzylidene)pyrrolidine-2,5-dione (3-DBP). *Biochim Biophys Acta* **2012**, *7*, 962-969.
48. Baran, Y., and Saydam, G. Cumulative clinical experience from a decade of use: imatinib as first-line treatment of chronic myeloid leukemia. *J Blood Med* **2012**, *3*, 139-150.
49. Bernstein, D. I., Schoenwetter, W. F., Nathan, R. A., Storms, W., Ahlbrandt, R., and Mason, J. Efficacy and safety of fexofenadine hydrochloride for treatment of seasonal allergic rhinitis. *Ann Allergy Asthma Immunol* **1997**, *79*, 443-448.
50. Overington, J. P., Al-Lazikani, B., and Hopkins, A. L. How many drug targets are there? *Nat Rev Drug Discov* **2006**, *5*, 993-996.
51. Tanrikulu, Y., Krüger, B., and Proschak, E. The holistic integration of virtual screening in drug discovery. *Drug Discovery Today* **2013**, *18*, 358-364.
52. McInnes, C. Virtual screening strategies in drug discovery. *Current Opinion in Chemical Biology* **2007**, *11*, 494-502.
53. Siegel, M. M. Early discovery drug screening using mass spectrometry. *Curr Top Med Chem* **2002**, *2*, 13-33.
54. Westerfeld, J. Detection trends in high throughput screening. *Analytical and Bioanalytical Chemistry* **2002**, *372*, 43-43.
55. de Boer, A. R., Lingeman, H., Niessen, W. M. A., and Irth, H. Mass spectrometry-based biochemical assays for enzyme-inhibitor screening. *TrAC Trends in Analytical Chemistry* **2007**, *26*, 867-883.
56. Bertucci, C., Pistolozzi, M., Felix, G., and Danielson, U. H. HSA binding of HIV protease inhibitors: a high-performance affinity chromatography study. *Journal of Separation Science* **2009**, *32*, 1625-1631.
57. Hage, D. S., Anguizola, J. A., Bi, C., Li, R., Matsuda, R., Papastavros, E., Pfaumiller, E., Vargas, J., and Zheng, X. Pharmaceutical and biomedical applications of affinity chromatography: Recent trends and developments. *Journal of Pharmaceutical and Biomedical Analysis* **2012**, *69*, 93-105.
58. Vuignier, K., Guillaume, D., Veuthey, J.-L., Carrupt, P.-A., and Schappler, J. High performance affinity chromatography (HPAC) as a high-throughput screening tool in drug discovery to study drug-plasma protein interactions. *Journal of Pharmaceutical and Biomedical Analysis* **2013**, *74*, 205-212.
59. de Moraes, M. C., Vanzolini, K. L., Cardoso, C. L., and Cass, Q. B. New trends in LC protein ligand screening. *Journal of Pharmaceutical and Biomedical Analysis* **2014**, *87*, 155-166.

60. Loo, J. C. K., Jordan, N., and Ho Ngoc, A. Application of a high-performance gel permeation liquid chromatographic procedure to the determination of binding of prednisolone to high-affinity binding sites in human serum. *Journal of Chromatography B: Biomedical Sciences and Applications* **1984**, 305, 194-198.
61. Jonker, N., Kool, J., Irth, H., and Niessen, W. M. Recent developments in protein-ligand affinity mass spectrometry. *Analytical and Bioanalytical Chemistry* **2011**, 399, 2669-2681.
62. Slon-Usakiewicz, J. J., Ng, W., Foster, J. E., Dai, J.-R., Deretey, E., Toledo-Sherman, L., Redden, P. R., Pasternak, A., and Reid, N. Frontal Affinity Chromatography with MS Detection of EphB2 Tyrosine Kinase Receptor. 1. Comparison with Conventional ELISA. *Journal of Medicinal Chemistry* **2004**, 47, 5094-5100.
63. Myszka, D. G. Kinetic analysis of macromolecular interactions using surface plasmon resonance biosensors. *Current Opinion in Biotechnology* **1997**, 8, 50-57.
64. Viht, K., Schweinsberg, S., Lust, M., Vaasa, A., Raidaru, G., Lavogina, D., Uri, A., and Herberg, F. W. Surface-plasmon-resonance-based biosensor with immobilised bisubstrate analog inhibitor for the determination of affinities of ATP- and protein-competitive ligands of cAMP-dependent protein kinase. *Analytical Biochemistry* **2007**, 362, 268-277.
65. Zhang, Y., Shi, S., Guo, J., You, Q., and Feng, D. On-line surface plasmon resonance-high performance liquid chromatography–tandem mass spectrometry for analysis of human serum albumin binders from Radix Astragali. *J Chromatogr A* **2013**, 1293, 92-99.
66. van Breemen, R. B., Huang, C.-R., Nikolic, D., Woodbury, C. P., Zhao, Y.-Z., and Venton, D. L. Pulsed Ultrafiltration Mass Spectrometry: A New Method for Screening Combinatorial Libraries. *Analytical Chemistry* **1997**, 69, 2159-2164.
67. Nikolic, D., Habibi-Goudarzi, S., Corley, D. G., Gafner, S., Pezzuto, J. M., and van Breemen, R. B. Evaluation of Cyclooxygenase-2 Inhibitors Using Pulsed Ultrafiltration Mass Spectrometry. *Analytical Chemistry* **2000**, 72, 3853-3859.
68. Moaddel, R., Marszał, M. P., Bigli, F., Yang, Q., Duan, X., and Wainer, I. W. Automated Ligand Fishing Using Human Serum Albumin-Coated Magnetic Beads. *Analytical Chemistry* **2007**, 79, 5414-5417.
69. Marszał, M. P., Moaddel, R., Kole, S., Gandhari, M., Bernier, M., and Wainer, I. W. Ligand and Protein Fishing with Heat Shock Protein 90 Coated Magnetic Beads. *Analytical Chemistry* **2008**, 80, 7571-7575.
70. Cubrilovic, D., Haap, W., Barylyuk, K., Ruf, A., Badertscher, M., Gubler, M., Tetaz, T., Joseph, C., Benz, J., and Zenobi, R. Determination of Protein–Ligand Binding Constants of a Cooperatively Regulated Tetrameric Enzyme Using Electrospray Mass Spectrometry. *ACS Chemical Biology* **2013**.
71. Maple, H. J., Garlish, R. A., Rigau-Roca, L., Porter, J., Whitcombe, I., Prosser, C. E., Kennedy, J., Henry, A. J., Taylor, R. J., Crump, M. P., and Crosby, J. Automated Protein–Ligand Interaction Screening by Mass Spectrometry. *Journal of Medicinal Chemistry* **2011**, 55, 837-851.
72. El-Hawiet, A., Kitova, E. N., Liu, L., and Klassen, J. S. Quantifying Labile Protein–Ligand Interactions Using Electrospray Ionisation Mass Spectrometry. *Journal of the American Society for Mass Spectrometry* **2010**, 21, 1893-1899.
73. Czuczy, N., Katona, M., and Takats, Z. Selective Detection of Specific Protein–Ligand Complexes by Electrosonic Spray–Precursor Ion Scan Tandem Mass Spectrometry. *Journal of the American Society for Mass Spectrometry* **2009**, 20, 227-237.
74. Liu, P., Zhang, J., Ferguson, C. N., Chen, H., and Loo, J. A. Measuring Protein–Ligand Interactions Using Liquid Sample Desorption Electrospray Ionisation Mass Spectrometry. *Analytical Chemistry* **2013**.
75. Yanes, O., Aviles, F. X., Roepstorff, P., and Jorgensen, T. J. Exploring the "intensity fading" phenomenon in the study of noncovalent interactions by MALDI-TOF mass spectrometry. *J Am Soc Mass Spectrom* **2007**, 18, 359-367.
76. Mireuta, M., Hancock, M. A., and Pollak, M. Binding between insulin-like growth factor 1 and insulin-like growth factor-binding protein 3 is not influenced by glucose or 2-deoxy-D-glucose. *J Biol Chem* **2011**, 286, 16567-16573.

77. Villanueva, J., Yanes, O., Querol, E., Serrano, L., and Aviles, F. X. Identification of protein ligands in complex biological samples using intensity-fading MALDI-TOF mass spectrometry. *Anal Chem* **2003**, *75*, 3385-3395.
78. Obregón, W. D., Ghiano, N., Tellechea, M., Cisneros, J. S., Lazza, C. M., López, L. M. I., and Avilés, F. X. Detection and characterisation of a new metalloproteinase inhibitor from *Solanum tuberosum* cv. Desirée using proteomic techniques. *Food Chemistry* **2012**, *133*, 1163-1168.
79. Sanglas, L., Aviles, F. X., Huber, R., Gomis-Rüth, F. X., and Arolas, J. L. Mammalian metalloproteinase inhibition at the defense barrier of *Ascaris* parasite. *Proceedings of the National Academy of Sciences* **2009**, *106*, 1743-1747.
80. Yanes, O., Nazabal, A., Wenzel, R., Zenobi, R., and Aviles, F. X. Detection of noncovalent complexes in biological samples by intensity fading and high-mass detection MALDI-TOF mass spectrometry. *J Proteome Res* **2006**, *5*, 2711-2719.
81. Yanes, O., Villanueva, J., Querol, E., and Aviles, F. X. Functional screening of serine protease inhibitors in the medical leech *Hirudo medicinalis* monitored by intensity fading MALDI-TOF MS. *Mol Cell Proteomics* **2005**, *4*, 1602-1613.
82. Yanes, O., Villanueva, J., Querol, E., and Aviles, F. X. Detection of non-covalent protein interactions by 'intensity fading' MALDI-TOF mass spectrometry: applications to proteases and protease inhibitors. *Nat Protoc* **2007**, *2*, 119-130.
83. Yanes, Ó., Villanueva, J., Querol, E., and Aviles, F. X. Intensity-fading MALDI-TOF-MS: novel screening for ligand binding and drug discovery. *Drug Discovery Today: TARGETS* **2004**, *3*, 23-30.
84. Gimenez-Oya, V., Villacanas, O., Fernandez-Busquets, X., Rubio-Martinez, J., and Imperial, S. Mimicking direct protein-protein and solvent-mediated interactions in the CDP-methylerythritol kinase homodimer: a pharmacophore-directed virtual screening approach. *J Mol Model* **2009**, *15*, 997-1007.
85. Hu, F., Zhang, H., Lin, H., Deng, C., and Zhang, X. Enzyme inhibitor screening by electrospray mass spectrometry with immobilised enzyme on magnetic silica microspheres. *J Am Soc Mass Spectrom* **2008**, *19*, 865-873.
86. Liu, W., Liu, S., Li, H., Song, F., and Liu, Z. Binding of alpha 1-acid glycoprotein with aconitum alkaloids: an investigation using an intensity fading matrix-assisted laser desorption/ionisation Fourier transform mass spectrometry method. *Rapid Commun Mass Spectrom* **2011**, *25*, 973-978.
87. Mishra, M., Tamhane, V. A., Khandelwal, N., Kulkarni, M. J., Gupta, V. S., and Giri, A. P. Interaction of recombinant CanPIs with *Helicoverpa armigera* gut proteases reveals their processing patterns, stability and efficiency. *Proteomics* **2010**, *10*, 2845-2857.
88. Shabab, M., Kulkarni, M. J., and Khan, M. I. Study of papain-cystatin interaction by intensity fading MALDI-TOF-MS. *Protein J* **2008**, *27*, 7-12.
89. Wang, Z., Yu, X., Cui, M., Liu, Z., Song, F., and Liu, S. Investigation of calmodulin-Peptide interactions using matrix-assisted laser desorption/ionisation mass spectrometry. *J Am Soc Mass Spectrom* **2009**, *20*, 576-583.
90. van Elswijk, D. A., Diefenbach, O., van der Berg, S., Irth, H., Tjaden, U. R., and van der Greef, J. Rapid detection and identification of angiotensin-converting enzyme inhibitors by on-line liquid chromatography-biochemical detection, coupled to electrospray mass spectrometry. *J Chromatogr A* **2003**, *5*, 45-58.
91. Falck, D., Pirkolachachi, F. R., Giera, M., Honing, M., Kool, J., and Niessen, W. M. A. Comparison of (bio-)transformation methods for the generation of metabolite-like compound libraries of p38 $\alpha$  MAP kinase inhibitors using high-resolution screening. *Journal of Pharmaceutical and Biomedical Analysis*.
92. Yamashita, M., and Fenn, J. B. Electrospray ion source. Another variation on the free-jet theme. *The Journal of Physical Chemistry* **1984**, *88*, 4451-4459.
93. Konermann, L., Ahadi, E., Rodriguez, A. D., and Vahidi, S. Unraveling the Mechanism of Electrospray Ionisation. *Analytical Chemistry* **2012**, *85*, 2-9.
94. Temporini, C., Pochetti, G., Fracchiolla, G., Piemontese, L., Montanari, R., Moaddel, R., Laghezza, A., Altieri, F., Cervoni, L., Ubiali, D., Prada, E., Loiodice, F., Massolini, G., and Calleri, E. Open tubular

- columns containing the immobilised ligand binding domain of peroxisome proliferator-activated receptors  $\alpha$  and  $\gamma$  for dual agonists characterization by frontal affinity chromatography with mass spectrometry detection. *Journal of Chromatography A* **2013**, 1284, 36-43.
95. Besanger, T. R., Hodgson, R. J., Guillon, D., and Brennan, J. D. Monolithic membrane-receptor columns: Optimization of column performance for frontal affinity chromatography/mass spectrometry applications. *Analytica Chimica Acta* **2006**, 561, 107-118.
96. Olesen, K., Karlsson, R., Lind, U., Davidson, M., Blomberg, A., and Karlsson, A. Detection of ligand-receptor binding using microfluidic frontal affinity chromatography on proteoliposomes derived directly from native cell membranes. *Journal of Chromatography B* **2013**, 931, 84-89.
97. Sleno, L., and Volmer, D. A. Ion activation methods for tandem mass spectrometry. *Journal of Mass Spectrometry* **2004**, 39, 1091-1112.
98. Jiang, K., Zhang, H., Wang, J., Li, F., and Qian, M. Fragmentation of Deprotonated Diacylhydrazine Derivatives in Electrospray Ionisation Tandem Mass Spectrometry: Generation of Acid Anions via Intramolecular Rearrangement. *PLoS ONE* **2013**, 8, e63097.
99. Dubber, M. J., Sewram, V., Mshicileli, N., Shephard, G. S., and Kanfer, I. The simultaneous determination of selected flavonol glycosides and aglycones in Ginkgo biloba oral dosage forms by high-performance liquid chromatography-electrospray ionisation-mass spectrometry. *Journal of Pharmaceutical and Biomedical Analysis* **2005**, 37, 723-731.
100. de Souza, L. M., Cipriani, T. R., Serrato, R. V., da Costa, D. E., Iacomini, M., Gorin, P. A. J., and Sasaki, G. L. Analysis of flavonol glycoside isomers from leaves of *Maytenus ilicifolia* by offline and online high performance liquid chromatography-electrospray mass spectrometry. *Journal of Chromatography A* **2008**, 1207, 101-109.
101. Ma, Y.-L., Vedernikova, I., Van den Heuvel, H., and Claeys, M. Internal glucose residue loss in protonated O-diglycosyl flavonoids upon low-energy collision-induced dissociation. *Journal of the American Society for Mass Spectrometry* **2000**, 11, 136-144.
102. Feketeová, L., Barlow, C. K., Benton, T. M., Rochfort, S. J., and O'Hair, R. A. J. The formation and fragmentation of flavonoid radical anions. *International Journal of Mass Spectrometry* **2011**, 301, 174-183.
103. Kazuno, S., Yanagida, M., Shindo, N., and Murayama, K. Mass spectrometric identification and quantification of glycosyl flavonoids, including dihydrochalcones with neutral loss scan mode. *Analytical Biochemistry* **2005**, 347, 182-192.
104. Chen, S., Wu, B.-H., Fang, J.-B., Liu, Y.-L., Zhang, H.-H., Fang, L.-C., Guan, L., and Li, S.-H. Analysis of flavonoids from lotus (*Nelumbo nucifera*) leaves using high performance liquid chromatography/photodiode array detector tandem electrospray ionisation mass spectrometry and an extraction method optimized by orthogonal design. *Journal of Chromatography A* **2012**, 1227, 145-153.
105. Zhou, D.-y., Xu, Q., Xue, X.-y., Zhang, F.-f., and Liang, X.-m. Identification of O-diglycosyl flavanones in *Fructus aurantii* by liquid chromatography with electrospray ionisation and collision-induced dissociation mass spectrometry. *Journal of Pharmaceutical and Biomedical Analysis* **2006**, 42, 441-448.
106. Domon, B., and Costello, C. A systematic nomenclature for carbohydrate fragmentations in FAB-MS/MS spectra of glycoconjugates. *Glycoconjugate Journal* **1988**, 5, 397-409.
107. Cunningham, O. D., and Edwards, R. Modifying the acylation of flavonols in *Petunia hybrida*. *Phytochemistry* **2008**, 69, 2016-2021.
108. Zhao, H.-Y., Sun, J.-H., Fan, M.-X., Fan, L., Zhou, L., Li, Z., Han, J., Wang, B.-R., and Guo, D.-A. Analysis of phenolic compounds in *Epimedium* plants using liquid chromatography coupled with electrospray ionisation mass spectrometry. *Journal of Chromatography A* **2008**, 1190, 157-181.
109. Barnes, J. S., and Schug, K. A. Structural characterization of cyanidin-3,5-diglucoside and pelargonidin-3,5-diglucoside anthocyanins: Multi-dimensional fragmentation pathways using high performance liquid chromatography-electrospray ionisation-ion trap-time of flight mass spectrometry. *International Journal of Mass Spectrometry* **2011**, 308, 71-80.

110. Kelly, R. T., Tolmachev, A. V., Page, J. S., Tang, K., and Smith, R. D. The ion funnel: Theory, implementations, and applications. *Mass Spectrometry Reviews* **2010**, *29*, 294-312.
111. Karas, M., Bachmann, D., and Hillenkamp, F. Influence of the wavelength in high-irradiance ultraviolet laser desorption mass spectrometry of organic molecules. *Analytical Chemistry* **1985**, *57*, 2935-2939.
112. Tanaka, K., Waki, H., Ido, Y., Akita, S., Yoshida, Y., Yoshida, T., and Matsuo, T. Protein and polymer analyses up to  $m/z$  100 000 by laser ionisation time-of-flight mass spectrometry. *Rapid Communications in Mass Spectrometry* **1988**, *2*, 151-153.
113. Karas, M., and Hillenkamp, F. Laser desorption ionisation of proteins with molecular masses exceeding 10,000 daltons. *Analytical Chemistry* **1988**, *60*, 2299-2301.
114. D'Imperio, M., Della Corte, A., Facchiano, A., Di Michele, M., Ferrandina, G., Donati, M. B., and Rotilio, D. Standardized sample preparation phases for a quantitative measurement of plasma peptidome profiling by MALDI-TOF. *Journal of Proteomics* **2010**, *73*, 1355-1367.
115. Zenobi, R., and Knochenmuss, R. Ion formation in MALDI mass spectrometry. *Mass Spectrometry Reviews* **1998**, *17*, 337-366.
116. Shah, B., Kozlowski, R. L., Han, J., and Borchers, C. H. Emerging mass spectrometry-based technologies for analyses of chromatin changes: analysis of histones and histone modifications. *Methods Mol Biol* **2011**, *773*, 259-303.
117. Arıca, M. Y., Bayramođlu, G., and Bıçak, N. Characterisation of tyrosinase immobilised onto spacer-arm attached glycidyl methacrylate-based reactive microbeads. *Process Biochemistry* **2004**, *39*, 2007-2017.
118. Wang, H.-Y., Chu, X., Zhao, Z.-X., He, X.-S., and Guo, Y.-L. Analysis of low molecular weight compounds by MALDI-FTICR-MS. *J Chromatogr B* **2011**, *879*, 1166-1179.
119. Vermillion-Salsbury, R. L., and Hercules, D. M. 9-Aminoacridine as a matrix for negative mode matrix-assisted laser desorption/ionisation. *Rapid Communications in Mass Spectrometry* **2002**, *16*, 1575-1581.
120. Guo, Z., and He, L. A binary matrix for background suppression in MALDI-MS of small molecules. *Analytical and Bioanalytical Chemistry* **2007**, *387*, 1939-1944.
121. Shroff, R., and Svatoš, A. Proton Sponge: A Novel and Versatile MALDI Matrix for the Analysis of Metabolites Using Mass Spectrometry. *Analytical Chemistry* **2009**, *81*, 7954-7959.
122. Chiang, C.-K., Chen, W.-T., and Chang, H.-T. Nanoparticle-based mass spectrometry for the analysis of biomolecules. *Chemical Society Reviews* **2011**, *40*, 1269-1281.
123. Law, K. P., and Larkin, J. Recent advances in SALDI-MS techniques and their chemical and bioanalytical applications. *Analytical and Bioanalytical Chemistry* **2011**, *399*, 2597-2622.
124. Sunner, J., Dratz, E., and Chen, Y.-C. Graphite surface-assisted laser desorption/ionisation time-of-flight mass spectrometry of peptides and proteins from liquid solutions. *Analytical Chemistry* **1995**, *67*, 4335-4342.
125. Chiang, C.-K., Lin, Y.-W., Chen, W.-T., and Chang, H.-T. Accurate quantitation of glutathione in cell lysates through surface-assisted laser desorption/ionisation mass spectrometry using gold nanoparticles. *Nanomedicine: Nanotechnology, Biology and Medicine* **2010**, *6*, 530-537.
126. Chiu, T.-C., Chang, L.-C., Chiang, C.-K., and Chang, H.-T. Determining Estrogens Using Surface-Assisted Laser Desorption/Ionisation Mass Spectrometry with Silver Nanoparticles as the Matrix. *Journal of the American Society for Mass Spectrometry* **2008**, *19*, 1343-1346.
127. Kawasaki, H., Yonezawa, T., Watanabe, T., and Arakawa, R. Platinum Nanoflowers for Surface-Assisted Laser Desorption/Ionisation Mass Spectrometry of Biomolecules. *The Journal of Physical Chemistry C* **2007**, *111*, 16278-16283.
128. Gholipour, Y., Giudicessi, S. L., Nonami, H., and Erra-Balsells, R. Diamond, Titanium Dioxide, Titanium Silicon Oxide, and Barium Strontium Titanium Oxide Nanoparticles as Matrixes for Direct Matrix-Assisted Laser Desorption/Ionisation Mass Spectrometry Analysis of Carbohydrates in Plant Tissues. *Analytical Chemistry* **2010**, *82*, 5518-5526.



129. Lee, K. H., Chiang, C. K., Lin, Z. H., and Chang, H. T. Determining enediol compounds in tea using surface-assisted laser desorption/ionisation mass spectrometry with titanium dioxide nanoparticle matrices. *Rapid Commun Mass Spectrom* **2007**, *21*, 2023-2030.
130. Watanabe, T., Kawasaki, H., Yonezawa, T., and Arakawa, R. Surface-assisted laser desorption/ionisation mass spectrometry (SALDI-MS) of low molecular weight organic compounds and synthetic polymers using zinc oxide (ZnO) nanoparticles. *Journal of Mass Spectrometry* **2008**, *43*, 1063-1071.
131. Chen, W.-Y., and Chen, Y.-C. Affinity-based mass spectrometry using magnetic iron oxide particles as the matrix and concentrating probes for SALDI MS analysis of peptides and proteins. *Analytical and Bioanalytical Chemistry* **2006**, *386*, 699-704.
132. Shin, W. J., Shin, J. H., Song, J. Y., and Han, S. Y. Effects of ZnO nanowire length on surface-assisted laser desorption/ionisation of small molecules. *J Am Soc Mass Spectrom* **2010**, *21*, 989-992.
133. Montsko, G., Vaczy, A., Maasz, G., Mernyak, E., Frank, E., Bay, C., Kadar, Z., Ohmacht, R., Wolfling, J., and Mark, L. Analysis of nonderivatized steroids by matrix-assisted laser desorption/ionisation time-of-flight mass spectrometry using C70 fullerene as matrix. *Analytical and Bioanalytical Chemistry* **2009**, *395*, 869-874.
134. Yonezawa, T., Kawasaki, H., Tarui, A., Watanabe, T., Arakawa, R., Shimada, T., and Mafune, F. Detailed investigation on the possibility of nanoparticles of various metal elements for surface-assisted laser desorption/ionisation mass spectrometry. *Anal Sci* **2009**, *25*, 339-346.
135. Distler, A. M., and Allison, J. Additives for the stabilization of double-stranded DNA in UV-MALDI MS. *J Am Soc Mass Spectrom* **2002**, *13*, 1129-1137.
136. Soltzberg, L. J., and Patel, P. Small molecule matrix-assisted laser desorption/ionisation time-of-flight mass spectrometry using a polymer matrix. *Rapid Communications in Mass Spectrometry* **2004**, *18*, 1455-1458.
137. Lee, J. H., Choi, H. S., Nasr, K. A., Ha, M., Kim, Y., and Frangioni, J. V. High-Throughput Small Molecule Identification Using MALDI-TOF and a Nanolayered Substrate. *Analytical Chemistry* **2011**, *83*, 5283-5289.
138. Li, Y., and Gross, M. Ionic-liquid matrices for quantitative analysis by MALDI-TOF mass spectrometry. *Journal of the American Society for Mass Spectrometry* **2004**, *15*, 1833-1837.
139. Turillazzi, S., Mastrobuoni, G., Dani, F., Moneti, G., Pieraccini, G., Marca, G., Bartolucci, G., Perito, B., Lambardi, D., Cavallini, V., and Dapporto, L. Dominulin A and B: Two new antibacterial peptides identified on the cuticle and in the venom of the social paper wasp *Polistes dominulus* using MALDI-TOF, MALDI-TOF/TOF, and ESI-ion trap. *Journal of the American Society for Mass Spectrometry* **2006**, *17*, 376-383.
140. Wattenberg, A., Organ, A., Schneider, K., Tyldesley, R., Bordoli, R., and Bateman, R. Sequence dependent fragmentation of peptides generated by MALDI quadrupole time-of-flight (MALDI Q-TOF) mass spectrometry and its implications for protein identification. *Journal of the American Society for Mass Spectrometry* **2002**, *13*, 772-783.
141. Schaiberger, A., and Moss, J. Optimized sample preparation for MALDI mass spectrometry analysis of protected synthetic peptides. *Journal of the American Society for Mass Spectrometry* **2008**, *19*, 614-619.
142. Du, Z., and McManus, M. T. Identification of proteins in leaf tissues of white clover using MALDI-TOF mass spectrometry. *Biologia Plantarum* **2011**, *55*, 261-268.
143. Meetani, M., and Voorhees, K. MALDI mass spectrometry analysis of high molecular weight proteins from whole bacterial cells: Pretreatment of samples with surfactants. *Journal of the American Society for Mass Spectrometry* **2005**, *16*, 1422-1426.
144. Liu, Z., and Schey, K. L. Fragmentation of Multiply-Charged Intact Protein Ions Using MALDI TOF-TOF Mass Spectrometry. *Journal of the American Society for Mass Spectrometry* **2008**, *19*, 231-238.
145. Lin, M., Campbell, J. M., Mueller, D. R., and Wirth, U. Intact protein analysis by matrix-assisted laser desorption/ionisation tandem time-of-flight mass spectrometry. *Rapid Communications in Mass Spectrometry* **2003**, *17*, 1809-1814.

146. Amini, N., Shariatgorji, M., and Thorsen, G. SALDI-MS signal enhancement using oxidised graphitized carbon black nanoparticles. *J Am Soc Mass Spectrom* **2009**, *20*, 1207-1213.
147. Tang, H.-W., Ng, K.-M., Lu, W., and Che, C.-M. Ion Desorption Efficiency and Internal Energy Transfer in Carbon-Based Surface-Assisted Laser Desorption/Ionisation Mass Spectrometry: Desorption Mechanism(s) and the Design of SALDI Substrates. *Analytical Chemistry* **2009**, *81*, 4720-4729.
148. Lim, A. Y., Ma, Z., Ma, J., and Rowell, F. Separation of fingerprint constituents using magnetic silica nanoparticles and direct on-particle SALDI-TOF-mass spectrometry. *J Chromatogr B* **2011**, *879*, 2244-2250.
149. Rowell, F., Seviour, J., Lim, A. Y., Elumbaring-Salazar, C. G., Loke, J., and Ma, J. Detection of nitro-organic and peroxide explosives in latent fingermarks by DART- and SALDI-TOF-mass spectrometry. *Forensic Science International* **2012**, *221*, 84-91.
150. Duan, J., Linman, M. J., Chen, C.-Y., and Cheng, Q. J. CHCA-Modified Au Nanoparticles for Laser Desorption Ionisation Mass Spectrometric Analysis of Peptides. *Journal of the American Society for Mass Spectrometry* **2009**, *20*, 1530-1539.
151. Lee, J., Lee, J., Chung, T. D., and Yeo, W.-S. Nanoengineered micro gold shells for LDI-TOF analysis of small molecules. *Analytica Chimica Acta* **2012**, *736*, 1-6.
152. Dupré, M., Cantel, S., Durand, J.-O., Martinez, J., and Enjalbal, C. Silica nanoparticles pre-spotted onto target plate for laser desorption/ionisation mass spectrometry analyses of peptides. *Analytica Chimica Acta* **2012**, *741*, 47-57.
153. Chen, W.-T., Chiang, C.-K., Lee, C.-H., and Chang, H.-T. Using Surface-Assisted Laser Desorption/Ionisation Mass Spectrometry to Detect Proteins and Protein-Protein Complexes. *Analytical Chemistry* **2012**, *84*, 1924-1930.
154. Lo, C.-Y., Lin, J.-Y., Chen, W.-Y., Chen, C.-T., and Chen, Y.-C. Surface-Assisted Laser Desorption/Ionisation Mass Spectrometry on Titania Nanotube Arrays. *Journal of the American Society for Mass Spectrometry* **2008**, *19*, 1014-1020.
155. Law, K. P. Laser desorption/ionisation mass spectrometry on nanostructured semiconductor substrates: DIOS™ and QuickMass™. *International Journal of Mass Spectrometry* **2010**, *290*, 72-84.
156. Gallifuoco, A., Alfani, F., Cantarella, M., Spagna, G., and Pifferi, P. G. Immobilised  $\beta$ -glucosidase for the winemaking industry: study of biocatalyst operational stability in laboratory-scale continuous reactors. *Process Biochemistry* **1999**, *35*, 179-185.
157. Yao, C., Qi, L., Qiao, J., Zhang, H., Wang, F., Chen, Y., and Yang, G. High-performance affinity monolith chromatography for chiral separation and determination of enzyme kinetic constants. *Talanta* **2010**, *82*, 1332-1337.
158. Henriksson, H., Muñoz, I. G., Isaksson, R., Pettersson, G., and Johansson, G. Cellobiohydrolase 58 (P.c. Cel 7D) is complementary to the homologous CBH I (T.r. Cel 7A) in enantioseparations. *J Chromatogr A* **2000**, *898*, 63-74.
159. Ho, J.-a. A., Wu, L.-c., Fan, N.-C., Lee, M.-S., Kuo, H.-Y., and Yang, C.-S. Development of a long-life capillary enzyme bioreactor for the determination of blood glucose. *Talanta* **2007**, *71*, 391-396.
160. Cheng, Y., Ho, E., Subramanyam, B., and Tseng, J.-L. Measurements of drug-protein binding by using immobilised human serum albumin liquid chromatography-mass spectrometry. *J Chromatogr B* **2004**, *809*, 67-73.
161. Mallik, R., Yoo, M. J., Briscoe, C. J., and Hage, D. S. Analysis of drug-protein binding by ultrafast affinity chromatography using immobilised human serum albumin. *J Chromatogr A* **2010**, *1217*, 2796-2803.
162. Bartolini, M., Greig, N. H., Yu, Q.-s., and Andrisano, V. Immobilised butyrylcholinesterase in the characterization of new inhibitors that could ease Alzheimer's disease. *J Chromatogr A* **2009**, *1216*, 2730-2738.
163. Bartolini, M., Cavrini, V., and Andrisano, V. Characterization of reversible and pseudo-irreversible acetylcholinesterase inhibitors by means of an immobilised enzyme reactor. *J Chromatogr A* **2007**, *1144*, 102-110.

164. Green, N. M. Avidin. 1. The Use of (14-C)Biotin for Kinetic Studies and for Assay. *Biochem J* **1963**, *89*, 585-591.
165. Chan, N. W., Lewis, D. F., Rosner, P. J., Kelly, M. A., and Schriemer, D. C. Frontal affinity chromatography-mass spectrometry assay technology for multiple stages of drug discovery: applications of a chromatographic biosensor. *Anal Biochem* **2003**, *319*, 1-12.
166. Schriemer, D. C., Bundle, D. R., Li, L., and Hindsgaul, O. Micro-Scale Frontal Affinity Chromatography with Mass Spectrometric Detection: A New Method for the Screening of Compound Libraries. *Angewandte Chemie International Edition* **1998**, *37*, 3383-3387.
167. Ng, E. S., Yang, F., Kameyama, A., Palczic, M. M., Hindsgaul, O., and Schriemer, D. C. High-throughput screening for enzyme inhibitors using frontal affinity chromatography with liquid chromatography and mass spectrometry. *Anal Chem* **2005**, *77*, 6125-6133.
168. Hochuli, E., Bannwarth, W., Dobeli, H., Gentz, R., and Stuber, D. Genetic Approach to Facilitate Purification of Recombinant Proteins with a Novel Metal Chelate Adsorbent. *Nat Biotech* **1988**, *6*, 1321-1325.
169. Chen, Y., Li, Y., Liu, P., Sun, Q., and Liu, Z. Optimized expression in *Pichia pastoris* eliminates common protein contaminants from subsequent His-tag purification. *Biotechnology Letters* **2013**, 1-8.
170. Hartwig, S., Frister, T., Alemdar, S., Li, Z., Krings, U., Berger, R. G., Scheper, T., and Beutel, S. Expression, purification and activity assay of a patchoulol synthase cDNA variant fused to thioredoxin in *Escherichia coli*. *Protein Expression and Purification*.
171. Cardi, M., Chibani, K., Castiglia, D., Cafasso, D., Pizzo, E., Rouhier, N., Jacquot, J.-P., and Esposito, S. Overexpression, purification and enzymatic characterization of a recombinant plastidial glucose-6-phosphate dehydrogenase from barley (*Hordeum vulgare* cv. Nure) roots. *Plant Physiology and Biochemistry* **2013**, *73*, 266-273.
172. Moaddel, R., and Wainer, I. W. Development of immobilised membrane-based affinity columns for use in the online characterization of membrane bound proteins and for targeted affinity isolations. *Anal Chim Acta* **2006**, *564*, 97-105.
173. Girelli, A. M., and Mattei, E. Application of immobilised enzyme reactor in on-line high performance liquid chromatography: A review. *Journal of Chromatography B* **2005**, *819*, 3-16.
174. Brady, D., and Jordaan, J. Advances in enzyme immobilisation. *Biotechnology Letters* **2009**, *31*, 1639-1650.
175. Coríci, L. N., Frissen, A. E., van Zoelen, D.-J., Eggen, I. F., Peter, F., Davidescu, C. M., and Boeriu, C. G. Sol-gel immobilisation of Alcalase from *Bacillus licheniformis* for application in the synthesis of C-terminal peptide amides. *Journal of Molecular Catalysis B: Enzymatic* **2011**, *73*, 90-97.
176. Batista, K. A., Lopes, F. M., Yamashita, F., and Fernandes, K. F. Lipase entrapment in PVA/Chitosan biodegradable film for reactor coatings. *Materials Science and Engineering: C* **2013**, *33*, 1696-1701.
177. Kumar, R. S. S., Vishwanath, K. S., Singh, S. A., and Rao, A. G. A. Entrapment of  $\alpha$ -amylase in alginate beads: Single step protocol for purification and thermal stabilization. *Process Biochemistry* **2006**, *41*, 2282-2288.
178. Iucci, G., Battocchio, C., Dettin, M., Ghezzi, F., and Polzonetti, G. An XPS study on the covalent immobilisation of adhesion peptides on a glass surface. *Solid State Sciences* **2010**, *12*, 1861-1865.
179. Karakuş, E., and Pekyardımcı, Ş. Immobilisation of apricot pectinesterase (*Prunus armeniaca* L.) on porous glass beads and its characterization. *Journal of Molecular Catalysis B: Enzymatic* **2009**, *56*, 13-19.
180. Calleri, E., Fracchiolla, G., Montanari, R., Pochetti, G., Lavecchia, A., Liodice, F., Laghezza, A., Piemontese, L., Massolini, G., and Temporini, C. Frontal affinity chromatography with MS detection of the ligand binding domain of PPAR $\gamma$  receptor: Ligand affinity screening and stereoselective ligand-macromolecule interaction. *Journal of Chromatography A* **2012**, *1232*, 84-92.
181. Nelson, M. A., Moser, A., and Hage, D. S. Biointeraction analysis by high-performance affinity chromatography: Kinetic studies of immobilised antibodies. *J Chromatogr B Analyt Technol Biomed Life Sci* **2010**, *878*, 165-171.

182. Yoo, M. J., Schiel, J. E., and Hage, D. S. Evaluation of affinity microcolumns containing human serum albumin for rapid analysis of drug-protein binding. *J Chromatogr B Analyt Technol Biomed Life Sci* **2010**, *878*, 1707-1713.
183. Sobansky, M. R., and Hage, D. S. Identification and analysis of stereoselective drug interactions with low-density lipoprotein by high-performance affinity chromatography. *Analytical and Bioanalytical Chemistry* **2012**, *403*, 563-571.
184. Kahraman, M. V., Bayramoğlu, G., Kayaman-Apohan, N., and Güngör, A.  $\alpha$ -Amylase immobilisation on functionalized glass beads by covalent attachment. *Food Chem* **2007**, *104*, 1385-1392.
185. Ogata, Y., Scampavia, L., Carter, T. L., Fan, E., and Tureček, F. Automated affinity chromatography measurements of compound mixtures using a lab-on-valve apparatus coupled to electrospray ionisation mass spectrometry. *Analytical Biochemistry* **2004**, *331*, 161-168.
186. Luo, H., Chen, L., Li, Z., Ding, Z., and Xu, X. Frontal immunoaffinity chromatography with mass spectrometric detection: a method for finding active compounds from traditional Chinese herbs. *Anal Chem* **2003**, *75*, 3994-3998.
187. Ota, S., Miyazaki, S., Matsuoka, H., Morisato, K., Shintani, Y., and Nakanishi, K. High-throughput protein digestion by trypsin-immobilised monolithic silica with pipette-tip formula. *Journal of Biochemical and Biophysical Methods* **2007**, *70*, 57-62.
188. Buck, M. E., Zhang, J., and Lynn, D. M. Layer-by-Layer Assembly of Reactive Ultrathin Films Mediated by Click-Type Reactions of Poly(2-Alkenyl Azlactone)s. *Advanced Materials* **2007**, *19*, 3951-3955.
189. Peterson, D. S., Rohr, T., Svec, F., and Frechet, J. M. Dual-function microanalytical device by in situ photolithographic grafting of porous polymer monolith: integrating solid-phase extraction and enzymatic digestion for peptide mass mapping. *Anal Chem* **2003**, *75*, 5328-5335.
190. Brne, P., Lim, Y. P., Podgornik, A., Barut, M., Pihlar, B., and Štrancar, A. Development and characterization of methacrylate-based hydrazide monoliths for oriented immobilisation of antibodies. *J Chromatogr A* **2009**, *1216*, 2658-2663.
191. Xu, S., Peng, B., and Han, X. Hydrazide-functionalized hollow porous poly(2-hydroxyethyl methacrylate-co-ethylene dimethacrylate) spheres for immobilisation of enzyme. *European Polymer Journal* **2006**, *42*, 2801-2806.
192. Xuan, H., Joseph, K. S., Wa, C., and Hage, D. S. Biointeraction analysis of carbamazepine binding to  $\alpha$ 1-acid glycoprotein by high-performance affinity chromatography. *Journal of Separation Science* **2010**, *33*, 2294-2301.
193. Jiang, Y., Guo, C., Xia, H., Mahmood, I., Liu, C., and Liu, H. Magnetic nanoparticles supported ionic liquids for lipase immobilisation: Enzyme activity in catalyzing esterification. *Journal of Molecular Catalysis B: Enzymatic* **2009**, *58*, 103-109.
194. Ren, Y., Rivera, J. G., He, L., Kulkarni, H., Lee, D. K., and Messersmith, P. B. Facile, high efficiency immobilisation of lipase enzyme on magnetic iron oxide nanoparticles via a biomimetic coating. *BMC Biotechnol* **2011**, *11*, 1472-6750.
195. Ranjbakhsh, E., Bordbar, A. K., Abbasi, M., Khosropour, A. R., and Shams, E. Enhancement of stability and catalytic activity of immobilised lipase on silica-coated modified magnetite nanoparticles. *Chemical Engineering Journal* **2012**, *179*, 272-276.
196. Girelli, A. M., Mattei, E., Messina, A., and Papaleo, D. Immobilisation of mushroom tyrosinase on controlled pore glass: Effect of chemical modification. *Sensors and Actuators B: Chemical* **2007**, *125*, 48-54.
197. Ponomareva, E. A., Kartuzova, V. E., Vlach, E. G., and Tennikova, T. B. Monolithic bioreactors: effect of chymotrypsin immobilisation on its biocatalytic properties. *J Chromatogr B Analyt Technol Biomed Life Sci* **2010**, *878*, 567-574.
198. Marin-Zamora, M. E., Rojas-Melgarejo, F., Garcia-Canovas, F., and Garcia-Ruiz, P. A. Effects of the immobilisation supports on the catalytic properties of immobilised mushroom tyrosinase: a comparative study using several substrates. *J Biotechnol* **2007**, *131*, 388-396.

199. Cuatrecasas, P., and Wilchek, M. Single-step purification of avidine from egg white by affinity chromatography on biocytin-Sepharose columns. *Biochem Biophys Res Commun* **1968**, *33*, 235-239.
200. Kasai, K., and Ishii, S. Affinity chromatography of trypsin using a Sepharose derivative coupled with peptides containing L-arginine in carboxyl termini. *J Biochem* **1972**, *71*, 363-366.
201. Duhamel, R. C., Schur, P. H., Brendel, K., and Meezan, E. pH gradient elution of human IgG1, IgG2 and IgG4 from protein A-sepharose. *J Immunol Methods* **1979**, *31*, 211-217.
202. Grodzki, A., and Berenstein, E., 'Antibody Purification: Affinity Chromatography – Protein A and Protein G Sepharose', in *Immunocytochemical Methods and Protocols*, ed. by Oliver, C. and Jamur, M. C. Humana Press, 2010), pp. 33-41.
203. KASAI, K.-i., and ISHII, S.-i. Quantitative Analysis of Affinity Chromatography of Trypsin: A New Technique for Investigation of Protein-ligand Interaction. *Journal of Biochemistry* **1975**, *77*, 261-264.
204. Kasai, K.-I., Oda, Y., Nishikata, M., and Ishii, S.-I. Frontal affinity chromatography: Theory for its application to studies on specific interactions of biomolecules. *Journal of Chromatography B: Biomedical Sciences and Applications* **1986**, *376*, 33-47.
205. Moaddel, R., Cloix, J.-F., Ertem, G., and Wainer, I. Multiple Receptor Liquid Chromatographic Stationary Phases: The Co-Immobilisation of Nicotinic Receptors,  $\gamma$ -Amino-Butyric Acid Receptors, and N-Methyl D-Aspartate Receptors. *Pharmaceutical Research* **2002**, *19*, 104-107.
206. Moaddel, R., Musyimi, H. K., Sanghvi, M., Bashore, C., Frazier, C. R., Khadeer, M., Bhatia, P., and Wainer, I. W. Synthesis and characterization of a cellular membrane affinity chromatography column containing histamine 1 and P2Y(1) receptors: a multiple G-protein coupled receptor column. *J Pharm Biomed Anal* **2010**, *52*, 416-419.
207. Song, L., Wellman, A. D., Yao, H., and Adcock, J. Electron capture atmospheric pressure photoionisation mass spectrometry: analysis of fullerenes, perfluorinated compounds, and pentafluorobenzyl derivatives. *Rapid Commun Mass Spectrom* **2007**, *21*, 1343-1351.
208. Gritti, F., and Guiochon, G. Adsorption mechanism in reversed-phase liquid chromatography: Effect of the surface coverage of a monomeric C18-silica stationary phase. *Journal of Chromatography A* **2006**, *1115*, 142-163.
209. Moaddel, R., Rosenberg, A., Spelman, K., Frazier, J., Frazier, C., Nocerino, S., Brizzi, A., Mugnaini, C., and Wainer, I. W. Development and characterization of immobilised cannabinoid receptor (CB1/CB2) open tubular column for on-line screening. *Analytical Biochemistry* **2011**, *412*, 85-91.
210. Zhang, B., Palcic, M. M., Schriemer, D. C., Alvarez-Manilla, G., Pierce, M., and Hindsgaul, O. Frontal affinity chromatography coupled to mass spectrometry for screening mixtures of enzyme inhibitors. *Anal Biochem* **2001**, *299*, 173-182.
211. Zhu, L., Chen, L., Luo, H., and Xu, X. Frontal affinity chromatography combined on-line with mass spectrometry: a tool for the binding study of different epidermal growth factor receptor inhibitors. *Anal Chem* **2003**, *75*, 6388-6393.
212. Calleri, E., Ceruti, S., Cristalli, G., Martini, C., Temporini, C., Parravicini, C., Volpini, R., Daniele, S., Caccialanza, G., Lecca, D., Lambertucci, C., Trincavelli, M. L., Marucci, G., Wainer, I. W., Raghino, G., Fantucci, P., Abbracchio, M. P., and Massolini, G. Frontal affinity chromatography-mass spectrometry useful for characterization of new ligands for GPR17 receptor. *J Med Chem* **2010**, *53*, 3489-3501.
213. Temporini, C., Ceruti, S., Calleri, E., Ferrario, S., Moaddel, R., Abbracchio, M. P., and Massolini, G. Development of an immobilised GPR17 receptor stationary phase for binding determination using frontal affinity chromatography coupled to mass spectrometry. *Analytical Biochemistry* **2009**, *384*, 123-129.
214. Svec, F. Preparation and HPLC applications of rigid macroporous organic polymer monoliths. *Journal of Separation Science* **2004**, *27*, 747-766.
215. Svec, F. Porous polymer monoliths: amazingly wide variety of techniques enabling their preparation. *J Chromatogr A* **2010**, *5*, 902-924.

216. Tjunelyte, I., Babinot, J., Guerrouache, M., Valincius, G., and Carbonnier, B. Hydrophilic monolith with ethylene glycol-based grafts prepared via surface confined thiol-ene click photoaddition. *Polymer* **2012**, *53*, 29-36.
217. Delaunay-Bertoncini, N., Demesmay, C., and Rocca, J. L. Development and in situ synthesis of monolithic stationary phases for electrochromatographic separations. *Electrophoresis* **2004**, *25*, 3204-3215.
218. Salwiński, A., Roy, V., Agrofoglio, L. A., and Delépée, R. In Situ One-Step Method for Synthesis of "Click"-Functionalized Monolithic Stationary Phase for Capillary Electrochromatography. *Macromolecular Chemistry and Physics* **2011**, *212*, 2700-2707.
219. Chen, B., Peng, H., Zheng, F., Hu, B., He, M., Zhao, W., and Pang, D. Immunoaffinity monolithic capillary microextraction coupled with ICP-MS for immunoassay with quantum dot labels. *Journal of Analytical Atomic Spectrometry* **2010**, *25*, 1674-1681.
220. Zhang, L., Chen, B., Peng, H., He, M., and Hu, B. Aminopropyltriethoxysilane-silica hybrid monolithic capillary microextraction combined with inductively coupled plasma mass spectrometry for the determination of trace elements in biological samples. *Journal of Separation Science* **2011**, *34*, 2247-2254.
221. Ishizuka, N., Kobayashi, H., Minakuchi, H., Nakanishi, K., Hirao, K., Hosoya, K., Ikegami, T., and Tanaka, N. Monolithic silica columns for high-efficiency separations by high-performance liquid chromatography. *Journal of Chromatography A* **2002**, *960*, 85-96.
222. Yan, L., Zhang, Q., Zhang, J., Zhang, L., Li, T., Feng, Y., Zhang, L., Zhang, W., and Zhang, Y. Hybrid organic-inorganic monolithic stationary phase for acidic compounds separation by capillary electrochromatography. *Journal of Chromatography A* **2004**, *1046*, 255-261.
223. Haddad, P. R. Editorial on "Porous polymer monoliths: Amazingly wide variety of techniques enabling their preparation" by F. Svec. *Journal of Chromatography A* **2010**, *1217*, 901.
224. Preinerstorfer, B., Bicker, W., Lindner, W., and Lammerhofer, M. Development of reactive thiol-modified monolithic capillaries and in-column surface functionalization by radical addition of a chromatographic ligand for capillary electrochromatography. *J Chromatogr A* **2004**, *30*, 1-2.
225. Brne, P., Lim, Y. P., Podgornik, A., Barut, M., Pihlar, B., and Strancar, A. Development and characterization of methacrylate-based hydrazide monoliths for oriented immobilisation of antibodies. *J Chromatogr A* **2009**, *27*, 2658-2663.
226. Salwiński, A., and Delépée, R. Comparison of monolithic capillary electrochromatography and micellar electrokinetic chromatography for the separation of polycyclic aromatic hydrocarbons. *Talanta* **2014**, *122*, 180-186.
227. Hilder, E. F., Svec, F., and Frechet, J. M. Shielded stationary phases based on porous polymer monoliths for the capillary electrochromatography of highly basic biomolecules. *Anal Chem* **2004**, *76*, 3887-3892.
228. Okay, O. Macroporous copolymer networks. *Progress in Polymer Science* **2000**, *25*, 711-779.
229. Svec, F. CEC: selected developments that caught my eye since the year 2000. *Electrophoresis* **2009**, *30*, 200900062.
230. Jiang, Z., Reilly, J., Everatt, B., and Smith, N. W. Novel zwitterionic polyphosphorylcholine monolithic column for hydrophilic interaction chromatography. *Journal of Chromatography A* **2009**, *1216*, 2439-2448.
231. Viklund, C., and Irgum, K. Synthesis of Porous Zwitterionic Sulfobetaine Monoliths and Characterization of Their Interaction with Proteins. *Macromolecules* **2000**, *33*, 2539-2544.
232. Siouffi, A. M. Silica gel-based monoliths prepared by the sol-gel method: facts and figures. *Journal of Chromatography A* **2003**, *1000*, 801-818.
233. Zhou, Y., Schattka, J. H., and Antonietti, M. Room-Temperature Ionic Liquids as Template to Monolithic Mesoporous Silica with Wormlike Pores via a Sol-Gel Nanocasting Technique. *Nano Letters* **2004**, *4*, 477-481.

234. Dai, S., Ju, Y. H., Gao, H. J., Lin, J. S., Pennycook, S. J., and Barnes, C. E. Preparation of silica aerogel using ionic liquids as solvents. *Chemical Communications* **2000**, 243-244.
235. Wang, H. F., Zhu, Y. Z., Yan, X. P., Gao, R. Y., and Zheng, J. Y. A Room Temperature Ionic Liquid (RTIL)-Mediated, Non-Hydrolytic Sol-Gel Methodology to Prepare Molecularly Imprinted, Silica-Based Hybrid Monoliths for Chiral Separation. *Advanced Materials* **2006**, *18*, 3266-3270.
236. Kahraman, M. V., Bayramoğlu, G., Kayaman-Apohan, N., and Güngör, A.  $\alpha$ -Amylase immobilisation on functionalized glass beads by covalent attachment. *Food Chemistry* **2007**, *104*, 1385-1392.
237. Etienne, M., and Walcarius, A. Analytical investigation of the chemical reactivity and stability of aminopropyl-grafted silica in aqueous medium. *Talanta* **2003**, *59*, 1173-1188.
238. Smet, L. C. P. M. d., Ullien, D., Mescher, M., and Sudhölter, E. J. R., *Organic Surface Modification of Silicon Nanowire-Based Sensor Devices, Nanowires - Implementations and Applications*, (2011).
239. Yu, Y., Addai-Mensah, J., and Losic, D. Functionalized diatom silica microparticles for removal of mercury ions. *Science and Technology of Advanced Materials* **2012**, *13*, 015008.
240. Kulkarni, S. A., Ogale, S. B., and Vijayamohanan, K. P. Tuning the hydrophobic properties of silica particles by surface silanization using mixed self-assembled monolayers. *Journal of Colloid and Interface Science* **2008**, *318*, 372-379.
241. Ghose, B. N. Synthesis of some Schiff bases. *Journal of Chemical & Engineering Data* **1984**, *29*, 237-237.
242. Mallik, R., Xuan, H., and Hage, D. S. Development of an affinity silica monolith containing  $\alpha$ 1-acid glycoprotein for chiral separations. *Journal of Chromatography A* **2007**, *1149*, 294-304.
243. Walter, J., Steigemann, W., Singh, T. P., Bartunik, H., Bode, W., and Huber, R. On the disordered activation domain in trypsinogen: chemical labelling and low-temperature crystallography. *Acta Crystallographica Section B* **1982**, *38*, 1462-1472.
244. Olsen, J. V., Ong, S. E., and Mann, M. Trypsin cleaves exclusively C-terminal to arginine and lysine residues. *Mol Cell Proteomics* **2004**, *3*, 608-614.
245. Calleri, E., Temporini, C., Gasparri, F., Simone, P., Villani, C., Ciogli, A., and Massolini, G. Immobilised trypsin on epoxy organic monoliths with modulated hydrophilicity: Novel bioreactors useful for protein analysis by liquid chromatography coupled to tandem mass spectrometry. *Journal of Chromatography A* **2011**, *1218*, 8937-8945.
246. Manrich, A., Galvão, C. M. A., Jesus, C. D. F., Giordano, R. C., and Giordano, R. L. C. Immobilisation of trypsin on chitosan gels: Use of different activation protocols and comparison with other supports. *International Journal of Biological Macromolecules* **2008**, *43*, 54-61.
247. Caro, A., Humblot, V., Méthivier, C., Minier, M., Barbes, L., Li, J., Salmain, M., and Pradier, C.-M. Bioengineering of stainless steel surface by covalent immobilisation of enzymes. Physical characterization and interfacial enzymatic activity. *Journal of Colloid and Interface Science* **2010**, *349*, 13-18.
248. Nihei, K., and Kubo, I. Identification of oxidation product of arbutin in mushroom tyrosinase assay system. *Bioorg Med Chem Lett* **2003**, *13*, 2409-2412.
249. Kurinov, I. V., and Harrison, R. W. Two crystal structures of the leupeptin-trypsin complex. *Protein Science* **1996**, *5*, 752-758.
250. Kuramochi, H., Nakata, H., and Ishii, S. Mechanism of association of a specific aldehyde inhibitor, leupeptin, with bovine trypsin. *J Biochem* **1979**, *86*, 1403-1410.
251. Zor, T., and Selinger, Z. Linearization of the Bradford protein assay increases its sensitivity: theoretical and experimental studies. *Anal Biochem* **1996**, *236*, 302-308.
252. Balunas, M. J., and Kinghorn, A. D. Drug discovery from medicinal plants. *Life Sci.* **2005**, *78*, 431-441.
253. Barenbrock, J. S., and Köck, M. Screening enzyme-inhibitory activity in several ascidian species from Orkney Islands using protein tyrosine kinase (PTK) bioassay-guided fractionation. *J. Biotechnol.* **2005**, *117*, 225-232.

254. Yang, Z., Lu, W., Ma, X., and Song, D. Bioassay-guided isolation of an alkaloid with antiangiogenic and antitumor activities from the extract of *Fissistigma cavaleriei* root. *Phytomedicine* **2012**, *19*, 301-305.
255. Yang, Z., Wang, Y., Wang, Y., and Zhang, Y. Bioassay-guided screening and isolation of  $\alpha$ -glucosidase and tyrosinase inhibitors from leaves of *Morus alba*. *Food Chem.* **2012**, *131*, 617-625.
256. Engelbertz, J., Lechtenberg, M., Studt, L., Hensel, A., and Verspohl, E. J. Bioassay-guided fractionation of a thymol-deprived hydrophilic thyme extract and its antispasmodic effect. *J. Ethnopharmacol.* **2012**, *141*, 848-853.
257. Villanueva, J., Yanes, O., Querol, E., Serrano, L., and Aviles, F. X. Identification of protein ligands in complex biological samples using intensity-fading MALDI-TOF mass spectrometry. *Anal. Chem.* **2003**, *75*, 3385-3395.
258. Gimenez-Oya, V., Villacanas, O., Fernandez-Busquets, X., Rubio-Martinez, J., and Imperial, S. Mimicking direct protein-protein and solvent-mediated interactions in the CDP-methylerythritol kinase homodimer: a pharmacophore-directed virtual screening approach. *J. Mol. Model.* **2009**, *15*, 997-1007.
259. Liu, W., Liu, S., Li, H., Song, F., and Liu, Z. Binding of alpha 1-acid glycoprotein with aconitum alkaloids: an investigation using an intensity fading matrix-assisted laser desorption/ionisation Fourier transform mass spectrometry method. *Rapid Commun. Mass Spectrom.* **2011**, *25*, 973-978.
260. Mireuta, M., Hancock, M. A., and Pollak, M. Binding between insulin-like growth factor 1 and insulin-like growth factor-binding protein 3 is not influenced by glucose or 2-deoxy-D-glucose. *J. Biol. Chem.* **2011**, *286*, 16567-16573.
261. Obregón, W. D., Ghiano, N., Tellechea, M., Cisneros, J. S., Lazza, C. M., López, L. M. I., and Avilés, F. X. Detection and characterisation of a new metalloproteinase inhibitor from *Solanum tuberosum* cv. Desirée using proteomic techniques. *Food Chem.* **2012**, *133*, 1163-1168.
262. Sanglas, L., Aviles, F. X., Huber, R., Gomis-Rüth, F. X., and Arolas, J. L. Mammalian metalloproteinase inhibition at the defense barrier of *Ascaris* parasite. *Proc. Natl. Acad. Sci. U.S.A.* **2009**, *106*, 1743-1747.
263. Shabab, M., Kulkarni, M. J., and Khan, M. I. Study of papain-cystatin interaction by intensity fading MALDI-TOF-MS. *Protein J.* **2008**, *27*, 7-12.
264. Wang, Z., Yu, X., Cui, M., Liu, Z., Song, F., and Liu, S. Investigation of calmodulin-Peptide interactions using matrix-assisted laser desorption/ionisation mass spectrometry. *J. Am. Soc. Mass Spectrom.* **2009**, *20*, 576-583.
265. Yanes, O., Aviles, F. X., Roepstorff, P., and Jorgensen, T. J. Exploring the "intensity fading" phenomenon in the study of noncovalent interactions by MALDI-TOF mass spectrometry. *J. Am. Soc. Mass Spectrom.* **2007**, *18*, 359-367.
266. Yanes, O., Nazabal, A., Wenzel, R., Zenobi, R., and Aviles, F. X. Detection of noncovalent complexes in biological samples by intensity fading and high-mass detection MALDI-TOF mass spectrometry. *J. Proteome Res.* **2006**, *5*, 2711-2719.
267. Yanes, O., Villanueva, J., Querol, E., and Aviles, F. X. Functional screening of serine protease inhibitors in the medical leech *Hirudo medicinalis* monitored by intensity fading MALDI-TOF MS. *Mol. Cell. Proteomics* **2005**, *4*, 1602-1613.
268. Yanes, O., Villanueva, J., Querol, E., and Aviles, F. X. Detection of non-covalent protein interactions by 'intensity fading' MALDI-TOF mass spectrometry: applications to proteases and protease inhibitors. *Nat. Protoc.* **2007**, *2*, 119-130.
269. Wang, H.-Y., Chu, X., Zhao, Z.-X., He, X.-S., and Guo, Y.-L. Analysis of low molecular weight compounds by MALDI-FTICR-MS. *J. Chromatogr. B* **2011**, *879*, 1166-1179.
270. Vermillion-Salsbury, R. L., and Hercules, D. M. 9-Aminoacridine as a matrix for negative mode matrix-assisted laser desorption/ionisation. *Rapid Commun. Mass Spectrom.* **2002**, *16*, 1575-1581.
271. Shroff, R., and Svatoš, A. Proton Sponge: A Novel and Versatile MALDI Matrix for the Analysis of Metabolites Using Mass Spectrometry. *Anal. Chem.* **2009**, *81*, 7954-7959.
272. Law, K. P., and Larkin, J. Recent advances in SALDI-MS techniques and their chemical and bioanalytical applications. *Anal. Bioanal. Chem.* **2011**, *399*, 2597-2622.



273. Sunner, J., Dratz, E., and Chen, Y.-C. Graphite surface-assisted laser desorption/ionisation time-of-flight mass spectrometry of peptides and proteins from liquid solutions. *Anal. Chem.* **1995**, *67*, 4335-4342.
274. Chiang, C.-K., Lin, Y.-W., Chen, W.-T., and Chang, H.-T. Accurate quantitation of glutathione in cell lysates through surface-assisted laser desorption/ionisation mass spectrometry using gold nanoparticles. *Nanomedicine* **2010**, *6*, 530-537.
275. Chiu, T.-C., Chang, L.-C., Chiang, C.-K., and Chang, H.-T. Determining Estrogens Using Surface-Assisted Laser Desorption/Ionisation Mass Spectrometry with Silver Nanoparticles as the Matrix. *J. Am. Soc. Mass Spectrom.* **2008**, *19*, 1343-1346.
276. Kawasaki, H., Yonezawa, T., Watanabe, T., and Arakawa, R. Platinum Nanoflowers for Surface-Assisted Laser Desorption/Ionisation Mass Spectrometry of Biomolecules. *J. Phys. Chem. C* **2007**, *111*, 16278-16283.
277. Gholipour, Y., Giudicessi, S. L., Nonami, H., and Erra-Balsells, R. Diamond, Titanium Dioxide, Titanium Silicon Oxide, and Barium Strontium Titanium Oxide Nanoparticles as Matrixes for Direct Matrix-Assisted Laser Desorption/Ionisation Mass Spectrometry Analysis of Carbohydrates in Plant Tissues. *Anal. Chem.* **2010**, *82*, 5518-5526.
278. Lee, K. H., Chiang, C. K., Lin, Z. H., and Chang, H. T. Determining enediol compounds in tea using surface-assisted laser desorption/ionisation mass spectrometry with titanium dioxide nanoparticle matrices. *Rapid Commun. Mass Spectrom.* **2007**, *21*, 2023-2030.
279. Watanabe, T., Kawasaki, H., Yonezawa, T., and Arakawa, R. Surface-assisted laser desorption/ionisation mass spectrometry (SALDI-MS) of low molecular weight organic compounds and synthetic polymers using zinc oxide (ZnO) nanoparticles. *J. Mass Spectrom.* **2008**, *43*, 1063-1071.
280. Chen, W.-Y., and Chen, Y.-C. Affinity-based mass spectrometry using magnetic iron oxide particles as the matrix and concentrating probes for SALDI MS analysis of peptides and proteins. *Anal. Bioanal. Chem.* **2006**, *386*, 699-704.
281. Tanaka, K., Waki, H., Ido, Y., Akita, S., Yoshida, Y., Yoshida, T., and Matsuo, T. Protein and polymer analyses up to  $m/z$  100 000 by laser ionisation time-of-flight mass spectrometry. *Rapid Commun. Mass Spectrom.* **1988**, *2*, 151-153.
282. Cao, J., Wang, Y., Yu, J., Xia, J., Zhang, C., Yin, D., and Häfeli, U. O. Preparation and radiolabeling of surface-modified magnetic nanoparticles with rhenium-188 for magnetic targeted radiotherapy. *J. Magn. Magn. Mater.* **2004**, *277*, 165-174.
283. Smith, C. A., O'Maille, G., Want, E. J., Qin, C., Trauger, S. A., Brandon, T. R., Custodio, D. E., Abagyan, R., and Siuzdak, G. METLIN: a metabolite mass spectral database. *Ther Drug Monit* **2005**, *27*, 747-751.
284. Zhu, Z. J., Schultz, A. W., Wang, J., Johnson, C. H., Yannone, S. M., Patti, G. J., and Siuzdak, G. Liquid chromatography quadrupole time-of-flight mass spectrometry characterization of metabolites guided by the METLIN database. *Nat. Protoc.* **2013**, *8*, 451-460.
285. Horai, H., Arita, M., Kanaya, S., Nihei, Y., Ikeda, T., Suwa, K., Ojima, Y., Tanaka, K., Tanaka, S., Aoshima, K., Oda, Y., Kakazu, Y., Kusano, M., Tohge, T., Matsuda, F., Sawada, Y., Hirai, M. Y., Nakanishi, H., Ikeda, K., Akimoto, N., Maoka, T., Takahashi, H., Ara, T., Sakurai, N., Suzuki, H., Shibata, D., Neumann, S., Iida, T., Tanaka, K., Funatsu, K., Matsuura, F., Soga, T., Taguchi, R., Saito, K., and Nishioka, T. MassBank: a public repository for sharing mass spectral data for life sciences. *Journal of Mass Spectrometry* **2010**, *45*, 703-714.
286. Arica, M. Y., Bayramoğlu, G., and Bıçak, N. Characterisation of tyrosinase immobilised onto spacer-arm attached glycidyl methacrylate-based reactive microbeads. *Process Biochem.* **2004**, *39*, 2007-2017.
287. Girelli, A. M., Mattei, E., Messina, A., and Papaleo, D. Immobilisation of mushroom tyrosinase on controlled pore glass: Effect of chemical modification. *Sens. Actuator B Chem.* **2007**, *125*, 48-54.
288. Nerya, O., Vaya, J., Musa, R., Izrael, S., Ben-Arie, R., and Tamir, S. Glabrene and isoliquiritigenin as tyrosinase inhibitors from licorice roots. *J. Agric. Food Chem.* **2003**, *51*, 1201-1207.
289. Kurinov, I. V., and Harrison, R. W. Two crystal structures of the leupeptin-trypsin complex. *Protein Sci.* **1996**, *5*, 752-758.

290. KURAMOCHI, H., NAKATA, H., and ISHIJ, S.-i. Mechanism of Association of a Specific Aldehyde Inhibitor, Leupeptin, with Bovine Trypsin. *Journal of Biochemistry* **1979**, *86*, 1403-1410.
291. Han, J., Ye, M., Qiao, X., Xu, M., Wang, B.-r., and Guo, D.-A. Characterization of phenolic compounds in the Chinese herbal drug *Artemisia annua* by liquid chromatography coupled to electrospray ionisation mass spectrometry. *Journal of Pharmaceutical and Biomedical Analysis* **2008**, *47*, 516-525.
292. Farag, M. A., Porzel, A., and Wessjohann, L. A. Comparative metabolite profiling and fingerprinting of medicinal licorice roots using a multiplex approach of GC-MS, LC-MS and 1D NMR techniques. *Phytochemistry* **2012**, *76*, 60-72.
293. Jayaprakasam, B., Doddaga, S., Wang, R., Holmes, D., Goldfarb, J., and Li, X. M. Licorice flavonoids inhibit eotaxin-1 secretion by human fetal lung fibroblasts in vitro. *J Agric Food Chem* **2009**, *57*, 820-825.
294. Masamoto, Y., Ando, H., Murata, Y., Shimoishi, Y., Tada, M., and Takahata, K. Mushroom tyrosinase inhibitory activity of esculetin isolated from seeds of *Euphorbia lathyris* L. *Biosci Biotechnol Biochem* **2003**, *67*, 631-634.
295. Lin, L., Dong, Y., Zhao, H., Wen, L., Yang, B., and Zhao, M. Comparative evaluation of rosmarinic acid, methyl rosmarinate and pedalin isolated from *Rabdosia serra* (MAXIM.) HARA as inhibitors of tyrosinase and  $\alpha$ -glucosidase. *Food Chem.* **2011**, *129*, 884-889.
296. Karioti, A., Protopappa, A., Megoulas, N., and Skaltsa, H. Identification of tyrosinase inhibitors from *Marrubium velutinum* and *Marrubium cylleneum*. *Bioorganic & Medicinal Chemistry* **2007**, *15*, 2708-2714.
297. Stratford, M. R. L., Ramsden, C. A., and Riley, P. A. Mechanistic studies of the inactivation of tyrosinase by resorcinol. *Bioorganic & Medicinal Chemistry* **2013**, *21*, 1166-1173.

298. Deville-Bonne, D., El Amri, C., Meyer, P., Chen, Y., Agrofoglio, L. A., and Janin, J. Human and viral nucleoside/nucleotide kinases involved in antiviral drug activation: structural and catalytic properties. *Antiviral Res* **2010**, *86*, 101-120.
299. De Clercq, E., and Field, H. J. Antiviral prodrugs - the development of successful prodrug strategies for antiviral chemotherapy. *Br J Pharmacol* **2006**, *147*, 1-11.
300. Van Rompay, A. R., Johansson, M., and Karlsson, A. Substrate specificity and phosphorylation of antiviral and anticancer nucleoside analogues by human deoxyribonucleoside kinases and ribonucleoside kinases. *Pharmacology & Therapeutics* **2003**, *100*, 119-139.
301. Auvynet, C., Topalis, D., Caillat, C., Munier-Lehmann, H., Seclaman, E., Balzarini, J., Agrofoglio, L. A., Kaminski, P. A., Meyer, P., Deville-Bonne, D., and El Amri, C. Phosphorylation of dGMP analogs by vaccinia virus TMP kinase and human GMP kinase. *Biochemical and Biophysical Research Communications* **2009**, *388*, 6-11.
302. Elion, G. B. Mechanism of action and selectivity of acyclovir. *Am J Med* **1982**, *73*, 7-13.
303. Topalis, D., Collinet, B., Gasse, C., Dugue, L., Balzarini, J., Pochet, S., and Deville-Bonne, D. Substrate specificity of vaccinia virus thymidylate kinase. *FEBS J* **2005**, *272*, 6254-6265.
304. Tolonen, N., Doglio, L., Schleich, S., and Krijnse Locker, J. Vaccinia virus DNA replication occurs in endoplasmic reticulum-enclosed cytoplasmic mini-nuclei. *Mol Biol Cell* **2001**, *12*, 2031-2046.
305. Smee, D. F., Sidwell, R. W., Kefauver, D., Bray, M., and Huggins, J. W. Characterization of wild-type and cidofovir-resistant strains of camelpox, cowpox, monkeypox, and vaccinia viruses. *Antimicrob Agents Chemother* **2002**, *46*, 1329-1335.
306. Caillat, C., Topalis, D., Agrofoglio, L. A., Pochet, S., Balzarini, J., Deville-Bonne, D., and Meyer, P. Crystal structure of poxvirus thymidylate kinase: an unexpected dimerization has implications for antiviral therapy. *Proc Natl Acad Sci U S A* **2008**, *105*, 16900-16905.
307. Ostermann, N., Schlichting, I., Brundiers, R., Konrad, M., Reinstein, J., Veit, T., Goody, R. S., and Lavie, A. Insights into the phosphoryltransfer mechanism of human thymidylate kinase gained from crystal structures of enzyme complexes along the reaction coordinate. *Structure* **2000**, *8*, 629-642.

308. Riffault, L., Destandau, E., Pasquier, L., André, P., and Elfakir, C. Phytochemical analysis of *Rosa hybrida* cv. 'Jardin de Granville' by HPTLC, HPLC-DAD and HPLC-ESI-HRMS: Polyphenolic fingerprints of six plant organs. *Phytochemistry* **2014**, *99*, 127-134.
309. Kartnig, T., and Göbel, I. Effect of fluorescence intensifiers on the fluorodensitometric determination of flavones and flavonols after detection with diphenylboric acid 2-aminoethyl ester. *Journal of Chromatography A* **1996**, *740*, 99-107.
310. Lobasso, S., Lopalco, P., Angelini, R., Vitale, R., Huber, H., Muller, V., and Corcelli, A. Coupled TLC and MALDI-TOF/MS analyses of the lipid extract of the hyperthermophilic archaeon *Pyrococcus furiosus*. *Archaea* **2012**, *957852*, 8.
311. Fuchs, B., Schiller, J., Suss, R., Zscharnack, M., Bader, A., Muller, P., Schurenberg, M., Becker, M., and Suckau, D. Analysis of stem cell lipids by offline HPTLC-MALDI-TOF MS. *Analytical and Bioanalytical Chemistry* **2008**, *392*, 849-860.
312. Fuchs, B., Schiller, J., Suss, R., Schurenberg, M., and Suckau, D. A direct and simple method of coupling matrix-assisted laser desorption and ionisation time-of-flight mass spectrometry (MALDI-TOF MS) to thin-layer chromatography (TLC) for the analysis of phospholipids from egg yolk. *Analytical and Bioanalytical Chemistry* **2007**, *389*, 827-834.
313. Lay, J. O., Gidden, J., Liyanage, R., Emerson, B., and Durham, B. Rapid characterization of lipids by MALDI MS. Part 2: Artifacts, ion suppression, and TLC MALDI imaging. *Lipid Technology* **2012**, *24*, 36-40.
314. Sommerer, D., Suss, R., Hammerschmidt, S., Wirtz, H., Arnold, K., and Schiller, J. Analysis of the phospholipid composition of bronchoalveolar lavage (BAL) fluid from man and minipig by MALDI-TOF mass spectrometry in combination with TLC. *J Pharm Biomed Anal* **2004**, *35*, 199-206.
315. Vieler, A., Wilhelm, C., Goss, R., Suss, R., and Schiller, J. The lipid composition of the unicellular green alga *Chlamydomonas reinhardtii* and the diatom *Cyclotella meneghiniana* investigated by MALDI-TOF MS and TLC. *Chem Phys Lipids* **2007**, *150*, 143-155.
316. Ivleva, V. B., Sapp, L. M., O'Connor, P. B., and Costello, C. E. Ganglioside analysis by thin-layer chromatography matrix-assisted laser desorption/ionisation orthogonal time-of-flight mass spectrometry. *J Am Soc Mass Spectrom* **2005**, *16*, 1552-1560.
317. Kim, J., Han, S.-p., Kim, J., and Kim, Y.-J. Detection of Long Alkyl Esters of Succinic and Maleic Acid Using TLC-MALDI-MS. *Bull Korean Chem Soc* **2011**, *32*, 915-920.
318. Crecelius, A., Clench, M. R., Richards, D. S., and Parr, V. Quantitative determination of Piroxicam by TLC-MALDI TOF MS. *J Pharm Biomed Anal* **2004**, *35*, 31-39.
319. Mehl, J. T., and Hercules, D. M. Direct TLC-MALDI coupling using a hybrid plate. *Anal Chem* **2000**, *72*, 68-73.
320. Isbell, D. T., Gusev, A. I., Taranenko, N. I., Chen, C. H., and Hercules, D. M. Analysis of nucleotides directly from TLC plates using MALDI-MS detection. *Fresenius' Journal of Analytical Chemistry* **1999**, *365*, 625-630.
321. Chen, Y. C., Shiea, J., and Sunner, J. Thin-layer chromatography-mass spectrometry using activated carbon, surface-assisted laser desorption/ionisation. *J Chromatogr A* **1998**, *826*, 77-86.

# Aleksander SALWIŃSKI

## Développement de nouvelles approches basées sur la spectrométrie de masse pour le criblage d'inhibiteurs de la tyrosinase en milieu complexe.

Ce manuscrit de thèse présente le développement de méthodes basées sur la spectrométrie de masse consacrées à la recherche d'inhibiteurs d'enzymes en milieux complexes, tels que les extraits de plantes. L'enzyme Tyrosinase a été utilisée comme principale cible biologique du fait de son implication dans les processus d'hyperpigmentation cutanée. De ce fait, la recherche d'inhibiteurs de cette enzyme, présente un grand intérêt pour l'industrie cosmétique.

La première partie de ce manuscrit décrit la mise en place de la chromatographie d'affinité frontale (FAC), permettant d'obtenir le classement simultané des inhibiteurs présent dans un mélange complexe en fonction de leurs affinités avec la cible biologique. Deux capillaires hydrophiles de phase monolithiques ont été évalués afin de réduire au maximum les interactions non spécifiques indésirables entre les analytes et le support solide d'immobilisation. De plus, nous avons étudié la faisabilité de l'utilisation de phases à base de silice comme support solide d'immobilisation des enzymes dans le cadre de ces analyses par chromatographie d'affinité frontale.

La seconde partie du manuscrit de thèse est consacrée au développement et à l'optimisation de l'approche nommée ENALDI-MS (Enzyme-coupled Nanoparticles-Assisted Laser Desorption/Ionisation Mass Spectrometry) permettant d'accéder à une gamme des faibles masses ( $m/z$  500 Da). Elle est déclinée en une première approche dite par 'extinction d'ions' (Ion Fading, IF-ENALDI), basée sur l'identification directe de la liaison des inhibiteurs vis-à-vis de l'enzyme sans pré-traitement de l'échantillon végétal. Une seconde déclinaison de l'ENALDI-MS concerne une approche dite par 'Ion Hunting' (IH - ENALDI MS), basée sur une méthode de pré-concentration sélective des inhibiteurs présents dans l'échantillon.

**Mots clés :** tyrosinase, chromatographie d'affinité frontale, monolithes, immobilisation d'enzymes, désorption/ionisation laser assistée par surface

## Development of novel mass spectrometry-based approaches for searching for low-mass tyrosinase inhibitors in complex mixtures

This thesis report presents the development of mass spectrometry-based methods for searching for inhibitors of enzymes in complex mixtures, such as plant extracts. Tyrosinase enzyme was used as the main biological target for the reason of a significant importance of its inhibitors in the cosmetic industry as the skin whitening agents.

The first part of this report describes **Frontal Affinity Chromatography (FAC)**, an approach enabling simultaneous ranking the inhibitors within the complex mixture according to their affinities to the biological target. Two hydrophilic capillary-scale polymer-based bioaffinity stationary phases were evaluated in the context of the presence of undesirable nonspecific interactions between the analyte and the solid immobilisation support. In addition, we explored the usability of two types of silica-based particles as a solid support for enzyme immobilisation for FAC.

The second part of the thesis manuscript is devoted to **Enzyme-coupled Nanoparticle-Assisted Laser Desorption/Ionisation Mass Spectrometry (ENALDI MS)** as a low-mass compatible extension of the **Intensity ion Fading MALDI MS (IF-MALDI MS)** method for high-throughput screening of the inhibitors in the complex mixtures. Two variations of ENALDI MS were evaluated: 'Ion Fading' (IF-ENALDI MS), based on on-the-spot binding of inhibitors by enzyme molecules and 'Ion Hunting' (IH-ENALDI MS), based on selective pre-concentration of inhibitors present in the sample.

**Keywords:** tyrosinase, frontal affinity chromatography, monoliths, enzyme immobilisation, surface-assisted laser desorption/ionisation



Université d'Orléans,  
CNRS, ICOA  
UMR 7311  
rue de Chartres  
45067 Orléans, France

